

WestminsterResearch

<http://www.westminster.ac.uk/westminsterresearch>

**Preparation of polysaccharide-based nanoemulsions to reduce
melanoma drug resistance and inflammation markers**

Hatami Fard, G.

This is an electronic version of a PhD thesis awarded by the University of Westminster.

© Miss Ghazal Hatami Fard, 2020.

The WestminsterResearch online digital archive at the University of Westminster aims to make the research output of the University available to a wider audience. Copyright and Moral Rights remain with the authors and/or copyright owners.

Preparation of polysaccharide-based nano-emulsions to reduce melanoma drug resistance and inflammation markers

Ghazal Hatami Fard

A thesis submitted in partial fulfilment of the requirements of the
University of Westminster
for the degree of Doctor of Philosophy

College of Liberal Arts and Sciences
University of Westminster

September 2020

Abstract

Melanoma is the most aggressive type of skin cancer and various treatments have been investigated to treat this disease. However, an intrinsic issue in the clinical setting is the development of multidrug resistance. So far no single approach has emerged that may overcome such drug resistance by drug delivery. Alongside this, inflammation is an important marker of melanoma relating both to the incidence and progression of the disease, with upregulation in COX-2 and iNOS reported as playing a role in melanoma progression.

The work embodied in this thesis describes the development, optimisation, and characterisation of alginate, chitosan, and pullulan nano-emulsions as a delivery platform to target melanoma. In this study, a novel nano-emulsion delivery system was designed and optimised using a series of experimental steps including, *in vitro* drug release, cell viability (MTT), Cellular apoptosis ELISA, confocal and fluorescent microscopy, PCR, and Western blot to address melanoma chemo-resistance, and COX-2 and iNOS expression.

Chitosan-pullulan, pullulan-alginate, and alginate-chitosan polymer blends were prepared as nano-emulsions. A comparative analysis of their effect on melanoma (A375) and keratinocyte (HaCaT) cells was conducted. The “pullulan-chitosan” formulation was taken forward with folate-modification and used to target A375 cells. Subsequently, the melanocortin type 1 and 3 receptor agonists BMS-470539-dihydrochloride and [DTrp⁸]- γ -MSH were delivered to A375 cells using folate-modified pullulan-chitosan nano-emulsion, to target regulation of iNOS and COX-2 as important markers in melanoma progression.

Folate-modified pullulan-chitosan nano-emulsion enabled the delivery of doxorubicin and dacarbazine to A375 cells and diminished cell viability to 14 and 48% for doxorubicin and dacarbazine loaded nano-emulsions, respectively. Furthermore, BMS470539-dihydrochloride [DTrp⁸]- γ -MSH loaded nano-emulsions were able to decrease the regulation of iNOS and COX-2 to zero, after 72 hours.

Optimal delivery of therapeutics has been successfully applied to address chemo-resistance and enhanced apoptosis induction to melanoma cells. A novel optimal pullulan-chitosan nano-emulsion delivery system was developed for malignant melanoma. The nano-emulsion provided a controlled delivery of the chemotherapeutics to defeat chemo-resistance. Furthermore, the anti-inflammatory compound loaded pullulan-chitosan nano-emulsion decreased the iNOS and COX-2 expression in the A375 cell. This indicates that the compounds are more effective while delivered intracellularly, as opposed to the attachment to surface melanocortin receptors. This novel approach can be a promising tool to be used alongside treatments to prevent melanoma progression in its early stages.

Dedication

I dedicate this thesis

To my beloved grand mother

*For all your never ending love, support, and encouragement all my life
My strong woman role model and partner in crime*

And

*To the loving memory of my grandfather
Who always reminded me to smile, when I was not*

And

To all my loved ones

To my country

Iran...

Acknowledgements

Ph.D. was the most challenging journey of my life, I would like to express my deepest gratitude to all who supported me through this journey. Professor Tajalli Keshavarz, I am grateful for all your support and supervision.

Thanks to my supervisory team, Dr. Miriam Dwek, Dr. Hafiz Iqbal, and especially Dr. Stephen Getting for all the contributions and advice.

I appreciate the support of the Cavendish research scholarship, for allowing me to undertake my Ph.D. at the University of Westminster.

I am very grateful to Dr Rachith Kalgudi for all his kind assistance, support and help all along my PhD journey.

I am extremely grateful to Dr Louise Usher, for her unlimited and kind assistance, encouragement, and support.

I am grateful to Dr Karima Brima, and Dr Nasrin Berruie, for their selfless support, encouragement, and more importantly their friendship.

Special thanks to Pouyan, for encouraging me to be the best version of myself, for all the support and advice. I am very grateful for all your positive energy and selfless support.

Thanks to Adele, Amara, and Polly for their kind assistance and support.

I am in debt to University technical staff, specially Thakor Tandel, and Vanita Amin, for their generous support.

Declaration

I declare that all the material presented in this thesis, is wholly my own work, unless otherwise referenced or acknowledged. The document has not been submitted for qualifications at any other academic institution.

Relevant publications

- Asefi, S., Seifi, M., **Fard, G.H.** and Lotfi, A., 2018. Innovative evaluation of local injective gel of curcumin on the orthodontic tooth movement in rats. *Dental research journal*, 15(1), p.40.
- Seifi, M., Asefi, S., **Hatamifard, G.**, & Lotfi, A. (2017). Effect of local injection of Zolena, zoledronic acid made in Iran, on orthodontic tooth movement and root and bone resorption in rats. *Journal of dental research, dental clinics, dental prospects*, 11(4), 257–264.
<https://doi.org/10.15171/joddd.2017.045>

Table of Contents

Abstract	II
Dedication.....	IV
Acknowledgements	V
Declaration.....	VI
Relevant publications	VII
Table of Contents	VIII
List of figures.....	XIII
List of tables	XIX
List of abbreviations	XXI
1 Introduction.....	1
1.1 Cancer and its challenges	2
1.2 Cancer treatment.....	6
1.3 Cancer drug delivery	9
1.3.1 How anti-cancer drugs work, general principles	9
1.3.2 Cancer drug delivery and nano-medicine	12
1.3.3 Intracellular delivery of the drugs	15

1.4	Challenges in cancer drug delivery	20
1.5	Skin structure and function	23
1.5.1	Skin cancer	23
1.5.2	Drug resistance in skin cancer	26
1.6	Melanoma	28
1.6.1	Anti-cancer treatments for melanoma alleviation	36
1.6.2	Melanoma drug delivery	39
1.6.3	Polysaccharides in melanoma drug delivery	47
1.6.4	Nano-emulsion delivery system for melanoma treatment	54
1.6.5	Classification of nano-emulsions for melanoma treatment based on the rout of administration	58
1.7	Effect of inflammation on melanoma	59
1.7.1	Mediators that drive the host inflammatory response	62
1.7.2	Inflammation and cancer.....	62
1.7.3	Current treatments for inflammatory pathologies.....	65
1.7.4	Novel therapeutics for treating inflammatory pathologies.....	65
1.8	Research approach.....	68
1.9	Research aim and objectives	69
2	Materials and methods.....	71
2.1	Materials	72
2.1.1	Chemicals and reagents.....	72
2.2	Methods	80

2.2.1	Preparation of drug-loaded polysaccharide-based nano-emulsion	80
2.2.2	Measurement of the drug encapsulation efficiency of optimised nano-emulsion	85
2.2.3	Coumarin-6 and doxorubicin <i>in vitro</i> release tests.....	86
2.2.4	Nano-emulsion characterisation	86
2.2.5	Preparation of drug-loaded Folic Acid surface-modified nano-emulsion.....	87
2.2.6	Encapsulation of anti-inflammatory compound in optimised nano-emulsion	88
2.2.7	Cell culture.....	89
2.2.8	Mitochondrial activity (MTT) cytotoxicity assay	90
2.2.9	Cellular uptake test using confocal microscopy	91
2.2.10	Fluorescent microscopy	92
2.2.11	DNA fragmentation ELISA.....	94
2.2.12	Folate binding protein ELISA	95
2.2.13	Co-culture of HaCaT and A375 cells	96
2.2.14	Polymerase chain reaction	96
2.2.15	Western blotting	101
2.3	Statistical analysis.....	104
3	Results.....	105
3.1	Synthesis and optimisation of nano-emulsion for enhanced drug delivery to melanoma	
	106	
3.1.1	Introduction.....	106
3.1.2	Synthesis and evaluation of polymeric nano-emulsions characteristics	108

3.2	Modification of optimised pullulan-chitosan nano-emulsion for enhanced uptake in A375 cells.....	144
3.2.1	Introduction.....	144
3.2.2	Characterisation of pullulan-chitosan nano-emulsion.....	146
3.2.3	Cell viability screening of modified nano-emulsion.....	151
3.2.4	Fluorescent microscopy.....	154
3.3	Evaluation of anti-inflammatory compounds encapsulated in nano-emulsions on melanoma cells	181
3.3.1	Introduction: Encapsulation of BMS-470539-dihydrochloride and [DTrp ⁸]- γ -MSH in pullulan-chitosan nano-emulsion as a novel tool for melanoma treatment.....	181
3.3.2	Viability of A375 cells treated with encapsulated BMS-470539-dihydrochloride and [DTrp ⁸]- γ -MSH in folate-modified pullulan-chitosan nano-emulsion	182
3.3.3	iNOS and COX-2 expression analysis	186
3.3.4	Fluorescent microscopy of A375 and HaCaT cells in co-culture, treated with encapsulated BMS-470539-dihydrochloride and [DTrp ⁸]- γ -MSH and non-encapsulated BMS-470539-dihydrochloride and [DTrp ⁸]- γ -MSH.....	192
4	Discussion.....	196
4.1	Introduction.....	197
4.2	Nano-emulsion optimisation.....	198
4.2.1	<i>In vitro</i> release test.....	198
4.2.2	Cell viability test.....	201
4.2.3	Cellular uptake and intracellular drug release studies	202

4.2.4	Cellular apoptosis induction ability of the nano-emulsions	204
4.2.5	Nano-emulsion characterisation	205
4.3	Modification of optimised chitosan-pullulan nano-emulsion	207
4.3.1	Folate-modification of nano-emulsion	207
4.3.2	Viability of melanoma and keratinocyte cells treated with surface modified optimized nano-emulsion	208
4.3.3	Fluorescent microscopy of melanoma and keratinocyte cells in co-culture	209
4.3.4	Polymerase chain reaction	211
4.4	Investigation of cell viability and iNOS and COX-2 downregulation after treating with encapsulated anti-inflammatory compounds	212
4.4.1	iNOS and COX-2 expression	213
4.4.2	Toxicity induced by encapsulated compounds on A375 cells.....	215
4.4.3	Fluorescent microscopy of melanoma-keratinocyte co-culture treated with encapsulated compounds.....	216
5	Conclusion	217
6	Future work	219
7	Appendix	221

List of figures

Figure 1.1 Intrinsic and extrinsic apoptosis pathways	4
Figure 1.2 Irregular proliferation of cancerous cells leading to tumour formation	5
Figure 1.3 Understanding tumour microenvironment and how it limits drug delivery	22
Figure 1.4 Skin cancer types	25
Figure 1.5 Skin layers showing the location of melanocytes in the skin	30
Figure 1.6 Various melanoma separated in terms of physical shape	32
Figure 2.1 Mitochondrial reduction happening during MTT assay	91
Figure 2.2 Organic, interface, and aqueous phases after treating with TRIzol	97
Figure 2.3 Western blot stained Ponceau S	104
Figure 3.1 Flow-chart of the development and optimisation of nano-emulsions	107
Figure 3.2 Coumarin-6 cumulative release from chitosan nano-emulsions	110
Figure 3.3 Coumarin-6 cumulative release profile from pullulan nano-emulsions	111
Figure 3.4 Coumarin-6 cumulative release profile from alginate nano-emulsion	112
Figure 3.5 Doxorubicin cumulative release profile from chitosan nano-emulsion	113
Figure 3.6 Doxorubicin cumulative release profile from pullulan nano-emulsions	114
Figure 3.7 Doxorubicin cumulative release profile from alginate nano-emulsions	115
Figure 3.8 Coumarin-6 cumulative release profile from blended nano-emulsions	118
Figure 3.9 Doxorubicin cumulative release profile from blended nano-emulsions	119

Figure 3.10 Viability screening keratinocyte (HaCaT) cells treated with non-loaded nano-emulsions	122
Figure 3.11 Viability screening melanoma (A375) cells treated with non-loaded nano-emulsions	123
Figure 3.12 Viability of A375 cells treated with top-nine blended nano-emulsions	125
Figure 3.13 Viability of A375 cells in 4-hour treatment with non-loaded and doxorubicin-loaded blended nano-emulsion	127
Figure 3.14 Viability of A375 cells in 24-hour treatment with non-loaded and doxorubicin-loaded blended nano-emulsion	128
Figure 3.15 Viability of A375 cells in 48-hour treatment with non-loaded and doxorubicin-loaded blended nano-emulsion	129
Figure 3.16 Viability of A375 cells in 72-hour treatment with non-loaded and doxorubicin-loaded blended nano-emulsion	130
Figure 3.17 Viability of HaCaT cells in 4-hour treatment with non-loaded and doxorubicin-loaded blended nano-emulsion	131
Figure 3.18 Viability of HaCaT cells in 24-hour treatment with non-loaded and doxorubicin-loaded blended nano-emulsion	132
Figure 3.19 Viability of HaCaT cells in 48-hour treatment with non-loaded and doxorubicin-loaded blended nano-emulsion	133
Figure 3.20 Viability of HaCaT cells in 72-hour treatment with non-loaded and doxorubicin-loaded blended nano-emulsion	134

Figure 3.21 Coumarin-6 intracellular release in A375 cells treated with top-nine C6 loaded nano-emulsions	136
Figure 3.22 Confocal images of A375 and HaCaT cells treated with C6 loaded nano-emulsions	139
Figure 3.23 Confocal images of A375 and HaCaT cells treated with doxorubicin-loaded nano-emulsions	140
Figure 3.24 Induced apoptosis trend by doxorubicin-loaded nano-emulsions measured by DNA fragmentation ELISA.....	142
Figure 3.25 Flow-chart of nano-emulsion characterization and experiments for surface modification of optimised nano-emulsions.....	145
Figure 3.26 Encapsulation efficiency of drug-loaded optimal nano-emulsion.....	147
Figure 3.27 Nano-particle tracking analysis using NanoSight	149
Figure 3.28 Nano-particle tracking analysis using NanoSight	150
Figure 3.29 Viability screening of A375 and HaCaT cells treated with drug-loaded nano-emulsion and naïve drugs.....	152
Figure 3.30 Fluorescent microscopy of HaCaT and A375 in co-culture	155
Figure 3.31 Fluorescent microscopy of A375 and HaCaT in co-culture (dacarbazine-loaded nano-emulsion)	157
Figure 3.32 Fluorescent microscopy of A375 and HaCaT in co-culture (doxorubicin-loaded nano-emulsion)	158

Figure 3.33 Fluorescent microscopy of A375 and HaCaT in co-culture (dacarbazine-loaded modified nano-emulsion)	159
Figure 3.34 Fluorescent microscopy of A375 and HaCaT in co-culture (naïve doxorubicin)	160
Figure 3.35 Fluorescent microscopy of A375 and HaCaT in co-culture (naïve dacarbazine)	161
Figure 3.36 Fluorescent microscopy of A375 and HaCaT in co-culture (doxorubicin-loaded modified nano-emulsion)	162
Figure 3.37 CMFDA and DAPI labelled A235 cells treated with drug-loaded nano-emulsions	164
Figure 3.38 Comparison of CMTPX labelled HaCaT treated with nano-emulsions	165
Figure 3.39 Quantified DNA band intensities analysed with PCR and gel electrophoresis (Caspase 3)	169
Figure 3.40 Quantified DNA band intensities analysed with PCR and gel electrophoresis (Caspase 9)	170
Figure 3.41 Quantified DNA band intensities analysed with PCR and gel electrophoresis (Bax)	171
Figure 3.42 Quantified DNA band intensities analysed with PCR and gel electrophoresis (Bcl2)	172
Figure 3.43 DNA bands detected in agarose gel	173
Figure 3.44 DNA bands detected in agarose gel	174
Figure 3.45 DNA bands detected in agarose gel	175

Figure 3.46 DNA bands detected in agarose gel.....	176
Figure 3.47 DNA bands detected in agarose gel.....	177
Figure 3.48 DNA bands detected in agarose gel.....	178
Figure 3.49 Standard curve of different concentrations of the folate binding protein detected in ELISA	180
Figure 3.50 Viability of the A375 cells treated with encapsulated and naïve BMS-470539-dihydrochloride	183
Figure 3.51 Viability of the A375 cells treated with encapsulated and naïve [DTrp ⁸]- γ -MSH	184
Figure 3.52 Viability of the A375 cells treated with LPS.....	185
Figure 3.53 iNOS and COX-2 expression analysis by Western blot.....	187
Figure 3.54 iNOS and COX-2 expression over 24 hours in melanoma cells treated with encapsulated and naïve compounds	189
Figure 3.55 iNOS and COX-2 expression over 48 hours in melanoma cells treated with encapsulated and naïve compounds	190
Figure 3.56 iNOS and COX-2 expression over 72 hours in melanoma cells treated with encapsulated and naïve compounds	191
Figure 3.57 Fluorescent imaging of HaCaT and A375 co-cultures treated with encapsulated and naïve BMS-470539-dihydrochloride	194
Figure 3.58 Fluorescent imaging of HaCaT and A375 co-cultures treated with encapsulated and naïve [DTrp ⁸]- γ -MSH	195

Figure 7.1 HPLC peak detected at 2 minutes for doxorubicin	221
Figure 7.2 SEM image of the optimal pullulan-chitosan nano-emulsion	222
Figure 7.3 iNOS and COX-2 expression analysis by Western blot.....	223

List of tables

Table 1.1 Chemotherapy drugs and their characteristics	11
Table 1.2 Drug delivery systems used for melanoma	40
Table 1.3 Characteristics of selected polysaccharides	49
Table 1.4 Nano-emulsions used in cancer research	55
Table 2.1 Materials and reagents	72
Table 2.2 Characteristics of cytotoxic drugs used for drug delivery	75
Table 2.3 Cell lines	75
Table 2.4 Primer sequences used for PCR (Si et al, 2018)	76
Table 2.5 ELISA kits	76
Table 2.6 antibodies	76
Table 2.7 Buffers used in the experiments.....	77
Table 2.8 Equipment.....	77
Table 2.9 Software	79
Table 2.10 Chitosan nano-emulsion preparation ratios	81
Table 2.11 Alginate nano-emulsion preparation ratios.....	82
Table 2.12 Pullulan nano-emulsion preparation ratios	82
Table 2.13 IDs for in-house prepared nano-emulsions	84
Table 2.14 RNA quantification and quality by nano-drop	98
Table 2.15 RNA purification and reagents	99
Table 2.16 PCR cycles and conditions	100

Table 3.1 Particle size and charge of doxorubicin-loaded nano-emulsions.....	148
Table 3.2 Folate receptor concentration.....	180

List of abbreviations

ACTH	Adrenocorticotrophic hormone	DTT	Dithiothreitol
BCC	Basal cell carcinoma	SDS	Sodium dodecyl sulfate
C6	Coumarin-6	TAE	Tris-acetate EDTA
cAMP	Cyclic adenosine monophosphate		
cDNA	Complementary DNA		
COX	Cyclooxygenase		
Coxib	Cyclooxygenase inhibitors		
DD	Deacetylation degree		
DNA	Deoxy ribonucleic acid		
Dox	Doxorubicin		
DTIC	Dacarbazine		
ECM	Extracellular		
EDTA	Ethylenediaminetetraacetic acid		
EPR	Enhanced permeation and retention		
ER	Endoplasmic reticulum		
HCl	Hydrochloric Acid		
iNOS	Induced nitric oxide synthase		
MAPK	Mitogen-activated protein kinase		

MCR	Melanocortin receptors		
MTT	3-(4,5-dimethylthiazol-2-yl)-2,5-diphenyltetrazolium bromide		
NEAI	Alginate nano-emulsion		
NEC	Chitosan nano-emulsion		
NEPI	Pullulan nano-emulsion		
NPC	Nuclear pore complex		
NSAID	Non-steroidal anti-inflammatory drug		
PBS	Phosphate buffered saline		
PCL	Polycaprolactone		
PEG	Poly ethylene glycol		
POMC	Proopiomelanocortin		
RAS	Rat sarcoma		
SCC	Squamous cell carcinoma		
siRNA	Small interfering ribonucleic acid		
TNF	Tumour necrosis factor		
UV	Ultra violet		
αMSH	α Melanocyte stimulating hormone		

1 Introduction

1.1 Cancer and its challenges

Increased cancer-related incidents and mortality rates in recent years have raised a challenge towards cancer diagnosis tools and treatments. Cancer is amongst the most common cause of mortality across the globe (Bray et al., 2018). The number of patients diagnosed with various types of it is increasing worldwide and it is estimated that the numbers will rise further in the next 20 years (Bray et al., 2018, Siegel et al., 2019, Ferlay et al., 2019). Cancer mortality and incidents were studied in the UK. According to the cancer mapping incidents in the UK, half of the people in the UK will develop cancer in their lifetime (Oke et al., 2018). Until 2018, cancer incidents and mortality rates were reported to raise in western Europe by 34.9% and 27.7% incidents for men and women respectively. While the mortality was reported as 13.3% and 8.8% for men and women respectively (Rawla et al., 2019).

So far, researchers have undertaken extensive investigations on the diagnosis, prevention, causes, and cancer therapies (Arruebo et al., 2011). However, no particular cause or therapy for cancer has been reported so far. This is mainly due to the highly heterogeneous nature of tumours (Siegel et al., 2020). In simple terms, cancer is the irregular growth of the cells in any part of the body which leads to the development of a tumour (Sudhakar, 2009).

The function of the cell is based on the expression of proteins that regulate cell growth, division, and programmed cell death. However, this regularity is entirely altered in cancer cells (Guimarães and Linden, 2004). This also means that inherited or recently generated gene mutations may lead to changed signalling pathways and dysregulation of protein expression (Cheng et al., 2019b). This in turn may lead to an irregular proliferation of the cells as the result

of dysfunction of cellular apoptosis, caused in the result of dysregulated programmed cell death (Ruddon, 2007, Kim, Duesberg and McCormack, 2013). There are many factors involved in the process of cellular transformation of normal cells to “cancer cells”; these factors arise from the genetic mutation in cells (Xu et al., 2018). When the normal cell is transformed into a so-called “cancerous” cell, it will act autonomously; a cancer cell is completely independent of normal healthy cells in terms of growth and proliferation (Alibert et al., 2017). Cancerous tumours can be either benign or malignant (Weinberg, 2013) and can result from a variety of genetic or environmental factors.

The cell proliferation cycle plays a crucial role in controlling cell proliferation and apoptosis, in the body (Pucci et al., 2000). Cell apoptosis is a programmed cell death which is a combination of organised biochemical processes leading to cell destruction (Elmore, 2007). There are two main pathways for apoptosis, the mitochondrial pathway, and the death receptor pathway (intrinsic and extrinsic) (Figure 1.1). The mitochondrial pathway is triggered by any DNA damage in the cells (Jan and Chaudhry, 2019). The death receptor pathway is activated by external death ligands activating tumour necrosis factor receptor (TNFr). Activation of both pathways leads to activation of apoptosis initiator caspases (Li and Yuan, 2008).

While apoptosis is a crucial biological process for repair, healing, and regeneration, dysregulation in apoptotic pathways can lead to over-proliferation of the cells (Ryoo and Bergmann, 2012). Subsequently, irregular cell proliferation as the result of the absence of apoptotic factors will lead to the formation of tumours (Lee et al., 2018). Hence, resistance to apoptosis is a sign of malignant disease (Wong, 2011).

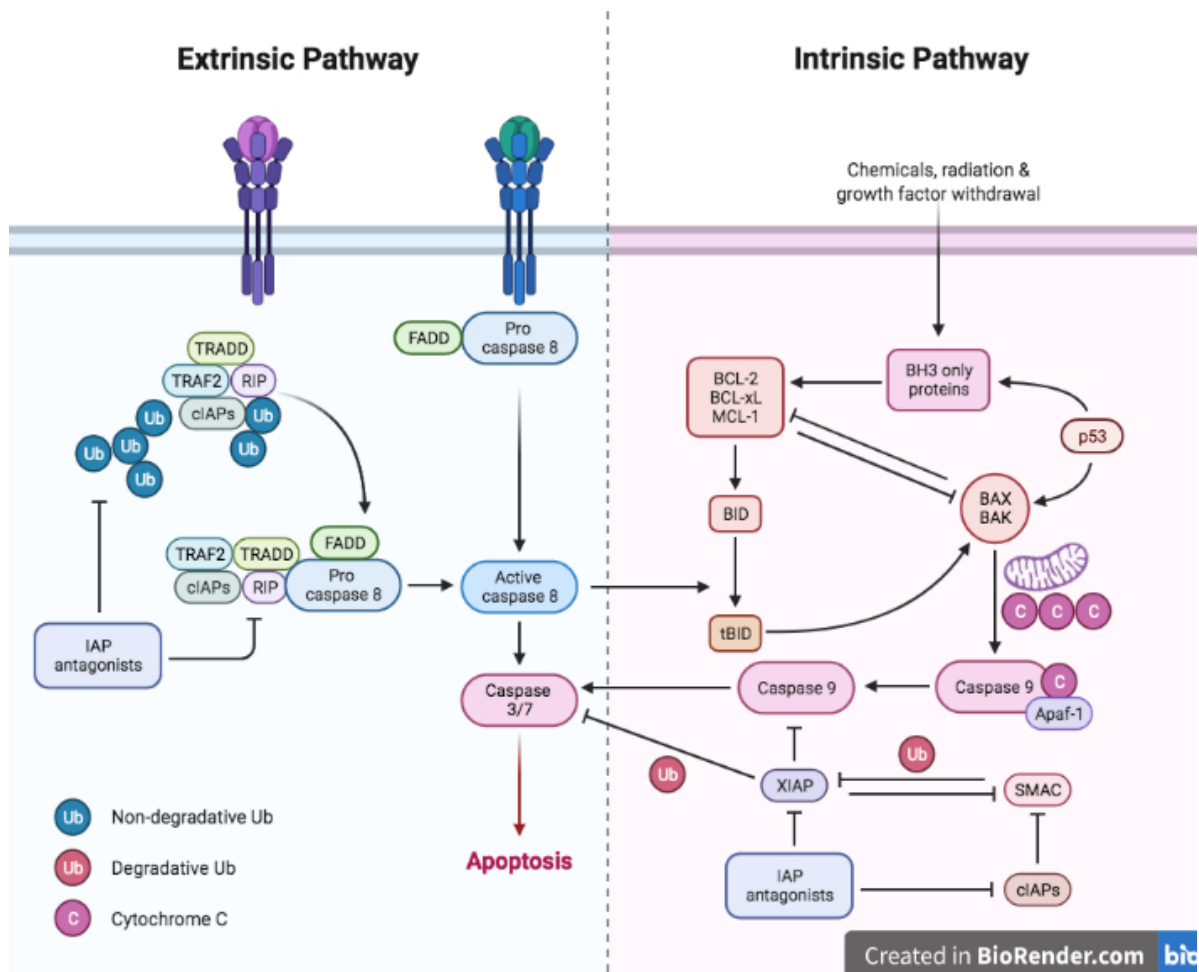


Figure 1.1 Intrinsic and extrinsic apoptosis pathways

Created in Biorender.com

Carcinogenesis happens in multiple steps that involve genetic and epigenetic (external factors which can cause damage or affect human genes) factors. Genetic instability is another important factor for carcinogenesis. Inherited or acquired DNA mutations will turn a healthy cell into a cancer cell. Existing mutations in patients also increase the risk of cancer (Coyle et al., 2017).

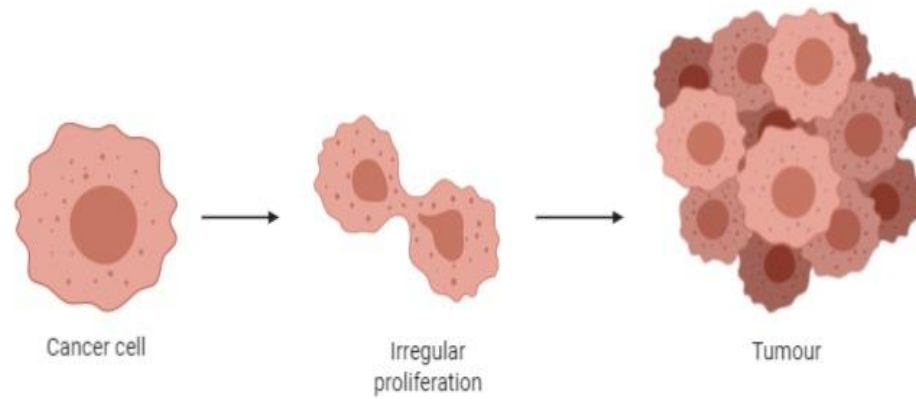


Figure 1.2 Irregular proliferation of cancerous cells leading to tumour formation

Created in BioRender.com

Malignant tumours are characterised by their invasiveness and ability to metastasise. The process of the growth of a tumour happens in a series of steps. The progression pace can be fast or slow, depending on the cancer type and/or the patient’s general health and immune system (van Zijl et al., 2011). Initially, a tumour consists of over proliferated cell clusters (Figure 1.2), called *hyperplasia*. This “overgrowth” starts to change appearance, a status called *dysplasia*. In the *dysplasia* phase, cells have the potential to spread over the healthy tissue, although, they have not done (invaded) so yet. With further progression, the cells lose their initial functions and this phase is called *anaplastic*. The cells in the anaplastic phase have the potential to invade the surrounding tissues and organs (Ruddon, 2007).

Cancer cells produce enzymes such as metalloproteinases that break down extracellular matrix (ECM) which enables them to move away from the primary tumour. They can migrate through

the tissue and infiltrate the blood vessels and lymphatics and travel through the vasculature to reach other sites in the body (Walker et al., 2018). Tumours formed from migrated cells in distant organs are called “secondary tumours”. The process of secondary tumour formation is metastasis and it is the main cause of mortality after cancer (Agliaio et al., 2017).

1.2 Cancer treatment

Cancer has been recognised throughout the millennia and early reports of cancer diagnosis date back to 1600 BC (Falzone et al., 2018b). Since then, investigators and physicians were in the quest for a cure to treat the disease. At that time, the most feasible treatment seemed to be surgery and removing the tumour mass (Samiee et al., 2012). Nevertheless, the mortality rate kept increasing (Jaffe et al., 2016).

The very first cancer treatments started in the early 1820s using surgery to remove solid tumours (Kuflik and Gage, 1990). However, this technique could only be used in the excision of accessible solid tumours with a specific border and did not have a significant effect on the long-term survival of cancer patients. During the late 1860s, a French doctor, Claudius Regaud, who is now known as the “father of radiation therapy” started treating cancer by X-ray radiations (Sgantzos et al., 2014). Afterward, X-ray treatment started to be used for breast cancer and a few types of skin cancer such as basal cell carcinoma (Silverman et al., 1992). In the 1920s, immune-stimulation by the injection of complex mixtures from tumours, was attempted as a complementary therapy to radiotherapy for cancer treatments (McCarthy, 2006a). This was done by injecting *streptococcal* organisms to a patient with advanced cancer (McCarthy,

2006b). Although the method was controversial at that time, it is now shown to have had some validity but the overall risk of this treatment was high (Wang, 2017). Chemotherapy remains the most common systemic cancer treatment with many chemotherapeutics synthesised, particularly by chemists commencing in the 1960s and beyond (DeVita and Chu, 2008). The chemicals for cancer treatments were partially successful. This means that although the survival rate of the patients increased, the mortality rate remained high (Huang et al., 2017). Moreover, the chemicals were severely toxic to the patients resulting in a significant decline in their general health conditions. Furthermore, most of the chemotherapeutics had poor bioavailability and were not able to specifically target cancer cells (De Souza et al., 2010, Gerber, 2008, Nurgali et al., 2018).

Most of the chemotherapeutics are cytotoxic reagents that can interfere with DNA and destroy the cells. Therefore, the presence of chemotherapeutics in the bloodstream can interact with healthy and crucially essential cells in the body, such as bone marrow cells (Dickens and Ahmed, 2018). Chemotherapy reagents are usually more effective when used in combination with surgery (Huang et al., 2017). Furthermore, depending on the biochemical nature of the drugs and/or their bioavailability, the therapy may fail to be efficiently delivered to cancer cells (Tharkar et al., 2019). Although chemotherapy in metastasised cancer is mostly considered as palliative care, which increases the patient's lifetime (Dickens and Ahmed., 2018), ultimately it may not be successful in eliminating cancer (Alfarouk et al., 2015).

Chemo-resistance is an important gap between initial cancer treatment and effective cure. This problem directly affects the patient's life quality and survival (Jo et al., 2018). Various approaches can be used which, depending on cancer type and progression, may change.

Nevertheless, effective and efficient delivery of chemotherapeutics to cancer cells and preventing chemo-resistance remain important factors in the therapy progress (Chatterjee and Bivona, 2019).

All the mentioned therapy procedures which have been developed over time were successful in increasing the survival rate of cancer patients particularly during the last half-century (Joo et al., 2013). Nevertheless, cancer-related mortality is still high. Furthermore, the side effects caused by the conventional therapy procedures are quite significant to the patient's overall health, their quality of life (QoL), and the cost is also notable (Love et al., 1989, Pearce et al., 2017).

Emerging novel targeted therapy procedures have had a great impact on cancer treatments and consequently have enhanced patients' QoL. The combination of chemotherapy and targeted drug delivery systems is called targeted drug delivery in cancer (Bayat Mokhtari et al., 2017). The main purpose of targeted therapy is to increase the efficacy of cancer treatment and diminish adverse effects on healthy tissues (Senapati et al., 2018). In this regard, targeted therapy approaches are promising tools with regards to increasing the scope for the treatment of cancer (Sawyers, 2004). Targeted therapy is a vast area of research that consists of various branches. The approaches to treat different cancer types and the progression stages are also different in targeted therapy procedures (Pucci et al., 2019).

1.3 Cancer drug delivery

A deeper understanding of cancer behaviour has driven researchers, particularly in the last decade, to seek improved delivery vehicles for chemotherapeutics (Falzone et al., 2018a). Due to the challenging nature of cancer and its treatments many investigations have been performed towards the effective delivery of therapeutics (Navya et al., 2019, Senapati et al., 2018b).

Common obstacles faced by traditional chemotherapy include lack of targeting, enzymatic digestion of the drug and biodegradation, and chemo-resistance (Liang et al., 2010). Through designing pertinent carrier systems for specific or non-specific drugs, these problems are starting to be addressed (Iwamoto, 2013).

1.3.1 How anti-cancer drugs work, general principles

The most conventional treatments for cancer are surgery, chemotherapy, and radiotherapy, depending on the stage of progression (Miller et al., 1981). Conventional chemotherapy acts non-selectively on all the cells in the body (Senapati et al., 2018a) and has a cytotoxic effect on the cells. However, recently novel biopharmaceuticals such as monoclonal antibodies and immunomodulators have improved the concept of conventional therapies (Kesik-Brodacka, 2018). Yet, cytotoxic drugs (chemotherapeutics) are principal components of cancer treatment along with surgery and radiotherapy (Schirrmacher, 2019). Cancer cells in a tumour exist in three states, dividing cells in active phases of the cell cycle, resting cells not dividing but potentially can, and cells that no longer have the capacity for cell division (Bertram, 2000). Cells in the first state, which are estimated to consist 5% of the tumour mass, are more prone

to be affected by cytotoxic drugs. The cells in the second state may not be affected by the cytotoxic drug, however, may start proliferating (Housman et al., 2014).

Most of the cytotoxic anti-cancer drugs act only against one aspect of the cancer cell cycle. The cytotoxic drugs affect the cells in the dividing phase (S phase) and usually have an anti-proliferative effect by damaging the cell DNA. However, along with cancer cells, most of the rapidly dividing healthy cells in the body can be affected by cytotoxic drugs. This may subsequently cause nausea, hair loss, vomiting, sterility, decreased resistance to infections, and growth suppression (mostly in children) (Mitchison, 2012).

Anti-cancer drugs are divided into three general groups (Table 1.1) namely cytotoxic drugs, hormones, protein kinase inhibitors, and monoclonal antibodies. Cytotoxic drugs include alkylating agents, antimetabolites, cytotoxic antibiotics, and plant derivatives (Chari, 2008).

Table 1.1 Chemotherapy drugs and their characteristics

	Alkylating agents	Antimetabolites	Cytotoxic antibiotics	Plant derivatives	Hormones	Protein kinase inhibitors	Monoclonal antibodies
Example	Bendamustine, melphalan, carboplatin, dacarbazine, procarbazine	Pemetrexed, Cytarabine, Decitabine, Fluorouracil, Gemcitabine, Cladribine,	Daunorubicin, Doxorubicin, Dactinomycin, Mitomycin, Epirubicin	Docetaxel, Paclitaxel, Vinblastine, Vincristine, Vindesine,	Medroxyproges Terone, Megestrol, Tamoxifen, Mitotane	Acalabrutinib, axitinib, crizotinib,	Brentuximab, ofatumumab, rituximab
Main mechanism	Intrastrand crosslinking of DNA	Blocking the synthesis of RNA and/or DNA	Effect on RNA and DNA synthesis,	Prevention of spindle formation	Inhibition of hormone dependant tumour growth	Inhibition of kinase involved in tumour growth factors	Preventing cell proliferation, inhibiting angiogenesis.

Chemotherapeutic drugs usually are used in combination but resistance to anticancer drugs can either happen in primary treatment or can be acquired during treatment mostly due to adaptation of the tumour cells or mutation (Bayat Mokhtari et al., 2017).

Several mechanisms leading to resistance have been described. These include low accumulation or uptake of the cytotoxic drug in the cells, increase in drug inactivation, increased concentration of target enzyme, decreased substrate, activation of alternative metabolic pathways, rapid repair of DNA damage caused by the drug, alteration in target activity (in the cell), and mutation in various or multiple genes (Vaidya et al., 2020). Accordingly, recent advances in cancer therapy involve drug treatment with lower side effects, targeted therapies for increase treatment efficiency, and a decrease in the chance of resistance (Pucci et al., 2019).

1.3.2 Cancer drug delivery and nano-medicine

Emerging nano-medicine has the potential to have a huge impact on cancer drug delivery (Bertrand et al., 2014). The utilization of nano-sized particles as carriers for chemotherapeutics has become an important tool in cancer therapy (Cho et al., 2008). Nano-sized particles have a high tendency to enter cells by an enhanced permeation and retention (EPR) effect which is known as passive targeting. The transport of nano-sized particles via the leaky vasculature in the tumour microenvironment (Dadwal et al., 2018) is known as passive targeting of cancer cells. These carrier particles can be further modified to especially target the cancer cells; this is called active targeting.

Besides the EPR effect, delivery via nano-particles has additional advantages. Therapeutics and drug conjugates entrapped in nano-particles tend to be more stable, particularly for drugs that, intrinsically do not have stability and long half-life (Parveen et al., 2012). The nano-particle shell can preserve the drug allowing for longer biological life (Nguyen, 2011). Also, the concentration of drug-containing particles will increase in the cancerous tissue site, due to the EPR effect (Senapati et al., 2018b). Furthermore, nano-particles can be used for entrapments of multiple drugs and they are suitable for multiple modes of delivery. The use of nano-particles can be advantageous for the delivery of drugs containing siRNA and protein as well since they can protect them from being degraded (Navya et al., 2019).

Nano-particles are investigated as suitable tools for both targeting cancer cells and addressing chemo-resistance at the same time (Sutradhar and Amin, 2014). Encapsulating chemotherapeutics within nano-particles can provide controlled release over time. This will happen by the slow degradation of the nano-sized shell encapsulating the drug (Rizvi and Saleh, 2018). The drug efflux delivered to the tumour will be limited and slower over time; this helps to prevent drug-efflux-dependent chemo-resistance (Navya et al., 2019, Da Silva et al., 2017). This feature of the delivery system can be manipulated to fit the final purpose.

Nano drug delivery systems can be prepared using various materials and different procedures. Liposomes (Allen and Cullis, 2013), micelles (Rapoport, 2007), polymeric nano-particles (Kumari et al., 2010), dendrimers (Tomalia et al., 2007), and hydrogels (Sharma et al., 2016), are the most common structures of nano-sized particles which can be used as drug carriers.

Micelles are among the very first novel drug delivery systems (Sutton et al., 2007). Micelles are known for their high specificity of delivery and controlled release. However, micelles lack

the properties for effective extravasation and there is the possibility of chronic liver toxicity in micellar drug delivery systems (Yokoyama, 2011).

After the successful application of micelles in delivering chemotherapy drugs such as doxorubicin, improvements to similar delivery systems for enhanced therapy and quality has gained importance (Fromherz and Ruppel, 1985). Lipid nano-carriers which emerged about three decades ago (Müller et al., 1997) were introduced as nano-sized delivery systems for therapeutics. Although these carriers have advantages like increased drug-loading efficiency and enhanced stability, other groups of non-toxic nano-sized particles made of natural and synthetic lipids show superior properties and provide controlled release with enhanced stability (Niu et al., 2016).

Another well-known nano-delivery vehicle is the dendrimer-based nano-particle composed of repetitively branched molecules, recognised for its very small size (1.5 to 10 nm), (Wolinsky and Grinstaff, 2008, Guo and Shi, 2012). Dendrimer's properties can be easily controlled by modifications and it can be used in a range of applications in nano-medicine and drug delivery (Bahrami and Arabi, 2016). Polymeric nano-structures made of various natural or synthetic polymers acting as nano-carriers for drugs or targeted therapies have very flexible preparation methods and controllable properties especially in cancer drug delivery (Wiradharma et al., 2009). Other than polymers, gold particles (Singh et al., 2017), magnetic nano-carriers (Tietze et al., 2015), albumin nano-carriers (Khandelia et al., 2015), viral particles (Biabanikhankahdani et al., 2016) and carbon-based carriers (Karimi et al., 2015) are alternative nano-carrier materials used for targeted and specific cancer drug delivery. Although nano-sized carriers can act as both passive and active delivery vehicles targeting cancer cells, there are still

challenges and sometimes disadvantages with each system. These include stability and cytotoxicity and particle accumulation in the body (Jong et al., 2008); however, these limitations can be addressed with further alterations, such as surface modification for active targeting, using peptides (Pang et al., 2019).

As mentioned above, the simplest tumour drug delivery mechanism using nano-particles is the EPR effect. It is capable of delivering chemotherapeutics to a cancer cell in a controlled fashion to overcome chemo-resistance and provide higher efficiency of chemotherapy. All of the nano-sized delivery systems mentioned above, have their pros and cons. The most important factor in choosing a delivery system for cancer is the nature of the tumour and its stage of progression (Patra et al., 2018). However, the fate of the nano-particles after entering the cell cytosol needs to be considered. Therefore, a cancer-specific drug delivery system should be designed based on both kinetic and histologic parameters, to meet the criteria for ultimate use (Blanco et al., 2015).

1.3.3 Intracellular delivery of the drugs

One of the major concerns of chemotherapeutics is the drug's action-site and its fate in the body and even its interactions with the cancer cell (Alfarouk et al., 2015). Since organelles are located within the cell walls, the drug carrier must first penetrate the cell, to be effective. Hence successful uptake of drug or drug-carrying particles is crucial. There is a basic mechanism for cancer cells to take up the drug-carrying particles (Sakhrani and Padh, 2013).

1.3.3.1 Cellular uptake of drug particles in cancer cells

Cells take up nano-particles and most chemotherapy therapeutics by endocytosis. However, due to endosomal entrapment, often they are degraded by the lysosome (Pei and Buyanova, 2019). Delivering drugs to cancer cells in a targeted manner requires surface functionalisation of the carrier particles, with specific ligands that will bind to cell surface receptors. The uptake of such functionalised particles is termed “receptor-mediated endocytosis” (Vácha et al., 2011, Devarajan et al., 2019), the aim is successful uptake of the drug carriers by the cells, however, this may not affect the ultimate treatment efficacy (Mo and Gu, 2016). Drug particle size and penetration mechanism are significant factors and other important considerations are that the therapeutic reaches and activates the cellular organelle(s) effectively (Barua and Mitragotri, 2014). As an instance, for doxorubicin to activate in the nucleus (Wang et al., 2017b), the drug delivery vehicle should be designed to penetrate the cytosol and reach the nucleus for ultimate effectiveness (Wei et al., 2018).

A drug delivery system requires energy to enter the cancer cells and remain in the cytoplasm rather than being degraded in lysosomes (Dong et al., 2018). So far, various tools have been developed to address this issue. For example, the modification of therapeutic carriers for enhanced cellular uptake (Dissanayake et al., 2017). Surface modification using cell-penetrating peptides is among the options for providing enhanced cellular uptake. As an instance, tat-peptide (a cell-penetrating peptide) was used in various targeted delivery systems and applications. Tat-modified drug-carrying nano-particles have demonstrated enhanced uptake in cancer cells (Cao et al., 2019). Cell-penetrating peptides have been used in drug

delivery systems and have shown an increased tendency to enter the cell without dependency on any external force. For example, this mechanism was used for doxorubicin which is a nucleus-specific drug (Hodoniczky et al., 2008). Cell-penetrating peptides are also used to address the drug-resistance issues, such as Acta-arginine (R8) delivering paclitaxel with high efficiency (Borrelli et al., 2018, Singh et al., 2018). Overexpressed in cancer cell lines, folate receptor is another option for surface modification of the drugs or drug carrier to provide increased uptake in cancer cells (Cheung et al., 2016). Vitamin B-9 occurs as folate in the body, which is an essential component for rapidly proliferating cells in the body (Curtis et al., 2017). Transferrin proteins (Daniels et al., 2006) and antigens such as CD19 and CD20 (Yu et al., 2010) which have been widely used in cancer drug delivery, are also alternatives for cancer targeting and providing enhanced uptake in cancer cells.

1.3.3.2 Intracellular release and fate of the drug

Reaching delivery target and controlling drug release pace can be achieved via manipulation of carriers to become stimuli-responsive as well, depending on the target and its specifications. The enzyme-redox potential, temperature, and pH-triggered releases are the most common elements for controlling drug release (Sheng et al., 2019). However, the fate of the drug particle may not be predictable even using these triggering factors. Hence, alternative triggering factors are being investigated. For example, nano-carriers can be triggered by ultrasound as they have been used for Paclitaxel delivery, and nano-emulsions can be activated by ultrasound (Cochran et al., 2011). Light-sensitive drug carriers can also be prepared where they can release the drug

once exposed to a light source such as UV light. However, there are concerns about this process due to polymerisation and *in vivo* degradation of polymer coatings (Viger et al., 2013).

Every single cellular organelle in cancer has a specific role. An efficient drug delivery system should be able to enter the cell and deliver the drug to the related organelle. Hence knowledge of the subcellular organelles specifications is important (Biswas and Torchilin, 2014).

Most of the cancer-targeting drugs can pass through the cell membrane and reach the cytosol (Yang and Hinner, 2015). However, a very negligible amount of them can reach into the subcellular organelles, such as the nucleus, where they exert their inhibitory effect on specific gene expression pathways. Subsequently, the cancer cell's fate is controlled (Kumar et al., 2020).

The nucleus is the main and most important part of a cell and it hosts the human DNA, the genetic material of the cell. Any upregulation or downregulation of genes may lead to lethal diseases like cancer (Mazzone et al., 2019). In cancer cell lines, the nucleus is the target for the delivery of most of the chemotherapy drugs (Vasir and Labhasetwar, 2005). For drugs to get to nuclei they should be able to pass the nuclear pore complex (NPC) passively or actively (Yasuhara et al., 2004). Nano-sized drug delivery systems have been developed to be compatible with cancer drug delivery applications but not all of them successfully deliver the drug to the nucleus for subsequent cell death induction. This means that more specific modifications to nano-particles are needed (Parta et al., 2018). As an instance, Tat-peptide-modified nano-particles have been developed to deliver doxorubicin more efficiently to the nucleus (Pan et al., 2012). Furthermore, the charge reversal process was also used to induce

nuclear-delivery by drug-loaded nano-particles. This method was simply used to deliver poly(ϵ -caprolactone)-block-polyethyleneimine nano-particle directly to the nucleus (Xu et al., 2007). Mitochondria are known as the powerhouse of the cells. They regulate cell cycle and proliferation and have an important role in cell apoptosis. Apoptosis messenger agents in the cytosol induce mitochondrial membrane permeabilisation leading to initiation of the apoptosis process (Costantini et al., 2000, D'Souza et al., 2011). An alteration with an inhibitory effect on mitochondrial membrane permeabilisation functions can consequently inhibit apoptosis. This process may ultimately end up as cancer. Considering the importance of mitochondria in cancer, the possibility of inducing apoptosis to cancer cells by targeting the mitochondria can be an option. So far various delivery systems have been designed, including nano-particle delivery systems, which can be functionalised to have mitochondrial selective delivery (Murphy, 1997, Chan et al., 2017).

Lysosomes have the most important role in endocytosis. They have a highly acidic environment and their role is to degrade the unwanted particles, recycle molecules, and receptors back to the cell. Cancer drug delivery systems need to escape this cycle (Piao and Amaravadi, 2016, Dielschneider et al., 2017) to be functional. On the other hand, failure of lysosomal function will lead to the accumulation of toxic materials in the cytosol which may end up in crucial diseases. However, this aspect can be taken for granted in a cancer cell drug delivery (Piao and Amaravadi, 2016). Accordingly, a major challenge for intracellular drug delivery is to find ways to prevent the drugs from entering the endocytosis cycle and keep the therapeutics in the cytosol, such as the utilization of modified polymer nano-complexes (Almeida et al., 2017).

Another cellular organelle, the Golgi apparatus, bears great importance in the drug delivery process. Any disorder in the Golgi apparatus may lead to serious disease, due to its role in processing macromolecules. It is known as an important target for cancer drug delivery (Vasir and Labhasetwar, 2005). Delivery systems that were targeted to the Golgi apparatus have appeared to be more functional and efficient (Tarragó-Trani and Storrie, 2007). Various pathways have been used to deliver the drugs to the Endoplasmic reticulum (ER) and then to the Golgi apparatus using specific receptors (Tarragó-Trani and Storrie, 2007). There are instances such as inhibition of breast cancer cell invasion by application of signaling proteins to target the Golgi (McKinnon and Mellor, 2017) and ADP-ribosylating bacterial toxin targeting cancer cell's Golgi and ER.

As mentioned above, many attempts have been tried to eliminate cancer cells efficiently and completely. Thus, the combination of the right delivery system and the right receptors to target the cell, and the organelle are crucially important. This requires a careful design of the delivery carrier to reach the appropriate target efficiently.

1.4 Challenges in cancer drug delivery

A multitude of factors has to be considered in the process of developing a novel delivery system. Type and stage of cancer, age of the patient, and immune response are among key factors influencing drug design and delivery (Hassanzadeh et al., 2019). Furthermore, the design should be based on essential therapeutics needed for specific target cells and must overcome the basic problems which cannot be addressed with traditional chemotherapy and radiotherapy

(Li et al., 2018b). So far various systems have been developed to achieve efficient delivery of chemotherapy drugs to cancer cells, a few of them address specific delivery along with overcoming resistance in cancer cells. A delivery system needs to address both to have a highly efficient therapy procedure.

Other than cancer type, the tumour microenvironment is an important factor in cancer drug delivery system design (Khawar et al., 2015). Heterogeneous cancer cells are surrounded by immune cells, growth factors, blood vessels, signalling molecules, and extracellular matrix (ECM) (Anderson et al., 2020). For a drug delivery system to be successful, the particles must cross the extracellular matrix, fibroblasts, and other cells of the tumour microenvironment to reach the cancer cells (Roma-Rodrigues et al., 2019). Thus, it is important to understand the tumour microenvironment structure to avoid drug resistance and provide more efficient delivery (Figure 1.3).

Stromal cells, one of the tumour microenvironment components, secrete connective tissue proteins including collagen, this can lead to fibrosis. When this happens, it may prevent the delivery of therapeutic agents from reaching cancer cells (Ria and Vacca, 2020). Hence, an active tumour microenvironment will lead the cancer cells to metastasise and invade the lymph nodes initially and ultimately to other organs. Additionally, the pressure-induced by stromal cells will affect the therapy adversely (Trédan et al., 2007). This will also happen through the entrapment of the drugs and lowered drug efflux due to the same mechanism, which inhibits the effect of therapy. This process may also lead to drug resistance in cancer (Yang and Gao, 2017, Sharma et al., 2012).

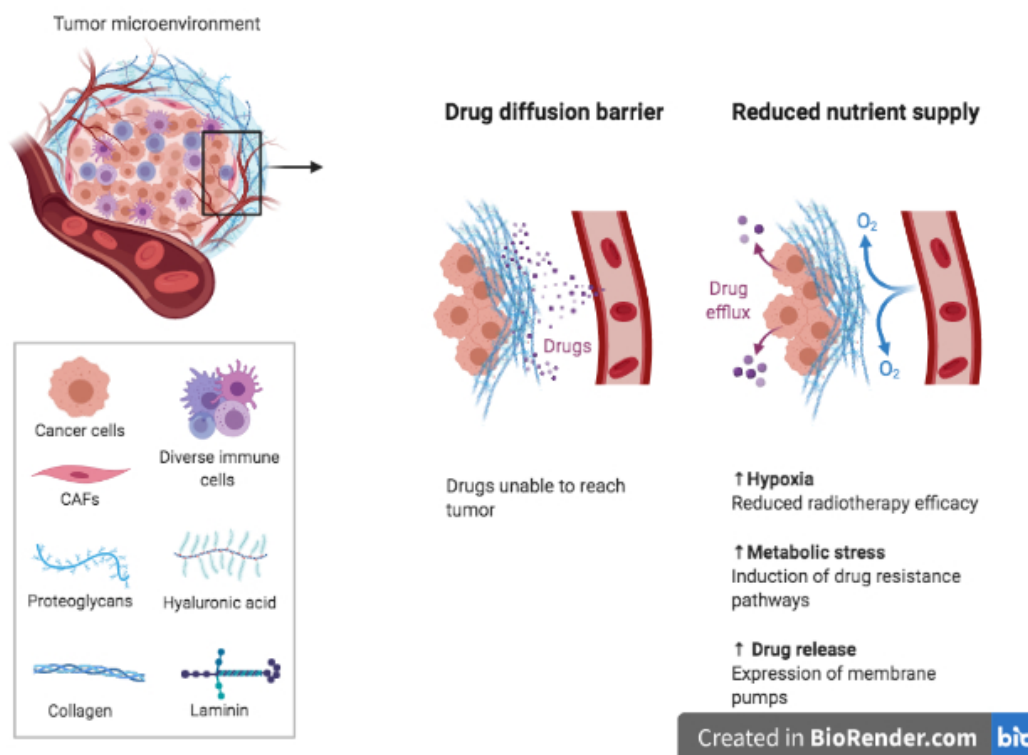


Figure 1.3 Understanding tumour microenvironment and how it limits drug delivery

Created with Biorender.com

Hence, the drug delivery system should be able to cross the tumour microenvironment and reach the cancer cells. Given the importance of tumour microenvironment, a drug delivery vehicle must be able to overcome these barriers (Stylianopoulos et al., 2018). Nano-particle-based delivery systems have demonstrated their ability to increase the yield and the quality of drug delivery and subsequently increases the therapy outcome. This will help to defeat tumour microenvironment-associated chemo-resistance (Xin et al., 2017).

1.5 Skin structure and function

Skin is the largest organ in our body and has the crucial protection role acting as a shield against pathogens and is responsible for synthesising vitamin D₃ (cholecalciferol) in presence of UVB (Mostafa and Hegazy, 2015). Three main layers are located in the skin, epidermis, dermis, and hypodermis (Agarwal and Krishnamurthy, 2019).

The epidermis is the outermost layer of the skin which consists of four layers, namely *Stratum corneum*, *Stratum lucidum*, *Stratum granulosum*, *Stratum spinosum*, and *Stratum Basale*. *Stratum Basale* is home to keratinocytes and melanocytes (Baroni et al., 2012). Melanocytes are responsible for producing granules of melanin in melanosomes (Cichorek et al., 2013). While keratinocytes divide and grow, they travel towards the surface of the skin.

The dermis is located below the epidermis and its thickness varies all over the body depending on the underlying tissue (Carroll, 2007). Fibroblasts are located in the dermis, it also contains blood vessels, lymphatics, hair follicles, sebaceous gland, and sweat gland.

The hypodermis, the most innermost layer of the skin, contains connective and adipocyte tissues and its thickness can change depending on its anatomical locations (Lee, 1953).

1.5.1 Skin cancer

Skin cancer is one of the most frequently diagnosed cancer types. The incidence is higher in people with fair and white skin types (Roider and Fisher, 2016). So far an increasing rate of skin cancer incidence and related mortality has been reported (Queen, 2017). According to the global cancer statistics, non-melanoma skin cancer incidents have fifth-place among other

cancers, which its 5-year mortality rate has increased by 0.7% until 2018 (Bray et al., 2018). Hence early detection, diagnosis, and treatment are vital in any kind of skin cancer type – aggressive or benign-(Diepgen and Mahler, 2002, Esteva et al., 2017).

Among the reasons for the increased rates of skin cancer diagnosis, environmental factors could be mentioned (Masoumi et al., 2018). Yet, various factors may be involved as an initiation point for skin cancer incidents, including inherited gene mutations or lifestyle. The genetic factor gains importance when the patient has a family history of skin cancer or a less pigmented skin type. The most important risk factor for skin cancer is increased exposure to UV light which increases the risk of skin cancer incidents which is most common in people aged 20-35 (O’Sullivan et al., 2019).

UV light is a primary reason for sunburn and skin cancers. It has three categories, UVA (320-400 nm), UVB (290-320 nm), and UVC (200-280 nm) (Harrison and Bergfeld, 2009). Only 5% of sun radiations are UV light, and about 0.3% of it reaches the earth after absorption by the ozone layer. However, even this amount can cause sunburns and skin defects (Gonzaga et al., 2009). UV light is known as an important reason for skin aging, benign skin defects, and rashes. It is known that UVB and UVA radiations are more responsible for skin cancer than UVC (Rass and Reichrath, 2008).

There are three most common skin cancer subtypes (Figure 1.4) squamous cell carcinoma, basal cell carcinoma, and malignant melanoma (Deinlein et al., 2016). Squamous cells are located on the outer layer of the skin. This type of skin cancer is also called non-melanoma skin cancer. It occurs most commonly on sun-exposed areas of the body. These cells grow slowly, and they rarely spread or metastasise. Early diagnosis and detection usually help to control squamous

cell carcinoma. Basal cell carcinoma is another non-melanoma skin cancer. About 80 percent of skin cancer cases are basal cell carcinoma (Rubin et al., 2005). This kind of skin cancer develops from UV exposure, in the lowest layer of the skin epidermis. Basal cell carcinoma is rarely lethal but it may be when left untreated (Helfand et al., 2001). On the other hand, melanoma which initiates from melanocytes is an aggressive type of skin cancer that has the potential to invade and spread in the body (Ioannides, 2017).

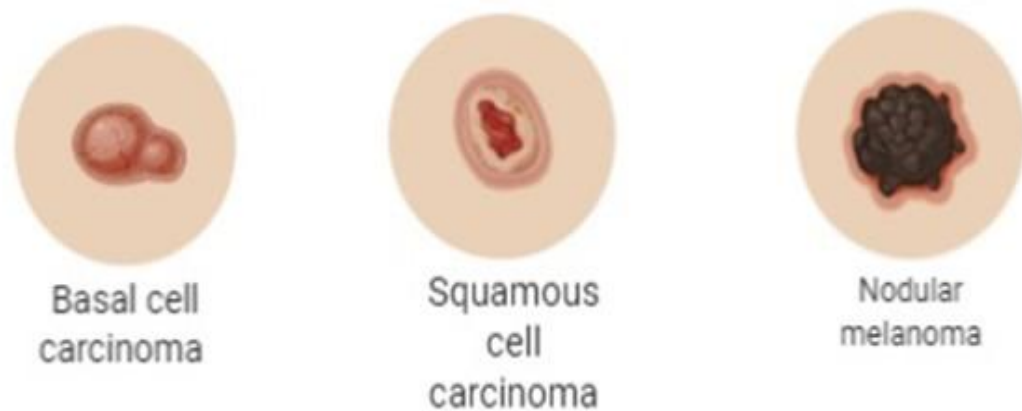


Figure 1.4 Skin cancer types

Basal cell carcinoma (left), Squamous cell carcinoma (middle), and malignant melanoma (right). Created with BioRender.com

1.5.2 Drug resistance in skin cancer

Surgery, chemotherapy, laser therapy, immunotherapy, and radiotherapy are the main treatment procedures for cancer, still, chemotherapy plays the main role in the treatment (Price and Sikora, 2020). However, about 90% of chemotherapy procedures will end up in failure due to drug resistance during the invasion and metastasis (Longley and Johnston, 2005). Hence, drug resistance is a serious problem in cancer treatments.

Various mechanisms are responsible for drug resistance. Multidrug resistance happens while cancer cells continue to survive despite the use of multiple anti-cancer drugs (Wu et al., 2014). This can happen due to the increased release of drugs outside of the cancer cells and reduced absorption of the drugs. ABC transporters including P-glycoproteins (P-gp), multidrug resistance-associated protein 1 (MRP1), and breast cancer resistance protein (BCRP/ABCG2), are a family of ATP-dependant transporters, are responsible for these phenomena (Leslie et al., 2005, Choi and Yu, 2014). Blocked pathways of apoptosis are another mechanism for drug resistance (Fernald and Kurokawa, 2013).

As mentioned in section 1.1, cellular apoptosis regulation plays a crucial role in cancer initiation and treatment. Cell death happens in three apoptosis, necrosis, and autophagy, and apoptosis happens through internal and external pathways (Chen et al., 2018). Cell death receptors such as TFN-R, FAS, linker proteins, caspases-3, -6, -7, -8 are involved in external pathways leading to apoptosis (Figure 1.1) (Elmore, 2007). As internal mitochondrial apoptosis pathway, upregulation of anti-apoptotic genes (Bcl2, AKT, etc) (Sharma et al., 2019) and downregulation

of pro-apoptotic genes (Bax, Bcl_{xl}, etc) in tumour cells will lead to the emergence of resistance (Campbell and Tait, 2018).

Alteration in drug metabolism is another factor leading to drug resistance (Lopes-Rodrigues et al., 2017). Enzyme reactions in the cells limit the drug resistance via reducing the activation of prodrug (reduced activity of some enzymes) (Ahmed et al., 2016) and increasing the drug activation (increased activity of some enzymes) (Hientz et al., 2017). Hence, alterations in enzyme activities associated with drugs and receptors may lead to drug resistance.

In some cases of skin cancer especially in melanoma, resistance happens with the alteration of chemotherapy drug targets (Kozar et al., 2019). In most of the melanoma cases bearing BRAFV600 mutation, resistance happens through the inactivation of MAPK/ERK pathways (Czarnecka et al., 2020). While the target of the chemotherapy drug, such as mutations and expression levels changes, the drugs will not be effective on that target (Wang et al., 2019b). So, the cell will continue proliferating without any damage. For instance, cancer cells having mutations of topoisomerase II will be resistant to the drug targeting topoisomerase II (Nitiss, 2009).

Imposing DNA damage (directly or indirectly) is one of the mechanisms of chemotherapy drugs (Woods and Turchi, 2013). Some mechanisms lead to the repair of the damaged DNA. These include the nucleotide excision repair system (NER) (Shuck et al., 2008) and homologous recombination repair mechanism (RRM), which can repair the DNA damage thus will trigger resistance (Li and Heyer, 2008).

Amplification of drug target genes is also a reason for the cancer cells to be drug-resistant. Some epigenetic factors such as DNA methylation and histone alterations will take a part in resistance as well (Lu et al., 2020).

There are also other factors at a cellular level, leading to resistance development. Namely tumour heterogeneity, drug efflux, tumour microenvironment, and cancer stem cells. Intra-tumoural pressure induces by stromal cells, hypoxia and paracrine signalling often lead to block the drug passage and inefficient delivery leading to drug resistance in tumour cells (Prasetyanti and Medema, 2017). Extracellular matrix (ECM) in tumour microenvironment also positively contributes to resistance emergence due to being home to cytokines and growth factors (Nallanthighal et al., 2019). Accordingly, to reach an efficient cancer therapy, the problem of drug resistance should be resolved.

1.6 Melanoma

Among the skin cancer categories, melanoma is the most aggressive and lethal type of skin cancer (Carreau and Pavlick, 2018). Similar to many other diseases, there are external factors that may be the initiation point for melanoma (Belter et al., 2017). UV radiation exposure is one of the critical environmental factors responsible for melanoma initiation and progression. Also, genetic and lifestyle factors should not be neglected, a weak immune system is likewise a factor that is important in the development of melanoma (Queen, 2017, Rangwala and Tsai, 2011).

Melanoma initiates from melanocytes (Figure 1.5), melanocytes are responsible for skin pigmentation. They produce melanin which changes skin colour when exposed to UV light. Melanocytes are located in the skin epidermis and have a protective effect on the skin from UV light. However, under triggering factors such as increased exposure to UV light, melanocytes start to proliferate irregularly and abnormally, which leads to malignant melanoma formation (Kozovska et al., 2016, Brenner and Hearing, 2008). Melanoma growth and progression have various types depending on the tumour cells spreading direction. Melanoma has 4 main subtypes Figure 1.6 superficial spreading melanoma, nodular melanoma, lentigo melanoma, and acral lentiginous melanoma (Garbe and Leiter, 2009).

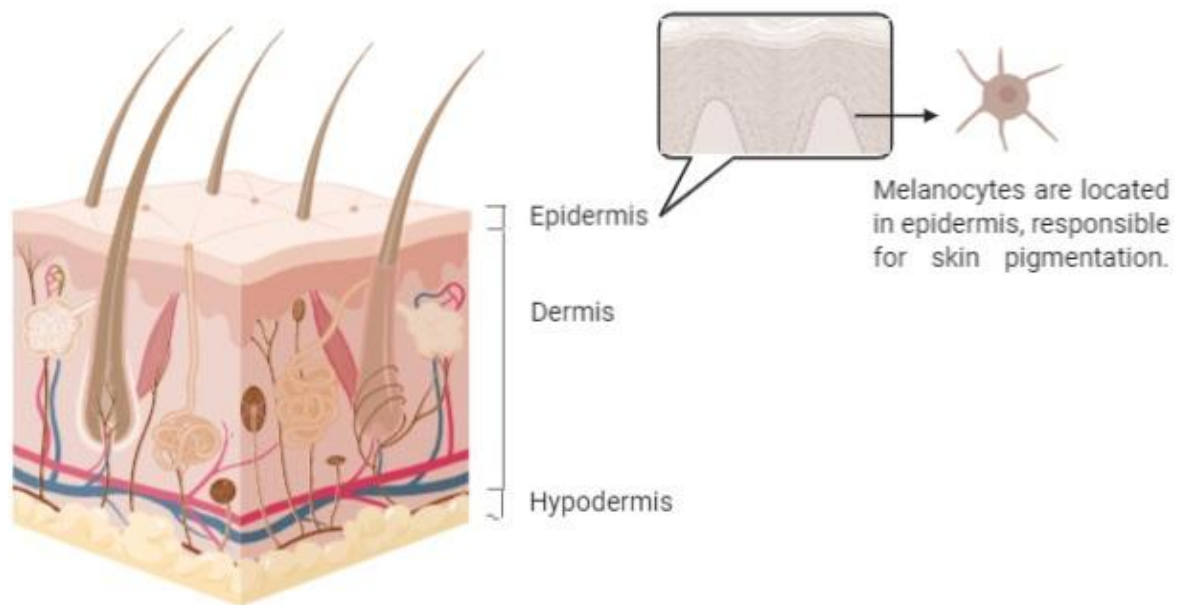


Figure 1.5 Skin layers showing the location of melanocytes in the skin

Melanoma initiates from the irregular proliferation of melanocytes, which are located in the epidermis. Created with BioRender.com.

The most common subtype of melanoma is superficial spreading melanoma (Forman et al., 2008). This type of melanoma has uneven borders and it is mostly on the surface of the skin and grows horizontally. It can also grow vertically penetrating the epidermis but the larger portion of the tumour is on the surface of the skin.

The second most common melanoma, nodular melanoma, grows deep into the skin layer (Erkurt et al., 2009). It grows fast and spreads very promptly. It is the worst type of melanoma. It is mushroom-shaped on the skin surface and usually dark-coloured but in some cases can be pinkish-red.

The third subtype of melanoma that is more common in old people is lentigo melanoma (DeWane et al., 2019). Lentigo melanoma is usually dark brown and grows in the epidermis. It can also grow within the skin layers after a long time of growth on the skin surface. The final subtype of melanoma is common in people with darker skin. Unlike other types of melanoma, Acral lentiginous melanoma is not so dependent on high UV exposure. This type of melanoma is more prone to develop and metastasise (Liu and Sheikh, 2014).

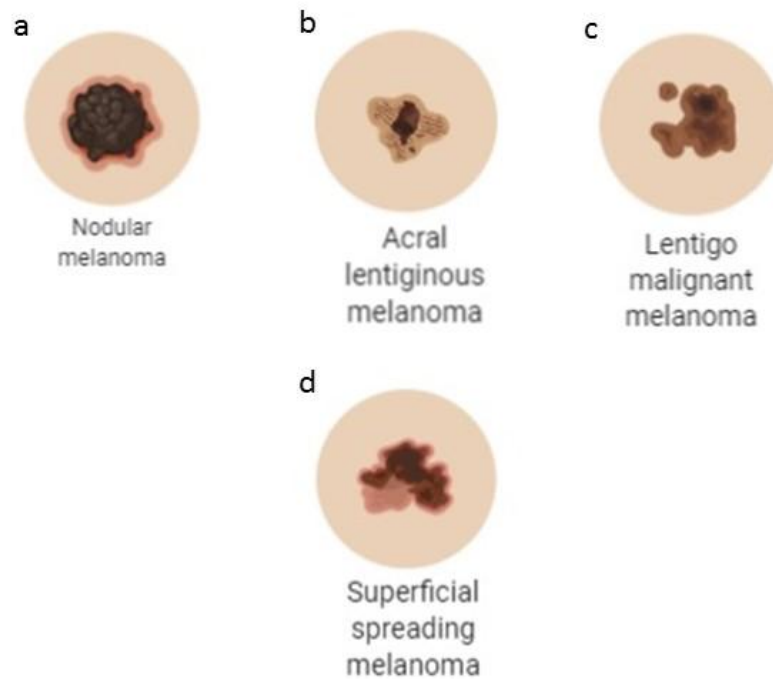


Figure 1.6 Various melanoma separated in terms of physical shape

Nodular melanoma, (b) Acral lentiginous melanoma, (c) Lentigo malignant melanoma and, (d) superficial spreading melanoma are four subtypes of melanoma. Created with BioRender.com.

Melanoma progression happens after a few evolutionary stages, to reach its malignant form. The initial sign of a melanoma is the development of a mole (Nevi), which on its own, is a benign skin lesion (Michael et al., 2017). However, most of the melanoma cases initiate from a mole (Bauman et al., 2018). With the abnormal proliferation of melanocytes, the mole will

start differentiating irregularly and turn into dysplastic nevi, which is stage two. In the third stage, dysplastic nevi start growing and turns into a tumour (Zaidi et al., 2008). It may grow vertically or horizontally, depending on the type of melanoma as mentioned above, until it reaches the epidermis but does not invade the dermis. In stage four, melanoma can invade the dermis. At this stage, melanoma has the potential to invade and differentiate faster. Following this stage, the tumour grows faster and metastatic lesions appear, which can invade other organs (Elder, 2016).

The mortality rate of melanoma patients is among the highest compared to other skin cancer types (Schadendorf et al., 2018). According to epidemiology studies in the United States, over the past 30 years, the population of patients diagnosed with melanoma has been increased (Erdei and Torres, 2010). Until 2017, 87,100 new patients were diagnosed with a progressed stage of melanoma in the United States. The mortality rate of patients was 11.15%; the majority of them being men (Matthews et al., 2017). In the UK, melanoma incidents had a sharp rise of 55% over 9 years until 2009 (Arnold et al., 2014). Since 2011, melanoma is the 5th most common cancer in the UK (Robertson and Fitzgerald, 2017). It is predicted that incidents will rise by 7% until 2035 in the UK (Mayers, 2018).

In the early stages, the melanoma lesion can be removed with surgery (Testori et al., 2009). The survival rate for early-stage patients is about 98% (Mohammadpour et al., 2019). However, the more developed it becomes, the treatment process becomes a challenge and the survival rate drops to 17% in the metastatic stage (Ugurel et al., 2017). Hence, early detection and highly efficient treatment can increase the survival time of melanoma patients (Eftekhari et al., 2019).

The treatment process for melanoma is a challenge. Due to difficulties of early diagnosis melanoma is hard to be diagnosed in the early stages and often presents a poor prognosis (Weyers, 2018). In most cases, it can be detected only when it is progressed to late stages and already invaded other organs, which makes the treatment process hard and lowers the patient's survival chance. More importantly, melanoma is highly drug-resistant which makes the treatment process a challenge (Nikolaou et al., 2018). Hence, conventional therapeutics used for cancer treatments are less effective.

Melanoma cells can develop alternative pathways to avoid apoptosis and resist therapeutics and can continue proliferating and spreading even after severe conditions of treatment. The malignancy of melanoma also depends on the stage of its progression (Winder and Virós, 2017). Melanoma may travel, initially, to the closest lymph nodes forming loco-regional deposits. These may seed out further metastases which may travel to distant organs, the wider the melanoma is disseminated, and the greater number of organs involved, so the poorer outlook and prognosis (Damsky et al., 2010).

However, the development of metastasis can be very fast, but only it forms after certain evolutionary stages, as mentioned above (Maddox, 2017). There are many factors and hypotheses which can be the initiating points of tumour metastasis, but the exact reason behind it is still a mystery. Distant metastasis to multiple organs is the most problematic stage of melanoma to treat and more efficient therapy procedures are desirable for advanced melanoma stages (Hua et al., 2016).

Depending on the stage of disease progression, common treatment procedures for a person diagnosed with melanoma are surgery, immunotherapy, adjuvant therapy, targeted therapy,

radiation therapy, and chemotherapy (Tran et al., 2009). Specifying the best treatment depends on how developed the melanoma is. Usually, four stages of its progression need to be considered. Surgery applies to melanoma in stages zero and one, in which the cancer cells are very superficial or have not grown deeply. Wide excision surgery is applied for the patients diagnosed with stage II melanoma in which lymph nodes are also involved, adjuvant therapy can also be advised (Koster et al., 2017). Adjuvant and radiation therapy are recommended for stage III melanoma patients, after surgery of the affected area, followed by chemo and targeted therapy (Blank et al., 2018). For stage IV of melanoma, the treatment will be the combination of radiotherapy, chemotherapy, and targeted therapy depending on how wide metastasis has been spread (Brossart et al., 1993, Garbe et al., 2010).

So far there are only a few therapy options that are approved by the FDA to treat metastatic melanoma, nevertheless, the overall chance of survival is still the same despite the high toxicity of the chemotherapeutics (Jacquelot et al., 2017). Later on, many of the therapeutics containing highly toxic components were removed from formulations in the markets (Bonifacio et al., 2014). As mentioned, there remain many challenges to have malignant melanoma treated without possible side effects, with enhanced efficiency and decreased multidrug resistance using conventional therapy systems. However, novel targeted therapy approaches can have promising effects on reducing the progression of melanoma.

The most important obstacle towards melanoma treatment is chemo-resistance (Kalal et al., 2017). There are various reasons behind the resistance mechanism in melanoma (Erdmann et al., 2019). Melanoma cells can develop various signalling pathways to regulate cell proliferation and differentiation. Downregulation or upregulation of these pathways can lead to

the development of the tumour or on the other hand, apoptosis induction to the tumour cells. The fundamental reason for resistance can be apoptosis dysregulation (Helmbach et al., 2001). More specifically, resistance in melanoma happens via altered DNA repair, altered enzymatic activation, dysregulation of apoptosis pathways, and drug transport efflux (Kalal et al., 2017). Recently, investigators have been focused on alternative resistance factors influencing melanoma treatment such as the physical environment of the tumours. There are possibilities that tumour microenvironment can be an escalating factor for resistance (Parkin et al., 2019). High intra-tumoural pressure induced by stromal cells, poor perfusion of drugs in the tumour microenvironment, drug efflux, and intracellular entrapment of therapeutics are the most important related factors (Somasundaram et al., 2016).

1.6.1 Anti-cancer treatments for melanoma alleviation

Dacarbazine (DTIC) was the first drug approved by the FDA for melanoma treatment (Velho, 2012). It was used as the main chemotherapy agent for treating melanoma. However, the 5-year mortality rate was still 96-98%. Hence, despite its high toxicity which is thought to be in result of photo-degradation (Koreich et al., 1981), the utilisation of dacarbazine continued to be used in combined chemotherapies (Wu et al., 2015). The most important side effects of dacarbazine are decreasing white blood cells and severe hepatotoxicity (Ma et al., 2013). Among chemotherapy drugs, doxorubicin (classified as anthracycline antibiotic) has been routinely used for multiple types of cancer treatments including melanoma (Licarete et al., 2020). Although doxorubicin is vastly used in melanoma treatment (Mukherjee et al., 2020), it is

among the drugs to which melanoma develops resistance (Fukunaga kalabis et al., 2012, Licarete et al., 2020). Furthermore, doxorubicin is severely cardiotoxic due to its reaction with free iron in the body, which can be prevented by combined therapy using iron chelators such as dexrazoxane (Thorn et al., 2012).

Improvements in melanoma treatment continued by using Temozolomide (TMZ), a prodrug derived from dacarbazine (Shah et al., 2010a). Although the development of Temozolomide was an important step, the survival rate of melanoma patients did not improve. According to the investigations, no significant difference in side effects of Temozolomide was detected compared to DTIC (Teimouri et al., 2013), hence the use of DTIC was recommended.

Electrochemotherapy (ECT) was later developed for treating melanoma. This system was designed for use of two cytotoxic drugs bleomycin and cisplatin (Fiorentzis et al., 2018). The base of treatment was facilitating the delivery of the drugs to cells by high-intensity electric pulses. This method was effective for treating subcutaneous melanoma nodules, however, it was highly toxic to the lymphatic system. Another treatment procedure for melanoma was introduced as photodynamic therapy (PDT), a light-based minimally invasive therapy for stage III/IV cutaneous melanoma (Naidoo et al., 2018). Although this method was non-toxic, it helped reactive oxygen species (ROS) to release. Hence the effect of PDT on melanoma was limited. However, it was suggested to be used in combination with chemotherapy drugs.

Cancer and the immune system are closely related, due to the presence of immune cells in tumour sites at the chronic inflammation site. Hence Immunotherapy was suggested for cancer treatment in the 19th century (Drake et al., 2014, Domingues et al., 2018). This procedure was a promising method for advanced stages of melanoma, yet again, it was more effective whilst

used in combination with chemotherapy. Interferons are important cytokines in immunotherapy. They have important immunomodulatory, antiangiogenic, antitumor, and antiproliferative. FDA approved the use of Interferon α -2b in 1995 for melanoma stage III/IIB. Approved in 2011 by FDA, Peg-interferon (Peg-INF α -2b) was used in stage III, melanoma treatment as a supplementary therapy (Medrano et al., 2017). Peg-INF was developed by combining Interferon α -2b with polyethylene glycol to prolong the stability of the Interferon α -2b (Shiffman, 2001). Hence its therapeutic effect was improved. IL-2 was another cytokine known for its antitumor effect and approved by the FDA in 1998 for metastatic melanoma treatment (Jiang et al., 2016). Another treatment approved by the FDA in 1999 for antitumor immune response suppression, were Treg inhibitors (Han et al., 2019). FDA also approved the use of Cytotoxic T lymphocyte-associated antigen 4 (CTLA-4) blockade in 2011, PD-I ligand blockade in 2014, oncolytic virus therapy in 2015, Toll-like receptor agonists, and adoptive T-cell therapy, as immune therapy approaches for cancer (Wang et al., 2011). However, all these approaches were more efficient while used in combination with other therapies such as chemotherapy.

Targeted therapy procedures significantly contributed to melanoma therapy. Approved in 2011, BRAF inhibitors were used in the treatment of melanomas harbouring BRAF mutations (Shah et al., 2019). Vemurafenib and Dabrafenib two BRAF inhibitor drugs used for metastatic melanoma patients were reported to show tumour regression in 90% of patients (Croce et al., 2019). Furthermore, Trametinib (MEK inhibitor) (Lugowska et al., 2015), Imatinib (CKIT inhibitor) (McLean et al., 2005), Bevacizumab (VEGF inhibitor) (Ferrara et al., 2005), rapamycin (PI3K-AKT-mTOR inhibitor) (Feldman and Shokat, 2010), ribociclib (CDK

inhibitor) (Spring et al., 2019), and lapatinib (ErbB4 inhibitor) (Qiu et al., 2008), demonstrated increased efficacy in melanoma targeted therapy.

1.6.2 Melanoma drug delivery

As mentioned in previous sections, the most important obstacle towards reaching efficient melanoma treatment is chemo-resistance (Xue and Liang, 2012). Furthermore, the drug release efflux delivered to the cell and its release from the drug carrier have to be controlled to prevent drug-efflux dependant resistance in melanoma. Due to the high potential of chemo-resistance in melanoma, drug delivery system design is even more challenging (Helmbach et al., 2001). Among the delivery systems, polymer-drug conjugates, and encapsulation of chemotherapeutics in nano-particles have shown a worthy performance regarding melanoma treatment (Li et al., 2015).

The table below (Table 1.2), indicates the most common delivery vehicles tested for melanoma treatment.

Table 1.2 Drug delivery systems used for melanoma

Delivery system	Drug	Material	Synthesis Method	Cell line	Experiment	Reference
Hydrogel Matrix (cell culture platform)	PLX 4032 (Vemurafenib)	PEG	Photopolymerization	WM35-A375 melanoma	<i>In vivo</i>	(Tokuda et al., 2014)
Magnetic based core-shell particles	Curcumin-doxorubicin	Poly (N-isopropyl acrylamide-allylamine) and a core of poly (lactic-co-glycolic acid) (PLGA) embedded with magnetite nanoparticles	Thermo-responsive	B16F10 melanoma	<i>In vivo</i>	(Wadajkar et al., 2012)
<i>In-situ</i> hydrogel	Curcumin-hydroxypropyl- β -cyclodextrin	Poloxamers	Thermos-responsive	B16-F10	<i>In vitro</i>	(Sun et al., 2014)
Nano-particles	Docetaxel-everolimus-LY294002	PEG-PCL	-	Metastatic melanoma	<i>In vivo</i>	(Doddapaneni et al., 2015)
Micellar-Nano particles	Doxorubicin	PEG-based	-	Melanoma	<i>In vivo</i>	(Li et al., 2019b)
Nano gel	5-Fluorouracil	Chitin	pH-responsive	A375 melanoma	<i>In vitro; Ex vivo</i>	(Sabitha et al., 2013)
Polymersomes	Doxorubicin	PMPC25-PDPA70	pH-sensitive	-	<i>In vitro</i>	(Pegoraro et al., 2013)

Bioactive polymer micelle	Doxorubicin	Poly(l-glutamic acid)n-b-poly(d, l-lactic acid)	pH responsive	A 375 melanoma	<i>In vitro; In vivo</i>	(Wang et al., 2014)
Hybrid Nano gel	5-Fluorouracil	PEG- Ni-Ag Nano gel	pH-responsive	B16-F10 melanoma	<i>In vitro</i>	(Wu et al., 2011)
Copolymer micelle	azobenzene and β -galactose	-	Light responsive	A375	<i>In vitro</i>	(Alfurhood, 2016)
Nano gel	5-Fluorouracil	Chitosan-PEG	pH responsive	B16F10	<i>In vitro</i>	(Maya et al., 2013)
Emulsion	SU5416	PEG based	-	C26-B16	-	(Ogawara et al., 2014)
Polymer-drug conjugate	Paclitaxel	PEG based	pH-redox sensitive	B16F1	<i>In vivo</i>	(Lv et al., 2014)
Liposome	Paclitaxel	PEG	Redox responsive	-	-	(Fu et al., 2015)
Liposome	N-Butyldeoxynojirimycin	cholesterylhemisuccinate (CHEMS), cholesterol (Chol), dioleoylphosphatidylethanolamine (DOPE), phosphatidylcholine (PC), phosphatidylethanolamine (PE), and phosphatidylserine (PS)	pH sensitive	B16-F1 mouse melanoma cells	<i>In vitro</i>	(Costin et al., 2002)
Hydrogel	Ni-Oxzaprozin	poly(2-hydroxypropyl acrylate/itaconic acid) (P(HPA/IA))	pH sensitive	Melanoma cell lines (FemX)	<i>In vitro</i>	(Babić et al., 2016)
Layer-by-layer Nano-particles	STAT3 (protein) siRNA	Chitosan coated gold	-	B16F10 murine	<i>In vitro</i>	(Labala, 2016)

				melanoma cells		
Solution	-	Chitosan	-	A375-SKMEL28-RPMI7951	<i>In vitro</i>	(Gibot et al., 2015)
Man-CTS-TCL NPs vaccine	-	Chitosan	-	B16	<i>In vivo- In vitro</i>	(Shi et al., 2017)
Nano-particles	Green tea polyphenol epigallocatechin-3-gallate (EGCG)	Chitosan	-	Human melanoma Mel 928 cells	<i>In vivo- In vitro</i>	(Siddiqui et al., 2014)
Gel	Doxorubicin	non-ionic hydroxyethylcellulose-cationic chitosan	-	B16F10	<i>In vitro-In vivo</i>	(Taveira et al., 2009)
Nano-particles	-	gadolinium-loaded chitosan	-	B16F10	<i>In vivo- In vitro</i>	(Naves and Almeida, 2015)
polypeptide-based micelle	Docetaxel- cisplatin	PLG-g-Ve/PEG		B16F1	<i>In vivo</i>	(Song et al., 2014)
Nano-particles	Paclitaxel	CpG-B 1826 thiophosphate (CpG)	-	DCs, CD11c+ B16-F10	<i>In vivo</i>	(Thomas et al., 2014)
Nano-gel	Decitabine	-	-	Melanoma cells, leukemia cells	-	(Vijayaraghavalu and Labhasetwar, 2013)
Polymer-drug conjugate	Docetaxel	Carboxymethyl chitosan	-	B16-HepG2	<i>In vitro- In vivo</i>	(Liu et al., 2013)
Liposome	Curcumin	Chitosan	-	B16-F10	<i>In vitro</i>	(Karewicz et al., 2013)

Nano-emulsion gel	Leflunomide	-	-	A375 and SK-MEL-2	<i>In vitro –In vivo</i>	(Pund et al., 2015)
Nano-ethosomes	Docetaxel	Epigallocatechin-3-O-gallate (EGCG)	-	A375	<i>In vivo</i>	(Liao et al., 2016)
cationic self-micro emulsifying drug delivery system (ECS)	-	-	-	B16F10	<i>In vivo-In vitro</i>	(Liao et al., 2016)
Intratumoral injection – nanoparticles	Doxorubicin	Gold nanoparticles	-	Murine B16, human SK-MEL-28	<i>In vitro-In vivo</i>	(Bagheri et al., 2018)
Nanoparticle	Docetaxel – cellax	Carboxymethyl cellulose -PEG	-	B16F10	<i>In vivo</i>	(Hoang et al., 2015)
Liposome	Doxorubicin	PEG based	-	B16F0- C26	-	(Teymouri et al., 2016)
Copolymeric Nanoparticles	-	methyl methacrylate (MMA) and N-vinylcaprolactam (VCL)	Thermos-responsive	B16F10	-	(Shah et al., 2010b)
Orally administrated Nanoparticles	Curcumin	Chitosan-PCL	-	B16F10	<i>In vivo-In vitro</i>	(Loch-Neckel et al., 2015)
Theranostic nanoparticles	PLX4032	BPLP-PLA	-	melanoma	<i>In vitro</i>	(Xie et al., 2017)
Injectable hydrogel	Doxorubicin	Sericin-Dextran	Chemical cross-linking	Melanoma	<i>In vitro</i>	(Liu et al., 2016)

Light responsive micelles	Nile red	Azobenzene and β -galactose polymer units	Self-assembly	A375	<i>In vitro</i>	(Pearson et al., 2015)
Edge activated liposome	siRNA	-	-	melanoma	<i>In vitro</i>	(Dorrani et al., 2016)
Cell-penetrating peptides	Paclitaxel	-	-	B10F16	<i>In vivo</i>	(Jiang et al., 2018)
Core-shell nano-fiber	5FU	Chitosan- PCL	-	B16F10	<i>In vitro</i>	(Zhu et al., 2019)
nanofiber mesh	-	PCL	Electrospinning	Melanoma	<i>In vitro</i>	(Lin et al., 2018)
Microneedle	Debrafenib – trametinib	-	-	A375	<i>In vivo</i>	(Tham et al., 2018)
Solid in oil peptide nano-carrier	Vaccine	-	-	B16F10	<i>In vivo</i>	(Wakabayashi et al., 2018)
Liposome	Indocyanine green	Chitosan coated	-	B16F10	<i>In vitro</i>	(Lee et al., 2019)
Dendritic nano-particles	Doxorubicin	Dendritic Fe ₃ O ₄	-	Melanoma	<i>In vivo</i>	(Nigam and Bahadur, 2018)
Redox responsive micelle	Paclitaxel	Hyaluronic acid – Tocopherol succinate	Self-assembly	B16F10	<i>In vivo</i>	(Xia et al., 2018)
Nano-particles	Curcumin	Bovine serum albumin	-	Murine melanoma	<i>In vivo</i>	(Camargo et al., 2018)

Prodrug micelle	Doxorubicin	Polysaccharide	-	A375	<i>In vivo</i>	(Li et al., 2018a)
Nano clay	Doxorubicin	Bentonite	Self-assembly	Melanoma	<i>in vitro</i>	(Hosseini et al., 2018)
Micelle	Doxorubicin-pheophorbide	Pluronic F127	-	B16F10	<i>In vivo</i>	(Zhang et al., 2018a)
Nano-particles	siRNA	Gold	-	B16-BL6	<i>In vitro</i>	(Zhang et al., 2018b)
Nano-gel	5FU	Chitosan	Ionic gelation	Melanoma-HaCaT	<i>In vitro-Ex vivo</i>	(Sahu et al., 2019a)
Nano-particle	Carboplatin	PCL	-	Melanoma	<i>In vivo</i>	(Bragta et al., 2018)
Polymeric nano-particle	-	Chitosan	-	B16F10	<i>In vitro</i>	(Ferraz et al., 2018)

The summary information provided in the table above indicates the variability of drug delivery systems used to combat melanoma *in vitro* and *in vivo*. Polymeric drug carriers seem to be more utilized as drug carriers for melanoma. Furthermore, among them, nano-sized delivery systems have acted more efficiently against melanoma (Table 1.2).

Chitosan is among the most utilized biopolymers for melanoma treatment, as indicated in Table 1.2. This can be due to chitosan's improved ability to permeate through skin cells (He et al., 2009). As mentioned, using the EPR effect, nano-particles can accumulate in the tumour via the leaky tumour vasculatures which have larger pore sizes (Maeda et al., 2009). Molecules having a range of nano-sized particles up to a few hundred nano-meters can penetrate tumour vasculatures easily (Zununi Vahed et al., 2019). On the other hand, these nano-sized particles cannot penetrate healthy tissues since the vasculature conditions are normal and this range of nano-sized particles is unable to extravasate. Hence the accumulation of nano-particles will be in the tumour environment. Consequently, they can provide targeted delivery to melanoma (Blanco et al., 2015).

In another perspective, the nano-particle shell protects the low molecular weight drugs from enzymatic digestion in the cell cytosol. The small molecules such as drugs can be lysed in the cell cytosol before affecting the cancer cell. Enzymatic digestion is one of the reasons that chemotherapy cannot be effective enough in the treatment of melanoma (Pfannenstiel et al., 2019).

Delivery of therapeutics using nano-particles is also important in terms of delivery dose and delivery flux of the drugs. A nano-sized delivery shell, rather than protecting the drugs encapsulated, can be designed to provide controlled delivery (Girdhar et al., 2018). This will

prevent increased drug accumulation in the cell and consequent resistance development (Yoncheva et al., 2019).

Among nano-sized delivery systems, polymeric nano-particles are the most common ones (Khalid and El-Sawy, 2017). A range of synthetic and natural, biodegradable, and biocompatible polymers have been used in the development of various drug delivery systems against melanoma treatment (Naves et al., 2017).

So far, Polymeric nanoparticles have been investigated as appropriate options to be used as melanoma delivery systems and to decrease chemo-resistance by adjusting drug release (Liu et al., 2018). Using careful design and optimisations, polymeric nano-particles can be designed to reach the appropriate initial burst followed by controlled release of the drugs. They can also be modified to increase or decrease the delivery rate. Surface modifications of the nano-particles can further increase the quality of delivery (Pathak et al., 2019).

1.6.3 Polysaccharides in melanoma drug delivery

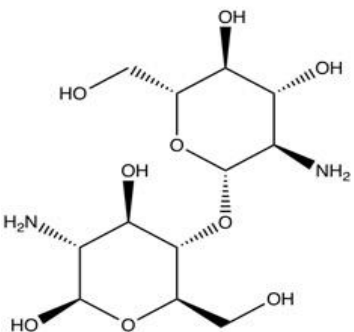
Due to their unique characteristics and wide availability, polysaccharides have gained importance specially in the cancer drug delivery field (Coviello et al., 2007, Debele et al., 2016). Furthermore, their low cost has made them a good option for medical and pharmaceutical applications (Debele et al., 2016). Additionally, polysaccharides have an increased tendency for cell membrane permeation and adherence. These features have made them a suitable choice for targeted cancer drug delivery (Dheer et al., 2017).

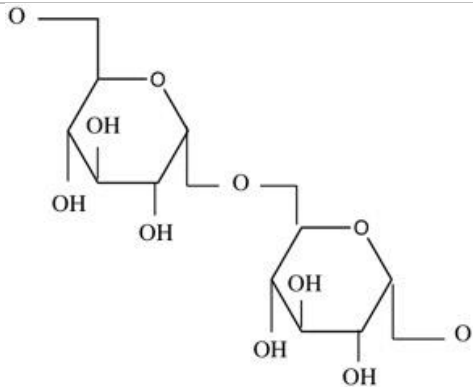
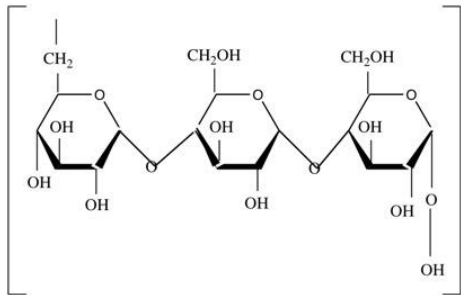
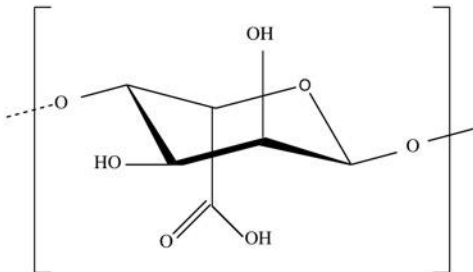
Polysaccharides are long-chain monosaccharides linked with glycosidic bonds. Based on their source, they can be found with various structures. Polysaccharides are also well-known for their

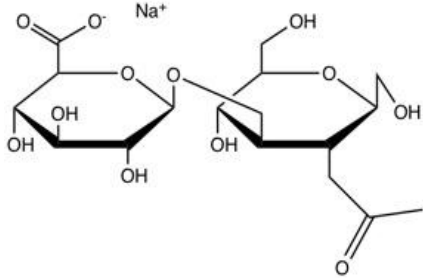
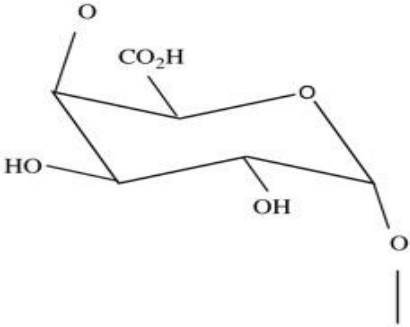
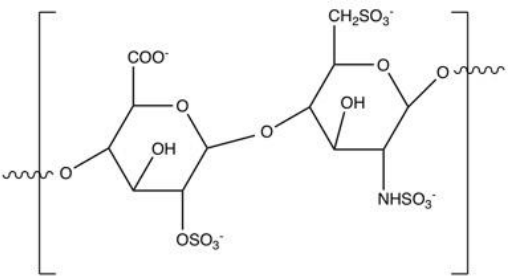
non-toxicity, low immunogenicity, bioactivity, muco-adhesion, are environmentally safe, and have the potential for targeting specific tissues (Gopinath et al., 2018). Various polymers include alginate, pectin, guar gum, dextran, xanthan gum, chitosan, chondroitin, hyaluronic acid, heparin, cyclodextrin, pullulan, and amylose are included in the polysaccharides family (abedini et al. 2018). Each of these polysaccharide-based polymers has a unique characteristic that can be used in a wide range of applications. Polysaccharide molecules have several reactive groups (depending on the polymer) which are accessible to various modifications. Based on their functional groups, they can be hydrophobic, hydrophilic, or neutral. Polymers from this category usually have a more extracellular matrix (ECM)-like backbone which is considered as a positive point for a delivery system (Liu et al., 2008). Hence, they are not considered as foreign material in the body consequently they will not be lysed readily and they are not immunogenic (Diekjürgen and Grainger, 2017). The most advantageous characteristics for polysaccharides nano-particles are their selective attachment to the target cancer site and successful uptake by the cells (Wang et al., 2006).

The following table (Table 1.3) shows a variety of polysaccharides and their structure, source, and characteristics.

Table 1.3 Characteristics of selected polysaccharides

Polymer	Structure	Source	Characteristics	Reference
Chitosan	 <p>The diagram shows the chemical structure of a chitosan repeating unit, which is a dimer of two N-acetylglucosamine (GlcNAc) units linked by a β-1,4-glycosidic bond. Each GlcNAc unit is a six-membered pyranose ring with an oxygen atom at the bottom. The top GlcNAc unit has a hydroxyl group (OH) at C2 (wedge), a hydroxymethyl group (CH₂OH) at C4 (wedge), and an amino group (NH₂) at C6 (wedge). The bottom GlcNAc unit has a hydroxyl group (OH) at C2 (wedge), a hydroxymethyl group (CH₂OH) at C4 (wedge), and an amino group (NH₂) at C6 (wedge). The two units are connected by a β-1,4-glycosidic bond between the C1 of the top unit and the C4 of the bottom unit.</p>	Chitin	<ul style="list-style-type: none"> -Non-toxic -Biodegradable -Biocompatible -Antimicrobial -Anti-inflammation -Analgesic -Mucoadhesive -Angiogenesis stimulator -Macrophage activator -Haemostatic -Easy modifications 	(Jaworska et al., 2003, Chung et al., 2004, Bano et al., 2017)
Dextran		Microorganism Leuconostoc mesenteroides	<ul style="list-style-type: none"> -Antithrombotic -Water-soluble -Biocompatible -Biodegradable -Stable for more than 5 years 	(Weissleder et al., 2018)

				
Pullulan		-Fungus (Aureobasidium pullulans)	-Non-toxic -Non-immunogenic -Water-soluble -Easy modification -adhesive -Oxygen impermeable -increase permeability	(Gibbs and Seviour, 2017)
Alginate		-Algal (Brown sea weed, <i>Azotobacter</i> and <i>P seudomonas</i>	-Non toxic -Anionic activity - Non toxic -Easy modification	(Wongkanya et al., 2017)

Hyaluronic acid	 <p>The diagram shows a repeating unit of hyaluronic acid. It consists of two pyranose rings linked by a 1-3 glycosidic bond. The left ring is a D-glucopyranose unit with a carboxylate group (COO⁻) at C5 and a sodium ion (Na⁺) nearby. The right ring is a 3-O-acetyl-D-glucopyranose unit with an acetyl group (CH₃CO-) at C2. The rings are connected at C1 of the left unit to C3 of the right unit.</p>	-Human (synovial fluid)	<ul style="list-style-type: none"> -Non-toxic -inducing cell proliferation and migration -wound healing and tissue repair 	(Wang et al., 2016)
Pectin	 <p>The diagram shows a repeating unit of pectin. It is a D-galacturonic acid unit in a chair conformation. It has a carboxylic acid group (CO₂H) at C5, a hydroxyl group (OH) at C2, and a hydroxyl group (OH) at C3. The C1 position is linked to the next unit in the chain via an oxygen atom.</p>	Plants primary cell walls	<ul style="list-style-type: none"> -Non-toxic -Fast hydration -Lowering cholesterol -Wound healing -Gel formation 	(Mohnen, 2008)
Heparin	 <p>The diagram shows a repeating unit of heparin. It consists of two pyranose rings linked by a 1-3 glycosidic bond, enclosed in brackets with wavy lines indicating the polymer chain. The left ring is a D-glucopyranose unit with a carboxylate group (COO⁻) at C5, a hydroxyl group (OH) at C2, and a sulfonate group (OSO₃⁻) at C3. The right ring is a 2-sulfamoyl-D-glucopyranose unit with a sulfonate group (CH₂SO₃⁻) at C6, a hydroxyl group (OH) at C2, and a sulfamoyl group (NHSO₃⁻) at C3. The rings are connected at C1 of the left unit to C3 of the right unit.</p>	<ul style="list-style-type: none"> -Human (mucosal tissue) -Synthetically made (2003-2008) 	<ul style="list-style-type: none"> -Anticoagulant -High water-soluble -Negatively charged 	(Lai et al., 2018)

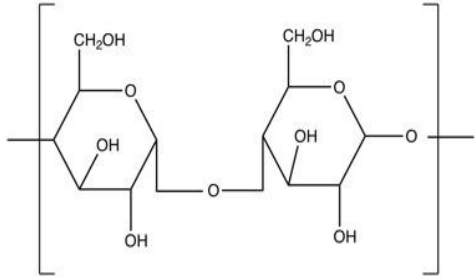
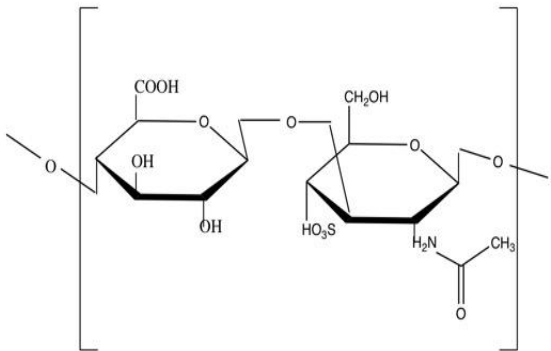
Amylose	 <p>The diagram shows the repeating unit of amylose, a linear polysaccharide of D-glucose. It consists of two glucose rings in their chair conformation, linked by an α-1,4-glycosidic bond. The entire unit is enclosed in large square brackets with horizontal bonds extending from the left and right sides, indicating its role as a repeating unit in a polymer chain.</p>	-Starch	-Hydrophobic -Unstable in the form of solution -Easy precipitation	(Koski and Bose, 2019)
Chondroitin	 <p>The diagram shows the repeating unit of chondroitin, a glycosaminoglycan. It consists of two sugar rings in their chair conformation, linked by a β-1,3-glycosidic bond. The left ring is a glucuronic acid derivative with a carboxylic acid group (COOH) at the C5 position. The right ring is a glucosamine derivative with a sulfonic acid group (HO₃S) at the C2 position and an N-acetyl group (H₂N-C(=O)-CH₃) at the C2 position. The unit is enclosed in large square brackets with horizontal bonds extending from the left and right sides.</p>	-Animal bone tissue	-Anti-inflammatory -Anti angiogenic -Tissue reconstruction ability	(Pal and Saha, 2019)

Table 1.3 shows the potential capability of polysaccharides for drug delivery and their unique characteristics. A few polysaccharides show enhanced activity to permeate skin cells making them suitable for skin cancer targeted delivery alternatives (Franze, 2015). Depending on their characteristics and the ultimate aim of application, each can perform different behaviours.

Chitosan, $\alpha(1-4)$ 2-amino 2-deoxy β -D glucan, one of the most abundantly available biopolymers is derived from chitin. Chitosan is a de-acetylated form of chitin and is a well-known polysaccharide that has been widely investigated for various applications (Mohammed et al., 2017). Positively charged chitosan can make a strong bonding through electrostatic interactions with negatively charged molecules, surfaces, and particles. Chitosan is soluble in acidic environments and hydrophilic in a neutral environment (Ali and Ahmed, 2018, Ghaz-Jahanian et al., 2015). This unique characteristic makes it a promising choice for cancer drug delivery, mostly due to the acidic environment of the tumours. A few of the chitosan properties depend on its deacetylation degree (DD), and others on molecular weight (Kumar et al., 2020). The lower the deacetylation degree, the more soluble the chitosan in increased pH and vice versa. Also, lower concentrations of chitosan usually have lower encapsulation efficiency (Ding et al., 2019). However, due to its functional groups, it is capable of various modifications to enhance its biological and biochemical properties. (Chellappan et al., 2019). Chitosan emerged in many investigations for various applications including skin tissue engineering and drug delivery due to its unique permeation ability (Liang et al., 2019).

Alginate is another linear well-known polyanionic polysaccharide, and it is initially sourced from algae. Its chemical structure is 1,4-linked α -L-guluronic acid and β -D-mannuronic acid. Negatively charged alginate can interact with positively charged particles. Modified sodium

alginate can act as a mildly pH-sensitive polymer and has been used in drug delivery systems (Bhunchu and Rojsitthisak, 2014, De Souza et al., 2010).

Pullulan is a highly water-soluble neutral polysaccharide derived from the fungi *Aureobasidium pullulans* and it is composed of α -1,6-linked maltotriose units (Tabasum et al., 2018). It is known to have promising characteristics and has been used in various medical, biological, and drug delivery applications. Pullulan is capable of adhering to cell surfaces and facilitates intracellular uptake and provides a time-based release (Ganeshkumar et al., 2014) of encapsulated molecules.

These three polymers separately have been used for skin and skin cancer delivery systems. However, the potential for improved drug delivery quality using mixing polysaccharides has not been greatly investigated.

1.6.4 Nano-emulsion delivery system for melanoma treatment

Nano-emulsion is a homogenized form of mixed immiscible reagents (oil/water) stabilized using an emulsifier (Jaiswal et al., 2015). Recently nano-emulsions have been increasingly used in the pharmaceutical fields (Rai et al., 2018a). This is potentially due to advantages such as increased drug loading efficiency, stability, decreased size of particles, and increased bioavailability. The use of nano-emulsions has also increased topical delivery systems such as cream and spray forms (Pathak et al., 2018). Simple preparation and functionalization abilities have also made nano-emulsions suitable for cancer drug delivery and specifically melanoma (Severino et al., 2013, Bagde et al., 2018). The table below lists some nano-emulsions used for skin cancer drug delivery (Table 1.4).

Table 1.4 Nano-emulsions used in cancer research

Material	Polymeric details	Characteristics	Nano-size preparation methods	Hydrophilicity	<i>In vivo</i> degradation	Reference
PLA	Aliphatic polyester-	thermoplastic, high-strength, high-modulus	solvent evaporation, solvent displacement, salting out, solvent diffusion	Hydrophobic	Scission to lactic acid monomers, as an intermediate for carbohydrate metabolism (no catalyst or enzyme needed)- degradation rate is dependent on size and hydrolysis temperature.	(Lassalle and Ferreira, 2007)
PLGA	PLA- PGA copolymer	Crystalline structure	Emulsification, evaporation, and precipitation	Less Hydrophilic	Hydrolysis of an ester linkage	(Fornaguera et al., 2015)
Nano-cellulose	homopolysaccharide composed of β - 1,4- anhydro-D- glucopyranose units	Both Crystalline and amorphous, high specific surface area, barrier properties, surface chemical reactivity, biocompatible	Emulsion polymerization	NA	Through cellulase enzyme - Biodegradable – slowly degradable in animal body (<i>in vivo</i>)	(Sarker, 2005)

Chitosan	glucosamine and N-acetylglucosamine	NA	ionotropic gelation, microemulsion, emulsification solvent diffusion, polyelectrolyte complex, self-assembly	Hydrophobic	<i>In vitro</i> : β -N-acetylhexosaminidase, chitosanase, chitinase and chitin deacetylase. <i>In vivo</i> : lysozyme, acid, gastrointestinal enzymes and colon bacteria	(Badawi et al., 2008)
Silk	Polysaccharide	Crystalline structure.	NA	Predominantly hydrophobic	<i>In vitro</i> degradation: Protease XIV Slowly biodegradable	(Khandavilli and Panchagnula, 2007)
PCL	Poly ester	Low melting point	nanoprecipitation, solvent displacement, solvent evaporation	Hydrophobic	Hydrolysis of ester linkage	(Wan et al., 2015)
PEG	Polyether	Non ionic	NA	Hydrophilic	<i>In vitro</i> degradation using proteinase K	(Constantinides et al., 2008)
Gelatine	Polypeptide	Physical and chemical crosslinking	Desolvation and emulsification- Through physical and chemical cross-linking	Hydrophilic	<i>In vivo</i> degradation in physiological conditions	(Date et al., 2010)
Pectin	Polysaccharide	Polyanionic nature	Cross linkable	Hydrophilic	Pectinase	(Burapapadh et al., 2012)

Alginate	Polysaccharide	Anionic	Covalent and Ionic cross-linking, thermo gelation	Hydrophilic	<i>In vitro</i> degradation using alginase. But Slightly oxidized alginate can degrade in aqueous media	(Li et al., 2013, Liu et al., 2008)
Pullulan	Polysaccharide	Neutral, high water solubility, adhesive	Crosslinking ability	Hydrophilic	<i>In vitro</i> degradation via pullulanase, and in vivo degradable	(Liu et al., 2008, Shingel, 2004)

As the table shows, a range of materials has been used for the preparation of nano-emulsions for skin cancer and melanoma drug delivery. The nano-emulsions can be prepared using various approaches depending on the ultimate application (Fofaria et al., 2016b). However, most of the nano-emulsion delivery systems lack stability and high drug loading capacity (Patel et al., 2017). Nano-emulsions were investigated to provide a potential solution for the flux-dependant melanoma drug resistance and a tool to increase therapy efficiency (Vecchione et al., 2017). This can happen through the nano-emulsion particles which can cross the tumour microenvironment barrier, and overcome intra-tumoural pressure. Hence they can reduce the resistance caused by alterations in drug efflux, due to their ability to provide a controlled release and increase the stability of the drug. Although to reach this, specific modifications may be needed (Patel et al., 2019).

1.6.5 Classification of nano-emulsions for melanoma treatment based on the route of administration

As melanoma has a poor response to existing treatment modalities and is highly resistant to conventional therapies, the development of a novel system to defeat it, is crucial (Mishra et al., 2018). Nano-emulsions are considered attractive drug delivery tools especially for skin diseases (McDonald et al., 2015). They are also well-known drug delivery systems for dermal and transdermal disorders (Shakeel et al., 2012). Increasing bioavailability of the drugs, nano-emulsions tend to be used in various administration routes (Rai et al., 2018a). Depending on

the size of nano-emulsion particles and the target disease, it can be designed to be used for particular administration routes.

Nano-emulsions have been successfully used in topical delivery of hydrophobic and toxic drugs such as Dacarbazine for melanoma, and facilitated use of the delivery system was consequently reported as an important point (Hafeez and Kazmi, 2017, Lasoń, 2020). Researchers also investigated the delivery of drug-loaded nano-emulsion by intramuscular injection, which decreased melanoma by 61% compared to untreated control (Tagne et al., 2008). Other administration routes of drug-loaded nano-emulsions for melanoma were also investigated, such as oral (Lin, 2018) and intravenous injection (Sánchez-López et al., 2019). However, topical delivery of nano-emulsion for skin cancer has been reported among the most common and effective routes of delivery (Giacone et al., 2020, Kaplan et al., 2019).

1.7 Effect of inflammation on melanoma

Inflammation is the body's response to damage caused in the body following exposure to pathogens, damaged cells, injury, and toxins. This process involves immune cells (Leukocytes), blood vasculatures, and some molecular mediators. The mediators including chemokines, cytokines, histamine, proteases, prostaglandin, leukotrienes, and serglycin proteoglycans are released during the host response (Chen et al., 2017).

When a tissue or part of the body is injured due to internal (autoimmune disorder) or external factors (bacteria, toxins, heat, and trauma), Histamine is released from mast cells immediately by the damaged tissue to aid in the repair. When the tissue repair process or healing, (resolution

of the host inflammatory response), is completed, inflammation subsides (Prockop, 2016). The physical signs of inflammation are usually redness (rubor), swelling (tumour), pain (dolor), and fever (calor) and correspond with acute inflammatory changes seen within the first 48 hours of an inflammatory response (Zetoune et al., 2014).

There are two types of inflammation, acute and chronic. Acute inflammation will stop after the injured part of the body is completely healed due to the body's prompt response to any trauma or injury (Coussens and Werb, 2002). It is characterised by the migration of neutrophils to the site of injury or infection via a repair process involving these stages. Initially, capillaries will expand to increase the blood flow following the release of histamine from mast cells causing a constriction in the endothelial cells, secondly, the microvascular structure will change with protein plasma exudation and finally, leukocytes migrate through the endothelium and accumulate at the damaged part (Hunter, 2012). This occurs by leukocytes passing from the bloodstream, adhering to the endothelium via upregulation of β_2 integrins (CD11a/CD18b) on the leukocyte cell surface and upregulation of adhesion molecules on the endothelium e.g. intracellular adhesion molecule 1 (ICAM1). This leads to a strong interaction of the leukocyte to the endothelium, subsequent flattening of the cell, and finally emigration through adjacent endothelial cells via upregulation of molecule CD31 (PECAM1) (Golias et al., 2007). Afterward, the foreign bodies will be removed by phagocytosis and the tissue will start to repair with subsequent scar formation.

Chronic inflammation is the failure of the inflammation to resolve due to a continued inflammatory response and may take weeks, months, or years to diminish as seen in diseases such as rheumatoid arthritis (Zaid et al., 2018). Chronic inflammation is prolonged acute

inflammation (Abudukelimu et al., 2018) and occurs due to various reasons such as prolonged exposure to *mycobacterium*, *fungi*, or *protozoa* which the body's immune system is unable to eliminate (Fulford and Stankiewicz, 2020, Bellamy et al., 2020), or chemical irritants (Bains and Fonacier, 2019). Alternatively, existing autoimmune disorders such as seen in Rheumatoid Arthritis or mitochondrial dysfunction can also lead to chronic inflammatory changes (Pahwa and Jialal, 2018) or via physical injury (Hughes, 2018), all these can lead to the 5th cardinal sign of inflammation, loss of function (function laesa).

Prolonged chronic inflammation may cause severe DNA damages and genomic changes which may be an initiation point for various diseases (Crusz and Balkwill, 2015) including cardiovascular diseases (Ferrucci and Fabbri, 2018), various cancer types, and diabetes (Chang and Yang, 2016).

There are two types of chronic inflammation, one is nonspecific proliferative inflammation, and the other granulomatous inflammation. The first type forms as a non-specific granulation in the presence of lymphocytes, macrophages, and plasma cells, and it continues proliferating in fibroblasts and connective tissue (Snape and Collins, 2020). Simple forms of this kind of inflammation are polyps and abscess, whilst the second types usually form as nodular lesions or granulomas. This type of inflammation can be due to a chronic infection such as tuberculosis or leprosy or in the presence of a foreign body or immune response (Billero et al., 2017). Some of these can be attributed to risk factors such as age, overweight, diet, smoking, and stress (Serhan et al., 2010).

1.7.1 Mediators that drive the host inflammatory response

For initiation of an inflammatory response, a message is delivered by inflammatory mediators which are released by injured or activated cells. These mediators are chemicals responsible as messengers. There are two types of mediators, plasma-derived mediators, and cell-derived mediators. Vasoactive amines (such as histamine and serotonin), arachidonic acid metabolites (Cyclooxygenase and Lipoxygenase pathways), liposomal components, platelet-activating factors, cytokines (IL-1, TNF- α , TNF- β , IF γ , and chemokines), and nitric oxide and nitrogen metabolites are cell-derived mediators of inflammation. On the other hand, plasma-derived mediators are derived from the kinin system, the clotting system, the fibrinolytic system, and the complement system (Abdulkhaleq et al., 2018). Each mediator has a particular role in the inflammation process and these responses such as pain, fever, and irritation. For instance, iNOS is the inducible form of Nitric Oxide synthetases (NOS), (Nakazawa et al., 2017), and cyclooxygenase-2 (COX-2), are enzymes that mediate inflammatory responses in the body (Gandhi et al., 2017) and are overexpressed in cancerous tissues (Murakami and Ohigashi, 2007, Singh et al., 2019).

1.7.2 Inflammation and cancer

Chronic inflammation has been proved to be an important hallmark in cancer occurrence and progression. The very first hypothesis of cancer initiation in chronic inflammation sites was mentioned in 1863 (Weber et al., 2010). The triggering factor is the proliferation of the cells in a microenvironment filled with inflammatory cells, growth factors, and stroma (Wang et al.,

2017a) with persistent inflammation potentially leading to cancer cell formation (Korniluk et al., 2017). Persistent inflammation could be due to immune deficiency problems, prolonged injury or infection, and long-term exposure to toxic chemicals and irritants (Mosenthal, 2018). There are two types of inflammatory mediators, pro-inflammatory ones (e.g. $\text{TNF-}\alpha$, $\text{IL-1}\beta$), and anti-inflammatory mediators (e.g. IL-10 , Heme-oxygenase 1) (Coras et al., 2019). The presence of increased pro-inflammatory chemokines and an uneven balance between catabolic pro-inflammatory vs anabolic anti-inflammatory chemokines are in part due to prolonged inflammatory response (Coussens and Werb, 2002). Consequently, due to long-lasting chronic inflammation phagocytic cells, Leukocytes and other inflammatory mediators will damage the DNA of the host cells, resulting in alterations in the proliferation cycle of the cells and subsequent abnormalities occurring (Kawanishi et al., 2017).

Studies have highlighted that cancer initiated from inflammation is responsible for 15-20% of cancer-related death worldwide (Okada, 2014). Rather than cancer initiation, inflammation can have a critical role in all stages of cancer and will positively affect cancer cell proliferation, migration, and invasion (Sui et al., 2017). Since inflammatory cells are known to be an abundant source of growth factors and cytokines prerequisites for cell survival and proliferation, this can affect the whole cancer therapy process including the response to the chemotherapeutics (Rajput and Wilber, 2010, Coussens and Werb, 2002). Several inflammatory mediators and chemokines are known to be directly related to cancer initiation and tumorigenesis. These include the pro-inflammatory, $\text{TNF-}\alpha$, IL-6 , $\text{TGF-}\beta$, $\text{NF-}\kappa\text{B}$, and STAT3 , which have great importance in carcinogenesis and metastasis. The enzymes, iNOS,

and COX-2 expression increase during the inflammatory process (Liu et al., 2003), with overexpression causing tumorigenesis and metastasis (Janakiram and Rao, 2012).

The cytokine IL-10 is anti-inflammatory which is associated with suppression of cancer-associated inflammatory changes with inhibition of pro-inflammatory genes including TNF- α , IL-1 β via inhibition of NF- κ B (Landskron et al., 2014).

Inflammation is also known as one of the important risk factors for skin cancer initiation and malignancy. As mentioned in previous sections, UV light has an important impact on skin cancer by inducing DNA damage (Prasad and Katiyar, 2017). When skin is inflamed by the action of UV light, inflammatory mediators, and cytokines such as IL-6 are released (Quist et al., 2016). Long-term accumulation of them in the skin will lead to the initiation of melanoma. The cytokines such as IL-1 β released from UV triggered keratinocytes, and melanocytes along with dendritic cells and Langerhans cells, during the melanoma inflammation process, promote aggressive tumour cell behaviour (Bou-Dargham et al., 2017).

Recent studies have shown a strong link between chronic inflammation and melanoma progression and metastasis (Maru et al., 2014, Tang and Wang, 2016). Non-melanoma skin cancers (Basal cell carcinoma (BCC) and squamous cell carcinoma (SCC)) are directly linked to inflammation (Voiculescu et al., 2018). Melanoma development is also strongly linked to inflammation due to the increased release of various cytokines such as IL-4, IL-10, and IL-13 by melanocytes (Neagu et al., 2019), due to paracrine signalling with the tumour microenvironment of the inflamed part. Hence the inflammation prevention and treatment gain importance (Xiao et al., 2016).

1.7.3 Current treatments for inflammatory pathologies

Nonsteroidal anti-inflammatory drugs (NSAIDs) are widely used to relieve pain, inflammation, and fever. These include aspirin, ibuprofen, and naproxen. NSAIDs have two categories, non-selective ones such as aspirin, ibuprofen, and diclofenac which inhibit the COX-1, and 2 pathways leading to a reduction in prostaglandins and COX-2 selective (Coxibs) such as celecoxib which decrease the pain and inflammation-mediated from COX-2 (Cairns, 2007).

However, although NSAIDs decrease the symptoms of inflammation, they may cause other side effects such as gastrointestinal diseases/bleeding via inhibition of the cytoprotective enzyme COX-1 (Matsui et al., 2011). On the other hand, specific COX-2 inhibitors (Coxibs) can inhibit inflammation by inhibiting PGE₂. However, the most important problem with Coxibs is substantial cardiotoxicity. This may lead to myocardial infarction through inhibition of prostacyclin tipping the balance in favour of thromboxane a prothrombotic eicosanoid (Zarghi and Arfaei, 2011).

1.7.4 Novel therapeutics for treating inflammatory pathologies

Melanocortin peptides are short amino acid sequences including alpha-melanocyte-stimulating hormone which corresponds to the first 13 amino acids of the parent hormone ACTH₁₋₃₉, a hormone derived from the larger precursor molecule the Proopiomelanocortin (POMC) gene (Getting et al., 2009).

Melanocortin peptides exert their biological effect by binding to a family of G-protein coupled receptors called the melanocortin receptors of which five have been identified and termed MC₁-

MC₅. Their activation leads to an increase in adenylate cyclase and a subsequent increase in cAMP (Wang et al., 2019a, Can et al., 2020). Studies have highlighted that melanocortin receptors can be expressed in various tissues in the body such as the brain and skin (Lisak and Benjamins, 2017). They have a notable effect on a few of the body functions including inflammation (Maaser et al., 2006). Activation of MC₁ and MC₃ has been shown to modulate the host inflammatory response and lead to an anti-inflammatory phenotype resulting in resolution of inflammation (Kaneva et al., 2012). To date, the most characterised peptide is an α -melanocyte stimulating hormone (α MSH) which is a naturally occurring melanocortin peptide. α MSH has a high affinity for the MC receptors and is involved in inflammation. Melanocortin peptides are expressed on immune cells such as neutrophils, macrophages, and also melanocytes responsible for skin pigmentation and melanoma metastasis and progression (Bulman et al., 2013). BMS-470539 dihydrochloride and [DTrp⁸]- γ -MSH are two commercially available melanocortin receptor agonists targeting the MC₁ and MC₃ receptor respectively and have been shown to modulate the host inflammatory response in *in vitro* models of osteoarthritis and *in vivo* models of stroke and ischaemic reperfusion injury (Can et al., 2020; Holloway et al., 2015; Leoni et al., 2010). These compounds inhibit leukocyte trafficking in models of stroke and ischaemic reperfusion injury in mice (Holloway et al., 2015; Leoni et al., 2010), modulate inflammatory markers including IL-6, IL-8 (Can et al., 2020), and induce an anti-inflammatory protein in *in vitro* models of osteoarthritis (Can et al., 2020; Kaneva et al., 2012).

As mentioned previously, chronic inflammatory markers are important factors influencing cancer initiation, progression, and metastasis (Yang, 2010, Qian, Greten, and Grivennikov,

2019). Malignant melanoma expresses high levels of MC₁ (Baumann et al., 1997, Park et al., 2019), which plays a crucial role in melanogenesis. Hence this can be utilized as a positive point towards melanoma treatment.

1.8 Research approach

The growing number of patients diagnosed with cancer, today is a global issue. The acquisition of genetic mutations due to environmental and lifestyle factors is increasingly important in influencing the incidence of melanoma. Cancer research is a vast field of study, so there are various factors to be considered in cancer therapy. Prevention, diagnosis, treatment, and palliative care are four major tasks in cancer research. In this project, the major focus is on treatment. To this end, an experimental approach was followed for this research.

The design of experiments was based on choosing appropriate polymers and cell lines for the particular aim of melanoma drug delivery and design a nano-emulsion for topical drug delivery. Initially, series of optimisation steps were carried out to reach a nano-emulsion providing a controlled release and lowest initial burst. Followed by reaching the optimal nano-emulsion, the nano-emulsion particles were surface modified.

The optimal drug-loaded nano-emulsion was further assessed using *in vitro* cellular assays. The related experimental assays were performed using A375, human malignant melanoma primary cell line, and HaCaT, keratinocyte cell line as control.

Furthermore, the downregulation of two important inflammation markers in melanoma was investigated. Current research contains a novel approach used for downregulation of iNOS and COX-2 by encapsulation and delivery of melanocortin peptides by nano-emulsion.

1.9 Research aim and objectives

This research aimed to develop a strategy to improve the drug delivery to A375 malignant melanoma human cell line. The intended drug delivery aims for successful apoptosis induction and decrease flux-dependant drug resistance.

To achieve the aim of this research a careful design and optimisation of the nano-emulsion were implemented to provide enhance uptake of the drug in A375 cells. Furthermore, the nano-emulsion was designed to be used as a topical delivery system in early-stage melanoma. Hence, the experimental part of the thesis was conducted using a comparison study between A375 and HaCaT cells as control healthy cells. Ultimately knockdown of two inflammation markers was tried to control melanoma progression.

To address the aim, the following objectives were implemented.

1. Development of chitosan/pullulan/alginate nano-emulsion to provide a slow and controlled release and optimisation of the nano-emulsions.
2. Tracking nano-emulsion particles in cell culture via encapsulation of coumarin-6 (C6, a fluorescent model drug) and comparing to the doxorubicin-loaded nano-emulsions.
3. Comparing the toxicity of doxorubicin/dacarbazine loaded nano-emulsions to naïve drugs in melanoma and keratinocytes.
4. Surface modification of optimised nano-emulsion to increase the uptake specifically in melanoma cells.
5. Increase the apoptosis induction to melanoma cells via surface-modified nano-emulsions.

6. Encapsulation of BMS-470539 dihydrochloride and [DTrp⁸]- γ -MSH in the surface modified-optimised nano-emulsion to inhibit melanoma growth and progression.

2 Materials and methods

2.1 Materials

2.1.1 Chemicals and reagents

Basic laboratory chemicals and reagents were purchased from Sigma, Thermo-Fischer Scientific, and Invitrogen. The list of materials and reagents, used in this research are outlined below in Table 2.1.

Table 2.1 Materials and reagents

Compound	Supplier	Catalog number
3,3',5,5'-Tetramethylbenzidine (TMB) Liquid Substrate System for ELISA	Sigma Aldrich-Merck	0440
Agarose (molecular biology grade)	Fischer scientific UK	10366603
Cell tracker green (CMFDA)	Thermo-Fischer scientific-Invitrogen	C7025
Cell tracker red (CMTPX)	Thermo-Fischer scientific-Invitrogen	C34552
Chitosan medium molecular weight (deacetylation \geq 75%)	Sigma Aldrich-Merck. UK	9012-76-4
Chloroform	Sigma Aldrich-Merck	67-66-3
Coumarin-6 (\geq99%)	Sigma Aldrich-Merck UK	38215-36-0
Dacarbazine (DTIC)	Sigma Aldrich-UK	4342-03-4
DAPI (4',6-Diamidino-2-Phenylindole, Dihydrochloride)	Thermo-Fischer scientific	D1306
Dimethyl Sulfoxide	Sigma Aldrich-Merck. UK	D2650
DMEM low high glucose	Sigma Aldrich-UK	MFCD00217342

DNA free, DNA removal kit	Thermo–Fischer scientific	AM1906
Doxorubicin hydrochloride	Sigma Aldrich-UK	25316-40-9
Ethanol absolute	VWR chemicals-UK	20821.310P
Fetal bovine serum	Sigma Aldrich-UK	MFCD00132239
Folic acid	Sigma Aldrich-Merck	F7876
Formaldehyde	Sigma Aldrich-Merck	F8775
Gene Ruler 1 kb DNA Ladder	Thermo-Fischer scientific	SM0311
Genipin	Sigma Aldrich-Merck	4796
Glacial acetic acid	Fischer scientific UK	15541152
Glycerol (molecular biology grade)	Sigma Aldrich-UK	56-81-5
Guanidine chloride	Sigma Aldrich-Merck	50-01-1
Isopropanol	VWR chemicals-UK	470301-456
Methanol	Fischer scientific	10365710
NuPAGE™ 10% Bis-Tris Protein Gels, 1.0 mm, 10-well	Thermo-Fischer scientific-Invitrogen	NP0301BOX
PCR master mix 2X	Thermo-Fischer scientific	K0171
Phosphate buffered saline (DPBS)	Sigma Aldrich-UK	MFCD00131855
Ponceau S Solution	Sigma Alrich-Merck UK	7170
Pre-stained protein molecular weight marker	Thermo-Fischer scientific	26612
Pullulan (aureobasidium pullulans)	Sigma Aldrich-Merck UK	9057-02-7
Sodium alginate	Sigma Aldrich-Merck UK	9005-38-3
Sodium dodecyl sulfate	Sigma Aldrich-Merck	151-21-3
SYBR™ Safe DNA Gel Stain	Sigma Aldrich-Merck	33102

TBE (tris-borate-EDTA)	Thermo-Fischer scientific-Invitrogen	LC6675
Thiazolyl Blue Tetrazolium Bromide	Sigma Aldrich-Merck	M2128
Tri reagent	Sigma Aldrich-Merck	93289
Tris-Acetate-EDTA 10x	Sigma Aldrich-UK	9650
Tris-HCl	Invitrogen	15-568-025
Trypan blue	Thermo-Fischer scientific	T10282
Trypan blue solution	Sigma Aldrich-Merck	T8154
Trypsin-EDTA 10X	Sigma Aldrich-UK	9002-07-7
Twin 20	Fischer scientific	9005-64-5
Twin 80	Fischer scientific	9005-65-6

The list of cytotoxic drugs used for drug delivery and their physicochemical characteristics are listed in the table below Table 2.2.

Table 2.2 Characteristics of cytotoxic drugs used for drug delivery

Anti-cancer drug	Molecular weight	Toxicity	LogP	pKa	Stability	Pharmacological classification
Doxorubicin	543.5 g/mol	Cardiotoxicity, hepatotoxicity, gastrointestinal problems	1.27	4.42	Neutral/ stable at room temperature	Topoisomerase II inhibitors
Dacarbazine	182.18 g/mol	Hepatotoxicity	-0.24	7.34	Unstable in presence of light	Anti-neoplastic agent, Alkylating

The list of cell lines used in this research is outlined below in Table 2.3.

Table 2.3 Cell lines

Cell line	Supplier	Order number	Mutations
A375	American tissue culture collection	ATCC® CRL-1619™	BRAFV600E/KRASG13D
HaCaT	Provided by University College London Hospital	NA	None

The list of oligonucleotide sequences, used in this research are outlined below in the Table 2.4

Table 2.4 Primer sequences used for PCR (Si et al, 2018)

Gene	Primers	Size (bp)	Company
Bax	F:5'-ACGAACTGGACAGTAACATGGAG-3' R:5'-CAGTTTGCTGGCAAAGTAGAAAAG-3'	839	IDT Integrated DNA Technologies, BVBA
Bcl-2	F:5'-ATGTGTGTGGAGAGCGTCAA-3' R:5'-GAGACAGCCAGGAGAAATCAA-3'	6492	IDT Integrated DNA Technologies, BVBA
Caspase-3	F:5'-CTGGACTGTGGCATTGAGAC-3' R:5'-ACAAAGCGACTGGATGAACC-3'	2689	IDT Integrated DNA Technologies, BVBA
Caspase-9	F:5'-AGGGTCGCTAATGCTGTTTC-3' R:5'-GCAAGATAAGGCAGGGTGAG-3'	1848	IDT Integrated DNA Technologies, BVBA
GAPDH	F:5'-CAAGGTCATCCATGACAACTTTG-3' R:5'-GTCCACCACCCTGTTGCTGTAG-3'	1513	IDT Integrated DNA Technologies, BVBA

The list of ELISA kits, used in this research is outlined below in Table 2.5

Table 2.5 ELISA kits

Kit	Supplier	Catalog number
Human folate binding protein ELISA	Abcam-UK	ab213781
DNA fragmentation ELISA	Sigma Aldrich-Roche	11585045001

The list of antibodies, used in this research is outlined below in Table 2.6

Table 2.6 antibodies

Antibody	Supplier	Catalog number
Human polyclonal Anti-COX-2 anti-body	Abcam-UK	ab15191
Human polyclonal Anti-iNOS anti-body	Abcam-UK	ab3523
Mouse anti-α-Tubulin antibody	Thermo-Fischer Scientific	A11126

The list of buffers, used in this research are outlined below in Table 2.7

Table 2.7 Buffers used in the experiments

Buffer	Preparation
1% SDS	1 gr SDS 100 ml H ₂ O
Lameali sample buffer	4% SDS, 10% 2-mercaptoethanol, 20% glycerol, 0.004% bromophenol blue, 0.125 M Tris-HCl, pH 6.8.
SDS page running buffer	25 mM Tris, 190 mM glycine, 0.1% SDS
TAE 1X	100 ml 10xTAE buffer, 900 ml milli Q water.
TBST 1x	10 ml 1M Tris-HCL, pH 8.0, 30 ml 5M NaCl, 500 µl Tween 20, ddH ₂ O up to 1L.
Western blot transfer buffer	25 mM Tris, 190 mM glycine, 20% methanol

The list of equipment, used in this research is outlined below in Table 2.8

Table 2.8 Equipment

Equipment	Model/Supplier	Serial number
Balance	Sartorius	M-Power SAR AZ64
C₁₈ HPLC column (4.6 mm x 10.0 mm) 3PK	Thermo-Scientific	071973
Centrifuge	Eppendorf	5418 R, 05-401-201
Confocal microscope	Leica TCS SP2	NA
Countess™ Cell Counting Chamber Slides	Thermo-Fischer Scientific-Invitrogen	C10228
Countess™ II FL Automated Cell Counter	Thermo-Fischer scientific-Applied Biosystems	A27974
Electrophoresis tank	Bio-rad Wide Mini sub-cell GT	170-4405
ELISA reader	BMG Labtech	NA
Fluorescent microscope	EVOS M5000 Thermo-Fischer Scientific	A40486
Glassware	Fischer brand, Doran laboratories	NA
Nano-particle tracking analyser	Nano sight NS300 Malvern UK	NA

Nano-drop	Thermo-Fischer Scientific	ND-One-W
Scanning electron microscopy	FEI Quanta 650 FEG-ESEM	NA
Sonicator	Phillip Harris Scientific	599006006
Sonicator probe-MS73 micro-tip, titanium alloy, 3 mm diameter	Sigma-Aldrich UK	659150
Spectrophotometer	JENWAY 6300 spectrophotometer	83054-05
Spectrum™ Labs Spectra/Por™ 5 12-14 kD MWCO Dialysis tubing	Fischer scientific	15340782
Thermo-cycler	Bio-Rad MJ Mini 48-well	PTC1148
UHPLC	Ultimate 3000 Thermo-scientific	IQLAAAGAAOFAMUMZZZ
UV gel imaging system	BioDoc-It UVP 3-Door Imaging System, 302nm 20x20cm Transilluminator; 115V	WZ-97701-82
Western blot tank	Thermo-Fischer Scientific XCell SureLock™ Mini-Cell	EI0001
Zeta sizer	Malvern UK	NA

The list of software, used in this research are outlined below in Table 2.9.

Table 2.9 Software

Software	Version
Biochem draw	Pro V.16.0.1
Biorender online drawing software	NA
Chromeleon	7
Endnote	X9
Graph pad Prism	8-win64bit
Image J	1.52d Java 1.7.0 – 60 (64 bit)
Microsoft office	Microsoft version 2013
NTA software	version 3.4 built 3.4.003
SPSS	25-win64bit

2.2 Methods

2.2.1 Preparation of drug-loaded polysaccharide-based nano-emulsion

Nano-emulsions were prepared using a high-energy sonication method (Fofaria et al., 2016a). Chitosan, pullulan, and alginate were used as main biopolymers. A range of nano-emulsions was prepared using different w/w ratios of the three polymers for coumarin-6 (Smith and Purr, 2019) or doxorubicin encapsulation to reach the formulation with an optimised and controlled release rate.

Starting with chitosan, the polymer powder was dissolved in ultrapure water containing the same ratio of acetic acid to chitosan Table 2.10. The solution was stir-mixed for 24 hours to reach homogeneity. Coumarin-6 solution (1mg/ml concentration), was prepared before the nano-emulsion preparations. Separately tween-80 was added to glycerol and then mixed for 2 hours. Fifty microliters of coumarin-6 solution were added to tween-80 and glycerol mixture and then left mixing for another hour. After preparing the oil phase (glycerol-tween-80), the chitosan solution was added to the oil mixture and was left for mixing for 2 hours to reach the oil in the water mixture. The mixture was sonicated using a high-energy sonicator for 20 minutes in an ice bucket to obtain coumarin-6 loaded nano-emulsion particles. The pH of prepared samples was adjusted to 7.4 using 1M sodium hydroxide. The ratios used for the preparation of nano-emulsions are shown in the tables below.

Table 2.10 Chitosan nano-emulsion preparation ratios

	Chitosan (w/v%)	Acetic acid/MQ water (v/v%)	Tween-80 (v/v%)	Glycerol (ml)	Coumarin-6 (μ l)
NEC1	0.2	0.2	1	20	50
NEC2	0.4	0.4	2	20	50
NEC3	0.6	0.6	3	20	50
NEC4	0.8	0.8	4	20	50
NEC5	1	1	5	20	50
NEC6	1.2	1.2	6	20	50
NEC7	1.4	1.4	7	20	50

Similarly, alginate powder was dissolved in ultrapure water. The solution was stir-mixed for 24 hours to obtain a homogenous mixture. Separately tween-80 with the ratio of 5:1 to alginate was added to glycerol and mixed for 2 hours. Fifty microliters of coumarin-6 solution were then added to tween-80 and glycerol mixture followed by another hour of stir-mixing. Alginate solution was added to the oil and tween-80 mixture then left for mixing for 2 hours to obtain oil/water mixture. The mixture was sonicated for 20 minutes to prepare nano-emulsion particles. The ratios of all prepared samples are shown in Table 2.11. the same preparation procedure as alginate was repeated to develop pullulan nano-emulsion and the ratios are available in the Table 2.12.

Table 2.11 Alginate nano-emulsion preparation ratios

Name	Alginate (w/v%)	MQ water (ml)	Tween 80 (v/v%)	Glycerol (ml)	Coumarin-6 (μ l)
NEA11	0.2	20	1	20	50
NEA12	0.4	20	2	20	50
NEA13	0.6	20	3	20	50
NEA14	0.8	20	4	20	50
NEA15	1	20	5	20	50
NEA16	1.2	20	6	20	50
NEA17	1.4	20	7	20	50

Table 2.12 Pullulan nano-emulsion preparation ratios

Name	Pullulan (w/v%)	MQ water (ml)	Tween 80 (v/v%)	Glycerol (ml)	Coumarin-6 (μ l)
NEP11	0.2	20	1	20	50
NEP12	0.4	20	2	20	50
NEP13	0.6	20	3	20	50
NEP14	0.8	20	4	20	50
NEP15	1	20	5	20	50
NEP16	1.2	20	6	20	50
NEP17	1.4	20	7	20	50

Each of the mentioned nano-emulsions was examined in the *in vitro* release test. Following the selection of one best sample from each polymer group, based on coumarin-6 and doxorubicin release, selected polymer samples were cross-linked. Accordingly, chitosan-pullulan, pullulan-alginate, and chitosan-alginate blended nano-emulsions were prepared using different w/w ratios (1:2, 2:1, 1:1). Genipin was used as a crosslinker, the solution was prepared with the

concentration of 1mg/ml and 500 microliters of genipin solution (1% v/v) were added to each polymer blend and stir mixed continuously for 72 hours to complete the cross-linking process. The cross-linking procedure was also applied to previously selected three non-composite formulations, chitosan, pullulan, and alginate. All the prepared blends were loaded with coumarin-6 and doxorubicin separately. Fifteen nano-emulsions were prepared with the same procedure. UV sterilisation was applied over two 20-minute cycles before uptake experiments. Coumarin-6 and doxorubicin release tests were also conducted for these samples under the same conditions as stated above. The same preparation and drug loading procedure were applied to prepare doxorubicin-loaded nano-emulsions. Blank coumarin-6 and doxorubicin were used as positive controls in the treatments and calculations.

Sample-coding is given in the following table Table 2.13.

Table 2.13 IDs for in-house prepared nano-emulsions

Polymer	Alginate (mg/ml)	Chitosan (mg/ml)	Pullulan (mg/ml)
Nano-emulsion			
NEC1-AI (2:1)	2	4	-
NEC1-AI (1:1)	2	2	-
NEC1-AI (1:2)	4	2	-
NEAI2-Cs (2:1)	8	4	-
NEAI2-Cs (1:1)	4	4	-
NEAI2-Cs (1:2)	4	8	-
NEPI2-Cs (1:1)	-	4	4
NEPI2-Cs (2:1)	-	4	8
NEPI2-Cs (1:2)	-	8	4
NEC1-PI (1:1)	-	2	2
NEC1-PI (2:1)	-	4	2
NEC1-PI (1:2)	-	2	4
NEPI2-AI (1:2)	8	-	4
NEPI2-AI (2:1)	4	-	8
NEPI2-AI (1:1)	4	-	4
NEC1	-	2	-
NEPI2	-	-	4
NEAI2	4	-	-

2.2.2 Measurement of the drug encapsulation efficiency of optimised nano-emulsion

To quantify the drug encapsulated within nano-emulsion particles dialysis methodology was used. All prepared coumarin-6, and doxorubicin-loaded nano-emulsions were dialyzed against phosphate-buffered saline (PBS). The buffer pH was adjusted to 7.4 using hydrochloric acid (HCl). To obtain the drug encapsulation efficiency, 1 ml of each sample was placed in a dialysis bag (10-12 KD molecular weight cut off (MWCO)) and then located in PBS buffer. The amount of free coumarin-6 in PBS was quantified by a spectrophotometer (JENWAY 6300, 83054-05) at 450 nm, and encapsulation efficiency was calculated using the following equation:

$$\text{Encapsulation efficiency} = \frac{\text{Total drug loaded} - \text{Free drug}}{\text{Total drug loaded}} * 100$$

The amount of free doxorubicin was quantified using high-performance liquid chromatography (HPLC) according to (Dharmalingam et al., 2014) with slight modifications. Briefly, UHPLC (Ultimate 3000 Thermo-scientific) was performed using a C₁₈ column (4.6 mm x 100 mm, 2.7 µm, Thermo-Scientific 071973). UV detection for doxorubicin was done at 233 nm. The mobile phase contained water and acetonitrile (25:75 v/v, adjusted to pH 3.0 using 85% w/v phosphoric acid) using the flow-rate of 1.0 ml per minute. The mobile phase was run using a gradient method as follows: acetonitrile gradient of 10% at 0 minutes, 20% at 3 minutes, 35% at 6 minutes, 55% at 8 minutes, 75% at 10 minutes, and 100% at 12 minutes was used. The peak

was identified, and the retention time of doxorubicin was detected at 2 minutes. Accordingly, the quantity of the doxorubicin released was measured (Appendix A).

2.2.3 Coumarin-6 and doxorubicin *in vitro* release tests

To identify the drug release profile for each prepared nano-emulsion, *in vitro* coumarin-6 release experiment was conducted. The experiment was carried out for all the prepared coumarin-6 and doxorubicin-loaded chitosan, alginate and pullulan, and blended nano-emulsion samples. A dialysis method was used to screen the *in vitro* release (Hua, 2014), 1 ml of each nano-emulsion was added to separate dialysis bags and placed into flasks containing PBS. The flasks moved into a shaker incubator, at 25°C and 55 rpm with continuous stirring. Liquid samples from the flasks analysed using UV-spectrophotometer at 450 nm wavelength for coumarin-6 and 479 nm for doxorubicin. The measurements were conducted for 21 days. The amount of liquid taken out was replaced each time. This protocol was applied to all the nano-emulsion samples in this experiment under the same conditions. Naïve coumarin-6 and doxorubicin solutions were used as control.

2.2.4 Nano-emulsion characterisation

To identify the particle size, size distribution, morphology, and stability of a nano-emulsion, it needs to be characterised. To characterise the size and concentration of nano-emulsion particles, a nanoparticle tracking analyser (NTA, Nano sight NS300, Malvern, UK) was used. To confirm the results further, the method was optimised and results were analysed by NTA software. The

optimisation was done by diluting the nano-emulsion sample in multiple steps (Grillo et al., 2019).

The experiment started by cleaning the lens over the flow cell. Initially, 1 ml of PBS was pumped into the system using a syringe to clean any previously remaining particles. The diluted nano-emulsion (1:200 PBS) was then syringe-pumped into the system. Images were captured using the following settings: laser type on blue 488, camera level set at 11, slider gain 146, syringe pump speed 50, detect threshold 2, and blur on auto. All the experiments were carried out at 25 °C and were performed in triplicates. The raw data was analysed by the software. The size, the mean concentration of particles, and the finite track length adjustment (FTLA) were collected during the total time of recording.

To identify the morphology of the nano-emulsion particles, scanning electron microscopy (SEM) was performed using FEI Quanta FEGSEM operating at 5.00 kV, 63k magnification, 50 pa pressure, dwelling 10 µseconds.

Zeta potential was determined at room temperature using Zetasizer nano (Malvern instrumentals, UK) in triplicates. The dilutions were made using PBS (1:100 v/v).

2.2.5 Preparation of drug-loaded Folic Acid surface-modified nano-emulsion

Modification of nano-emulsion was carried out in order to increase the uptake of particles in A375 cells. Hence, the previously, prepared drug-loaded nano-emulsions (section 2.2.1) were surface coated with folic acid.

Folic acid coating of the polymer was conducted via electrostatic interactions according to Song et al (Song et al., 2013) with slight modifications. Briefly, folic acid solution (20 w%) was prepared by dissolving folic acid in 1 M NaOH. The folic acid solution was added dropwise to the drug-loaded nano-emulsion while stirring for 12 hours. The solution was washed with PBS 3 to 4 times and centrifuged for 30 minutes at 16000 rpm to remove the unbound folic acid.

2.2.6 Encapsulation of anti-inflammatory compound in optimised nano-emulsion

According to the aims of the current research, to target iNOS and COX-2 expression in A375 cells anti-inflammatory compounds were used. The compounds aimed to target iNOS and COX-2 expression by means of the developed nano-emulsion. Hence, encapsulation of the anti-inflammatory compounds in nano-emulsion was conducted using the same procedure as mentioned above (section 2.2.2). However, due to the short half-life of the peptides (6 hours), the whole encapsulation procedure was done on ice. The compounds BMS-470539 dihydrochloride and [DTrp⁸]- γ -MSH (Can et al., 2020) were used to target human melanocortin receptors on melanoma (MC₁ and MC₃) (Zhang et al., 2017, Zhou, 2019). In this research, they are utilised to downregulate iNOS and COX-2 in A375 cells.

2.2.7 Cell culture

As the skin comprises fibroblasts, melanocytes, and keratinocytes. The HaCaT cell line was used as a highly proliferative epidermis *in-vitro* model in cell culture and viability (Souto et al., 2020, Bácskay et al., 2018) studies due to facilitated proliferation, propagation, and its phenotype (Lehmann, 1997, López-García et al., 2014). Similarly, the A375 metastatic melanoma human-derived primary cell line was chosen for *in-vitro* studies of drug optimisation and viability screening (Couto et al., 2019). A375 cells are chosen to study the features of the drug delivery system for early-stage melanoma. Hence, the HaCaT cell line was used as a control healthy cell to malignant A375 cell line in this study to investigate the effect of drug-loaded nano-emulsion as a topical delivery system (Bittkau et al., 2019).

A375 (malignant melanoma) and HaCaT (human immortalized keratinocyte) cell lines were cultured in T-75 flasks using Dulbecco's Modified Eagle Medium (DMEM) high glucose (4500 mg/L, no sodium pyruvate and containing L-Glutamin) and 10% (v/v) fetal bovine serum (FBS). The cell-containing flask was incubated at 37°C and 5% CO₂. After confluency of 80%, the cells were collected for seeding.

To seed the cells in multi-well plates, the medium was removed from the flask, and cells were washed with PBS. Trypsin-EDTA was added to the volume of 2 ml to the flask to detach the cells and left for incubation at 37 °C and 5% CO₂, 2 minutes for melanoma cells, and 4 minutes for keratinocytes. After the cells were detached, 6 ml of DMEM was added to the flask, and cells were suspended and collected. The media containing trypsin-ETDA was centrifuged for 5 minutes at 15,000 rpm. The supernatant was removed afterward, the cell pellet was re-

suspended in fresh DMEM and added to a new T-75 flask containing 10 ml of fresh DMEM. Passage numbers 13-17 were used for cell experiments.

To seed the cells in multi-well plates, the pellet was re-suspended in 1 ml DMEM and was transferred to an Eppendorf tube. To count the cells, 10 μ l of the cell suspension was mixed with 10 μ l Trypan Blue dye and incubated for 2 minutes. Then 10 μ l of the dyed cell suspension was pipetted into cell counting chamber slides and the cells were counted using Countess™ II FL Automated Cell Counter (Thermo-Fischer Scientific, A27974).

Subsequently, the cells were seeded in suitable multi-well plates with a density of 10^6 cells per well in 6 well plates, and 10^5 cells per well in 96 well plates. Plates were incubated under the same conditions. Cell treatments were done after 8 hours while the cells were attached to the plates. The cell culture condition remained unchanged for all the cell-culture-based experiments and for all the time points.

2.2.8 Mitochondrial activity (MTT) cytotoxicity assay

To explore the viability of cells treated with drug-loaded and non-loaded nano-emulsions, MTT (3-(4,5-dimethylthiazol-2-yl)-2,5-diphenyltetrazolium bromide) assay was conducted. Cells (A375 and/or keratinocyte) were collected from T-75 flasks and seeded in 96 well plates with a density of 10^5 cells per well, then they all were incubated with 1-18 nano-emulsion preparation using three doses of 10, 20, and 30 μ l/ml of culture medium during 72 hours. After the treatments, MTT dye (3-(4, 5-dimethylthiazol-2-yl)-2, 5-diphenyltetrazolium bromide)) (Figure m 5) (2.1g/ml) equivalent to 1/10 of culture medium was added to each well. The plate containing dye was incubated for 4 hours at 37 C° and 5% CO₂. After incubation, the culture

medium was removed. DMSO to the volume of 200 μ l was added to the wells and incubated overnight at room temperature (25°C) in dark. The optical density (OD) of the wells was obtained at 570nm by an ELISA reader. The results were obtained as the percentage of control (untreated cells).

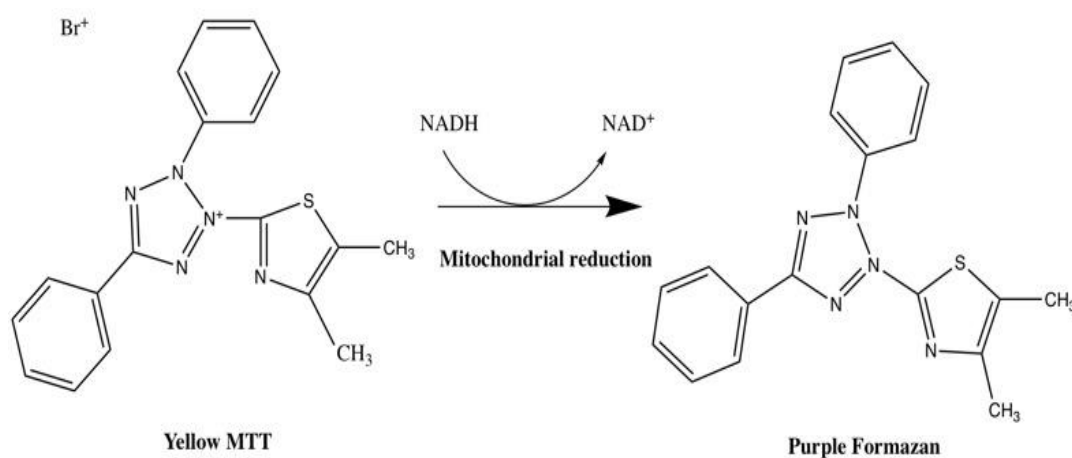


Figure 2.1 Mitochondrial reduction happening during MTT assay

2.2.9 Cellular uptake test using confocal microscopy

To screen the uptake of the nano-emulsion particles in A375 and HaCaT confocal microscopy was used. As nano-emulsions were loaded with doxorubicin and coumarine-6 separately, after the treatment the cells were imaged. The fluorescent intensity of both doxorubicin and coumarine-6 was used as to observe the nano-emulsion particle's uptake in the cells. To conduct cellular uptake experiments, cells were seeded into 6 well plates with a density of 5×10^6 cells per well and were treated with coumarin-6 and doxorubicin-loaded nano-emulsion. The uptake

of the coumarin-6 and doxorubicin-loaded nano-emulsions was measured for both HaCaT and A375 cells after specific treatment periods (4 hours, 24 hours, 48 hours, and 72 hours). After the treatments, the medium was removed from the wells, and all wells were washed with PBS twice. The cells were fixed using 4% (v/v) formaldehyde. For this, formaldehyde (50 μ l) was added to the media into each well and left for 5 minutes, then the media were removed and 250 μ l of formaldehyde was added to each well to cover all the cell surface and incubated for 20 minutes for cells to fix. Cells were washed with PBS twice and 2 ml of PBS were added to the wells for confocal microscopy (Leica TCS SP2).

To obtain images for coumarin-6, FITC filter was used (λ_{max} 488nm). Images were obtained along Z-axis (Z wide) and Z position was set to 0.1 μ m per turn (objective HCX APOLU-V-1 63X0.9W, pixels 1024 X 1024, pinhole 1 airy unit, stack 0.5 μ m thick). Images for doxorubicin (excitation 543 nm, emission long-pass filter 570 nm) were obtained under the same conditions. After the cells were observed using confocal microscopy, the fluorescence intensity was quantified using Image J, to identify the cellular uptake.

2.2.10 Fluorescent microscopy

For more investigation on the cell morphology after the treatments with drug loaded nano-emulsion, fluorescent microscopy was conducted. The microscopy imaging of the cells was conducted using an EVOS fluorescent microscope. The cells were initially labelled with cell tracker red (CMTPX) and cell tracker green (CMFDA) florescent probes according to the manufacturer's protocol (Zouani et al., 2013). For CMFDA labelling, 107 μ l of DMSO was added to one of the CMFDA vials provided by the manufacturer to make a 1 mM stock solution.

To make 10 μ M working solution, 50 μ l of the stock solution (1 mM) were diluted in 5 ml of serum-free DMEM. For CMT PX, 72 μ l of DMSO was added to the CMT PX vial; again 50 μ l of the stock solution was diluted in 5 ml serum-free DMEM to make 10 μ M working solution. To label the cells, HaCaT and A375 cells were previously passaged and seeded in a T-75 flask. After the cells became confluent, the media was removed and the cells were washed with PBS twice. Five ml of CMFDA working solution was added to the A375 flask and 5 ml of CMT PX working solution was added to the HaCaT flask. The flasks were incubated for 30 minutes in an incubator. Afterward, media from both flasks were removed and the cells were washed with PBS twice. The labelled cells were detached using trypsin-EDTA and collected for subsequent seeding in the 6 well plates. After the attachment of the cells, nano-emulsion treatments were applied. Cells were imaged for durations of 24 hours, 48 hours, and 72 hours afterward.

DAPI stain was used to image the cell nuclei. Deionized water (2 ml) was added to the entire content of the DAPI vial to make a 5 mg/ml stock solution. To make a 300 μ M DAPI intermediate solution, 2.1 μ l of DAPI stock solution, was added to 100 μ l of PBS. The intermediate solution was diluted 1:1000 in PBS to make a 300 nM solution. To commence the staining, the cells were washed with PBS twice. A sufficient amount of 300 nM DAPI solutions (approximately 250 μ l) was added to cells to cover their surface. The plates were incubated for 15 minutes protected from light, at room temperature. After incubation, the stain was removed and the cells were washed with PBS twice. They were then imaged using the DAPI filter in an EVOS microscope (M5000 Thermo-Fischer Scientific). Cells that demonstrated decreased nuclear size, condensation of chromatin, and intensive fluorescent emission are considered as apoptotic.

Images of CMFDA-probed cells were taken at excitation 492 nm and emission 517 nm and GFP filter on EVOS microscope. CMTPIX was imaged at excitation 577 nm and emission 602 nm using an RFP filter.

2.2.11 DNA fragmentation ELISA

The apoptosis process includes activation of endonucleases leading to fragmentation of chromatin to oligonucleosomal fragments (approximate sizes of 180 bp). These DNA fragments appear in the early stages of apoptosis. One of the approaches to detect these fragments is DNA fragmentation ELISA (Salgame et al., 1997). DNA fragmentation ELISA was used in this section to detect early apoptosis as it is a highly sensitive monoclonal-antibody-based assay (Jablonski et al., 2017, George and Rupasinghe, 2017).

Cellular apoptosis ELISA experiment was done to specify the doxorubicin-loaded nano-emulsions apoptosis induction-ability on melanoma and keratinocyte cells. A cellular apoptosis experiment was conducted using cellular fragmentation ELISA kit, following the manufacturer protocol. After confluency of about 80%, cells were treated with trypsin-EDTA to detach from the flask. After 30 seconds, 5 ml of media was added to the flask and the cell suspension was centrifuged for 5 minutes at 15000 rpm. The supernatant was removed, and the cell pellet was re-suspended in a fresh medium. BrdU (Bromodeoxyuridine/ 5-bromo-2'-deoxyuridine) labelling solution was added to the medium to prepare the final concentration of 10 μ M and the cell suspension was incubated overnight in the incubator. After incubation time, BrdU cell suspension was centrifuged for 10 minutes at 250 \times g. The supernatant was taken out and the labelled cells were re-suspended in a fresh medium. BrdU labelled cells were seeded into

triplicate wells of round bottom 96 well plates to a final concentration of 1×10^5 cells/ml. The cells were treated with 10 μ l/ml of nano-emulsions (section 2.2.5) and incubated for 4, 24, 48, and 72 hours. After the incubation, plates were centrifuged for 10 minutes at $250 \times g$, and supernatants were removed thoroughly. Incubation solution was added to the remaining cells to lyse them. For this, the plates were incubated for 30 minutes at room temperature and then centrifuged. Supernatants were collected from each well and then added to triplicate wells pre-coated plates for ELISA photometric measurements using an ELISA reader (BMG, Labtech).
Add the full protocol detail

2.2.12 Folate binding protein ELISA

Folate receptors are overexpressed in most cancer cell lines. However, to confirm and identify the folate receptor expression concentration on melanoma cells (A375) folate binding protein (FBP) ELISA was done (Ogboodu et al., 2015). Accordingly, cell supernatants from A375, HaCaT (negative control), and MDB MA-231 (positive control) cell lines were used for the assay. Preparation of all the reagents, samples, and standard stock solutions was based on the manufacturer's protocol. Standard solution (100 μ l) and sample solutions were added to the appropriate wells of the pre-coated ELISA plate. The plate was incubated at 37 °C for 90 minutes. The content of the plate was tapped out after the incubation and 100 μ l of biotinylated antibody was added to the wells and incubated for 60 minutes at 37 °C. The wells were washed with 300 μ l of 0.01 M PBS three times. After the washing, 100 μ l of Avidin-biotin-peroxidase complex (ABC) working solution was added and the plate was incubated at 37 °C for 30 minutes. The wells were washed again and 90 μ l of TMB (3,3',5,5'-Tetramethylbenzidine) was

added to the wells and incubated at 37 °C in dark for 15-20 minutes. TMB stop solution with the volume of 100 µl was added to the wells afterward, and the OD of the wells was read at 450 nm within 30 minutes.

2.2.13 Co-culture of HaCaT and A375 cells

To observe the effect of the drug-loaded nano-emulsions on both A375 and HaCaT cell lines, the treatments were conducted on the co-culture of both cells. The co-culture of HaCaT and A275 was also a primary monolayer model to study the effect of drug-loaded nano-emulsion as a topical delivery system for melanoma. Previously fluorescent labelled A375 and HaCaT cells 2.2.10) were seeded in 6 well plates with a ratio of 1:5 respectively and grown in DMEM. Plates were incubated at 37°C and 5% CO₂. After 12 hours, the seeded and labelled cells were treated with 10 µl/ml of drug-loaded nano-emulsions in duplicate wells, incubated for 72 hours, and imaged using fluorescent microscopy.

2.2.14 Polymerase chain reaction

Polymerase chain reaction (PCR) was performed to screen the apoptosis-associated proteins caspase-3 (Duan et al., 2020), and caspase-9 (Chen et al., 2019). Bax (Pan et al., 2019) a pro-apoptotic gene, and Bcl2 (Pan et al., 2019) an anti-apoptotic gene expression were also screened using a PCR methodology. This methodology was used as a qualitative method screening of the gene expressions in the treated cells.

2.2.14.1 RNA extraction using TRIzol method

Total RNA was extracted directly from the treated cells in 6 well plates (cell density of 5×10^6) using TRIzol reagent. Initially, the media was removed and cells were washed with PBS. Using 1ml of TRIzol, the content of 3 wells was pooled together and mixed well. The lysate was then transferred to 1.5 ml Eppendorf microcentrifuge tubes containing 1.5 μ l Glycobblue co-precipitant. Chloroform at 200 μ l/ml of TRIzol was added to each tube. The content of each tube was mixed by inversion for 10 seconds and left for incubation for 5 minutes at room temperature. The mixture was then centrifuged at $12,000 \times g$ for 15 minutes at 4 °C.

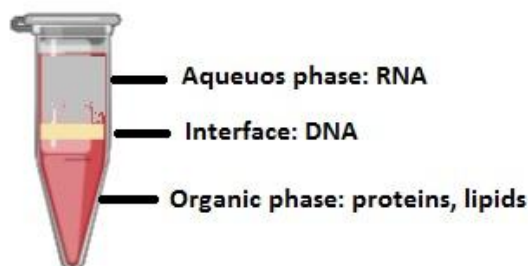


Figure 2.2 Organic, interface, and aqueous phases after treating with TRIzol.

After centrifugation, the upper phase was removed fully and accurately added to a new tube. Isopropanol at half of the original TRIzol was added to each tube and gently mixed by inversion three times followed by centrifugation at $12,000 \times g$ for 10 minutes at 4°C. The supernatant was removed leaving a blue pellet behind. The pellet was washed using 500 μ l of 75% ethanol by gentle inversion and flicking. The tube was centrifuged at $10,000 \times g$ for 5 minutes at 4°C.

The pellet was then air-dried and RNA was re-suspended in 44 µl of nuclease-free water. The RNA quality was measured and quantified using nano-drop in the table below (Table 2.14) (Thermoscientific UK).

Table 2.14 RNA quantification and quality by nano-drop

Treatment	A375 cell line (ng/µl)	HaCaT cell line (ng/µl)	260/280 ratio	260/230 ratio
Doxorubicin-loaded modified nano- emulsion	770.01	263.5	2.10	2.09
Dacarbazine-loaded modified nano- emulsion	810.08	351.1	2.12	2.08
Doxorubicin-loaded nano-emulsion	697.0	1084.5	2.10	2.10
Dacarbazine-loaded nano-emulsion	659.9	264.3	2.11	2.10
Naïve doxorubicin	332.3	313.3	2.25	2.07
Naïve dacarbazine	983.3	396.6	2.11	2.05
Control	683.5	248.2	2.11	2.13

2.2.14.2 RNA purification and DNase treatment

The extracted RNA samples were DNase treated using the DNA purification kit according to the manufacturer's recommendations. The volumes used are shown in the table below Table 2.15.

Table 2.15 RNA purification and reagents

RNA	17 µl
DNase (buffer)	2 µl
DNase enzyme	1 µl

The mixtures were incubated for 15 minutes at 25 °C in a thermocycler. EDTA was then added to all samples to the volume of 1 µl and incubated for 10 minutes at 65 °C. All the samples were run on the gels to detect the total, DNA-free RNA.

2.2.14.3 Preparation of cDNA

The extracted and purified RNA was used for complementary DNA synthesis. The RNA was converted to cDNA using a superscript II reverse transcriptase kit (Invitrogen). The total extracted and purified RNA (500 ng) was used for cDNA synthesis. To commence, Oligo (dT)₁₂₋₁₈ and dNTP mix was added to nuclease-free microcentrifuge tubes (1 µl each). Nuclease-free sterile water was added to each sample to the total volume of 12 µl. Finally, 4 µl of purified RNA was added to the tubes. The mixture was heated to 65°C for 5 minutes. Subsequently, the tubes were promptly chilled on ice. In the next step first strand buffer 5x, 0.1 M DTT, and

RNAse OUT to the volumes of 4, 2, and 1 µl respectively, were added to the tube. The mixture was gently mixed and 1µl of superscript II was added to the tube. The mixture was incubated at 42 °C for 50 minutes followed by reaction inactivation for 15 minutes at 70 °C.

2.2.14.4 Thermo-cycling, an agarose gel electrophoresis analysis

PCR was done using 5 µl of PCR master mix (2X), 0.5 µl forward and reverse primers, 1 µl of cDNA template, and Nuclease free water up to 12 µl (Si et al., 2018).

The mixtures were gently vortexed and spun down. The samples were put in a thermal cycler with the conditions as follows:

Table 2.16 PCR cycles and conditions

Step	Temperature °C	Time	Number of cycles
Initial denaturation	95	2 minutes	1
Denaturation	95	30 seconds	
Annealing	55	30 seconds	30
Extension	72	2 minutes	
Final extension	72	15 minutes	1

To visualise the amplified DNA, agarose gel electrophoresis was used. Agarose gel (1% w/v) was prepared before the experiment. The agarose powder (1 gr), was added to 100 ml of TAE (Tris-acetate-EDTA) buffer and heated in a microwave until the solution was clear and the agarose was dissolved. The agarose solution was cooled down at room temperature, and a 2% v/v Gel red DNA stain was added to the solution to visualise the DNA under UV light. The

agarose solution was then poured into the gel electrophoresis tray and was left to set at room temperature. After solidifying, the gel was placed in the tank and TAE buffer was added.

After the thermo-cycler step, the samples were collected and mixed with 3 μ l of loading dye (Thermo-Scientific 6X DNA loading dye). The mixture was then loaded into the wells of 1% agarose gel in the tank.

A molecular weight marker of 1Kb and 100 Kb were used alongside the cDNA samples. Electrophoresis was set to run for 60 minutes in the 100 V constant. After 60 minutes, the gel was imaged using the UV transilluminator at the wavelength of 200-280 nm and the DNA fragments were detected.

2.2.15 Western blotting

2.2.15.1 Protein extraction using TRIzol method

The western blot experiment was carried out in order to screen and identify the iNOS and COX-2 expression in A375 cells treated with anti-inflammatory compound-loaded nano-emulsion. Before performing Western blotting, the total protein content of the cells (5×10^6 cells per well) was extracted directly from the treated cells in 6 well plates, media was removed and cells washed with PBS once before the addition of, 1 ml of TRIzol, the content of 3 wells were pooled together and mixed well. The lysate was then transferred to 1.5 ml Eppendorf micro-centrifuge tubes, chloroform, 200 μ l per 1 ml of initial TRIzol was added to each tube. The content of tubes was mixed by inversion for 10 seconds and left for 5 minutes at room temperature and centrifuged at 12,000 x g for 15 minutes at 4 °C. The upper aqueous phase and

interface were discarded, and the organic phase was kept for protein extraction. Isopropanol was then added to each tube (0.8 ml per 1 ml of TRIzol). Samples were incubated for 10 minutes at 15-30 °C, and protein centrifuged at 7,500xg for 5 minutes at 2-8 °C. The supernatant was removed and the protein pellet washed three times using 0.3 M guanidine hydrochloride solution in 95% ethanol (2 ml of wash buffer was used per 1 ml of initially used TRIzol). During each wash step, the protein pellet was kept in the solution for 20 minutes at 15-30 °C, then centrifuged at 7,500xg for 5 minutes at 2-8 °C. Following the final wash step, the pellet was stored in ethanol for 20 minutes at 15-30 °C and then centrifuged at 7,500xg for 5 minutes at 2-8 °C. The pellet was vacuum dried and dissolved in 1% SDS by continuous pipetting. The step was completed on a heat block at 50 °C. Final centrifugation at 10,000xg for 10 minutes at 2-8°C was done and the supernatant was removed to a fresh tube and stored at -80 °C for western blotting.

2.2.15.2 SDS 10% polyacrylamide gel electrophoresis (SDS-PAGE)

Extracted proteins were prepared and loaded onto SDS page gel; Subsequently, 25 µl of each protein extracted was mixed with 25 µl of 2x laemmli loading buffer (4% SDS, 10% 2-mercaptoethanol, 20% glycerol, 0.004% bromophenol blue, 0.125 M Tris-HCL, pH 6.8), and boiled at 95 °C water for 5 minutes. Samples were centrifuged down at 12,000 g for 1 minute and 20 µl of each sample was loaded into each well of precast SDS 10% polyacrylamide gels along with protein molecular markers (prestained protein MW marker). The tank was filled with running buffer (containing 25 mM tris, 190 mM glycine, and 20% methanol) and the gel was run at 50 V constant for 5 minutes and then 100 V for 1 hour.

2.2.15.3 Protein transfer

Following running the gel, the gel cassette was placed in the Western blot running buffer for 10-15 minutes and the gel was removed from the cassette to prepare the transfer sandwich. Nitrocellulose membrane(s), Western blot papers, and sponges were soaked in Western blot buffer for a few minutes and the gel was placed in a Western blot sandwich, with the gel on the anode side and the blot on the cathode side. The cassette was placed in the Western blot tank alongside an ice block (-20 °C) to keep the buffer cold using a magnetic stirrer. The transfer was run for 150 minutes at 30 mA.

After the Western blotting step, the blot was removed and placed in TBST (Tris buffer saline containing tween 20). The blot was rinsed with dH₂O and stained with 0.2% Ponceau S in 10% v/v acetic acid for 1 minute to assess transfer quality (Figure 2.3) The blot was then blocked with 5% non-fat milk in TBST for 2 hours and rinsed with TBST for 5 minutes 3-5 times.

Following blocking, the blot was then incubated with primary antibodies against target proteins (anti-Cox-2 and anti iNOS antibodies (Abcam, ab15191 and ab 3523)). The antibody (dilution factor 1:200) was dissolved in TBST and then blot was incubated with the primary antibody at 4 °C overnight. Following incubation, the blot was washed with TBST 3-5 times and incubated with the secondary antibody -mouse α -tubulin antibody- solutions for 1 hour at room temperature.

The protein bands were visualized by incubating the blot in 3 ml of TMB solution for 10 minutes. The blot was washed with dH₂O and imaged using UVP Image Capture System.

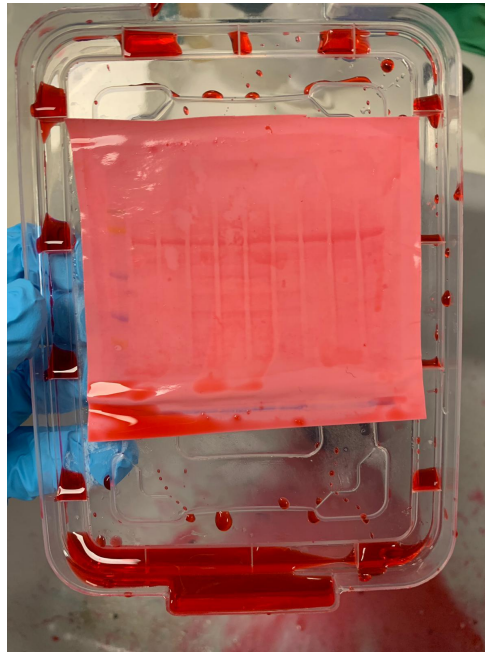


Figure 2.3 Western blot stained Ponceau S

2.3 Statistical analysis

The experiments conducted in this research were repeated at least three times ($n=3$) unless stated in the results. The acquired data were analysed using GraphPad software and ECXEL. Two-way ANOVA, Tukey's multiple comparison test was performed to compare the significant differences in the same treatment groups. Any set of data with $P<0.05$ is considered statistically significant.

3 Results

3.1 Synthesis and optimisation of nano-emulsion for enhanced drug delivery to melanoma

3.1.1 Introduction

One of the important factors causing an increase in drug-resistance in melanoma (at the cellular level) is the inefficient and uncontrolled (too low or too high) drug efflux (Xue and Liang, 2012) in delivering chemotherapeutics (Yuan et al., 2016). It has been reported that polysaccharides have unique potential in cancer drug delivery (Posocco et al., 2015), such as enhanced uptake in the cancer cells (Dheer et al., 2017). In this chapter, novel synergy of chitosan, pullulan and alginate were investigated with the intention of uptake enhancement and chemo-resistance defeat in melanoma (Gilani et al., 2018).

The *in vitro* characteristics of chitosan-pullulan, pullulan-alginate, and alginate-chitosan polymer blends as nano-emulsions, as described in this chapter. Based on release profiles, the nano-emulsion samples were narrowed down to top-nine.

Subsequently, the toxicity to the A375 and HaCaT cell lines, release, and uptake of drug-loaded nano-emulsions were measured.

Furthermore, apoptosis induction of doxorubicin delivery was evaluated by DNA fragmentation ELISA and based on the results, the optimal nano-emulsion was selected for further investigations.

The flow-chart below indicates the work carried out in brief Figure 3.1

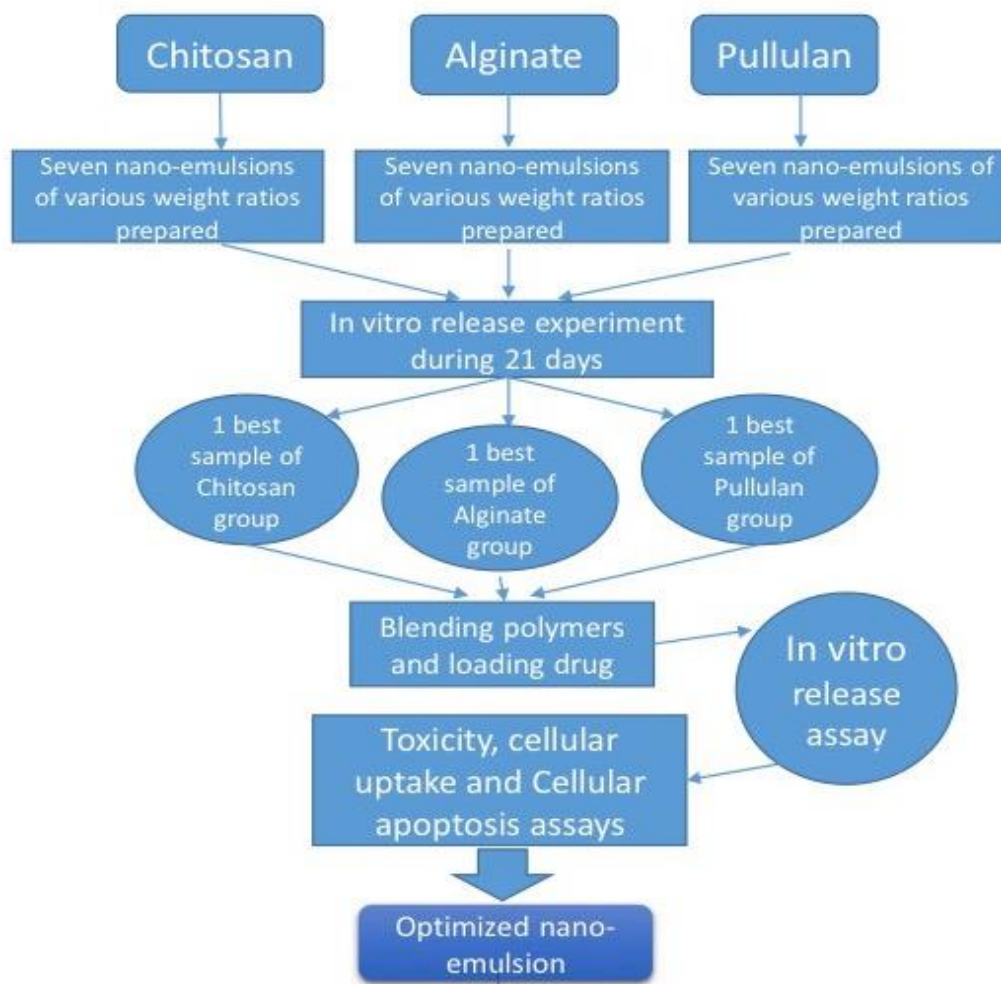


Figure 3.1 Flow-chart of the development and optimisation of nano-emulsions

3.1.2 Synthesis and evaluation of polymeric nano-emulsions characteristics

3.1.2.1 Evaluation of *in vitro* release of coumarin-6 and doxorubicin from chitosan, pullulan, and alginate nano-emulsions

A set of experiments were carried out to monitor the release of doxorubicin and coumarin-6 from pullulan, alginate, and chitosan nano-emulsions. In the previous investigations, the three polymers individually presented unique characteristics in drug delivery systems, and they were subjected to various modifications and combinations in previous investigations (Ahmed and Aljaeid, 2016, Vora et al., 2020, Cheng et al., 2019a, Yu et al., 2017).

However, in this research as a novel approach, the polymer combinations were compared to each other. Chitosan, alginate, and pullulan all have different surface charges. So the surface charge was considered as one of the factors influencing release profile and consequently the stability of the nano-emulsion.

Each of the nano-emulsions was prepared with different amounts of polymers. The profile of coumarin-6 and doxorubicin release from nano-emulsion was measured by the dialysis method for 21 days. Initial burst (release in 0-24 hours) of coumarin-6 from chitosan nano-emulsions ranged between 0 to 30%, for pullulan nano-emulsions the range was 1 to 17.5%, and for alginate ranged between 1 to 5%. The initial burst of doxorubicin from chitosan nano-emulsions ranged between 0 to 9% for pullulan nano-emulsions the range was 1.7 to 14%, and for alginate ranged between 2.25 to 11.9%. Nano-emulsions that showed the steadiest release (fewer fluctuations over 21 days) and the lowest initial burst were chosen for blending. The release

profiles were recorded for both coumarin-6 and doxorubicin-loaded nano-emulsions. In both cases, the data were collected from 3 independent experiments and calculated as percentages of naïve coumarin-6 and doxorubicin control values. Recorded profiles for doxorubicin release was steadier and showed less fluctuation with a lower initial burst.

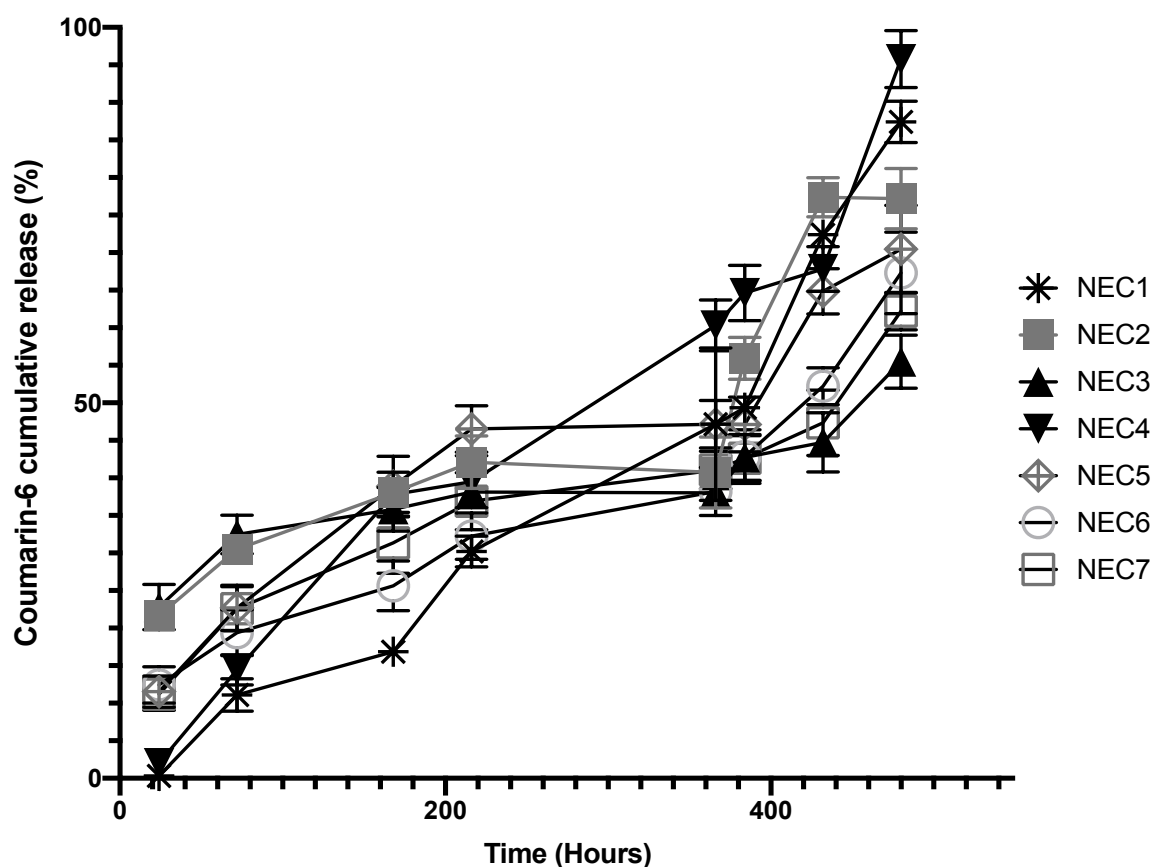


Figure 3.2 Coumarin-6 cumulative release from chitosan nano-emulsions

The nano-emulsions were prepared (0.1, 0.2, 0.3, 0.4, 0.5, 0.6 and 0.7 w/v %), loaded with coumarin-6 and screened for 21 days. The release data was measured by spectrophotometer at 7 different time points over 21 days. The experiment was conducted using the dialysis method at 25°C and 55 rpm with continuous stirring. Liquid samples from the flasks analysed using UV-spectrophotometer at 450 nm wavelength. The results were normalised to naïve coumarin-6 release (control) and are demonstrated as the percentage of the control. The data were obtained from 3 independent experiments and presented as mean \pm SD error bars.

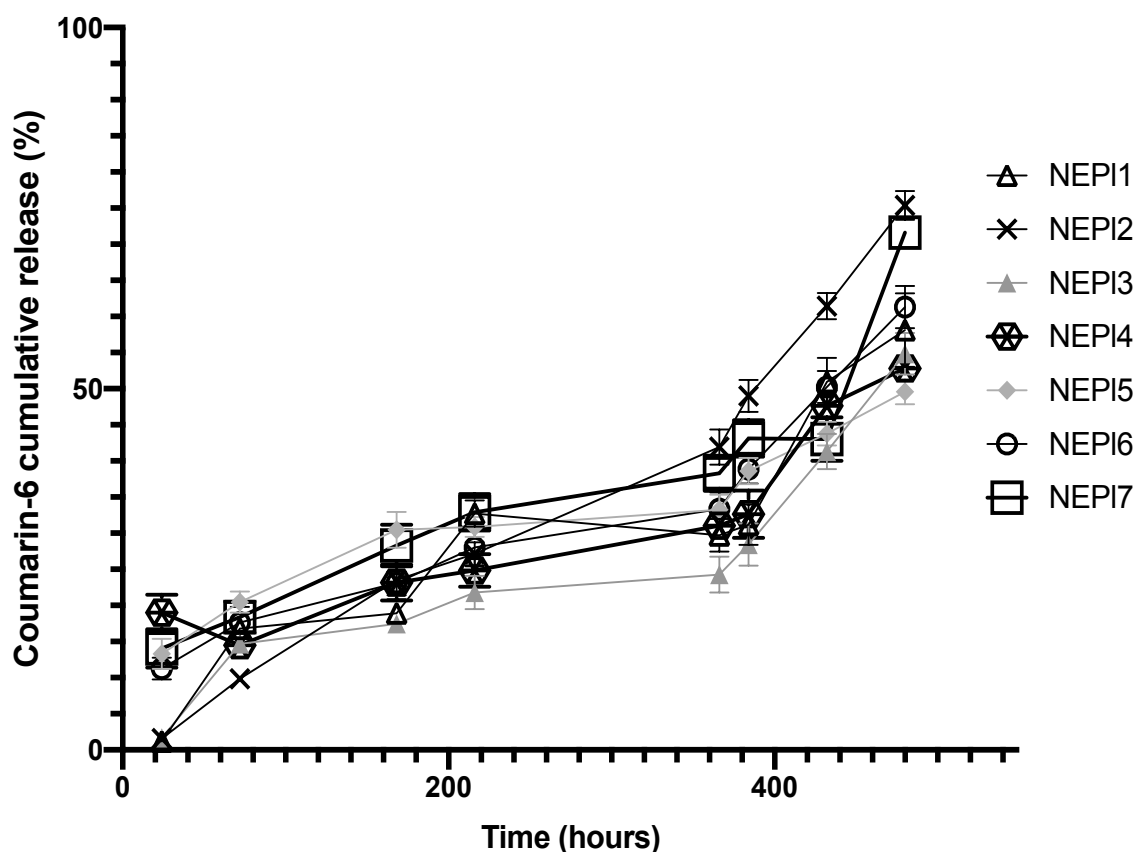


Figure 3.3 Coumarin-6 cumulative release profile from pullulan nano-emulsions

The nano-emulsions were prepared (0.1, 0.2, 0.3, 0.4, 0.5, 0.6 and 0.7 w/v %), loaded with coumarin-6 and screened for 21 days. The release data was measured by spectrophotometer at 7 different time points over 21 days (n=3). The experiment was conducted by dialysis method at 25°C and 55 rpm with continuous stirring. Liquid samples from the flasks analysed using UV-spectrophotometer at 450 nm wavelength. The results were normalised to naïve coumarin-6 release (control) and are demonstrated as the percentage of the control. The data are obtained from 3 independent experiments and presented as mean \pm SD error bars.

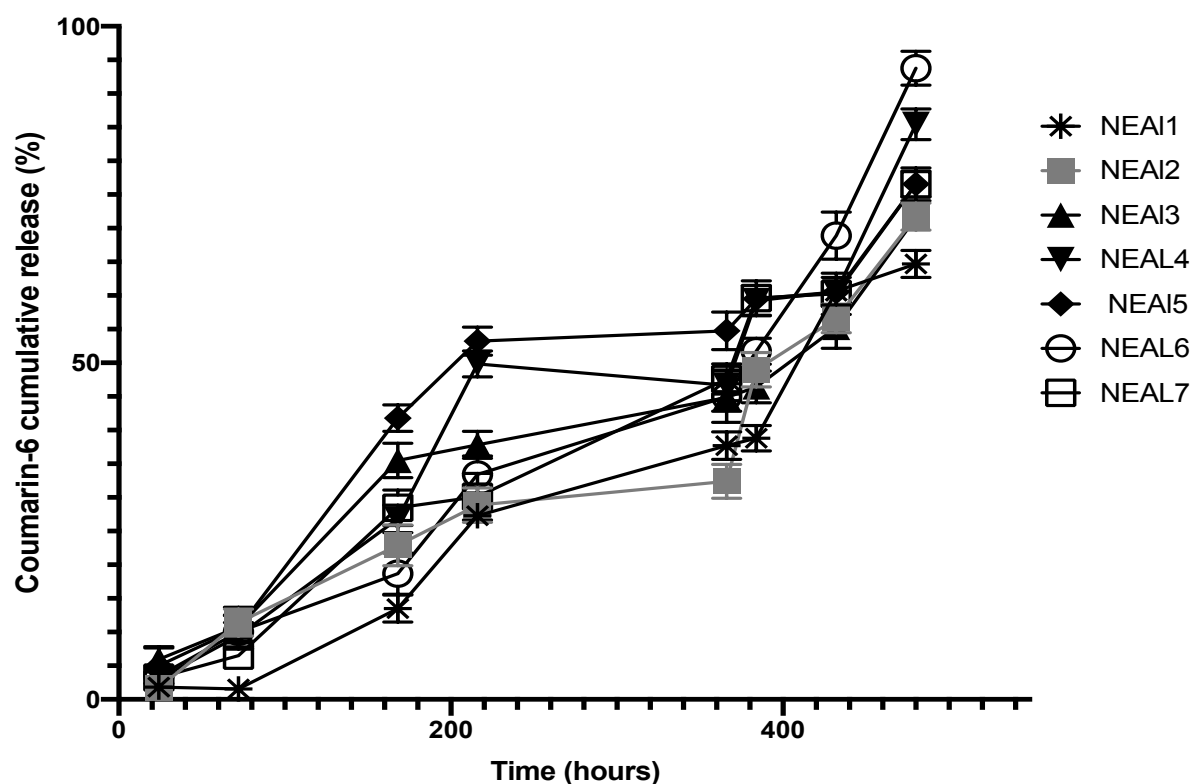


Figure 3.4 Coumarin-6 cumulative release profile from alginate nano-emulsion

The nano-emulsions were prepared (0.1, 0.2, 0.3, 0.4, 0.5, 0.6 and 0.7 w/v %), loaded with coumarin-6 and screened for 21 days. The release data was measured by spectrophotometer at 7 different time points over 21 days (n=3). The experiment was conducted using a dialysis method at 25°C and 55 rpm with continuous stirring. Liquid samples from the flasks analysed using UV-spectrophotometer at 450 nm wavelength. The results were normalised to naïve coumarin-6 release (control) and are demonstrated as the percentage of the control. The data are obtained from 3 independent experiments and presented as mean \pm SD error bars.

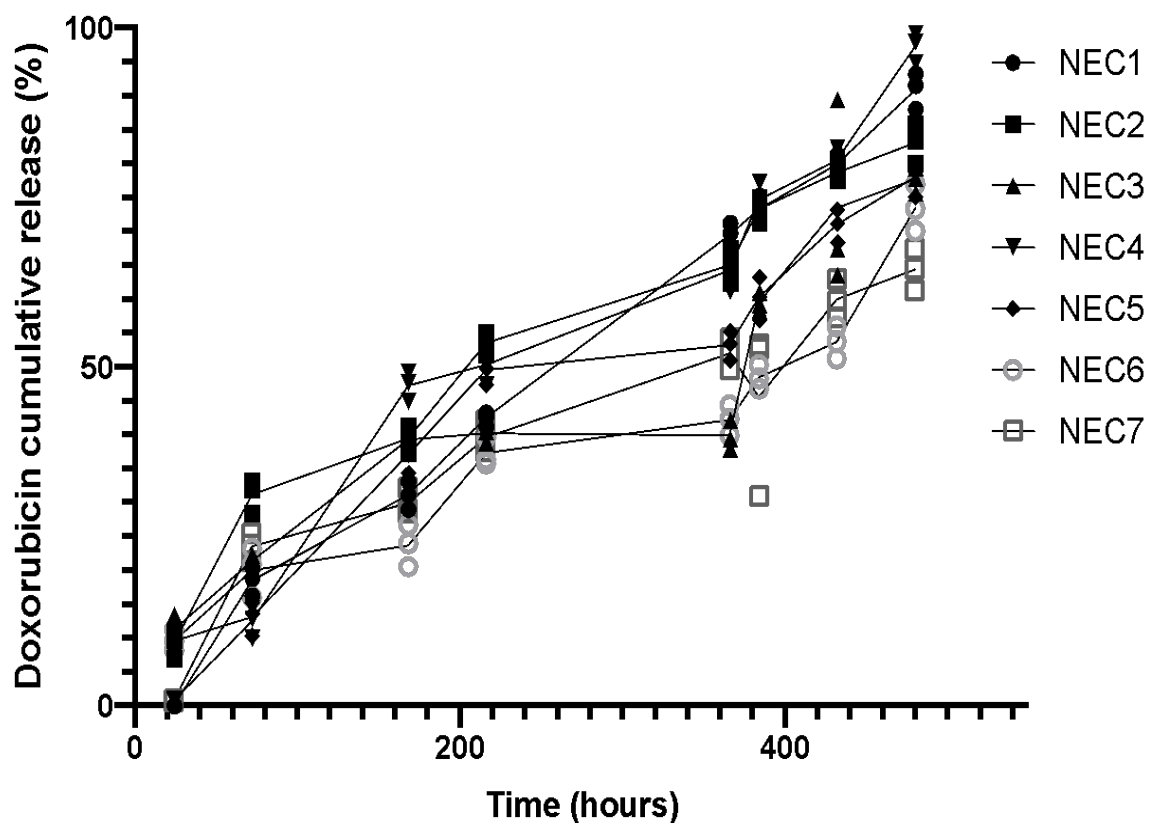


Figure 3.5 Doxorubicin cumulative release profile from chitosan nano-emulsion

The nano-emulsions were prepared (0.1, 0.2, 0.3, 0.4, 0.5, 0.6 and 0.7 w/v %), loaded with coumarin-6 and screened for 21 days. The release data was measured by spectrophotometer at 7 different time points over 21 days (n=3). The experiment was conducted using a dialysis method at 25°C and 55 rpm with continuous stirring. Liquid samples from the flasks analysed using UV-spectrophotometer at 479 nm wavelength. The results were normalised to naïve doxorubicin release (control) and are demonstrated as the percentage of the control. The data are obtained from 3 independent experiments and presented as mean \pm SD error bars.

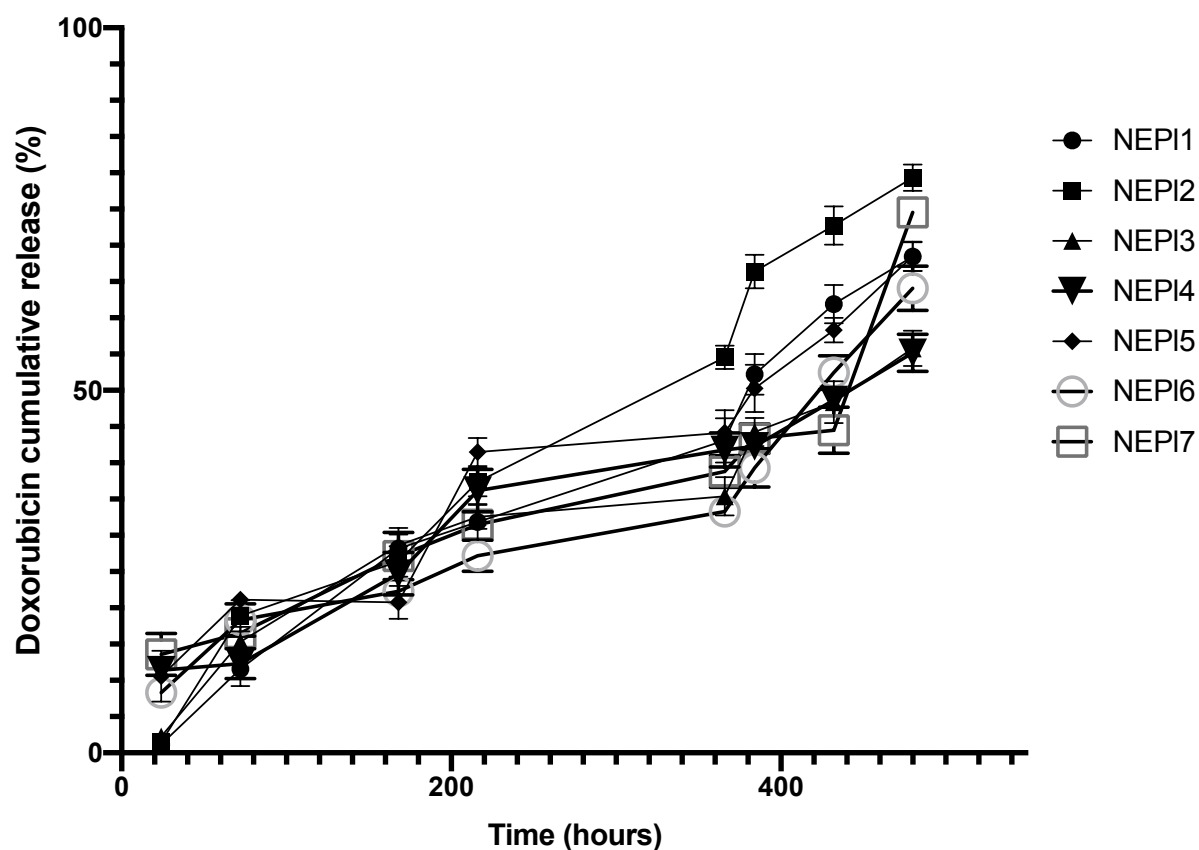


Figure 3.6 Doxorubicin cumulative release profile from pullulan nano-emulsions

The nano-emulsions were prepared (0.1, 0.2, 0.3, 0.4, 0.5, 0.6 and 0.7 w/v %), loaded with coumarin-6 and screened for 21 days. The release data was measured by spectrophotometer at 7 different time points over 21 days (n=3). The experiment was conducted using a dialysis method at 25°C and 55 rpm with continuous stirring. Liquid samples from the flasks analysed using UV-spectrophotometer at 479 nm wavelength. The results were normalised to naïve doxorubicin release (control) and are demonstrated as the percentage of the control. The data are obtained from 3 independent experiments and presented as mean \pm SD error bars.

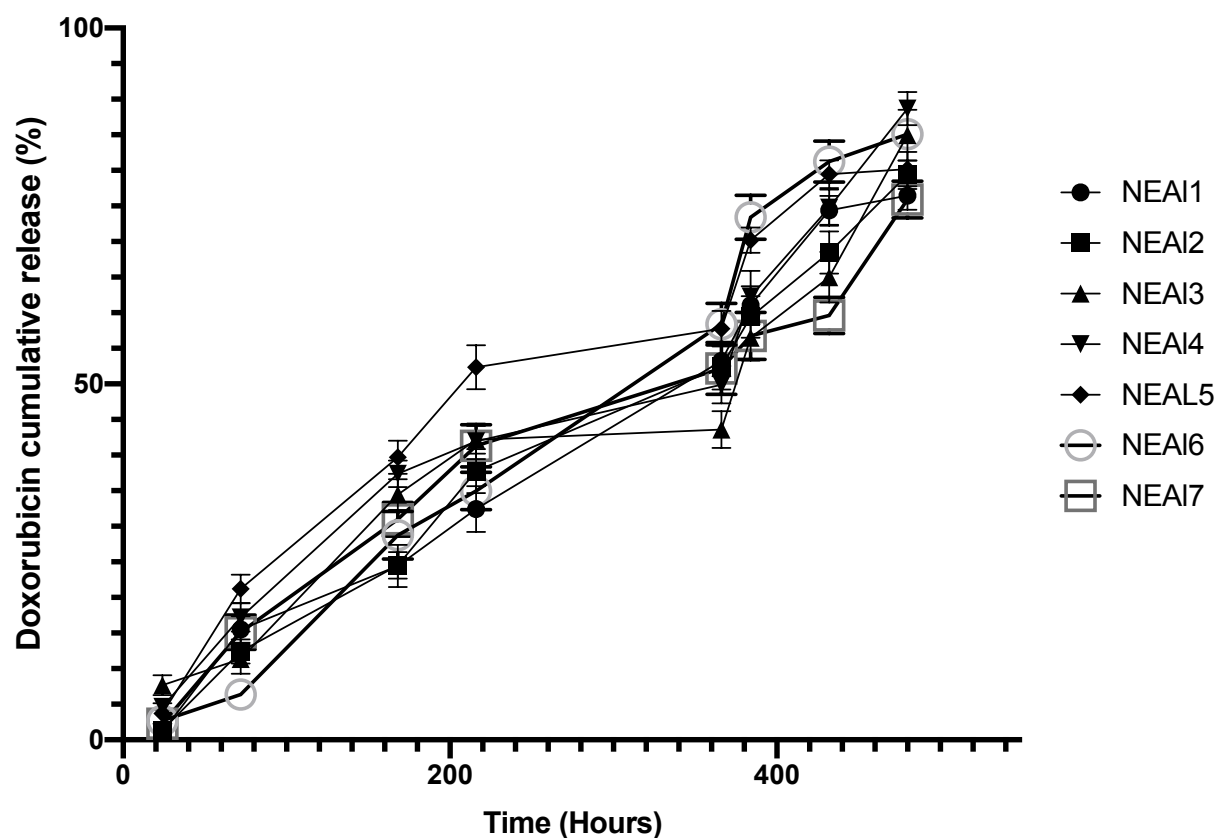


Figure 3.7 Doxorubicin cumulative release profile from alginate nano-emulsions

The nano-emulsions were prepared (0.1, 0.2, 0.3, 0.4, 0.5, 0.6 and 0.7 w/v %), loaded with coumarin-6 and screened for 21 days. The release data was measure by spectrophotometer at 7 different time points over 21 days (n=3). The experiment was conducted using a dialysis method at 25°C and 55 rpm with continuous stirring. Liquid samples from the flasks analysed using UV-spectrophotometer at 479 nm wavelength. The results were normalised to doxorubicin release (control) and are demonstrated as the percentage of the control. The data are obtained from 3 independent experiments and presented as mean \pm SD error bars.

According to the Figure 3.2 to Figure 3.7 overall release pattern for all nano-emulsions for 21 days increased over time. However, the cumulative release pattern of each nano-emulsion was different at each period.

Through the release optimisation assessment, the selection of nano-emulsions was based on the controlled and slow release pattern over time. Additionally, the minimal initial burst of release pattern was considered for the nano-emulsion selection exercise.

According to Figure 3.2 and Figure 3.5, the initial burst of chitosan nano-emulsions release profile was closest to zero for two of the samples. For pullulan nano-emulsions, three of the samples had initial bursts closest to zero. Among alginate nano-emulsions, four samples had initial bursts closest to zero.

The main objective for this experiment was to identify which nano-emulsions could provide the lowest initial burst and a steady release profile. To this end, initial bursts and overall release patterns for each nano-emulsion were carefully analysed. Accordingly, NEC1, NEPI2, and NEAI2 were chosen due to their lowest initial burst and lowest fluctuations over time.

3.1.2.2 Evaluation of in vitro release for blended chitosan, pullulan, and alginate nano-emulsions

To improve the physical characteristics of nano-emulsions, the selected nano-emulsions from section 2.2.1 were blended. Nano-emulsions that showed the steadiest release and lowest initial burst during the 21 days were chosen for blending. In section 3.1.2.1 nano-emulsions presented a slow release profile over time. However, the patterns did not concur with the desired controlled release to overcome flux-dependant resistance in melanoma. Consequently,

chitosan-pullulan, pullulan-alginate, and alginate-chitosan nano-emulsions were developed. Each of the blended nano-emulsions was prepared according to the method described in section 2.2.1 and the release profile of encapsulated coumarin-6 and doxorubicin was measured by the dialysis method for 21 days. The results were obtained from three independent experiments and were calculated as percentages of naïve coumarin-6 and doxorubicin control values. In comparison to single polymer nano-emulsions, all the initial bursts were improved and were closer to zero.

The initial burst of coumarin-6 loaded nano-emulsions ranged between 0 to 3.9%, and for doxorubicin-loaded nano-emulsions ranged between 0 to 2.7%. The release profile quality increased significantly. The initial burst reduced and the release profiles for the 21 days were steadier.

The release trends for all the samples were observed and recorded (Figure 3.8 and Figure 3.9). The best release profile for both doxorubicin and coumarin-6 release fitting the criteria appeared to be pullulan-chitosan. This nano-emulsion consisted of 4 mg/ml pullulan and 8 mg/ml chitosan (Table 2.13). However, after the analysis, the samples narrowed down to 9 best according to controlled release and steadiness over 21 days, to investigate further. Based on the findings, nine nano-emulsion samples were marked out for their superior performance: NEC1-AI 2:1, NEAI2-Cs 1:2, NEPI2-Cs 2:1, NEPI2-Cs 1:2, NEC-PI 1:1, NEC1-PI 2:1, NEPI2-AI 1:2, NEPI2-AI 2:1 and NEPI2-AI 1:1.

The drug release showed an increasing pattern over 21 days, in all cases. The release profile was detected to be about 80% during the first 72 hours for a few samples. Hence, a good extent of the drug was released, yet, in a controlled pattern to avoid resistance.

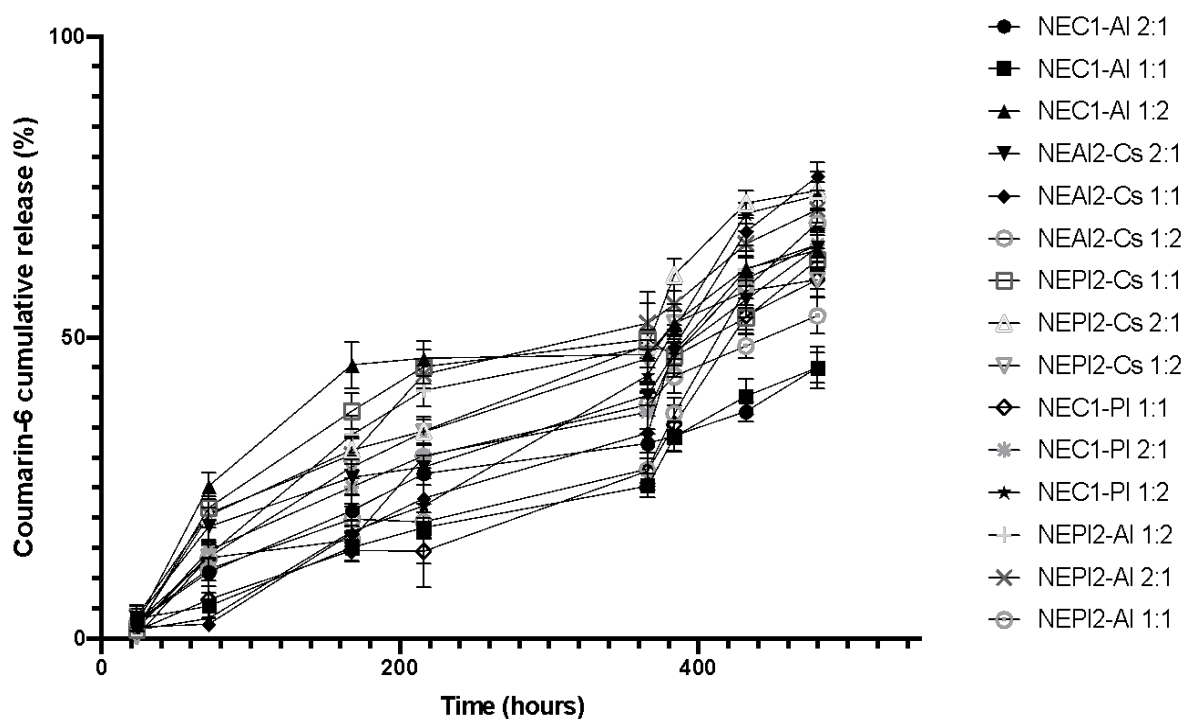


Figure 3.8 Coumarin-6 cumulative release profile from blended nano-emulsions

The nano-emulsions were prepared with three different weight ratios (1:1, 1:2, 2:1 w/w%) loaded with coumarin-6 and screened for 21 days. The release data was measured by spectrophotometer at 7 different time points over 21 days (n=3). The experiment was conducted using a dialysis method at 25°C and 55 rpm with continuous stirring. Liquid samples from the flasks analysed using UV-spectrophotometer at 450 nm wavelength. The results were normalised to coumarin-6 release (control) and are demonstrated as the percentage of the control. The data were obtained from 3 independent experiments and presented as mean \pm SD error bars.

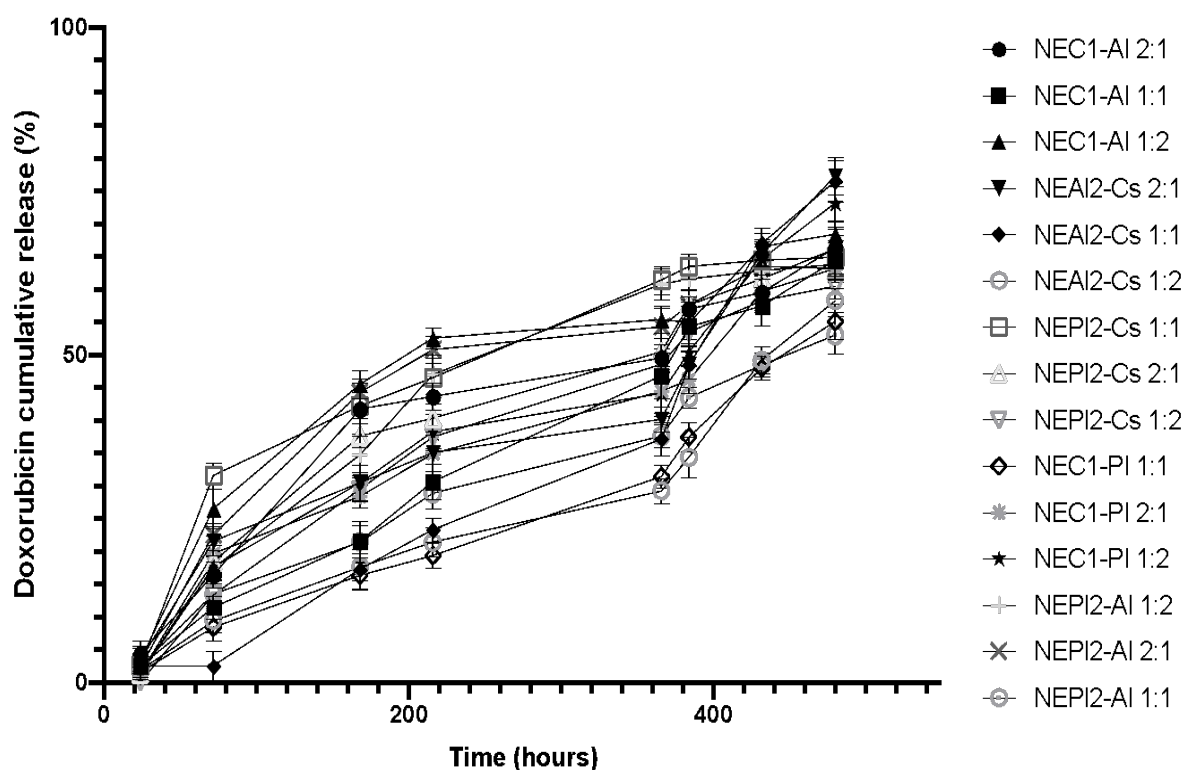


Figure 3.9 Doxorubicin cumulative release profile from blended nano-emulsions

The nano-emulsions were prepared with three different weight ratios (1:1, 1:2, 2:1 w/w%) loaded with doxorubicin and screened for 21 days. The release data was measured by spectrophotometer at 7 different time points over 21 days (n=3). The experiment was conducted using a dialysis method at 25°C and 55 rpm with continuous stirring. Liquid samples from the flasks analysed using UV-spectrophotometer at 479 nm wavelength. The results were normalised to doxorubicin release (control) and are demonstrated as the percentage of the control. The data are obtained from 3 independent experiments and presented as mean \pm SD error bars.

3.1.2.3 Viability screening of non-loaded blended nano-emulsions at three different doses

A375 and HaCaT cells were treated with 15 non-loaded blended nano-emulsions to screen the cell viability. The outcome was confirmed by MTT assay. The data were obtained from six independent experiments and outcomes are reported as a percentage of control.

Cytotoxicity assay was conducted for 15 blended nano-emulsions plus three single polymer nano-emulsions chosen in section 3.1.2.1. the cells were treated with three concentrations of 10, 20, and 30 $\mu\text{l/ml}$ of non-loaded nano-emulsions.

The viability of HaCaT cells ranged from 75.5 to 106.06% (NEPI2-AI 1:2 and NEPI2-Cs 1:2), 43.32 to 85% (NEAI2-Cs 2:1 and NEC1-AI 2:1) and 47.13 to 80% (NEAI2-Cs 2:1 and NEPI2-Cs 1:1) for treatment concentrations of 10, 20, and 30 $\mu\text{l/ml}$ respectively. A375 cell viabilities ranged from 70 to 107.48% (NEC1 and NEPI2-Cs 1:2), 56.14 to 87.71% (NEAI2-Cs 2:1 and NEC1-AI 2:1) and 28.16 to 96.99% (NEAI2-Cs 1:1 and NEPI2-AI 1:1) for treatment doses of 10, 20 and 30 $\mu\text{l/ml}$ respectively. This set of experiments aimed to choose the optimal concentration and find out the non-loaded nano-emulsions which do not decrease HaCaT viability but decrease the A375 viability. Nano-emulsion treatment concentration of 10 $\mu\text{l/ml}$ was chosen accordingly. This was used to narrow down the samples to the ones inducing higher toxicity to A375 and lower toxicity to HaCaT.

Increasing the dose to 20 and 30 $\mu\text{l/ml}$, significantly decreased the viability of both A375 and HaCaT cells to a maximum of 45% compared to untreated control, for a few treatments. Hence,

the lowest dose was chosen for treatments. However, the reason for decreased viability of both cell lines treated with increased concentration of the nano-emulsions can be further investigated with Annexin-V assay. A good example is sample NEPL2-Cs 1:2 which had a significant desirable (High HaCaT viability and low A375 viability) effect compared to other treatments.

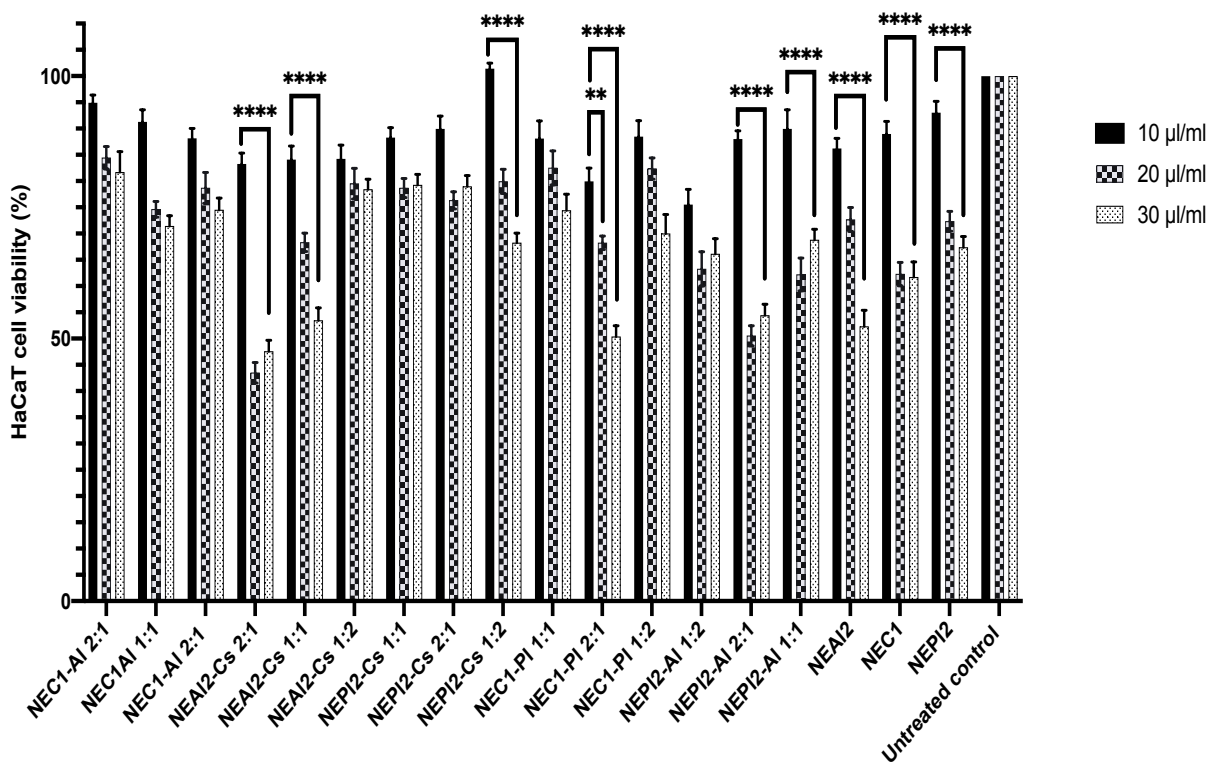


Figure 3.10 Viability screening keratinocyte (HaCaT) cells treated with non-loaded nano-emulsions

The cells were treated at three nano-emulsion concentrations of 10, 20, and 30 µl/ml. Cells were treated with 15 nano-emulsion and incubated for 72 hours. The viability data were obtained using the MTT method, results were calculated based on untreated control cells, and reported as the percentage of control. Bars represent the mean value of 6 independent experiments \pm SD error. The data were analysed with two-way ANOVA Tukey's comparison test, **** is indicating $P < 0.0001$, *** $P < 0.001$, ** $P < 0.01$, and * $P < 0.05$.

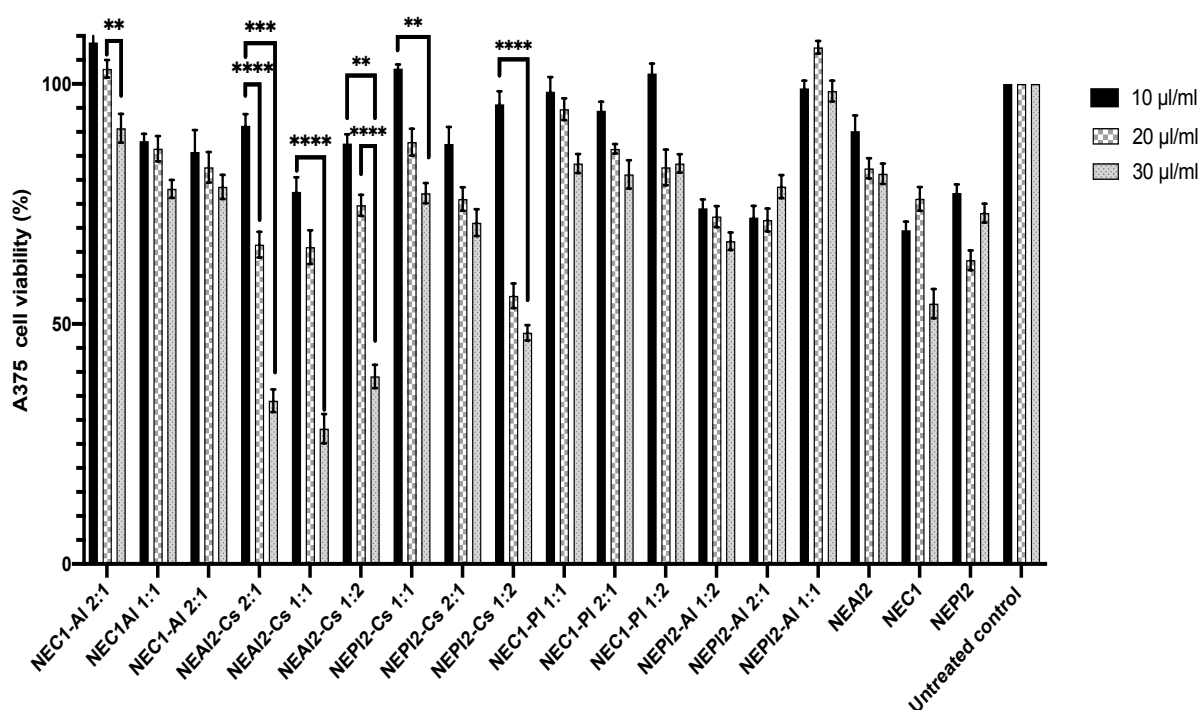


Figure 3.11 Viability screening melanoma (A375) cells treated with non-loaded nano-emulsions

The cells were treated at three nano-emulsion concentrations of 10, 20, and 30 µl/ml. Cells were treated with 15 nano-emulsion and incubated for 72 hours. The viability data were obtained using the MTT method, results were calculated based on untreated control cells, and reported as the percentage of control. Bars represent the mean value of 6 independent experiments \pm SD error. The data were analysed with two-way ANOVA Tukey's comparison test, **** is indicating $P < 0.0001$, *** $P < 0.001$, ** $P < 0.01$, and * $P < 0.05$.

3.1.2.4 Evaluation of the top-nine blended doxorubicin-loaded nano-emulsions to induce toxicity to melanoma

From the last three sections, based on MTT and release assays, the blended nano-emulsion samples were analysed and narrowed down to 9 top nano-emulsions as best fit designs for this project. The criteria for the top best were the highest possible viability for HaCaT compared to untreated HaCaT and decreased viability for A375 cells compared to untreated A375 cells. The data were obtained from 6 independent experiments and the values were calculated as a percentage of control. The results below, belong to the chosen 9 nano-emulsions.

The toxicity of top-nine nano-emulsions was monitored and compared to doxorubicin-loaded nano-emulsions and naïve doxorubicin.

The figure below (Figure 3.12) is a comparison of A375 cell viability treated with of non-loaded, doxorubicin-loaded, and naïve doxorubicin.

The viability of A375 cells treated with non-loaded nano-emulsions ranged from 35.82 to 107.07% and 25.62 to 47.22% for doxorubicin-loaded nano-emulsions while the viability of cells treated with doxorubicin is 104.55% (All the viability data assessed as percentage of untreated control). For the samples, NEC1-Al 2:1, NEPl2-Cs 2:1, NEC1-Pl 2:1, NEPL2-Al 1:2, and NEPl2-Al 1:1 viability of A375 cells significantly decreased by a range of 25-30% of control.

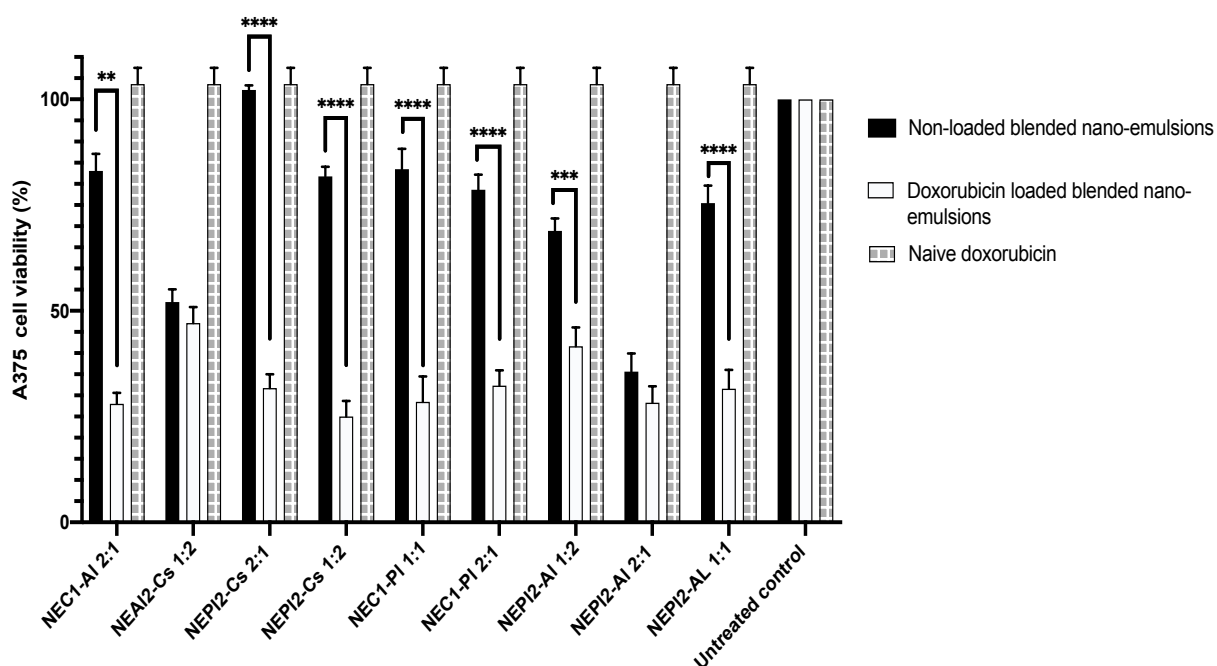


Figure 3.12 Viability of A375 cells treated with top-nine blended nano-emulsions

The cells were treated with non-loaded and doxorubicin-loaded nano-emulsions and naïve doxorubicin. The cells were incubated for 72 hours following the treatment. The viability data were obtained using the MTT method, results were calculated based on untreated control cells, and reported as the percentage of control. Bars represent the mean value of 6 independent experiments \pm SD error. The data were analysed with two-way ANOVA Tukey's comparison test, **** is indicating $P < 0.0001$, *** $P < 0.001$, ** $P < 0.01$, and * $P < 0.05$.

According to Figure 3.12 viability of the cells treated with blank nano-emulsions was significantly higher than the cells treated with doxorubicin-loaded nano-emulsions.

The results indicate that the encapsulation of doxorubicin is more effective to decrease the viability of A375 cells compared to blank blended nano-emulsions. Lower viability of cells treated with doxorubicin-loaded nano-emulsions may be the result of increased intracellular uptake of the drug-loaded nanoparticles and the subsequent effective action of the main drug (doxorubicin). Hence, while melanoma develops resistance to naïve doxorubicin (Xiao et al., 2018), encapsulated doxorubicin can be effective in treating melanoma.

3.1.2.5 Evaluation of the top-nine blended doxorubicin-loaded nano-emulsion to induce toxicity to melanoma and keratinocytes at 4, 24, 48, and 72 hours

The experiment in section 3.1.2.4 was repeated, the repeat was to screen the viability of cells treated with blank and doxorubicin-loaded nano-emulsions over 72 hours. The viability test was conducted for both A375 and HaCaT cells treated with blank blended nano-emulsions. Six independent experiments were carried on to obtain the data and the results were calculated as a percentage of control. In each treatment, the effect of both treatments on cell viability was compared. A significant decrease of viability was observed in both cell lines treated with doxorubicin-loaded blended nano-emulsions compared to the viability of cells treated with non-loaded nano-emulsion and control.

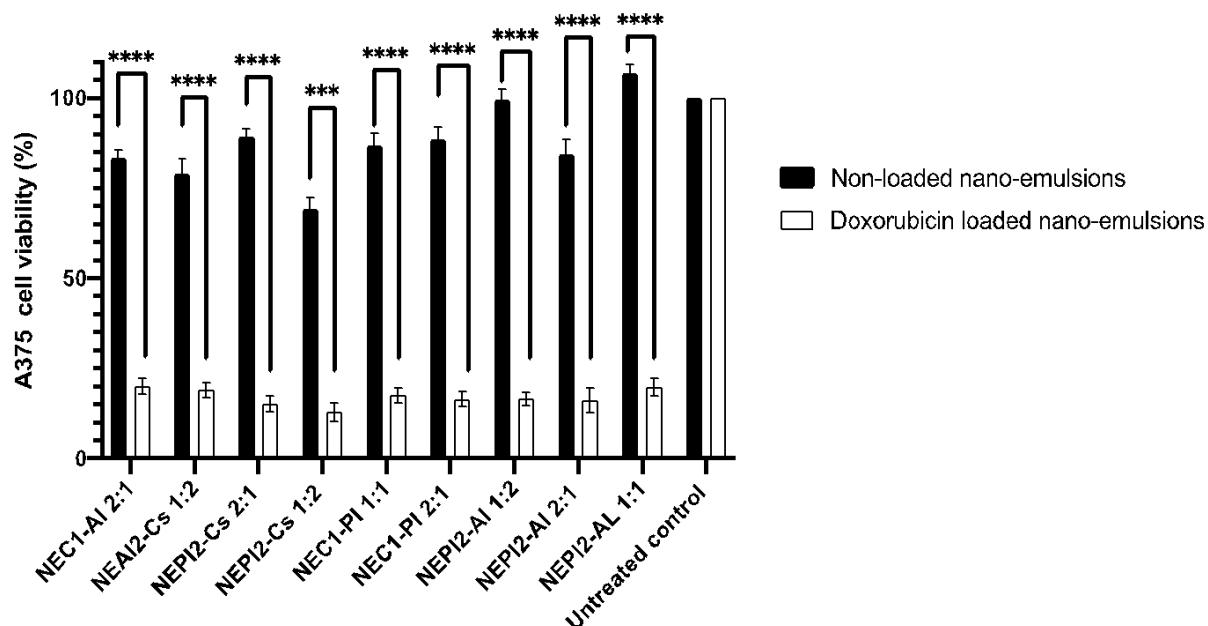


Figure 3.13 Viability of A375 cells in 4-hour treatment with non-loaded and doxorubicin-loaded blended nano-emulsion

The cells were treated with non-loaded and doxorubicin-loaded nano-emulsions and incubated for 4 hours. The viability data were obtained using the MTT method, results were calculated based on untreated control cells, and reported as the percentage of control. The experiment was conducted in 6 independent experiments and bars are indicating the mean value \pm SD error bars. The data were analysed with two-way ANOVA Tukey's comparison test, **** is indicating $P < 0.0001$, *** $P < 0.001$, ** $P < 0.01$, and * $P < 0.05$.

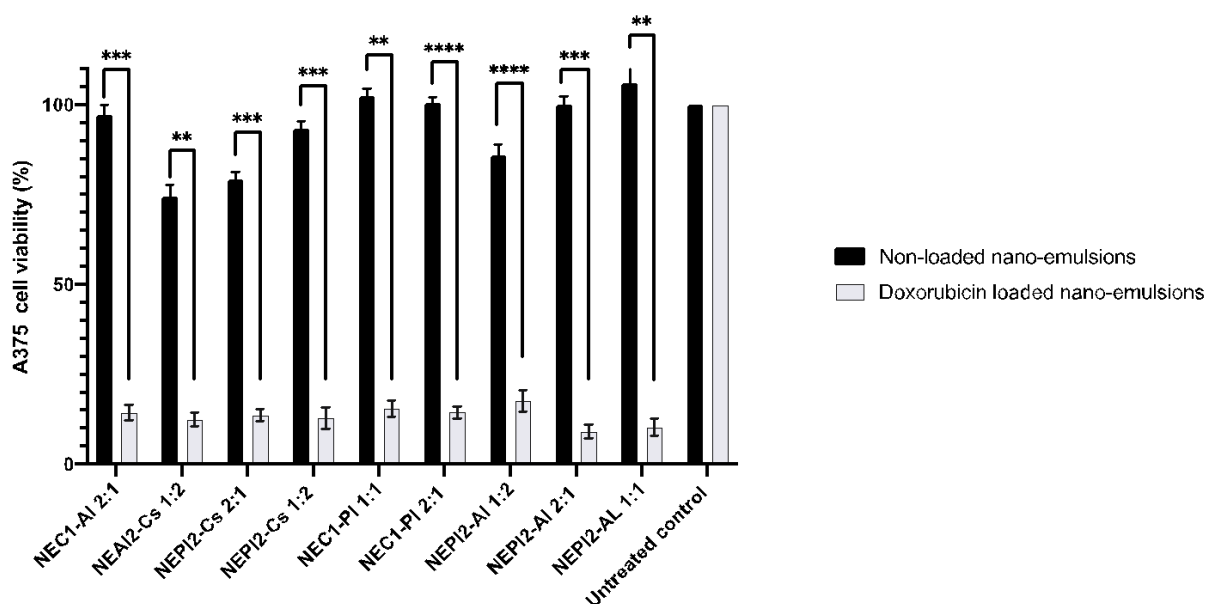


Figure 3.14 Viability of A375 cells in 24-hour treatment with non-loaded and doxorubicin-loaded blended nano-emulsion

The cells were treated with non-loaded and doxorubicin-loaded nano-emulsions and incubated for 24 hours. The experiment was conducted in 6 independent experiments and bars are indicating the mean value \pm SD error bars. The viability data were obtained using the MTT method, results were calculated based on untreated control cells, and reported as the percentage of control. The data were analysed with two-way ANOVA Tukey's comparison test, **** is indicating $P < 0.0001$, *** $P < 0.001$, ** $P < 0.01$, and * $P < 0.05$.

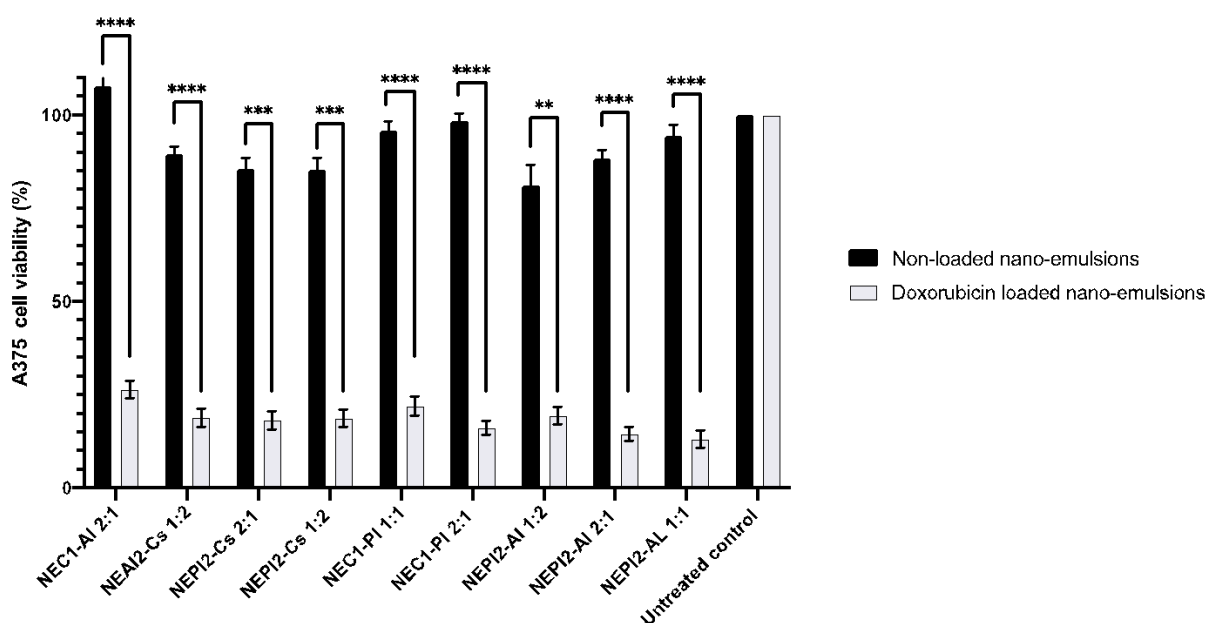


Figure 3.15 Viability of A375 cells in 48-hour treatment with non-loaded and doxorubicin-loaded blended nano-emulsion

The cells were treated with non-loaded and doxorubicin-loaded nano-emulsions and incubated for 48 hours. The experiment was conducted in 6 independent experiments and bars are indicating the mean value \pm SD error bars. The viability data were obtained using the MTT method, results were calculated based on untreated control cells, and reported as the percentage of control. The data were analysed with two-way ANOVA Tukey's comparison test, **** is indicating $P < 0.0001$, *** $P < 0.001$, ** $P < 0.01$, and * $P < 0.05$.

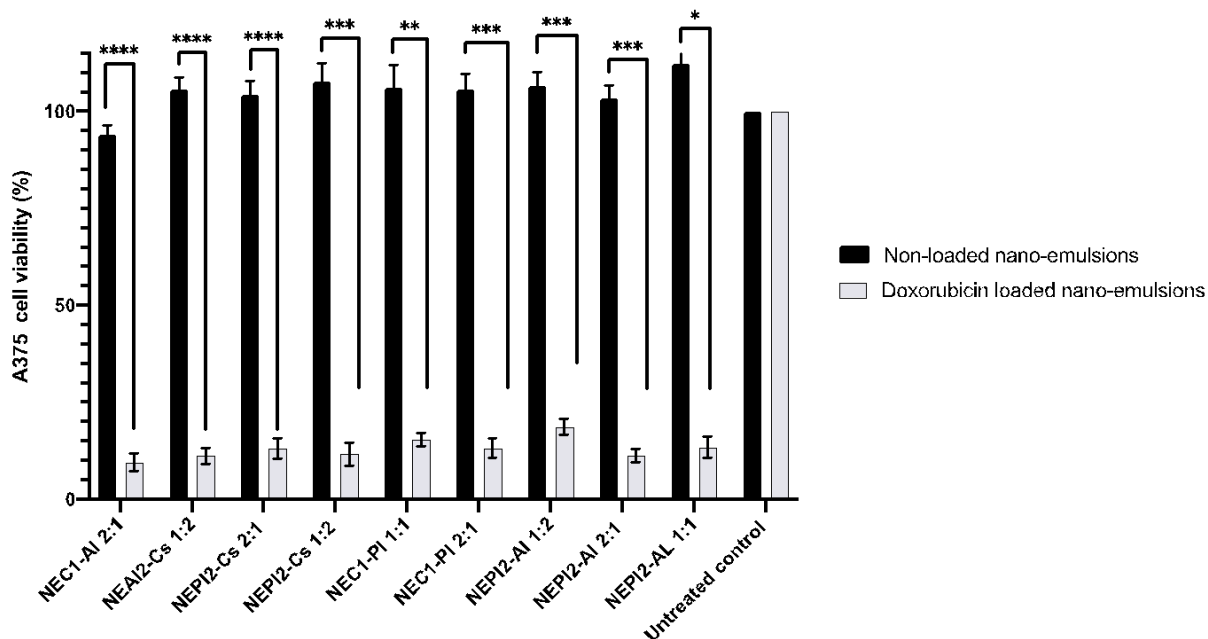


Figure 3.16 Viability of A375 cells in 72-hour treatment with non-loaded and doxorubicin-loaded blended nano-emulsion

The cells were treated with non-loaded and doxorubicin-loaded nano-emulsions and incubated for 72 hours. The experiment was conducted in 6 independent experiments and bars are indicating the mean value \pm SD error bars. The viability data were obtained using the MTT method, results were calculated based on untreated control cells, and reported as the percentage of control. The data were analysed with two-way ANOVA Tukey's comparison test, **** is indicating $P < 0.0001$, *** $P < 0.001$, ** $P < 0.01$, and * $P < 0.05$.

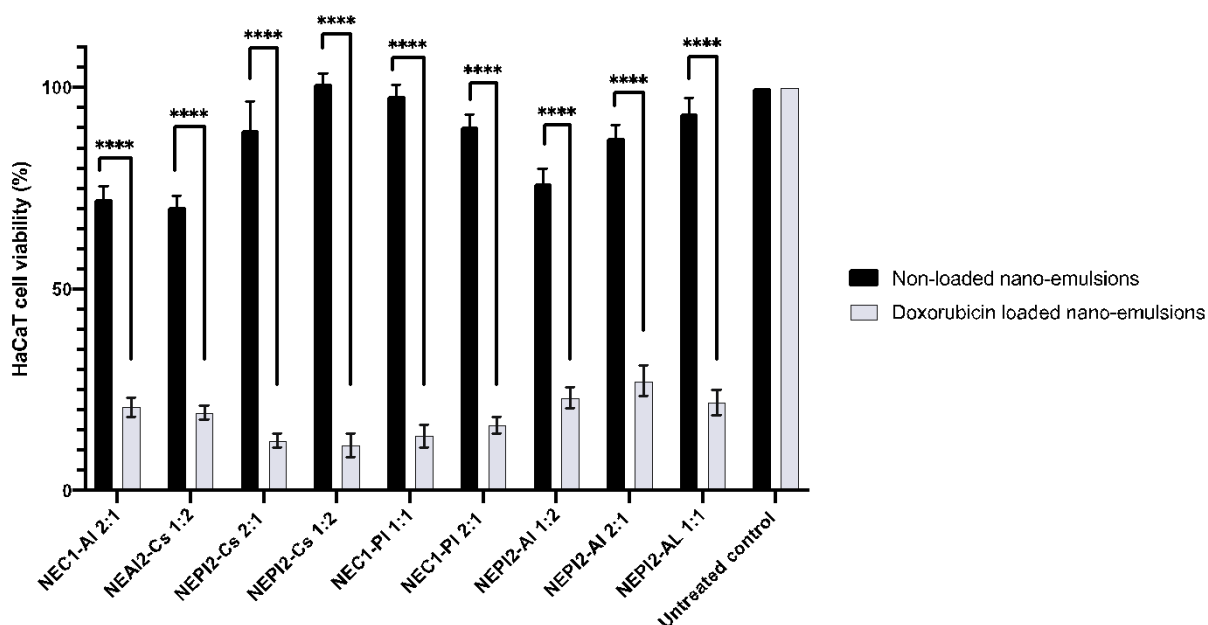


Figure 3.17 Viability of HaCaT cells in 4-hour treatment with non-loaded and doxorubicin-loaded blended nano-emulsion

The cells were treated with non-loaded and doxorubicin-loaded nano-emulsions and incubated for 4 hours. The experiment was conducted in 6 independent experiments and bars are indicating the mean value \pm SD error bars. The viability data were obtained using the MTT method, results were calculated based on untreated control cells, and reported as the percentage of control. The data were analysed with two-way ANOVA Tukey's comparison test, **** is indicating $P < 0.0001$, *** $P < 0.001$, ** $P < 0.01$, and * $P < 0.05$.

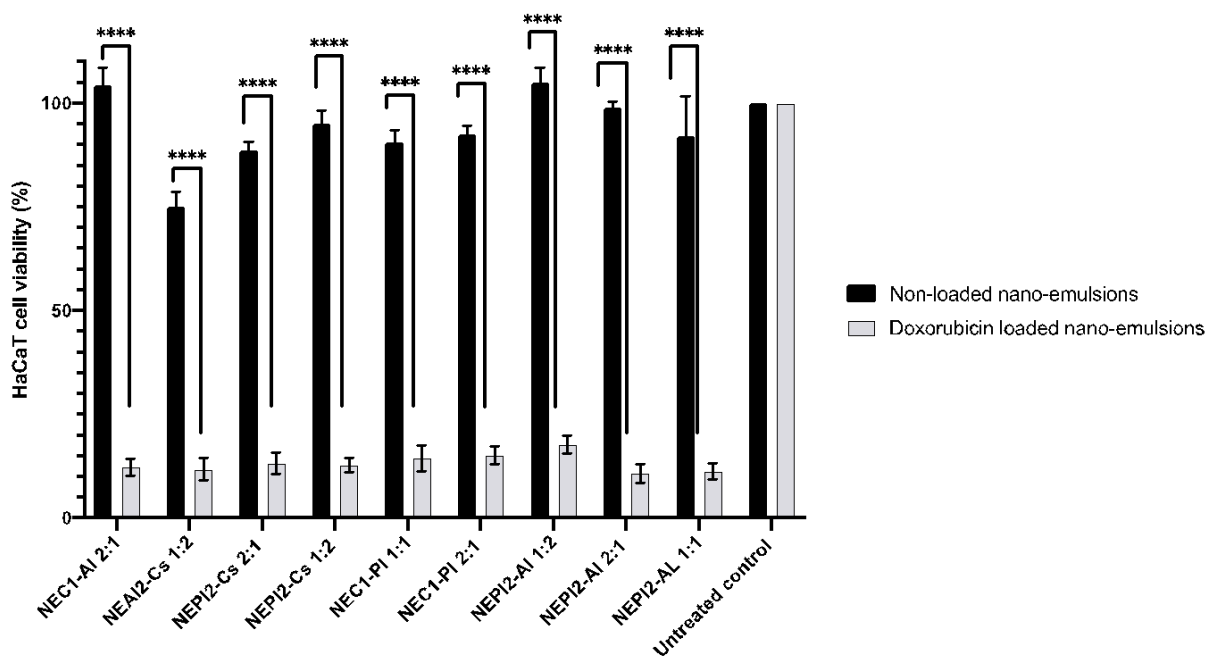


Figure 3.18 Viability of HaCaT cells in 24-hour treatment with non-loaded and doxorubicin-loaded blended nano-emulsion

The cells were treated with non-loaded and doxorubicin-loaded nano-emulsions and incubated for 24 hours. The experiment was conducted in 6 independent experiments and bars are indicating the mean value \pm SD error bars. The viability data were obtained using the MTT method, results were calculated based on untreated control cells, and reported as the percentage of control. The data were analysed with two-way ANOVA Tukey's comparison test, **** is indicating $P < 0.0001$, *** $P < 0.001$, ** $P < 0.01$, and * $P < 0.05$.

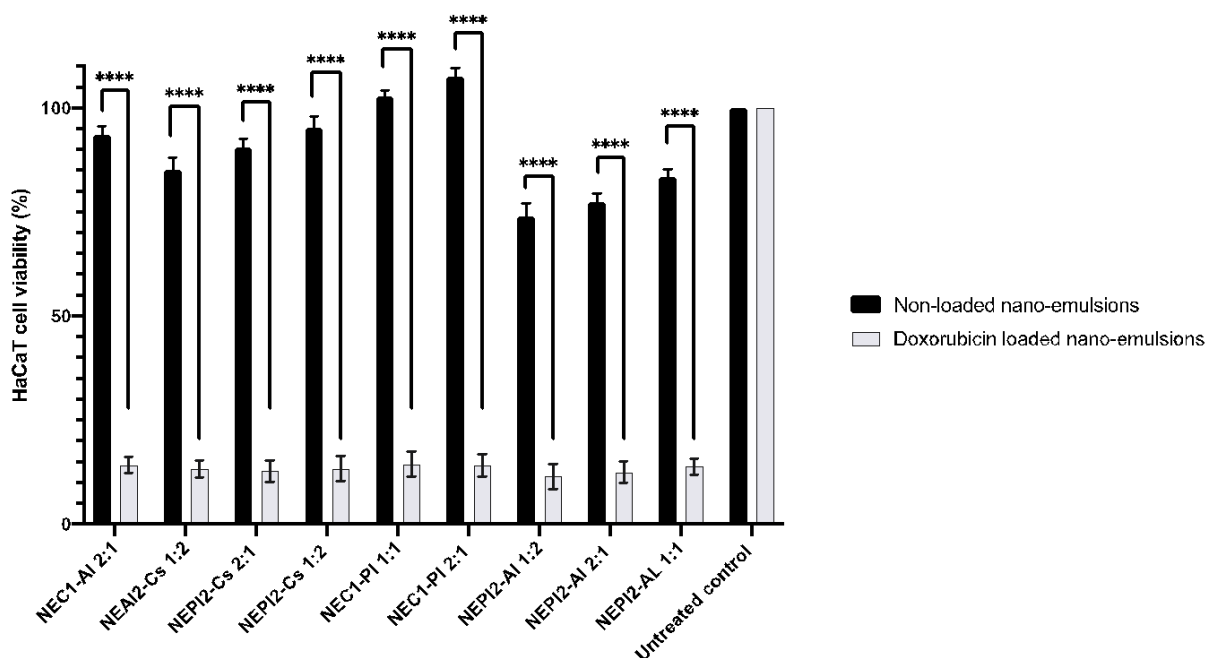


Figure 3.19 Viability of HaCaT cells in 48-hour treatment with non-loaded and doxorubicin-loaded blended nano-emulsion

The cells were treated with non-loaded and doxorubicin-loaded nano-emulsions and incubated for 48 hours. The experiment was conducted in 6 independent experiments and bars are indicating the mean value \pm SD error bars. The viability data were obtained using the MTT method, results were calculated based on untreated control cells, and reported as the percentage of control. The data were analysed with two-way ANOVA Tukey's comparison test, **** is indicating $P < 0.0001$, *** $P < 0.001$, ** $P < 0.01$, and * $P < 0.05$.

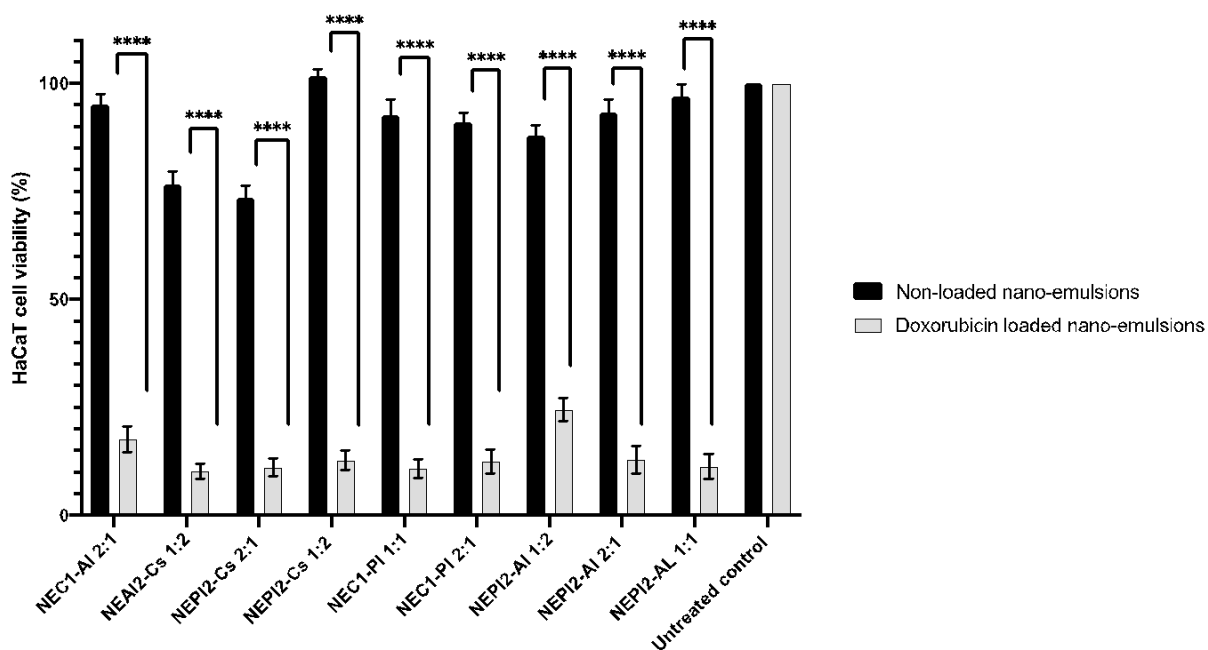


Figure 3.20 Viability of HaCaT cells in 72-hour treatment with non-loaded and doxorubicin-loaded blended nano-emulsion

The cells were treated with non-loaded and doxorubicin-loaded nano-emulsions and incubated for 72 hours. The experiment was conducted in 6 independent experiments and bars are indicating the mean value \pm SD error bars. The viability data were obtained using the MTT method, results were calculated based on untreated control cells, and reported as the percentage of control. The data were analysed with two-way ANOVA Tukey's comparison test, **** is indicating $P < 0.0001$, *** $P < 0.001$, ** $P < 0.01$, and * $P < 0.05$.

3.1.2.6 Quantification of *in vitro* coumarin-6 release in melanoma using confocal microscopy

Confocal microscopy images were captured to screen the uptake of drug-loaded nano-emulsions in A375 cells over 72 hours. Accordingly, the imaging was performed after 4, 24, 28, and 72 hours. In these experiments, the drug-loaded in the nano-emulsions was coumarin-6. The data was obtained from quantification of images (using ImageJ) from 3 independent experiments and calculated as a percentage of control. Figure 3.21 indicates the intracellular release of the coumarin-6 within the cell cytosol compared to naïve coumarin-6 uptake.

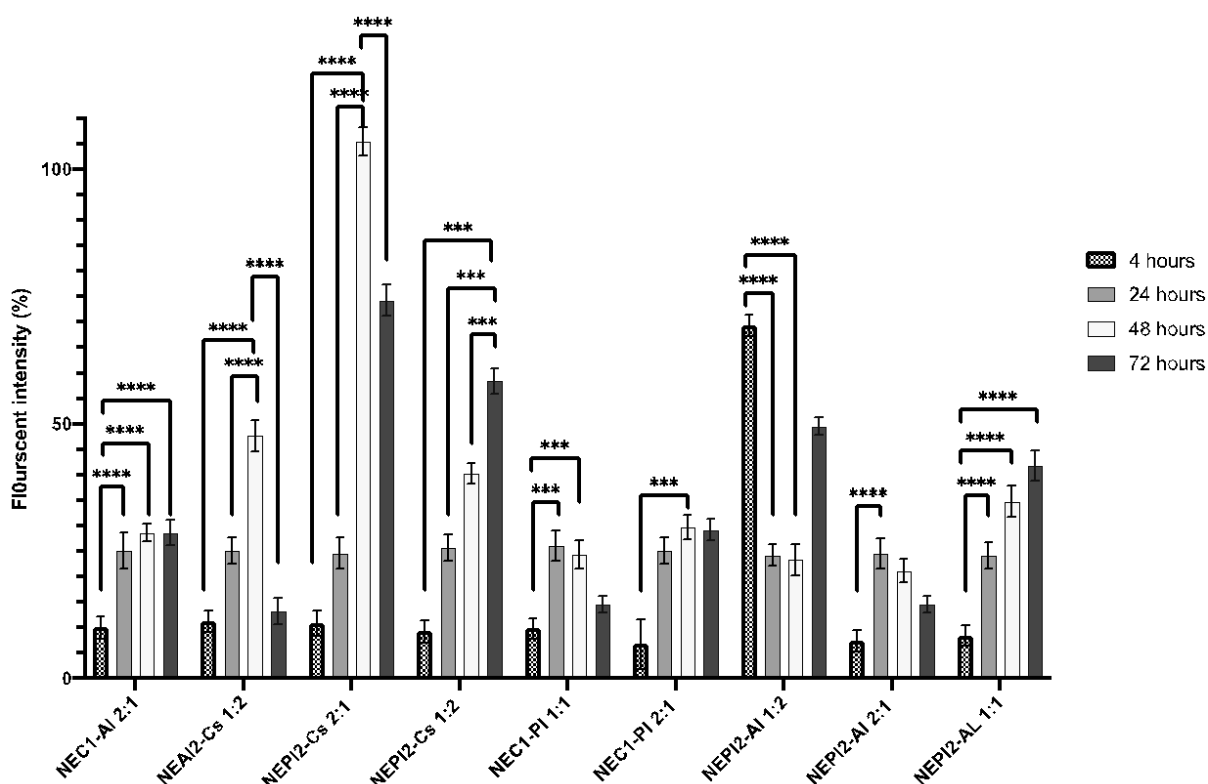


Figure 3.21 Coumarin-6 intracellular release in A375 cells treated with top-nine C6 loaded nano-emulsions

The cells were treated with C6 loaded top-nine nano-emulsions. The experiment was repeated four times in the same conditions, and treated cells were incubated for 4, 24, 48, and 72 hours respectively. The fluorescent images were obtained by confocal microscopy (λ_{\max} 488nm) and quantified using Image-J. The results are normalised to naïve coumarin-6 uptake and presented as the percentage of control. The experiment was conducted in 3 independent experiments and mean data are reported \pm SD error bars. The data were analysed with two-way ANOVA Tukey's comparison test, **** is indicating $P < 0.0001$, *** $P < 0.001$, ** $P < 0.01$, and * $P < 0.05$.

In Figure 3.21, based on coumarin-6 fluorescent intensity, the intracellular release of the drug from nano-emulsions can be estimated. Samples NEPI2-AI 1:1, NEPI2-Cs-1:2, NEC1-AI 2:1, and NEC1-PI 2:1 demonstrated the increasing pattern of release over 72 hours. Other samples did not exhibit a certain pattern, but a sudden increase and decrease of fluorescent intensity were detected. Samples which can provide an increasing and steady pattern during the 72 hours, such as NEPI2-Cs 1:2, are most relevant to this project. The fluorescent intensity recorded for NEPI2-Cs 1:2 was increased from 9.28 to 58%. This could be an indication of the abrupt release of the drug due to possible degradation of the nano-particles and needs to be further investigated using alternative fluorescent drugs or NTA.

Although there was a pattern for the release of coumarin-6 from the nano-emulsions, there was no significant difference in the release patterns. Samples NEPI2-Cs 2:1 and NEPI2-AI 1:2 have an abrupt decrease or increase in the fluorescent intensities which could be due to lysosomal degradation of coumarin-6 inside the cells.

3.1.2.7 Visualisation of coumarin-6 and doxorubicin uptake and release in A375 and HaCaT cells

To investigate the uptake of the nano-emulsions in the cell cytosol, both HaCaT and A375 cells were treated with coumarin-6 and doxorubicin-loaded nano-emulsions. Here the overall uptake after 72 hours were screened and the status for the two cell lines was compared.

Confocal photos obtained from 72 hours' treatments of doxorubicin-loaded nano-emulsions and coumarin-6 loaded nano-emulsions are demonstrated. The images were obtained from the A375 and HaCaT cells after treatments.

The uptake of drug-loaded nano-emulsion particles in A375 cells and HaCaT is presented in Figure 3.22 and 3.23. Interestingly, it can be observed that a few nano-emulsions, namely NEPI2-Cs 1:2, NEC1-Al 2:1, NEPI2-Al 1:1, NEPI2-Al 1:2 and NEAl2-Cs 1:2 provided a good fluorescent intensity in A375 cells, yet the fluorescent intensity in the HaCaT for the same treatments was not considerable. On the other hand, some nano-emulsion samples provide good uptake both in A375 and HaCaT. The samples showing less uptake (low fluorescent intensity) in the HaCaT and high uptake in A375 cells (high fluorescent intensity) were selected for further research (NEC1-PI 1:1, NEPI2-Cs 1:2, and NEPI2-Al 1:2).

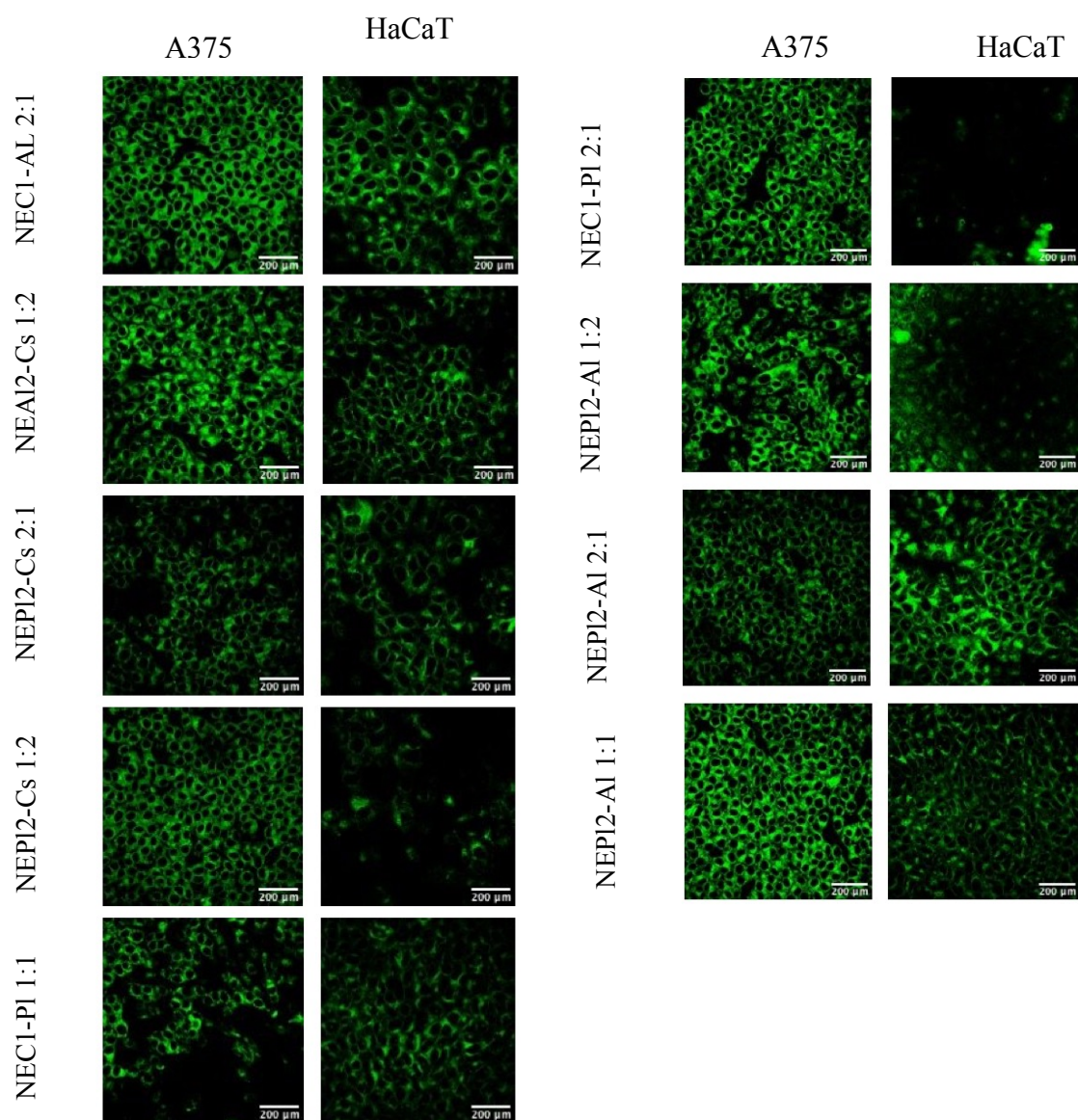


Figure 3.22 Confocal images of A375 and HaCaT cells treated with C6 loaded nano-emulsions

The A375 and HaCaT cells were treated with coumarin-6 loaded nano-emulsions for 72 hours. The cells were washed and fixed. PBS was added to the wells for confocal imaging. FITC filter was used (λ_{max} 488nm). Images were obtained along Z-axis (Z wide) and Z position was set to 0.1 μm per turn (objective HCX APOLU-V-1 63X0.9W, pixels 1024 X 1024, pinhole 1 airy unit, stack 0.5 μm thick) (scale bars 200 μm).

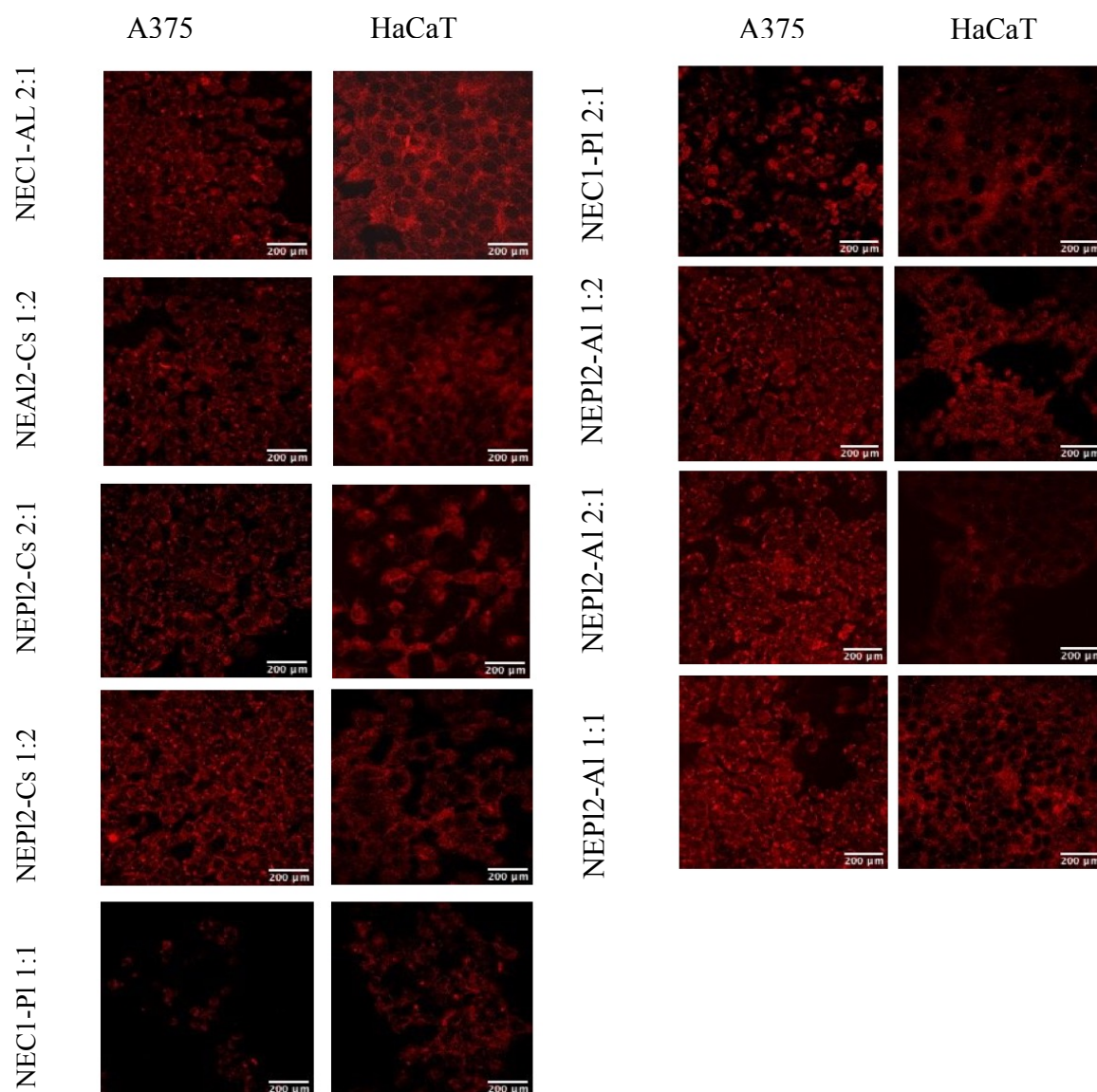


Figure 3.23 Confocal images of A375 and HaCaT cells treated with doxorubicin-loaded nano-emulsions

The A375 and HaCaT cells were treated with doxorubicin loaded nano-emulsions for 72 hours. The cells were washed and fixed. PBS was added to the wells for confocal Imaging. Images were obtained along Z-axis (Z wide) and Z position was set to 0.1 μm per turn (objective HCX APOLU-V-1 63X0.9W, pixels 1024 X 1024, pinhole 1 airy unit, stack 0.5 μm thick) (scale bars 200 μm).

According to Figure 3.22 Figure 3.23, drug-loaded (Coumarin-6/Doxorubicin) nano-emulsions had successful uptake in melanoma cells, for most of the samples. Among the nano-emulsion samples, NEPI2-Cs 1:2 showed good uptake in A375, yet decreased uptake in HaCaT compared to A375 cells.

3.1.2.8 DNA fragmentation ELISA measurement of apoptosis induction by the top-nine blended nano-emulsions delivering doxorubicin to A375 melanoma cells

DNA fragmentation ELISA was performed to confirm and monitor the apoptosis induction ability of the doxorubicin-loaded nano-emulsions on the best nine nano-emulsions chosen from the previous sections (3.1.2.1 and 3.1.2.3). The data were obtained from three independent experiments and calculated as the percentage of control.

The results from the ELISA indicate the apoptosis induction ability trend of nano-emulsions on A375 cells over 72 hours. Doxorubicin alone was used as the control in the analysis.

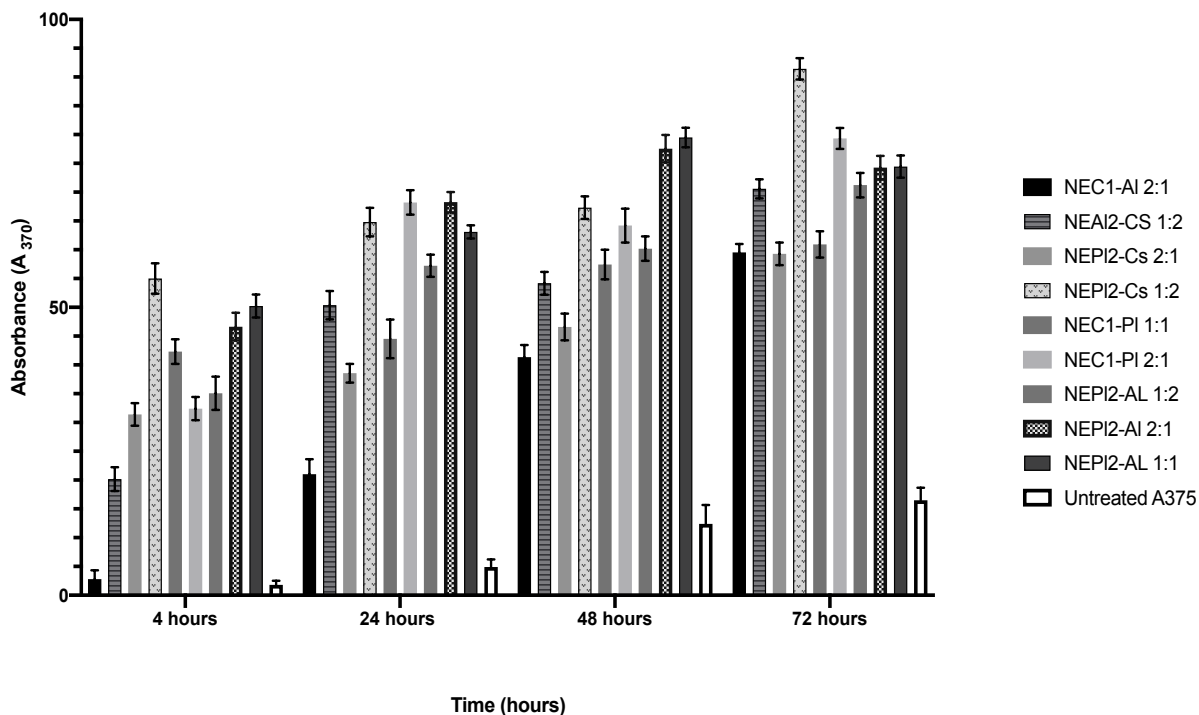


Figure 3.24 Induced apoptosis trend by doxorubicin-loaded nano-emulsions measured by DNA fragmentation ELISA

Apoptosis induction ability of doxorubicin-loaded top nine nano-emulsion was measured by treating BrdU labeled A375 cells with doxorubicin-loaded nano-emulsions. After 4, 24, 48, and 72 hours of incubations (in separate plates), The supernatant was tested with ELISA, and absorbance was measured (A_{370}). The control values were assessed separately for each time point. The results are indicating the mean values from three independent experiments normalised to untreated A375 control value \pm SD.

Figure 3.24 indicates the cellular apoptosis trend for doxorubicin-loaded nano-emulsions treated A375 cells. Samples NEC1-Al 2:1, NEPI2-Cs 1:2, and NEAl2-Cs 1:2 show increasing apoptosis trends over 72 hours. Sample NEAl2-Cs 1:2 apoptosis trend indicated absorbance increase from 20 to 70.8 at 370 nm over 72 hours. For NEPI2-Cs 1:2 absorbance increases from 55.52 to 91.67 at 370 nm, and from 2.67 to 59.79 for the nano-emulsion NEC1-Al 2:1.

The overall trend of apoptosis induced to A375 cells by doxorubicin-loaded nano-emulsion demonstrates an increasing pattern. Looking at nano-emulsion NEC1-PI 2:1, decreased apoptosis induction is observed. Yet, the best trends are the increasing ones with the highest yield (absorbance) for apoptosis induction (NEPI2-Cs 1:2, Figure 3.24).

Based on the experiments done, NEPI2-Cs 1:2 was chosen as the optimised nano-emulsion for further experiments to continue with.

3.2 Modification of optimised pullulan-chitosan nano-emulsion for enhanced uptake in A375 cells

3.2.1 Introduction

So far, preliminary experiments were conducted to find a nano-emulsion optimised in terms of release and toxicity. Pullulan-chitosan nano-emulsion was optimised in terms of physical characteristics. To have targeted uptake toward melanoma cells, the nano-emulsion was further modified. The modification was done using folic acid (folate). The procedure for nano-emulsion modification is briefed in Figure 3.25.

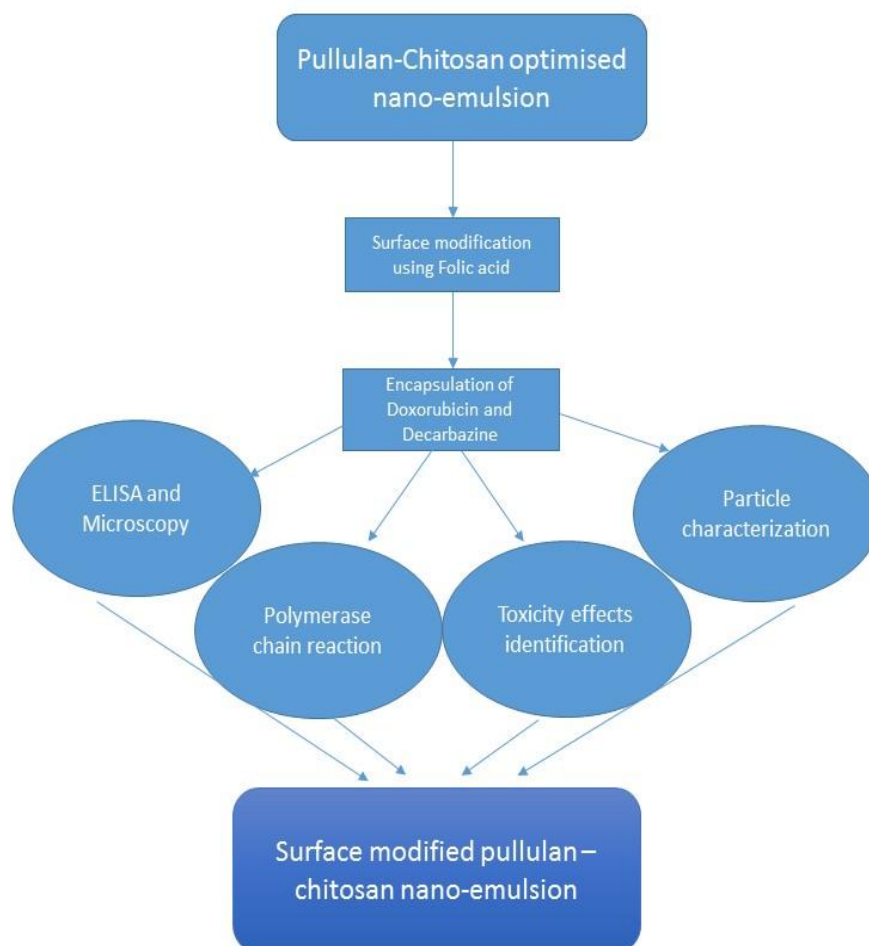


Figure 3.25 Flow-chart of nano-emulsion characterization and experiments for surface modification of optimised nano-emulsions

3.2.2 Characterisation of pullulan-chitosan nano-emulsion

Based on the results of the previous experiments (section 3.1), the best sample optimised based on increased toxicity to melanoma cells, controlled release, and optimised apoptosis induction were NEPl2-Cs 1:2 (pullulan- chitosan nano-emulsion containing 4 mg/ml pullulan and 8 mg/ml chitosan).

The characteristics for optimised pullulan-chitosan nano-emulsion were investigated before surface modification.

3.2.2.1 Drug encapsulation efficiency of pullulan-chitosan nano-emulsion

The encapsulation efficiency of the nano-emulsion was investigated using dialysis methodology. The nano-emulsion was investigated for encapsulation of doxorubicin and dacarbazine. The encapsulation efficiency of doxorubicin was detected as 87% and for dacarbazine was 86.12% (Figure 3.26).

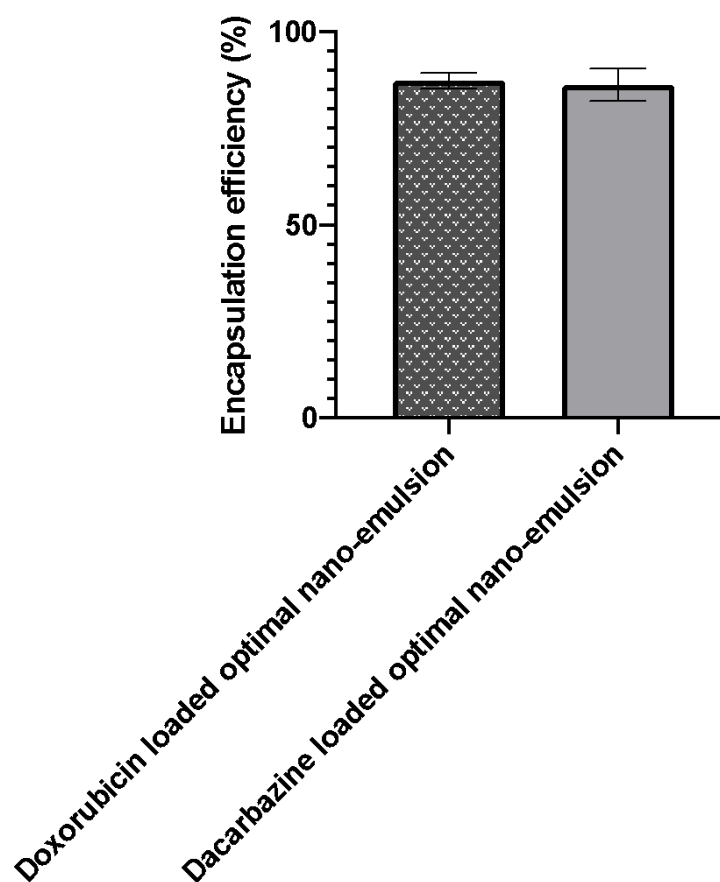


Figure 3.26 Encapsulation efficiency of drug-loaded optimal nano-emulsion

The experiment was conducted using the dialysis method at 25°C and 55 rpm with continuous stirring for 72 hours. Liquid samples from the flasks analysed using UV-spectrophotometer at 479 nm and 331 nm for doxorubicin and dacarbazine respectively. The bars are indicating the mean value of 3 independent experiments (n=3) \pm SD error bars.

The Figure 3.26 shows the encapsulation efficiency of pullulan-chitosan nano-emulsion loaded with dacarbazine and doxorubicin separately, they both indicate high encapsulation efficiency.

3.2.2.2 Evaluation of particle size and size distribution of drug-loaded pullulan-chitosan nano-emulsion

Defining the size of nano-emulsion plays an important role in its uptake and action in melanoma cells, hence the size was identified by a nano-particle tracking analyser. The method was optimised first and subsequently, the analysis was done for doxorubicin-loaded nano-emulsion and doxorubicin-loaded surface-modified nano-emulsion.

Accordingly, the mean particle size for doxorubicin-loaded nano-emulsion (9F-dox) was detected as 174.2 +/- 3.8 nm, the zeta potential of +5, and peak concentration of particles at 115 nm. The procedure was repeated with surface modified doxorubicin-loaded nano-emulsion and the mean particle size was measured as 238.7 +/- 10.7 nm, the zeta potential of +5.7, and peak concentration of particles was detected at 118 and 183 nm (Figure 3.27, Figure 3.28, and Table 3.1) (Appendix B).

Table 3.1 Particle size and charge of doxorubicin-loaded nano-emulsions

Nano-emulsion	Mean particle size (nm)	Standard deviation (nm)	Peak concentration (particles/ml)	Zeta potential (mV)
9F-dox	174.6	150.1	1.65e+10 +/- 1.67e+09	+5.0
FA9-dox	240.1	83.7	7.73e+09 +/- 5.02e+08	+5.7

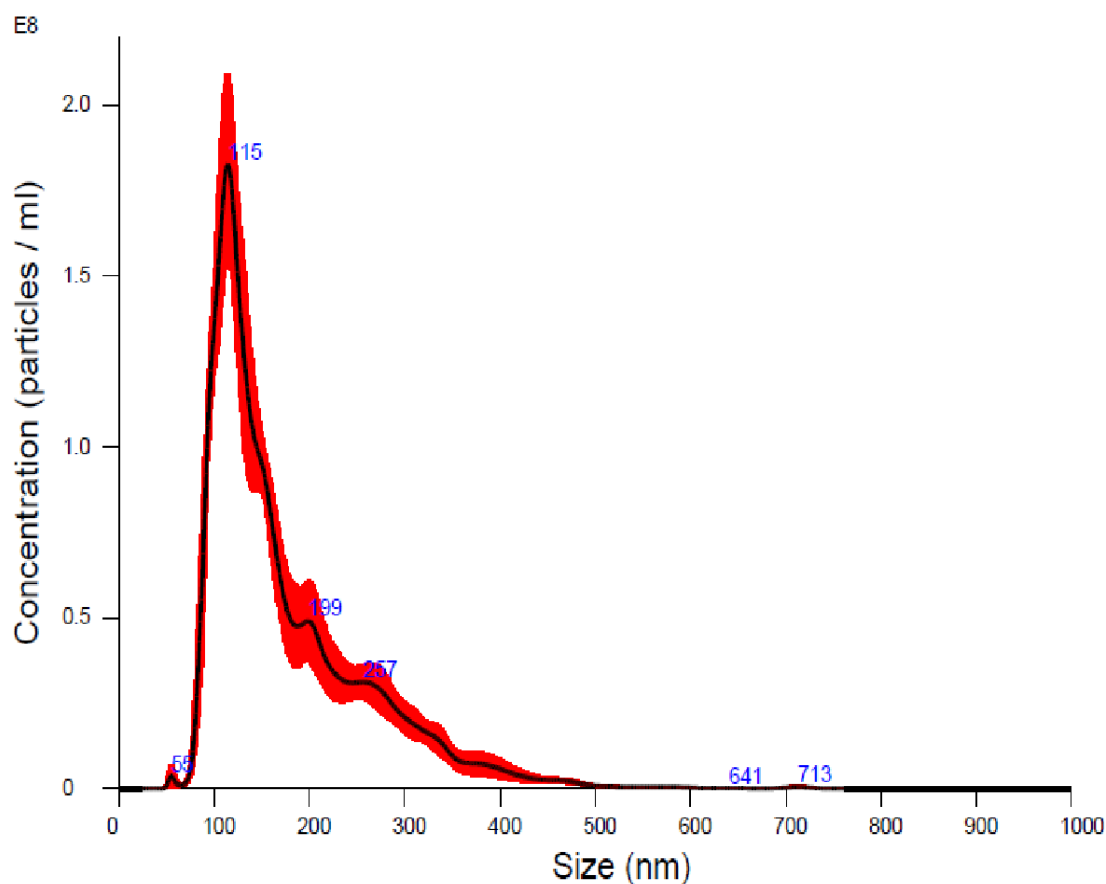


Figure 3.27 Nano-particle tracking analysis using NanoSight

The analysis was performed for doxorubicin-loaded pullulan-chitosan nano-emulsion. The diluted nano-emulsion (1:200 PBS) was syringe-pumped into the NTA equipment. Images were captured using the following settings: laser type on blue 488, camera level set at 11, slider gain 146, syringe pump speed 50, detect threshold 2, and blur on auto. The graphs are a single demonstration from 3 independent experiments carried on.

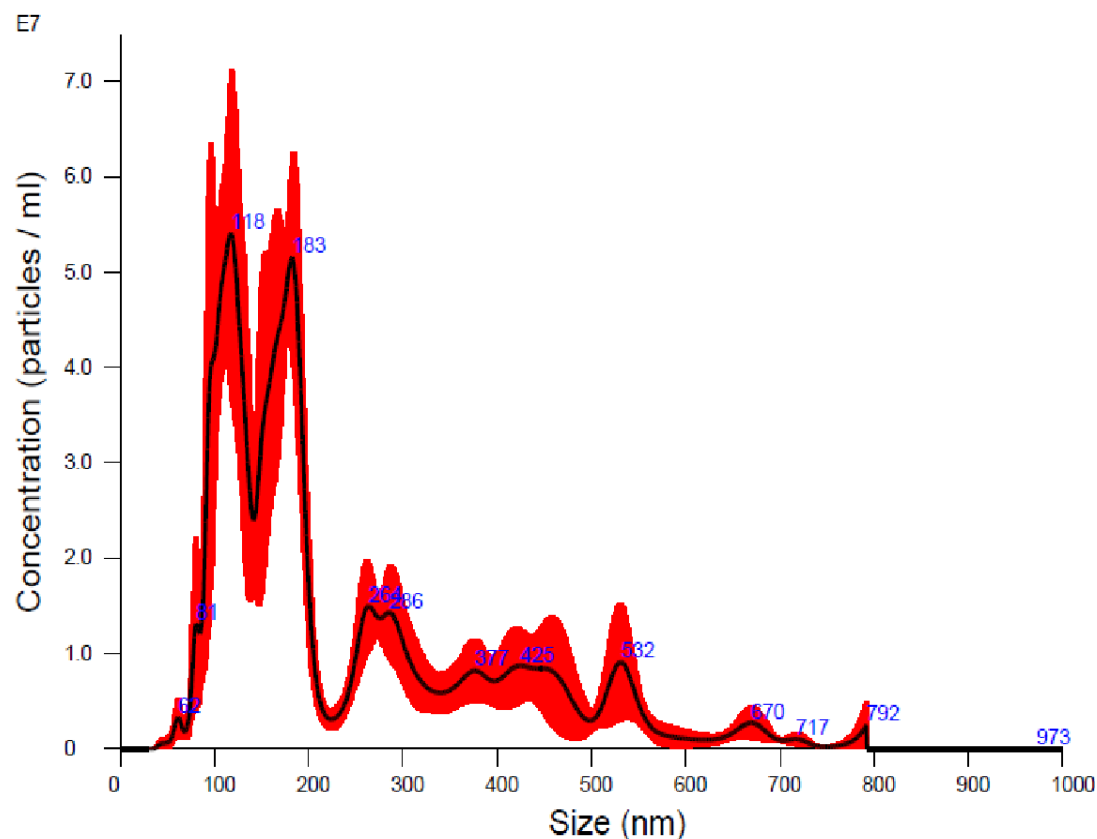


Figure 3.28 Nano-particle tracking analysis using NanoSight

The analysis was performed for folate-modified doxorubicin-loaded pullulan-chitosan nano-emulsion. The diluted nano-emulsion (1:200 PBS) was syringe-pumped into the NTA equipment. Images were captured using the following settings: laser type on blue 488, camera level set at 11, slider gain 146, syringe pump speed 50, detect threshold 2, and blur on auto. The graphs are a single demonstration from 3 independent experiments carried on.

3.2.3 Cell viability screening of modified nano-emulsion

3.2.3.1 Comparison of induced toxicity of modified and non-modified nano-emulsion on HaCaT and A375 cells

The cytotoxicity test was conducted on both melanoma (A375) and keratinocyte (HaCaT) cells to compare the effect of folate-modified nano-emulsion on cell viability. Briefly, doxorubicin and dacarbazine-loaded folate-modified nano-emulsions and non-modified ones versus naïve doxorubicin and dacarbazine were tested on both cell lines. The results are shown in Figure 3.29.

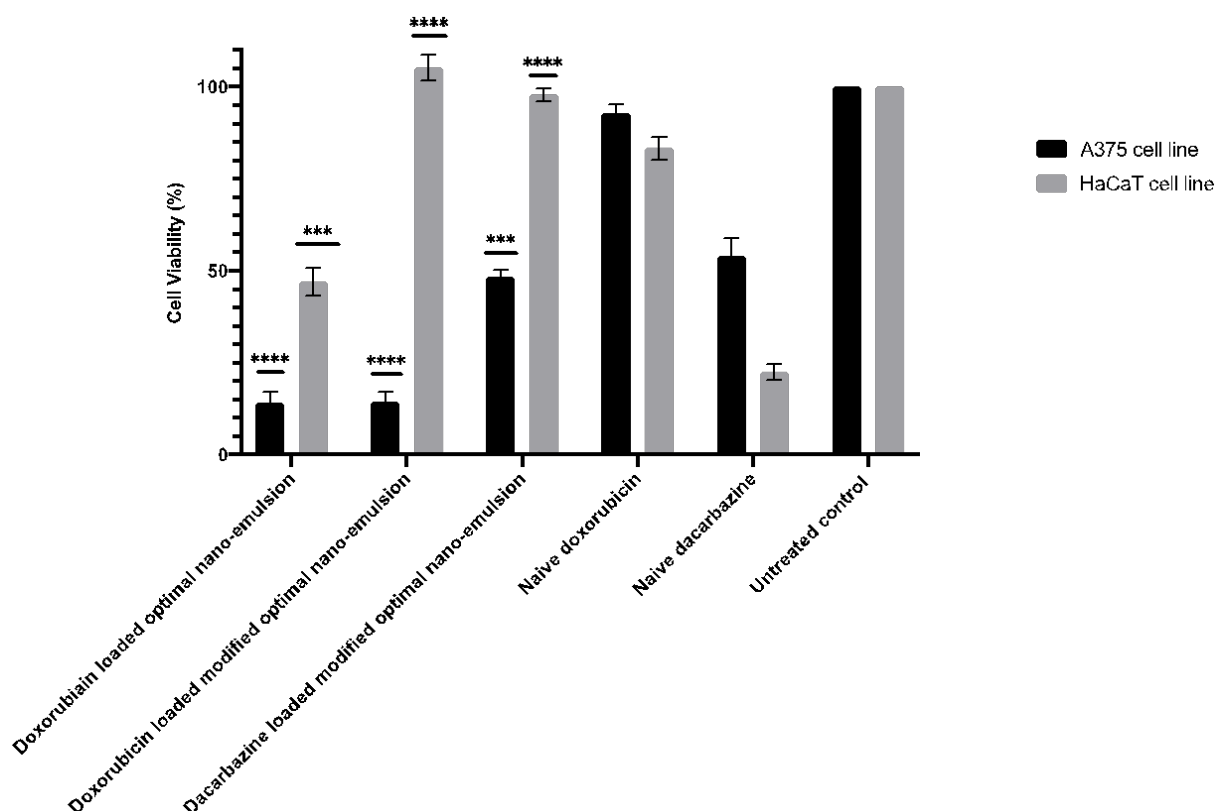


Figure 3.29 Viability screening of A375 and HaCaT cells treated with drug-loaded nano-emulsion and naïve drugs

The cells were treated with drug-loaded nano-emulsions and naïve drugs and the viability data were obtained using the MTT method. Results were calculated based on untreated control cells and reported as the percentage of control. The figure aims to exhibit the significant differences in HaCaT and A375 viability treated with modified and non-modified drug-loaded nano-emulsions compared to Naïve drugs. Bars represent the mean value of 6 independent experiments \pm SD error. The data were analysed with two-way ANOVA Tukey's comparison test, to compare the effect of drug encapsulation on cell viability compared to untreated control **** is indicating $P < 0.0001$, *** $P < 0.001$, ** $P < 0.01$, and * $P < 0.05$.

The figure presents the viability of both cell lines screened with the MTT cytotoxicity test.

The viability of A375 cells decreased by 17% and 14% for doxorubicin-loaded nano-emulsion and modified doxorubicin-loaded nano-emulsion treatments, compared to untreated A375 viability, respectively. On the other hand, A375 treated with folate-modified dacarbazine-loaded nano-emulsion detected as 48% viable, while the viability of A375 treated with naïve doxorubicin and dacarbazine detected as 92% and 53% respectively.

HaCaT cell was observed as 47% viable while treated with doxorubicin-loaded nano-emulsion. However, modified doxorubicin and dacarbazine-loaded nano-emulsions increased the HaCaT cell viability by 112% compared to untreated HaCaT, and decreased its viability to 97% compared to untreated HaCaT viability, respectively. Yet, viability decreased by 22% for HaCaT cells treated with naïve dacarbazine compared to untreated HaCaT viability. For Naïve doxorubicin treatment, contrarily, the viability increased by 83% for HaCaT cells compared to the viability of HaCaT cells treated with doxorubicin-loaded optimal nano-emulsion treatment.

A sharp decrease in melanoma viability by 14.8% was detected while treated with modified doxorubicin-loaded nano-emulsion. This decrease can be compared to the increase of keratinocytes viability by 112.37% while treated with the same treatment compared to untreated control. The obtained results provided a clear indication of increased uptake of modified nano-emulsion in A375 rather than HaCaT. On the other hand, the low viability of both cell lines (17.3 and 47% for A375 and HaCaT respectively) treated with non-modified nano-emulsion compared to untreated control was detected.

3.2.4 Fluorescent microscopy

3.2.4.1 Fluorescent imaging of modified and non-modified nano-emulsion on co-culture of HaCaT and A375 cells

To investigate a more realistic effect of the surface coated-nano-emulsion, the treatment was done on the co-culture of A375 and HaCaT, and the results were visually observed.

The co-culture of the A375 and HaCaT cells was done successfully after labelling the cells using fluorescent cell trackers, fluorescent tracker green (CMFDA) for A375 cells, and fluorescent tracker red (CMTPX) for HaCaT cells (Figure 3.30). Followed by labelling the cells and seeding in 6 well plates for co-culture, the wells were treated with 5 treatments including, doxorubicin-loaded nano-emulsion, modified doxorubicin-loaded nano-emulsion, modified dacarbazine-loaded nano-emulsion, naïve doxorubicin, and dacarbazine. The results are obtained from fixed cells after 72 hours of treatment using EVOS microscopy. The images are a single demonstration from three independent experiments.

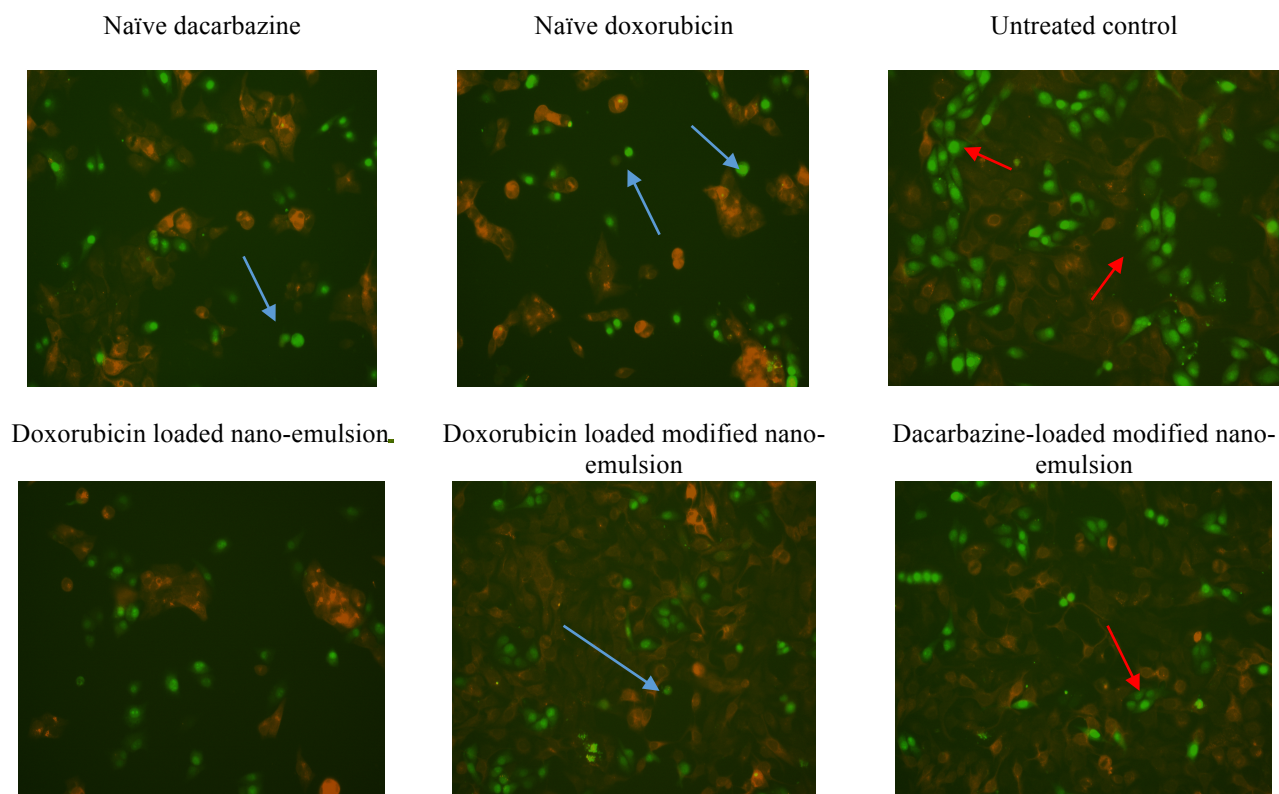


Figure 3.30 Fluorescent microscopy of HaCaT and A375 in co-culture

Fluorescent labelled HaCaT (CMTPX, red) and A375 (CMFDA, green) cells in co-culture. Two cell lines were seeded (1:5, A375: HaCaT) and incubated for 12 hours before the treatment, then incubated for 72 hours after the treatments. The cells were imaged on 72nd hour. Apoptotic melanoma cells are marked by blue arrows and healthy melanoma cells are pointed by red arrows. The images are a single demonstration from three independent experiments. The red arrow in the untreated figure, however, indicates healthy melanoma cells. The scale bar indicates 100 μ m.

According to images obtained from co-culture, the wells treated with modified drug-loaded nano-emulsion have more viable HaCaT (red) rather than A375 (green) cells compared to the ones treated with non-modified nano-emulsion or naïve doxorubicin and dacarbazine.

3.2.4.2 Imaging co-culture of A375 and HaCaT cells over 72 hours treated with modified and non-modified nano-emulsions

Treated keratinocyte and melanoma co-culture plates (containing DMEM) were screened consecutively, during 4, 24, 48, and 72 hours in a fluorescent microscope. The obtained images are single demonstrations from three independent experiments.

According to the images obtained, a reduction of melanoma cells (green fluorescent labelled), can be detected with the treatment of doxorubicin/dacarbazine loaded modified nano-emulsion. Although in the same treatment, keratinocytes are remaining healthy and proliferating. The result images obtained are demonstrated in the figures below.

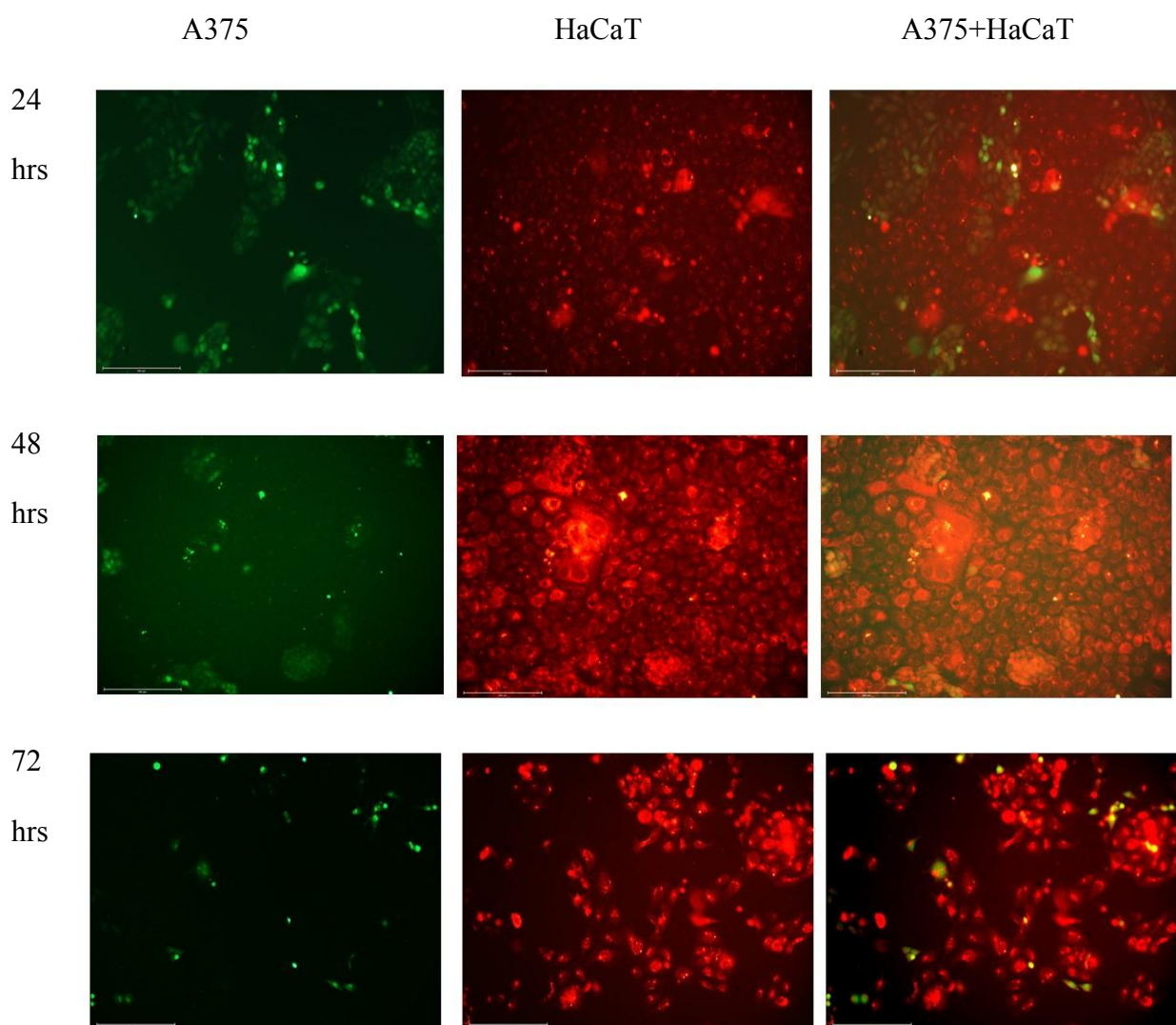


Figure 3.31 Fluorescent microscopy of A375 and HaCaT in co-culture (dacarbazine-loaded nano-emulsion)

Fluorescent labelled HaCaT (CMTPX, red) and A375 (CMFDA, green) cells in co-culture were treated with dacarbazine-loaded pullulan-chitosan nano-emulsion. Two cell lines were seeded (1:5, A375: HaCaT) in wells of a 6 well plate incubated for 12 hours before the treatment, then incubated and imaged on 24th, 48th, and 72nd hours after the treatments. The wells contained DMEM during the imaging. The Images are a single demonstration from three independent experiments conducted (scale bar: 125µm).

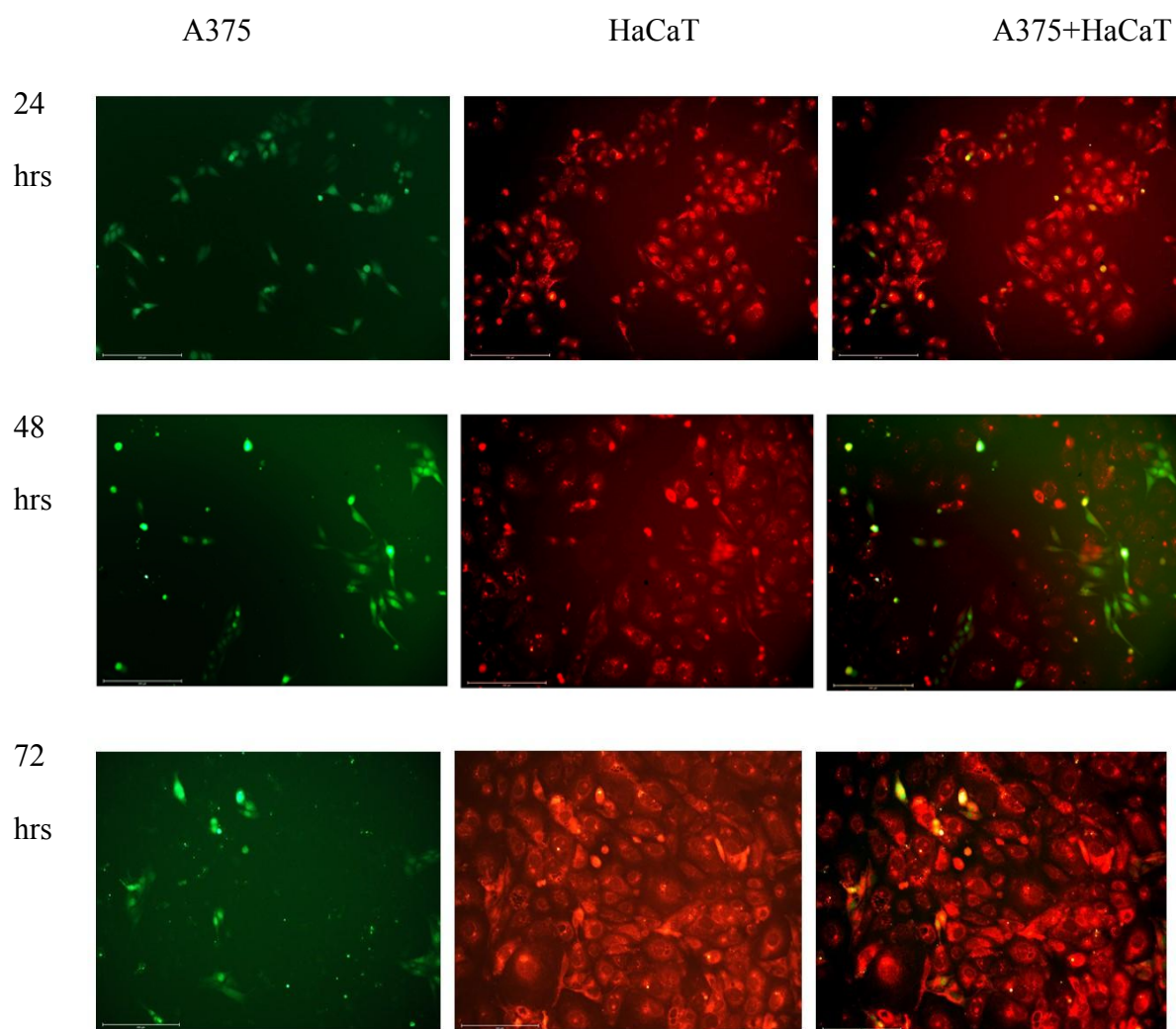


Figure 3.32 Fluorescent microscopy of A375 and HaCaT in co-culture (doxorubicin-loaded nano-emulsion)

Fluorescent labelled HaCaT (CMTPX, red) and A375 (CMFDA, green) cells in co-culture were treated with doxorubicin-loaded pullulan-chitosan nano-emulsion. Two cell lines were seeded (1:5, A375: HaCaT) in wells of a 6 well plate incubated for 12 hours before the treatment, then incubated and imaged on 24th, 48th, and 72nd hours after the treatments. The wells contained DMEM during the imaging. The Images are a single demonstration from three independent experiments conducted (scale bar: 125µm).

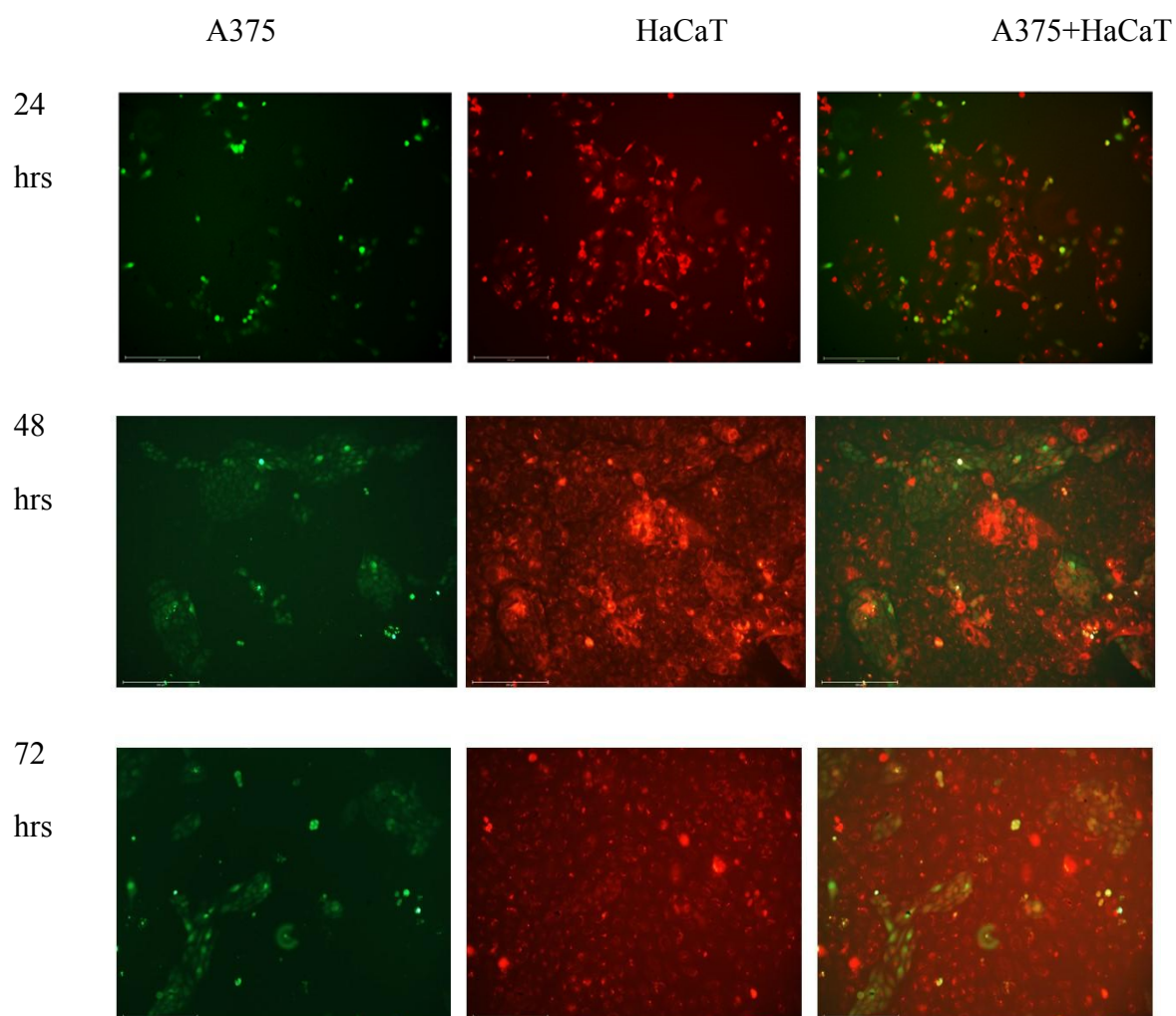


Figure 3.33 Fluorescent microscopy of A375 and HaCaT in co-culture (dacarbazine-loaded modified nano-emulsion)

Fluorescent labelled HaCaT (CMTPIX, red) and A375 (CMFDA, green) cells in co-culture were treated with dacarbazine-loaded modified pullulan-chitosan nano-emulsion. Two cell lines were seeded (1:5, A375: HaCaT) in wells of a 6 well plate incubated for 12 hours before the treatment, then incubated and imaged on 24th, 48th, and 72nd hours after the treatments. The wells contained DMEM during the imaging. The Images are a single demonstration from three independent experiments conducted (scale bar: 125 μ m).

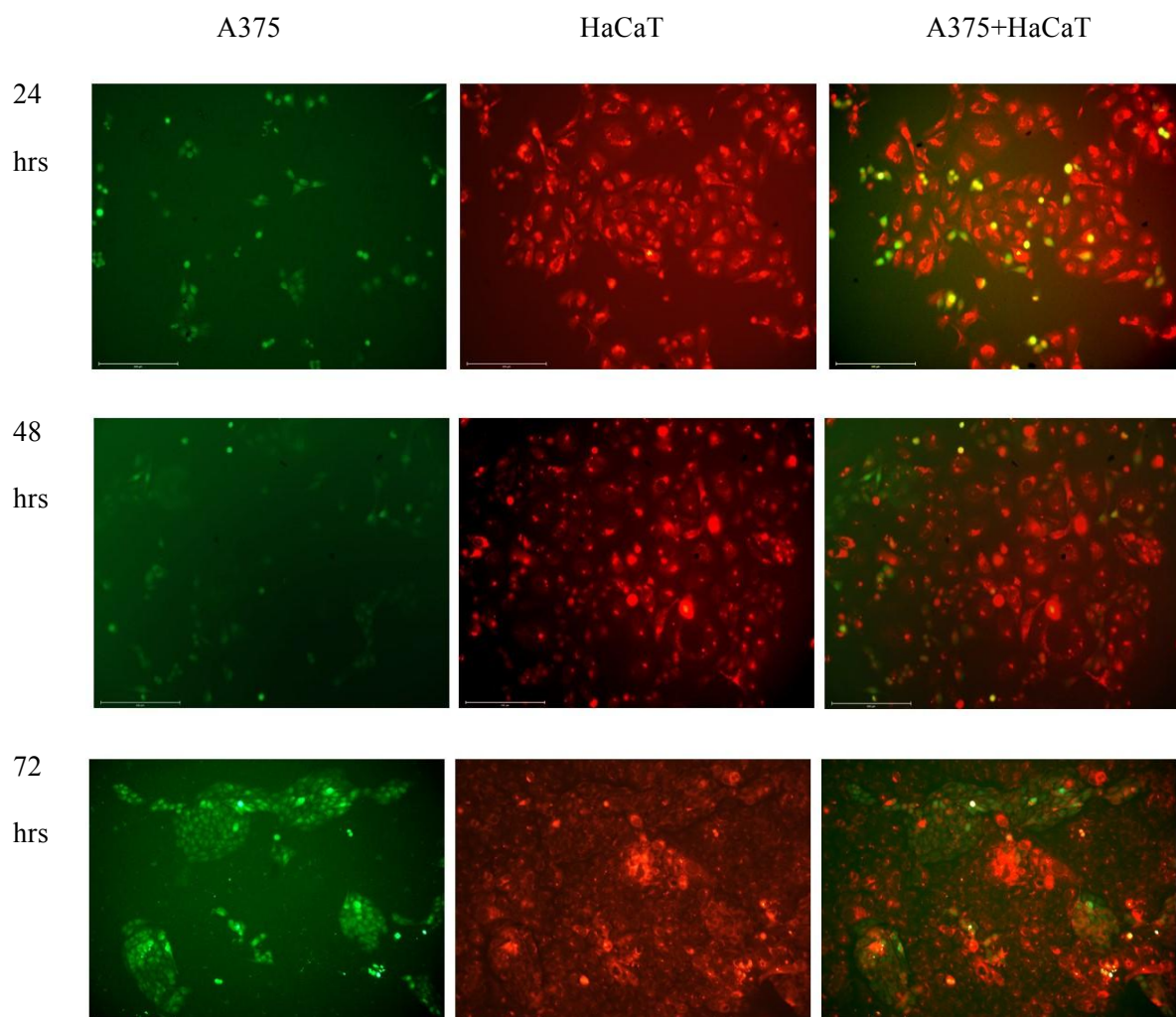


Figure 3.34 Fluorescent microscopy of A375 and HaCaT in co-culture (naïve doxorubicin)

Fluorescent labelled HaCaT (CMTPIX, red) and A375 (CMFDA, green) cells in co-culture were treated with naïve doxorubicin. Two cell lines were seeded (1:5, A375: HaCaT) in wells of a 6 well plate incubated for 12 hours before the treatment, then incubated and imaged on 24th, 48th, and 72nd hours after the treatments. The wells contained DMEM during the imaging. The Images are a single demonstration from three independent experiments conducted (scale bar: 125µm).

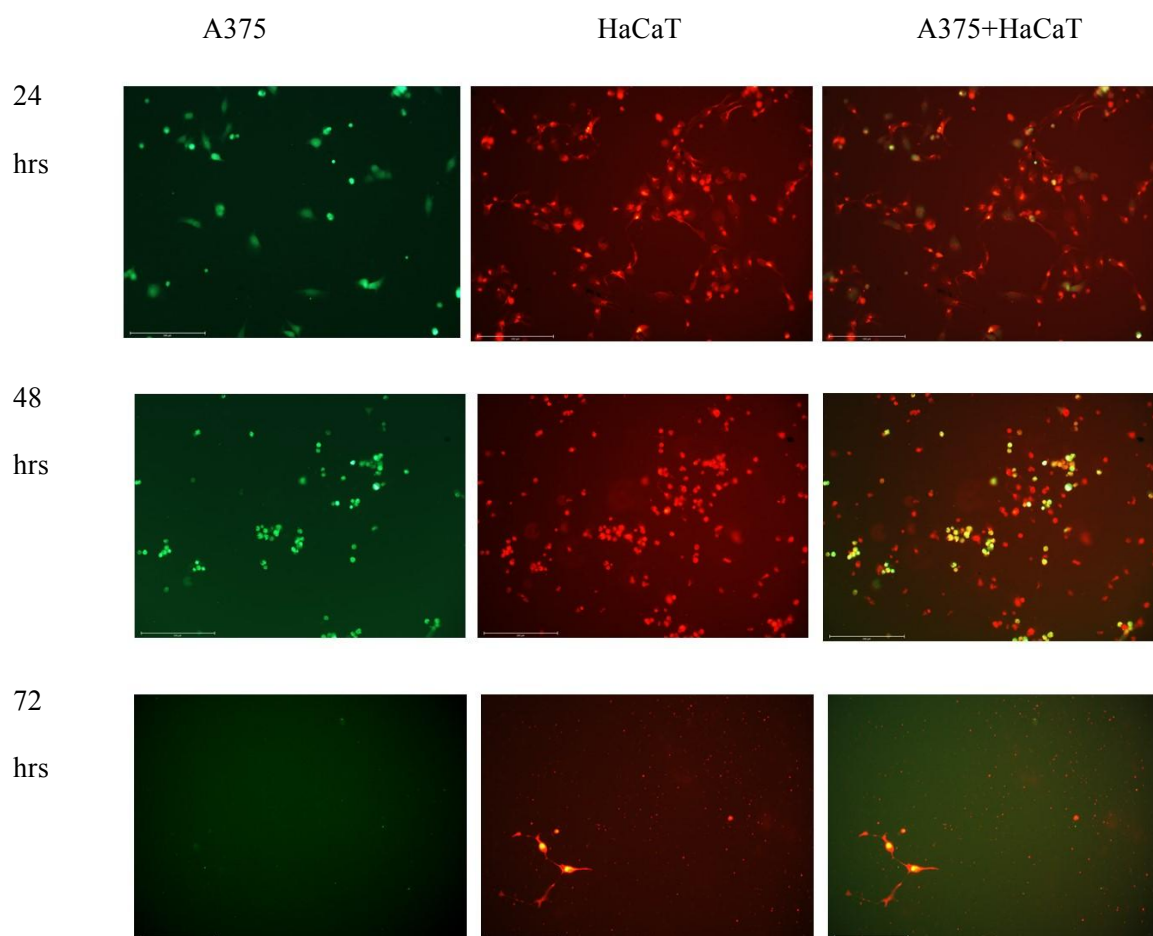


Figure 3.35 Fluorescent microscopy of A375 and HaCaT in co-culture (naïve dacarbazine)

Fluorescent labelled HaCaT (CMTPX, red) and A375 (CMFDA, green) cells in co-culture were treated with naïve dacarbazine. Two cell lines were seeded (1:5, A375: HaCaT) in wells of a 6 well plate incubated for 12 hours before the treatment, then incubated and imaged on 24th, 48th, and 72nd hours after the treatments. The wells contained DMEM during the imaging. The Images are a single demonstration from three independent experiments conducted (scale bar: 125µm).

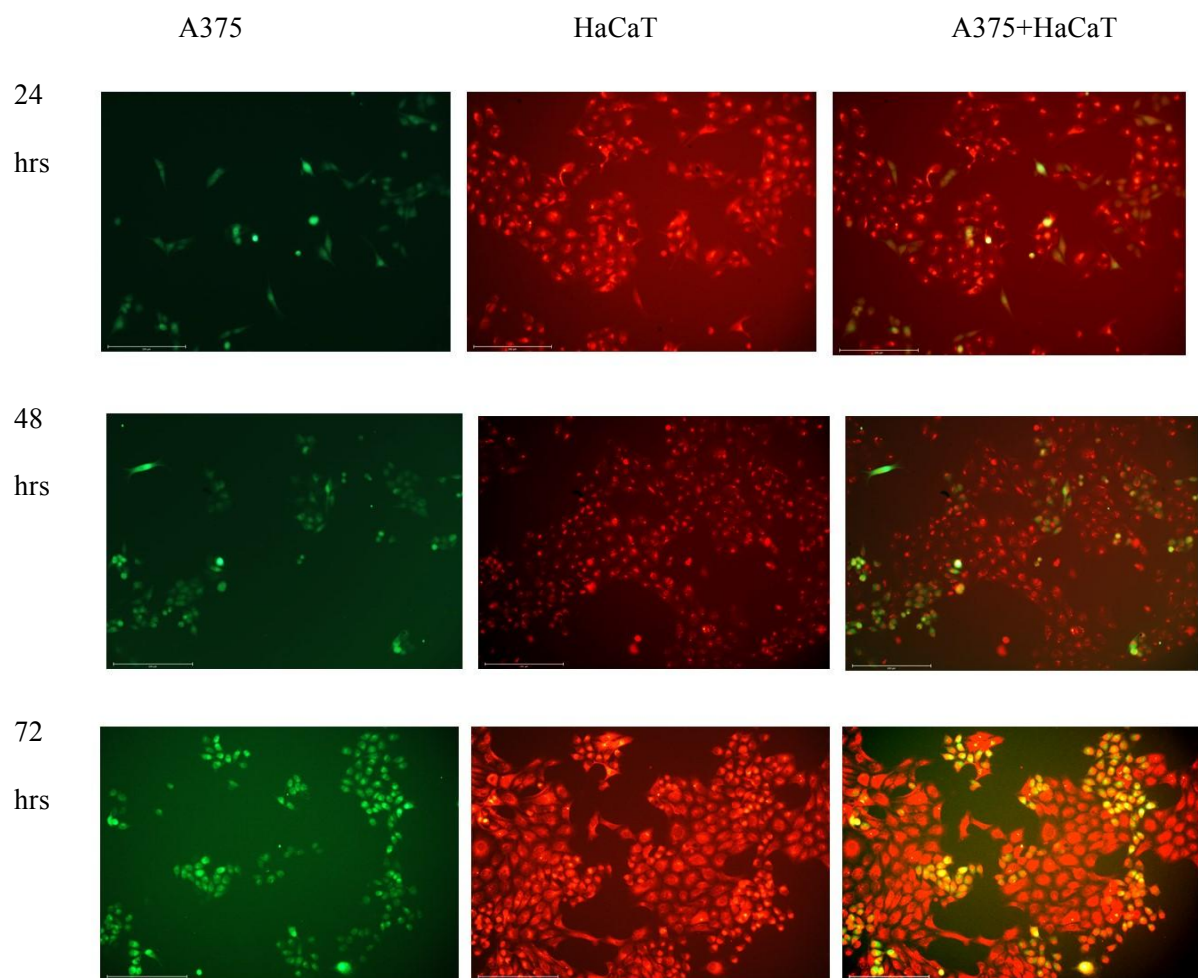


Figure 3.36 Fluorescent microscopy of A375 and HaCaT in co-culture (doxorubicin-loaded modified nano-emulsion)

Fluorescent labelled HaCaT (CMTPX, red) and A375 (CMFDA, green) cells in co-culture were treated with doxorubicin-loaded modified pullulan-chitosan nano-emulsion. Two cell lines were seeded (1:5, A375: HaCaT) in wells of a 6 well plate incubated for 12 hours before the treatment, then incubated and imaged on 24th, 48th, and 72nd hours after the treatments. The wells contained DMEM during the imaging. The Images are a single demonstration from three independent experiments conducted (scale bar: 125 μ m).

3.2.4.3 Fluorescent imaging of A375 and HaCaT cells in mono-cultures treated with modified and non-modified nano-emulsion

Melanoma (A375) and keratinocyte (HaCaT) cells were treated with doxorubicin-loaded nano-emulsion, modified doxorubicin-loaded nano-emulsion, modified dacarbazine-loaded nano-emulsion, naïve doxorubicin, and naïve dacarbazine, in mono-culture. The images obtained after 72 hours of treatment and are a single demonstration from three independent experiments. Melanoma cells were labelled with CMFDA, and keratinocyte cells were labelled with CMTPIX fluorescent labels for imaging before the treatment using the same procedure as the previous section.

After the treatment was done (after 72 hours) the cells were fixed and stained with DAPI nucleus stain and were imaged with an EVOS microscope.

The images below show the treated and the control melanoma (A375) and the keratinocyte (HaCaT) cells. The images below are obtained for DAPI, CMFDA, and CMTPIX.

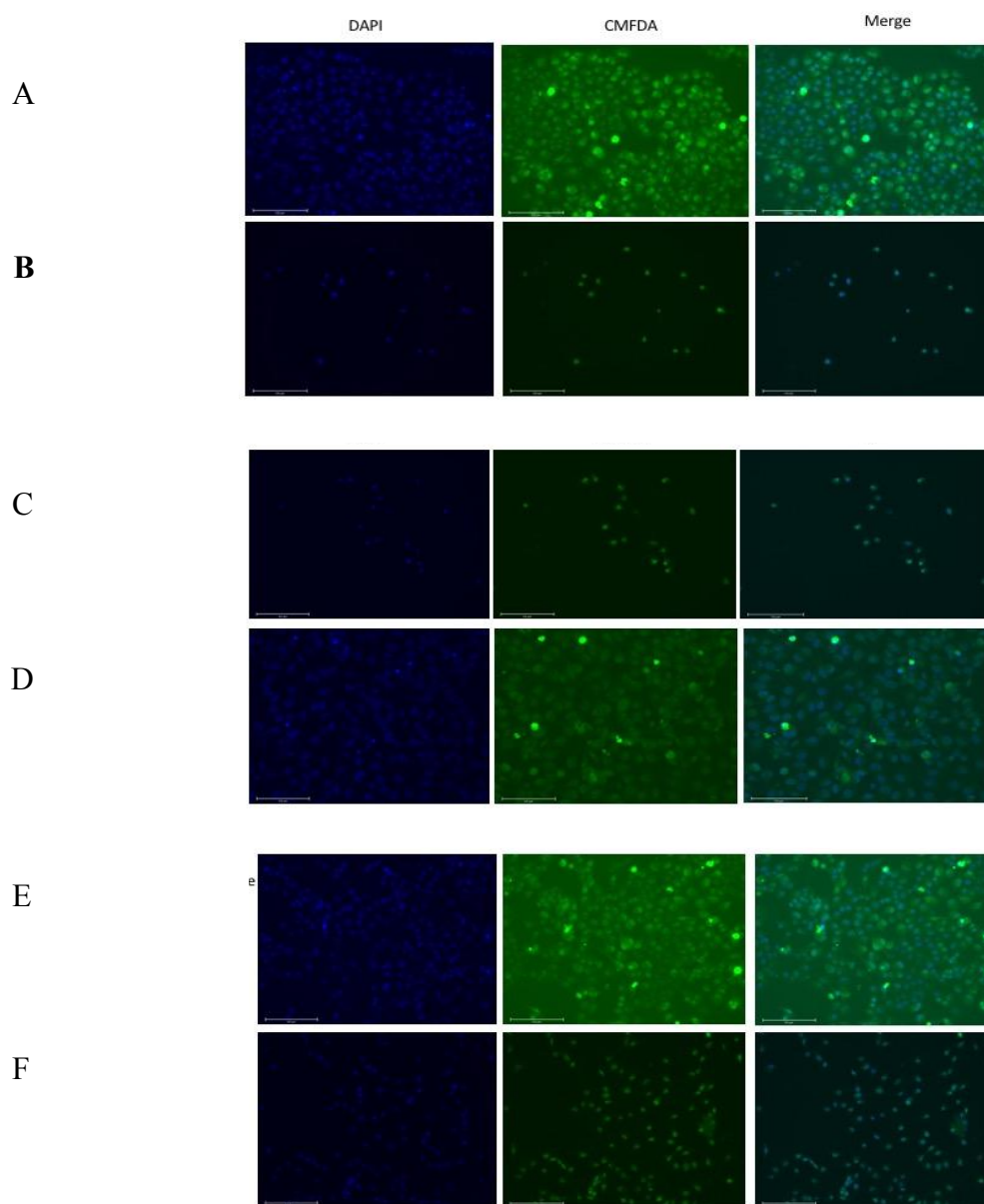


Figure 3.37 CMFDA and DAPI labelled A235 cells treated with drug-loaded nano-emulsions

Treatments are (A) untreated A375, (B) doxorubicin-loaded nano-emulsion, (C) modified doxorubicin-loaded nano-emulsion, (D) modified dacarbazine-loaded nano-emulsion, (E) naïve dacarbazine, and (F) naïve doxorubicin. The cells were imaged immediately after 72 hours of treatment. The images are a single demonstration from three independent experiments (scale 200 μ m).

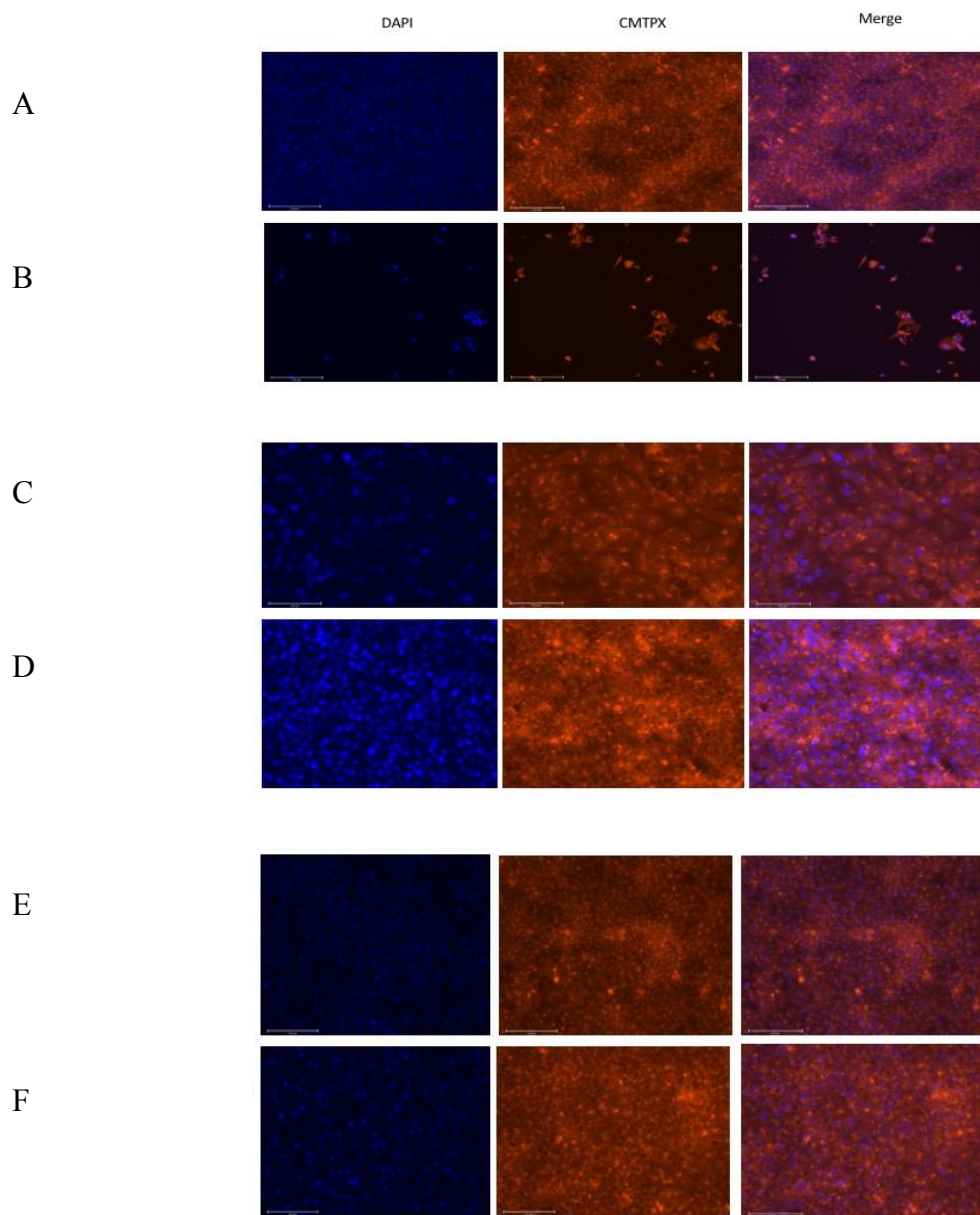


Figure 3.38 Comparison of CMPX labelled HaCaT treated with nano-emulsions

Treatments are (A) untreated A375, (B) doxorubicin-loaded nano-emulsion, (C) modified doxorubicin-loaded nano-emulsion, (D) modified dacarbazine-loaded nano-emulsion, (E) naïve dacarbazine, and (F) naïve doxorubicin. The cells were imaged immediately after 72 hours of treatment. The images are a single demonstration from three independent experiments (scale 200µm).

According to the images obtained from mono-cultures and DAPI staining, keratinocytes (HaCaT) that are treated with surface-modified nano-emulsions show an increased DAPI fluorescent intensity which indicates increased viability of cells. On the other hand, melanoma (A375) cells treated with surface-modified drug-loaded nano-emulsion indicate decreased fluorescent intensity of DAPI, this is an indication of lower viability. The decreased and apoptotic melanoma cells can be detected in the CMFDA image of the same treatment.

Figure 3.37-B indicates A375 cells treated with doxorubicin-loaded pullulan-chitosan nano-emulsion, compared to (A) untreated A375, the cell numbers decreased and visually seem apoptotic. In figure 3.37-C, folate-modified nano-emulsion also decreased the A375 cells. HaCaT cells treated with folate-modified dacarbazine/doxorubicin (figure 3.38 C and D) seem intact and healthy. Nevertheless, Figure 3.38-B indicates negatively affected HaCaT cells from non-modified nano-emulsion treatment.

Although surface-modified nano-emulsion is more toxic to melanoma cells, the non-surface-modified nano-emulsion reduces the numbers of both melanoma (A375) and keratinocytes (HaCaT). The scale bar for all the images obtained from EVOS fluorescent microscopy is 200 μm (Figures 3.37, 3.38).

3.2.4.4 Polymerase chain reaction and gene expression of the treated cells

The effect of nano-emulsion treatment on the melanoma and HaCaT cells were investigated at the molecular level by monitoring the expression of four genes (excluding house-keeping gene GAPDH). Therefore, the expression of Caspase 9, Caspase 3, Bax, and Bcl2 were investigated in both treated cell lines. The band intensities obtained from the PCR are demonstrated for Caspase3, caspase9, Bax, and Bcl2 respectively in Figure 3.43 to Figure 3.48.

Accordingly, the obtained bands were quantified using ImageJ (n=3), normalized using GAPDH band intensity, and gene expression intensities are demonstrated in Figures 3.39 to 3.42.

The figure indicates apoptosis gene, caspase 3, in A375 cells treated with folate-modified doxorubicin and dacarbazine-loaded pullulan-chitosan nano-emulsion expressed 67 and 63% respectively. While cells treated with naïve doxorubicin and dacarbazine expressed 11 and 16% caspase3, respectively. Caspase 3 expression in control A375 cells was 16%.

Caspase 9 was also measured. The expression of caspase 9 in control A375 cells was 23%, this value increased to 73 and 65% for folate-modified doxorubicin and dacarbazine-loaded nano-emulsion treatments.

Pro-apoptotic gene Bax was expressed 6% in A375 cells, while in cells treated with folate-modified doxorubicin and dacarbazine-loaded pullulan-chitosan nano-emulsion this figure was 87 and 65% respectively. Naïve doxorubicin and dacarbazine-expressed Bax to 28 and 27.5% respectively.

Anti-apoptotic gene Bcl2 was expressed 17% in folate-modified doxorubicin-loaded nano-emulsion, 19% in folate modified dacarbazine-loaded nano-emulsion, 57% in doxorubicin, and 35% in dacarbazine treated cells, compared to 86% expression in control A375.

Caspase 3, in HaCaT cells treated with folate-modified doxorubicin and dacarbazine-loaded pullulan-chitosan nano-emulsion, expressed 15 and 3% respectively. While cells treated with naïve doxorubicin and dacarbazine expressed 13 and 59% caspase 3, respectively. Caspase 3 expression in control HaCaT cells was 17%.

Caspase 9 was also measured. The expression of caspase 9 in control HaCaT cells was 25%, this value was 24 and 28% for folate-modified doxorubicin and dacarbazine-loaded nano-emulsion treatments.

Pre-apoptotic gene Bax was expressed 37% in HaCaT cells, while in cells treated with folate-modified doxorubicin and dacarbazine-loaded pullulan-chitosan nano-emulsion this figure was 41 and 31% respectively. Naïve doxorubicin and dacarbazine-expressed Bax to 93 and 86% respectively.

Pre anti-apoptotic gene Bcl2 was expressed 93% in folate-modified doxorubicin-loaded nano-emulsion, 68% in folate modified dacarbazine-loaded nano-emulsion, 40% in doxorubicin, and 12% in dacarbazine-treated cells, compared to 96% expression in control HaCaT.

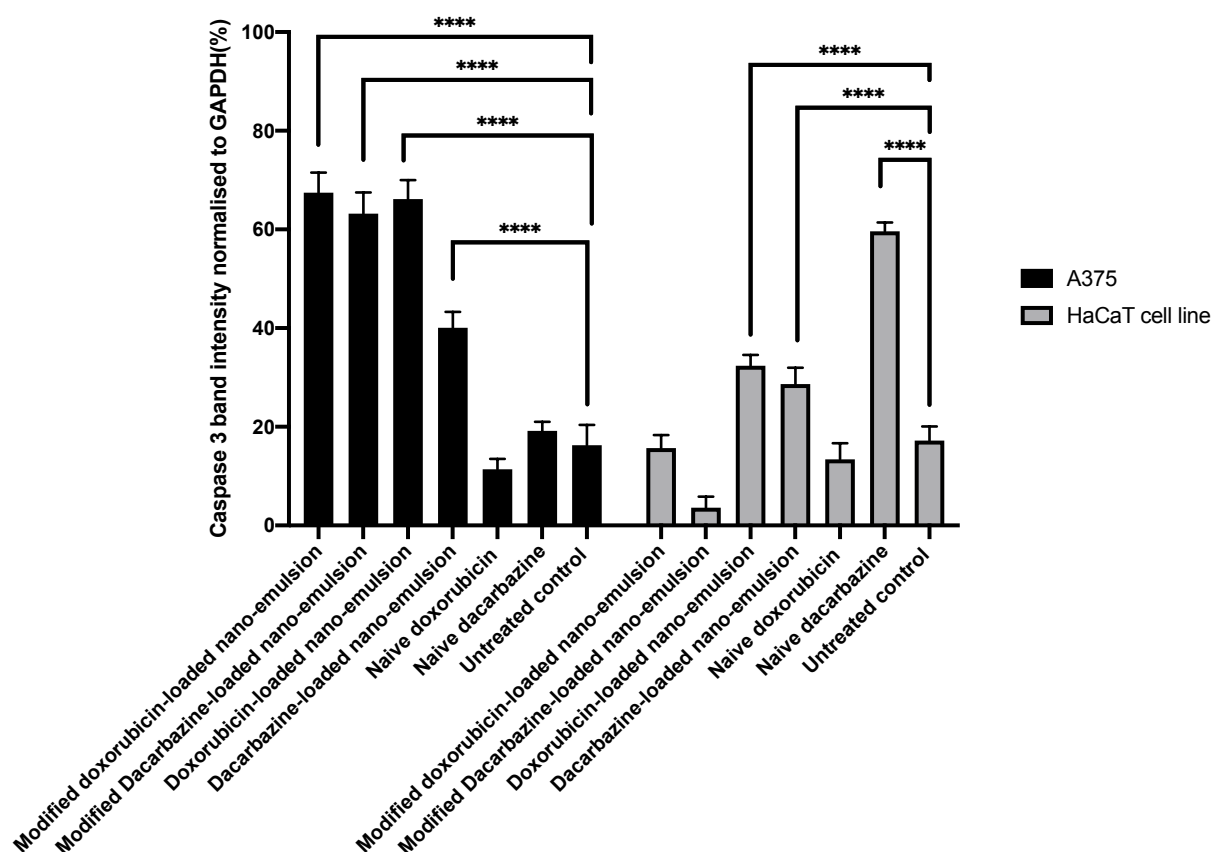


Figure 3.39 Quantified DNA band intensities analysed with PCR and gel electrophoresis (Caspase 3)

The figure demonstrates the expression of the caspase 3 gene in A375 and HaCaT cell lines treated with drug-loaded nano-emulsions and naïve drugs compared to untreated control cells. The band intensities were quantified using ImageJ. The Experiment was conducted after 72 hours of treatment. Complementary DNA was used to screen the gene expressions. The band intensity of each treatment was normalised to GAPDH (housekeeping gene) and is reported as a percentage of control (untreated cells). The data are representative of the mean values of 3 independent experiments \pm SD in the bar chart. The results were analysed with two-way ANOVA Tukey's comparison test, **** is indicating $P < 0.0001$, *** $P < 0.001$, ** $P < 0.01$, and * $P < 0.05$.

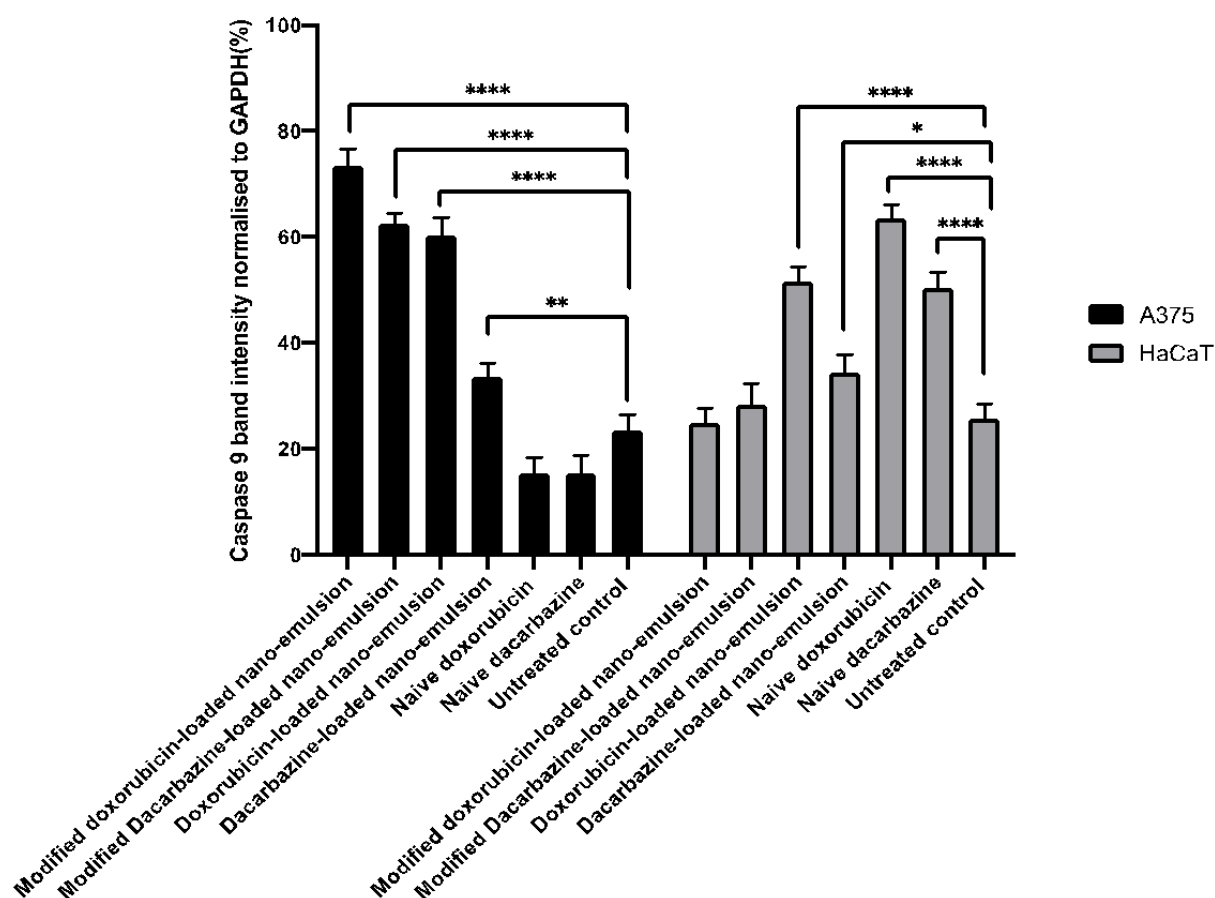


Figure 3.40 Quantified DNA band intensities analysed with PCR and gel electrophoresis (Caspase 9)

The figure demonstrates the expression of the caspase 9 gene in A375 and HaCaT cell lines treated with drug-loaded nano-emulsions and naïve drugs compared to untreated control cells. The band intensities were quantified using ImageJ. The Experiment was conducted after 72 hours of treatment. Complementary DNA was used to screen the gene expressions. The band intensity of each treatment was normalised to GAPDH (housekeeping gene) and is reported as a percentage of control (untreated cells). The data are representative of the mean values of 3 independent experiments \pm SD in the bar chart. The results were analysed with two-way ANOVA Tukey's comparison test, **** is indicating $P < 0.0001$, *** $P < 0.001$, ** $P < 0.01$, and * $P < 0.05$.

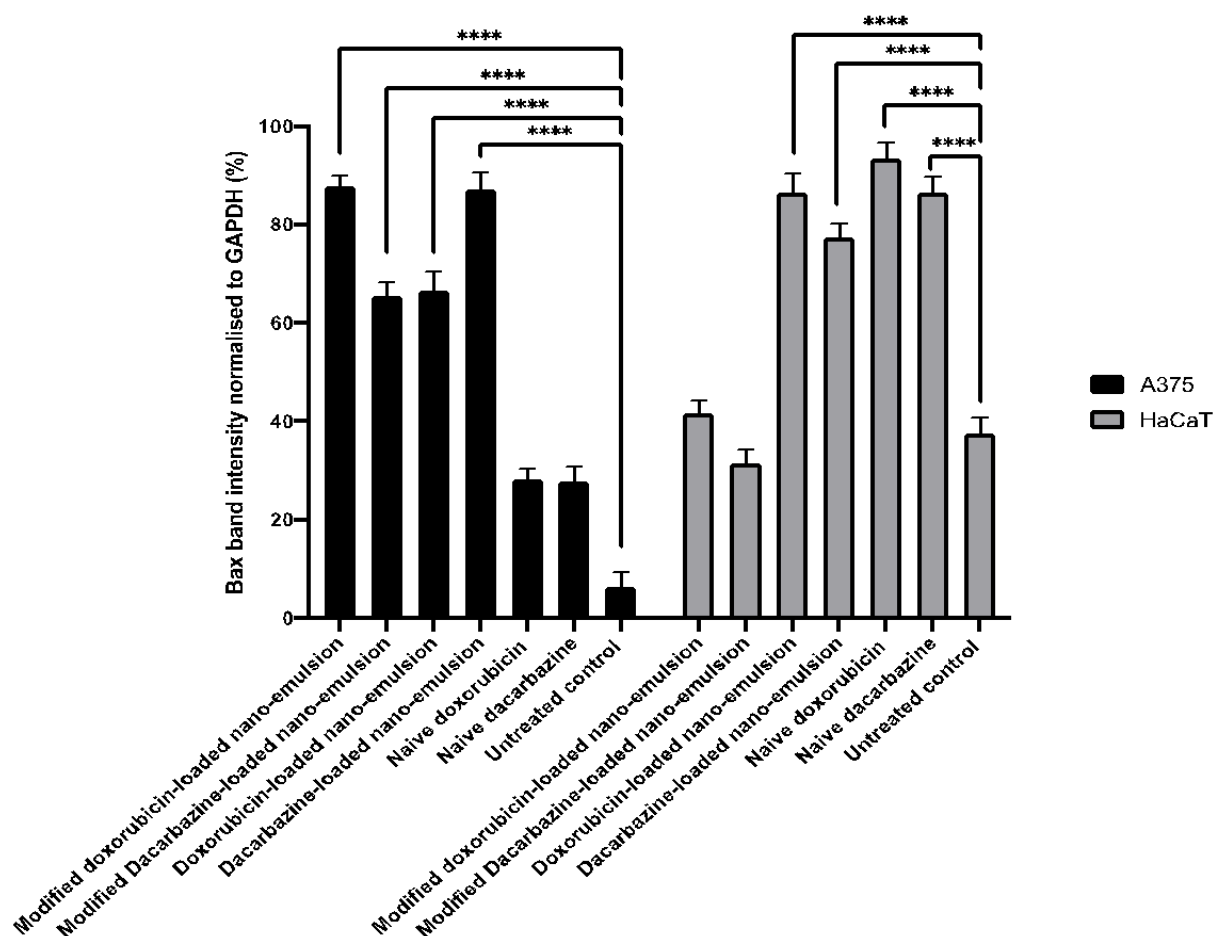


Figure 3.41 Quantified DNA band intensities analysed with PCR and gel electrophoresis (Bax)

The figure demonstrates the expression of the Bax gene in A375 and HaCaT cell lines treated with drug-loaded nano-emulsions and naïve drugs compared to untreated control cells. The band intensities were quantified using ImageJ. The Experiment was conducted after 72 hours of treatment. Complementary DNA was used to screen the gene expressions. The band intensity of each treatment was normalised to GAPDH (housekeeping gene) and is reported as a percentage of control (untreated cells). The data are representative of the mean values of 3 independent experiments \pm SD in the bar chart. The results were analysed with two-way ANOVA Tukey's comparison test, **** is indicating $P < 0.0001$, *** $P < 0.001$, ** $P < 0.01$, and * $P < 0.05$.

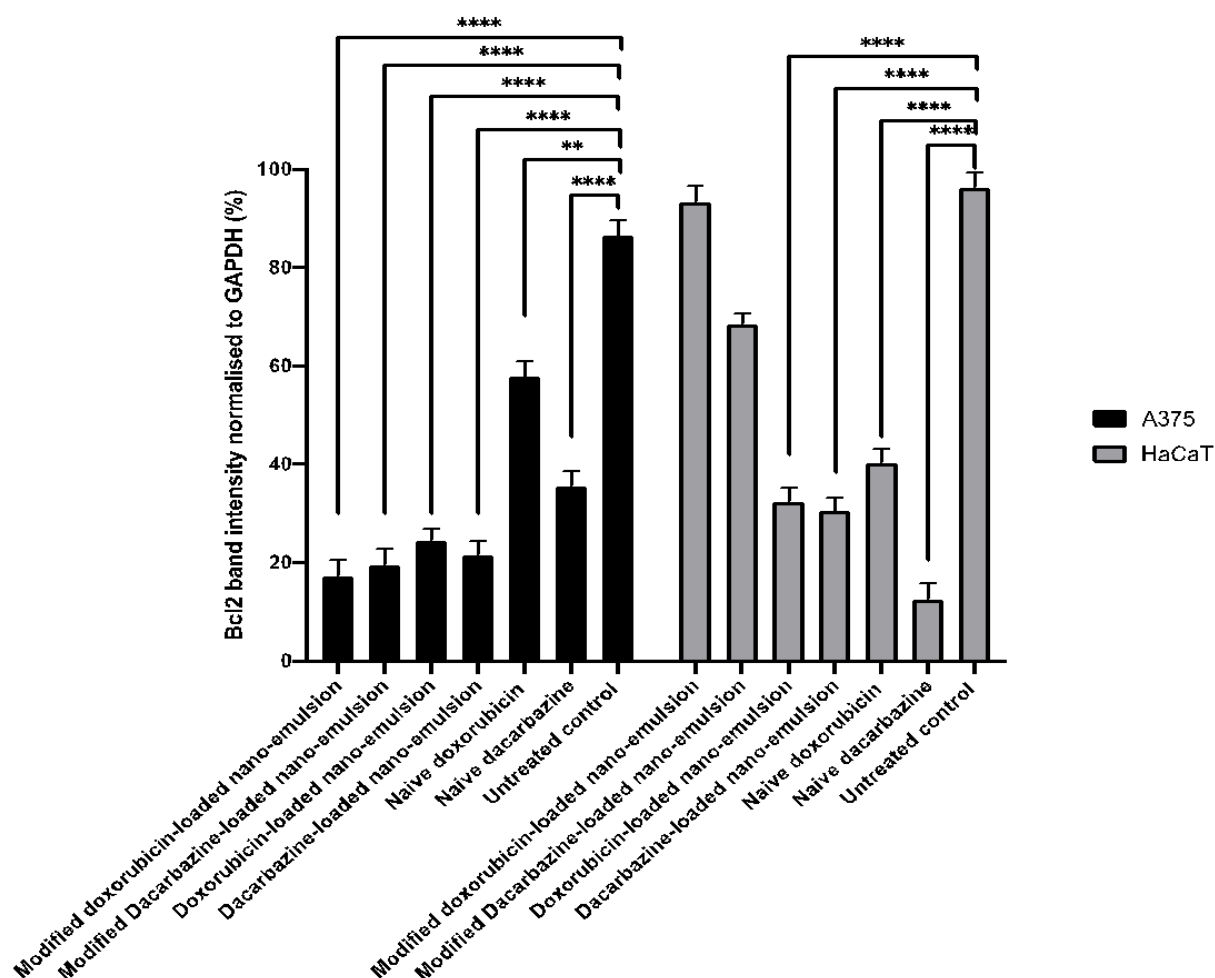


Figure 3.42 Quantified DNA band intensities analysed with PCR and gel electrophoresis (Bcl2)

The figure demonstrates the expression of the Bcl2 gene in A375 and HaCaT cell lines treated with drug-loaded nano-emulsions and naïve drugs compared to untreated control cells. The band intensities were quantified using ImageJ. The Experiment was conducted after 72 hours of treatment. Complementary DNA was used to screen the gene expressions. The band intensity of each treatment was normalised to GAPDH (housekeeping gene) and is reported as a percentage of control (untreated cells). The data are representative of the mean values of 3 independent experiments \pm SD in the bar chart. The results were analysed with two-way ANOVA Tukey's comparison test, **** is indicating $P < 0.0001$, *** $P < 0.001$, ** $P < 0.01$, and * $P < 0.05$.

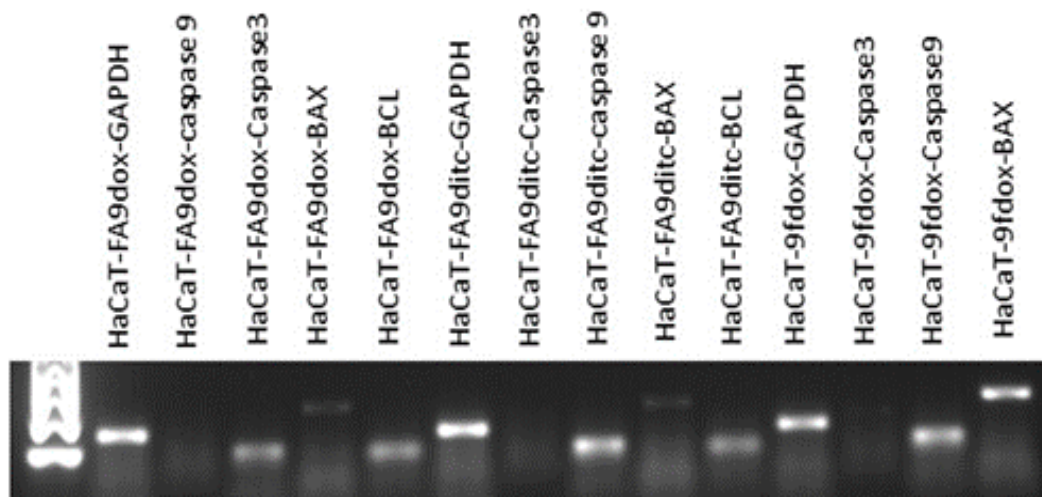


Figure 3.43 DNA bands detected in agarose gel

After the thermo-cycler step, the samples were collected and mixed with 3 μ l of loading dye. The mixtures were then loaded into the wells and run on the 1% agarose gel in the tank. A molecular weight marker of 1Kb and 100 Kb were used alongside the cDNA samples. Electrophoresis was set to run for 60 minutes in the 100 V constant. After 60 minutes, the gel was imaged using the UV transilluminator at the wavelength of 200-280 nm and the DNA fragments were detected.

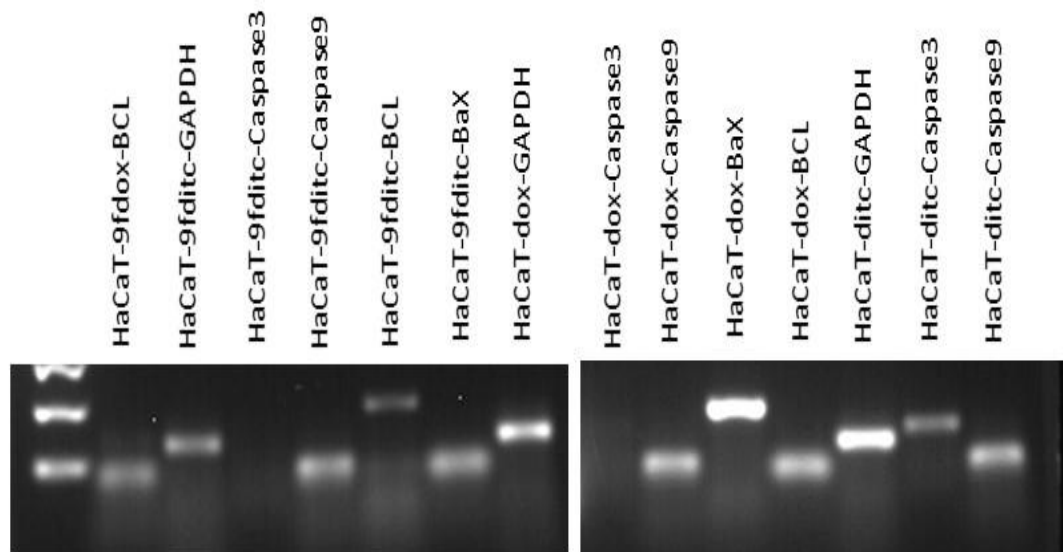


Figure 3.44 DNA bands detected in agarose gel

After the thermo-cycler step, the samples were collected and mixed with 3 μ l of loading dye. The mixtures were then loaded into the wells and run on the 1% agarose gel in the tank. A molecular weight marker of 1Kb and 100 Kb were used alongside the cDNA samples. Electrophoresis was set to run for 60 minutes in the 100 V constant. After 60 minutes, the gel was imaged using the UV transilluminator at the wavelength of 200-280 nm and the DNA fragments were detected.

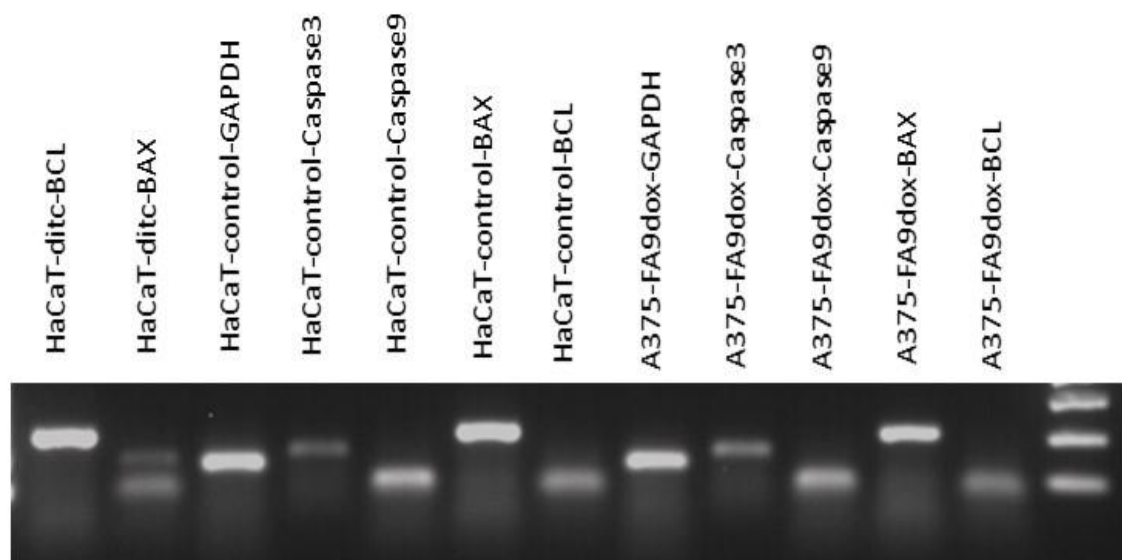


Figure 3.45 DNA bands detected in agarose gel

After the thermo-cycler step, the samples were collected and mixed with 3 μ l of loading dye. The mixtures were then loaded into the wells and run on the 1% agarose gel in the tank. A molecular weight marker of 1Kb and 100 Kb were used alongside the cDNA samples. Electrophoresis was set to run for 60 minutes in the 100 V constant. After 60 minutes, the gel was imaged using the UV transilluminator at the wavelength of 200-280 nm and the DNA fragments were detected.

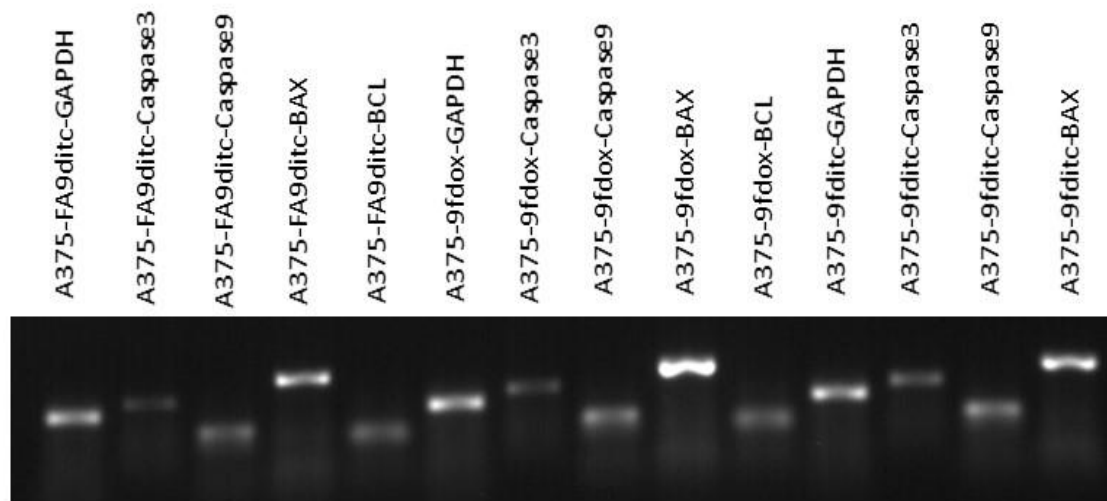


Figure 3.46 DNA bands detected in agarose gel

After the thermo-cycler step, the samples were collected and mixed with 3 μ l of loading dye. The mixtures were then loaded into the wells and run on the 1% agarose gel in the tank. A molecular weight marker of 1Kb and 100 Kb were used alongside the cDNA samples. Electrophoresis was set to run for 60 minutes in the 100 V constant. After 60 minutes, the gel was imaged using the UV transilluminator at the wavelength of 200-280 nm and the DNA fragments were detected.

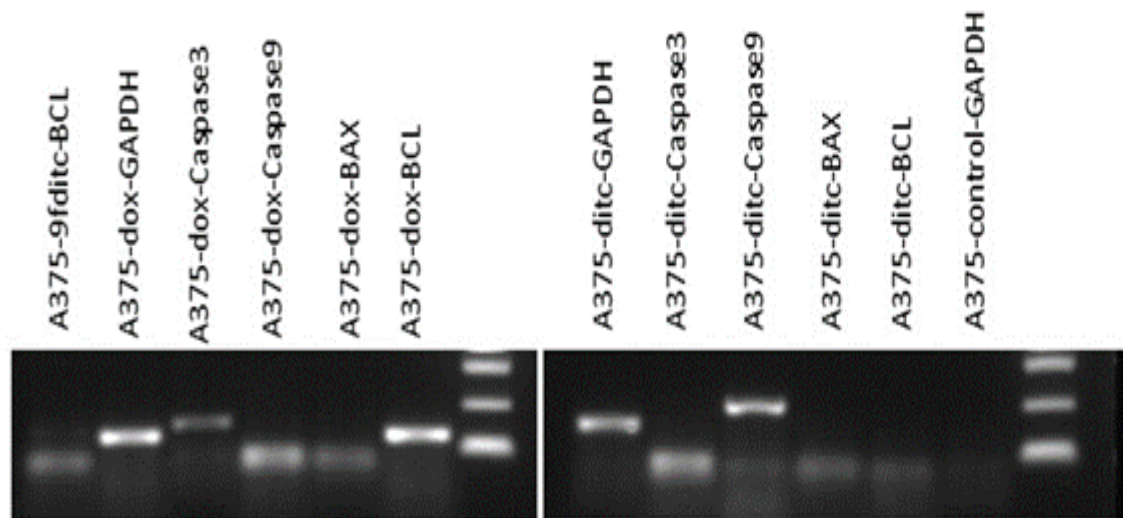


Figure 3.47 DNA bands detected in agarose gel

After the thermo-cycler step, the samples were collected and mixed with 3 μ l of loading dye. The mixtures were then loaded into the wells and run on the 1% agarose gel in the tank. A molecular weight marker of 1Kb and 100 Kb were used alongside the cDNA samples. Electrophoresis was set to run for 60 minutes in the 100 V constant. After 60 minutes, the gel was imaged using the UV transilluminator at the wavelength of 200-280 nm and the DNA fragments were detected.

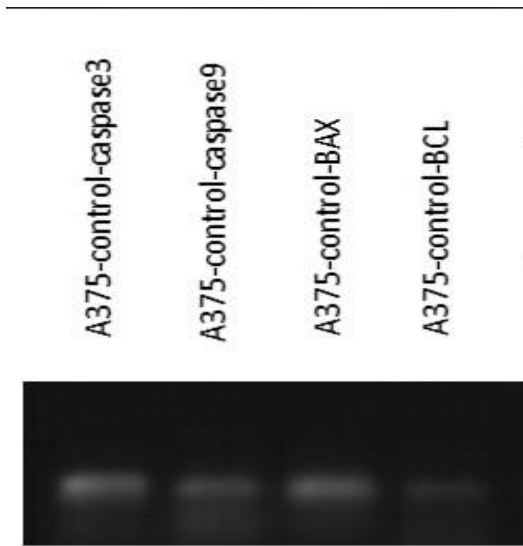


Figure 3.48 DNA bands detected in agarose gel

After the thermo-cycler step, the samples were collected and mixed with 3 μ l of loading dye. The mixtures were then loaded into the wells and run on the 1% agarose gel in the tank. A molecular weight marker of 1Kb and 100 Kb were used alongside the cDNA samples. Electrophoresis was set to run for 60 minutes in the 100 V constant. After 60 minutes, the gel was imaged using the UV transilluminator at the wavelength of 200-280 nm and the DNA fragments were detected.

3.2.4.5 Folate binding protein ELISA

To confirm folate receptors' quantity on A375 cell's surface, folate binding protein (FBP) ELISA was conducted. This was reported before by (Ogboodu et al., 2015), however, secondary confirmation was done in current research. Hence, the FBP ELISA was conducted to confirm and quantify the folate binding receptors on melanoma (A375) compared to keratinocytes (HaCaT) as negative control and epithelial breast cells (MDB-MA-231) as a positive control. This is to show that uptake of the folate-modified nano-emulsions in melanoma cells is via folate receptors. The results obtained from the colourimetric reading and using linear regression from the standard curve Figure 3.49. Table 3.2 is indicating the concentration of the folate receptors expressed in three cell lines. Accordingly, the folate concentration on the A375 surface is 179 pg/ml, for HaCaT and MDB-MA-231 the concentrations are 21.5 and 315 pg/ml respectively.

Three supernatants of three cell lines were used, A375, HaCaT, and MDB-MA-231. HaCaT cell line was used as negative control and MDB-MA-231 cell supernatant was used as a positive control. Subsequently, it was confirmed that A375 cells express folate receptors, however less than MDB-MA-231. HaCaT had negative amounts and on the other hand, MDB-MA-231 was containing an increased amount of folate receptors compared to A375 melanoma.

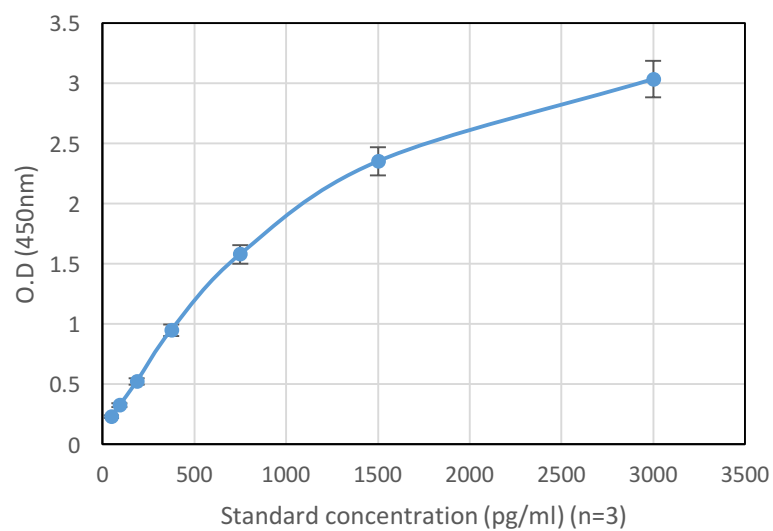


Figure 3.49 Standard curve of different concentrations of the folate binding protein detected in ELISA

The results are the mean value of three independent ELISA tests \pm SD.

Table 3.2 Folate receptor concentration

Cell line	FBP concentration (pg/ml)
A375	179
MDB-MA-231	315
HaCaT	21.5

3.3 Evaluation of anti-inflammatory compounds encapsulated in nano-emulsions on melanoma cells

3.3.1 Introduction: Encapsulation of BMS-470539-dihydrochloride and [DTrp⁸]- γ -MSH in pullulan-chitosan nano-emulsion as a novel tool for melanoma treatment

Previous studies have shown the expression of MC₁ on A375 cells (Nagy et al., 2017), and multiple studies have shown these to have anti-inflammatory effects in different models of inflammation including gout (Getting et al., 2006), asthma (Getting et al., 2008), Rheumatoid Arthritis (Patel et al., 2010), Osteoarthritis (Can et al., 2020, Kaneva et al., 2012) and Stroke (Holloway et al., 2015). MC₁ receptor is activated by the number of melanocortin peptides including α -Melanocyte stimulating hormone (α MSH), NDP- α -MSH, and POMC gene-derived peptides (Tafreshi et al., 2019). Hence, in this study, the effect of encapsulation of the anti-inflammatory compounds in nano-emulsion was investigated. This approach seeks to find out any improvement in their anti-inflammatory effect and consequently a reduction in melanoma viability. The approach involved encapsulation of BMS-470539-dihydrochloride and [DTrp⁸]- γ -MSH in pullulan-chitosan modified nano-emulsion and subsequent measurement of iNOS and COX-2 level in A375 cells.

Accordingly, the compounds were encapsulated in folate-modified pullulan-chitosan nano-emulsion and according to the methodology explained in section 2.2.6. However, due to the

limited half-life of the compounds, the encapsulation procedures were completed in less than 6 hours.

3.3.2 Viability of A375 cells treated with encapsulated BMS-470539-dihydrochloride and [DTrp⁸]- γ -MSH in folate-modified pullulan-chitosan nano-emulsion

To clarify the effect of naïve BMS-470539-dihydrochloride and [DTrp⁸]- γ -MSH and their encapsulation in nano-emulsion on the melanoma cell treatment, the MTT cytotoxicity test was performed to assess their effects on cell viability. The A375 cells were treated with BMS-470539-dihydrochloride (10 μ g/ml) and [DTrp⁸]- γ -MSH (3 μ g/ml) and encapsulated BMS-470539-dihydrochloride and [DTrp⁸]- γ -MSH for 24, 48, and 72 hours and the viability of A375 cells was measured and analysed accordingly.

The viability of cells treated with BMS-470539-dihydrochloride ranged from 78 to 86% and for encapsulated BMS-470539-dihydrochloride from 75 to 12% over the 24-72-hour time course. The viability of cells treated with [DTrp⁸]- γ -MSH ranged from 83 to 59% and for encapsulated [DTrp⁸]- γ -MSH were from 68.05 to 9% over the 24-72-hour time course (Figure 3.50-3.52).

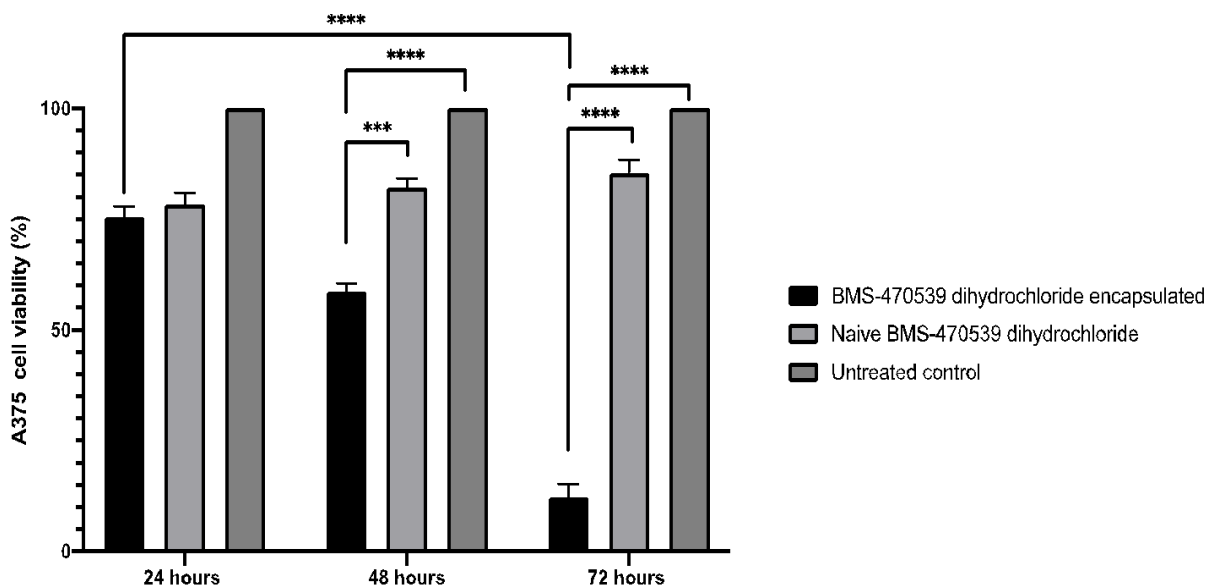


Figure 3.50 Viability of the A375 cells treated with encapsulated and naïve BMS-470539-dihydrochloride

A375 cells were treated with naïve and encapsulated BMS-470539-dihydrochloride (10µg/ml). Independent experiments were conducted for different time points. The test was conducted 24, 48, and 72 hours after treatments. The viability data were obtained using the MTT method, results were calculated based on untreated control cells, and reported as the percentage of control. Bars represent the mean value of 6 biological replicates \pm SD error. The data were analysed with two-way ANOVA Tukey's comparison test, **** is indicating $P < 0.0001$, *** $P < 0.001$, ** $P < 0.01$, and * $P < 0.05$.

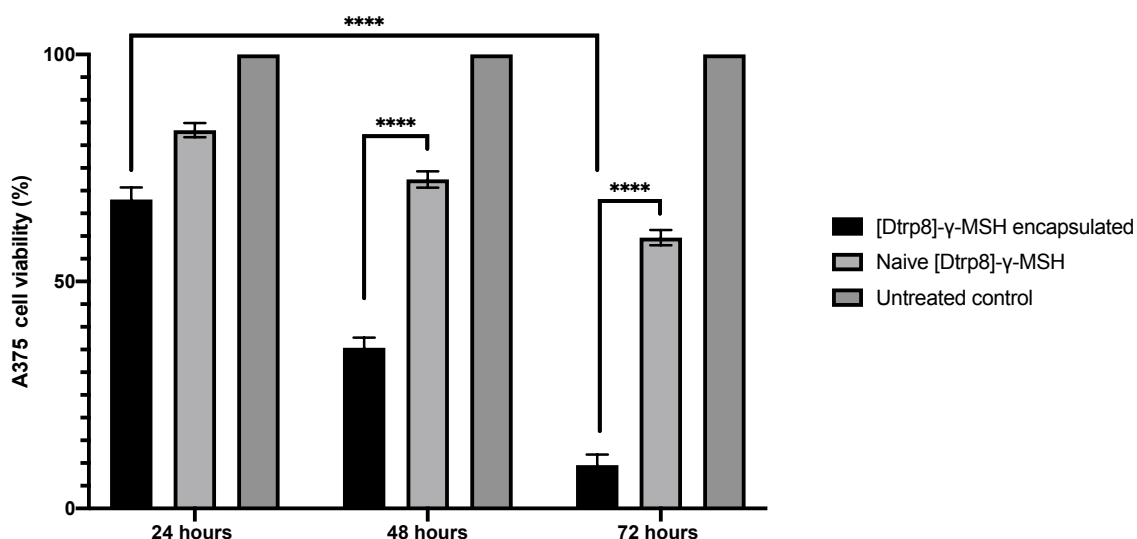


Figure 3.51 Viability of the A375 cells treated with encapsulated and naïve [DTrp⁸]-γ-MSH

A375 cells were treated with naïve and encapsulated [DTrp⁸]-γ-MSH (1μg/ml). Independent experiments were conducted for different time points. The test was conducted 24, 48, and 72 hours after treatments. The viability data were obtained using the MTT method, results were calculated based on untreated control cells, and reported as the percentage of control. Bars represent the mean value of 6 biological replicates ±SD error. The data were analysed with two-way ANOVA Tukey's comparison test, **** is indicating $P < 0.0001$, *** $P < 0.001$, ** $P < 0.01$, and * $P < 0.05$.

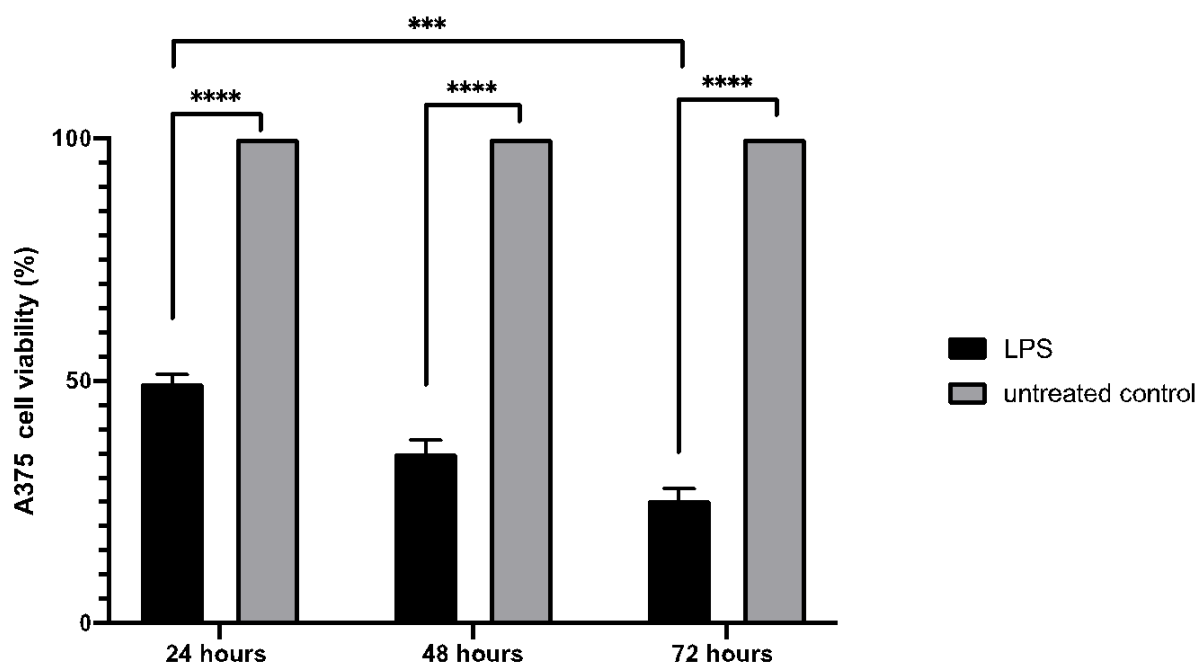


Figure 3.52 Viability of the A375 cells treated with LPS

A375 cells were treated with LPS. Independent experiments were conducted for different time points. The test was conducted 24, 48, and 72 hours after treatments. The viability data were obtained using the MTT method, results were calculated based on untreated control cells, and reported as the percentage of control. Bars represent the mean value of 6 biological replicates \pm SD error. The data were analysed with two-way ANOVA Tukey's comparison test, **** is indicating $P < 0.0001$, *** $P < 0.001$, ** $P < 0.01$, and * $P < 0.05$.

According to Figure 3.50 and 3.51, the viability of A375 cells treated with encapsulated compounds decreased drastically during 72 hours, compared to untreated control cells. The viability of A375 cells treated with naïve BMS-470539-dihydrochloride decreases to 84% over 72 hours, compared to untreated A375 cells. However, A375 cells treated with encapsulated BMS-470539-dihydrochloride were 15% viable after 72 hours. Likewise, A375 cells treated with naïve [DTrp⁸]- γ -MSH show decreased viability to 58.35% over 72 hours and to 23.29% for the cells treated with encapsulated [DTrp⁸]- γ -MSH. LPS decreased the viability of A375 cells from 49.36% to 25.17% both compared to control viable cells.

3.3.3 iNOS and COX-2 expression analysis

Expression of iNOS and COX-2 are important markers of inflammation and directly affect melanoma proliferation and invasion (Johansson et al., 2009). Hence, the effect of encapsulated peptides in decreasing cell viability and proliferation of melanoma cells is of importance to disease progression. Since increased iNOS and COX-2 are markers for inflammation and particularly a marker for progression and invasion of melanoma, expression of both during the treatment with encapsulated BMS-470539-dihydrochloride and [DTrp⁸]- γ -MSH in pullulan-chitosan modified nano-emulsion was measured.

A western blot experiment was done to screen the expression of iNOS and COX-2 proteins in treated melanoma cells. Cells were treated with both encapsulated and naïve compounds, in the presence or absence of LPS (1.0 μ g/ml).

The figure below (Figure 3.53) is an indication of the iNOS and COX-2 expressions that were conducted using western blot assay.

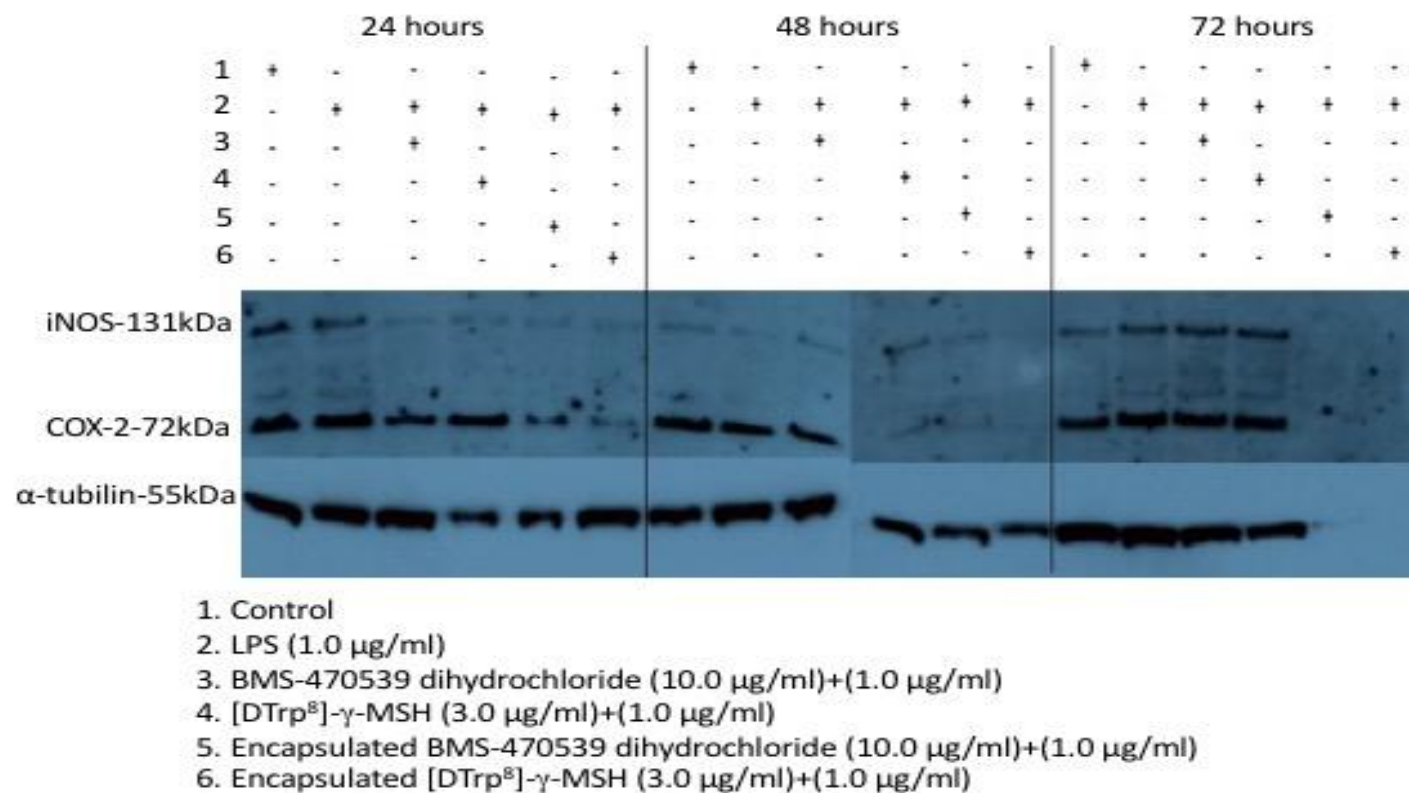


Figure 3.53 iNOS and COX-2 expression analysis by Western blot

This image is a single demonstration of three independent western blots (for each time point) conducted to analyse iNOS and COX-2 expressions in treated A375 cells. The experiment was conducted after 24, 48, and 72 of incubation with treatments. The results are normalised to α-tubulin. The full blots are presented in appendix C figure 7.4.

According to the figure, iNOS and COX-2 expression significantly decreased using encapsulated compound treatments at 48 and 72hour time points compared to their expression in A375 cells treated with non-encapsulated compound. At the earlier time point only a reduction was seen with respect to COX-2 with similar levels of expression observed for iNOS. Accordingly, the iNOS and COX-2 expressions were zero after 72 hours. However, the proteins were still expressed in the cells treated with only peptides. The Intensity of the bands obtained in the western blot was normalized with α -tubulin, quantified and presented in Figure 3.53.

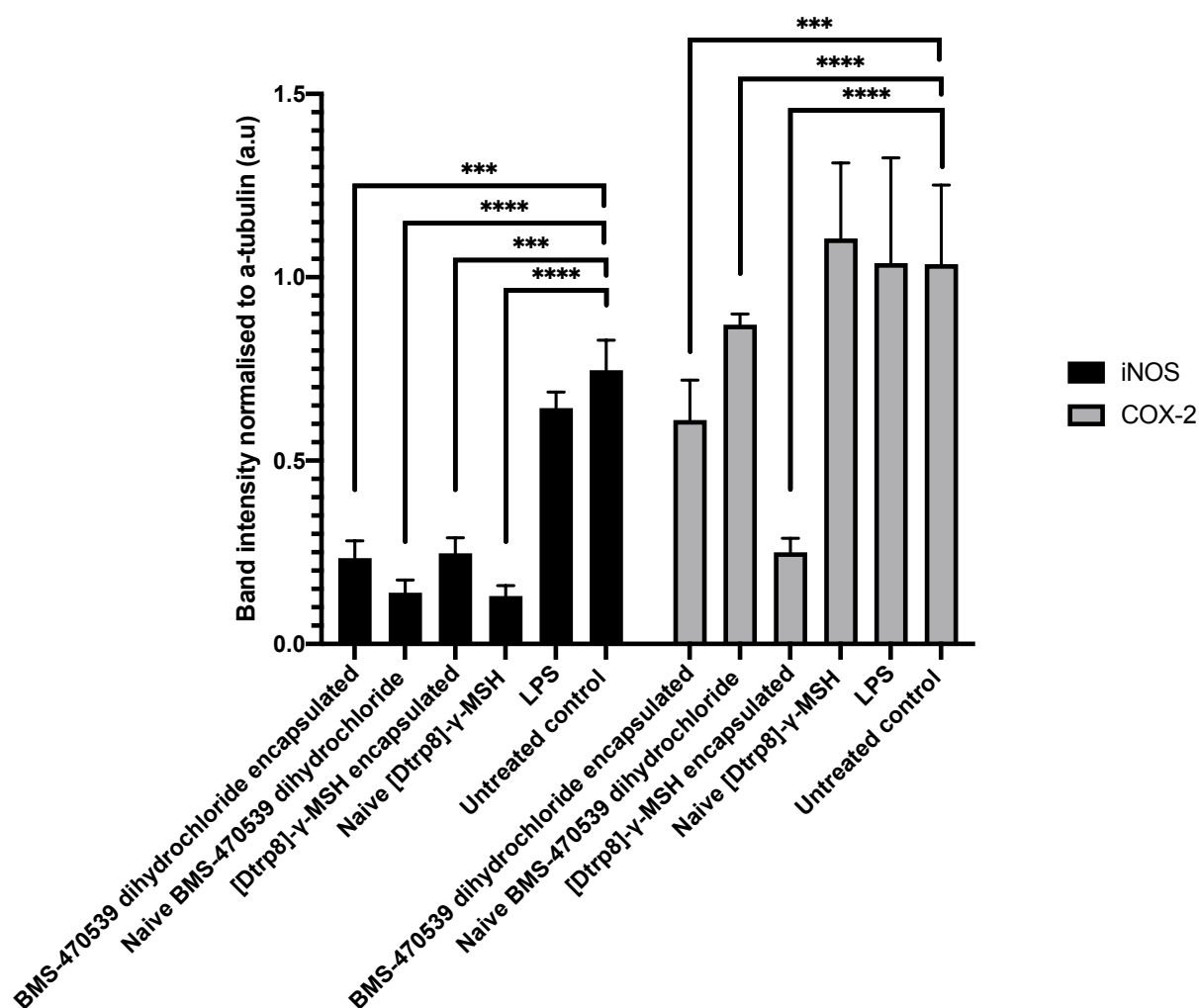


Figure 3.54 iNOS and COX-2 expression over 24 hours in melanoma cells treated with encapsulated and naïve compounds

Expression of iNOS and Cox-2 were evaluated by western blot. The experiment was conducted to analyse iNOS and COX-2 expressions in treated A375 cells. The results are reported as a mean value obtained from three independent western blots after 24 hours of treatment. The results are normalised to α-tubulin. Concentrations used for the treatments were , 10 µg/ml BMS-470539-dihydrochloride, 3.0 µg/ml [DTrp⁸]-γ-MSH and 1µg/ml LPS, the bars are indicating mean values ±SD error bar.

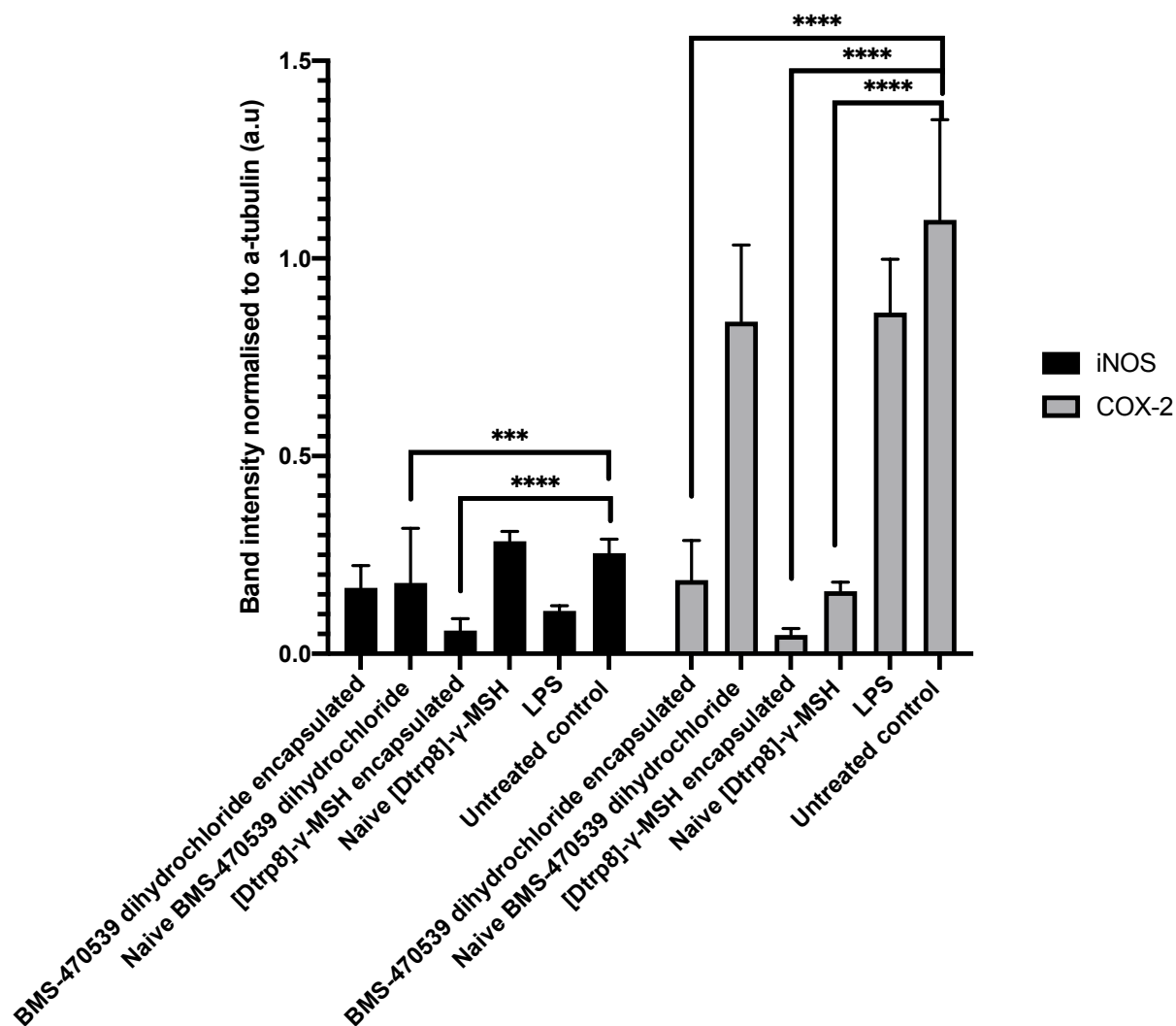


Figure 3.55 iNOS and COX-2 expression over 48 hours in melanoma cells treated with encapsulated and naïve compounds

Expression of iNOS and Cox-2 were evaluated by western blot. The experiment was conducted to analyse iNOS and COX-2 expressions in treated A375 cells. The results are reported as a mean value obtained from three independent western blots after 48 hours of treatment. The results are normalised to α -tubulin. Concentrations used for the treatments were, 10 μ g/ml BMS-470539-dihydrochloride, 3.0 μ g/ml [DTrp⁸]- γ -MSH, and 1 μ g/ml LPS, the bars are indicating mean values \pm SD error bar.

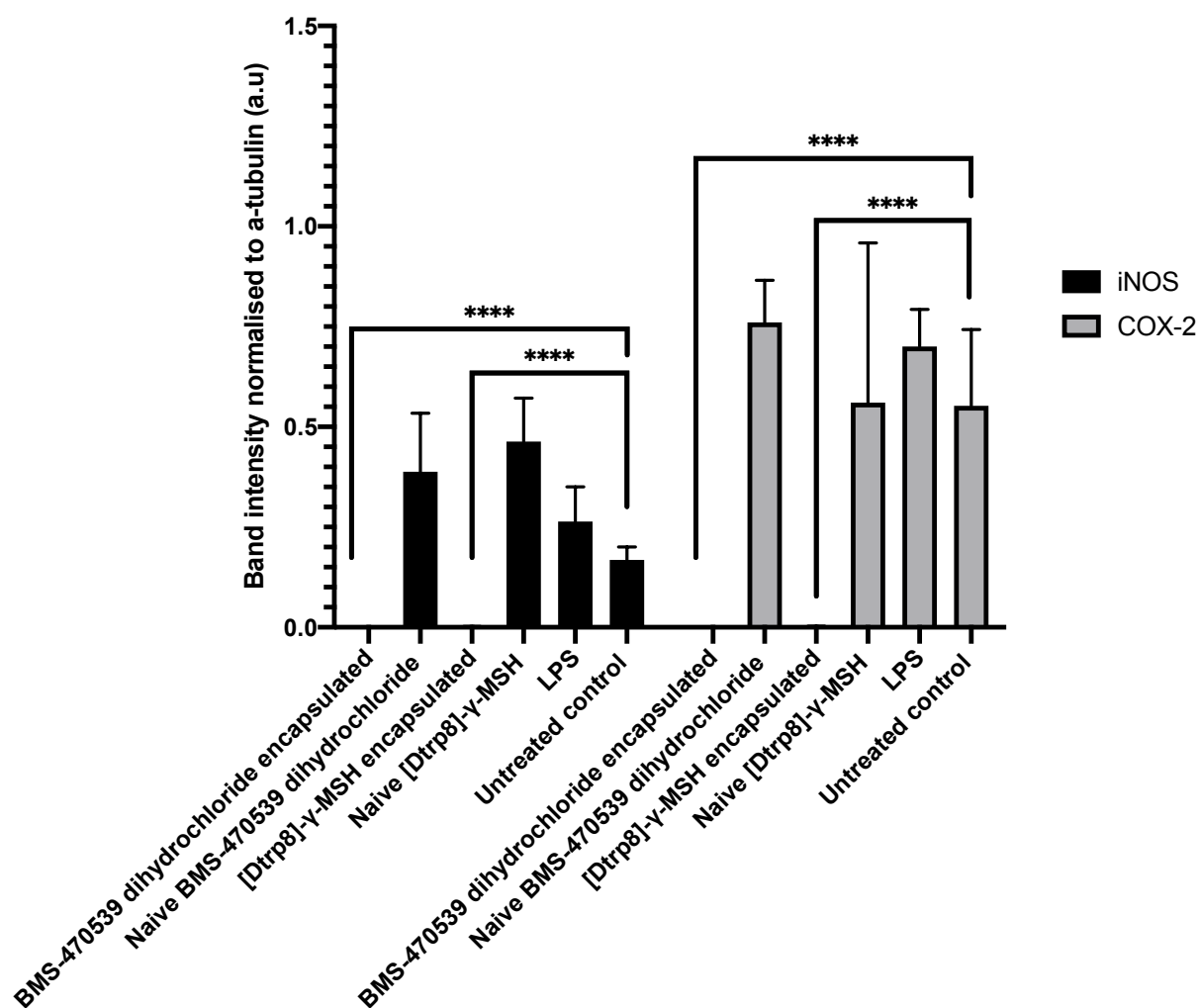


Figure 3.56 iNOS and COX-2 expression over 72 hours in melanoma cells treated with encapsulated and naïve compounds

Expression of iNOS and Cox-2 were evaluated by western blot. The experiment was conducted to analyse iNOS and COX-2 expressions in treated A375 cells. The results are reported as a mean value obtained from three independent western blots after 72 hours of treatment. The results are normalised to α -tubulin. Concentrations used for the treatments were , 10 μ g/ml BMS-470539-dihydrochloride, 3.0 μ g/ml [DTrp⁸]- γ -MSH and 1 μ g/ml LPS, the bars are indicating mean values \pm SD error bar

According to image 3.56, no bands are representing the expression of iNOS and COX-2 after 72 hours of treatment with encapsulated BMS-470539-dihydrochloride and [DTrp⁸]- γ -MSH. This is an indication of no iNOS and COX-2 expression in melanoma cells, on the other hand, the α -tubulin band associated with the 72hour treatment of encapsulated compounds displays low expression. This was due to the lower population of A375 cells in the wells after 72 hours of treatment with encapsulated compounds. As the results are consistent with the MTT viability experiment for 72hour treatment of the cells with encapsulated compounds (figures 3.50, and 3.51). The viability of A375 cells treated with encapsulated compounds was significantly lower compared to control and naïve compounds.

3.3.4 Fluorescent microscopy of A375 and HaCaT cells in co-culture, treated with encapsulated BMS-470539-dihydrochloride and [DTrp⁸]- γ -MSH and non-encapsulated BMS-470539-dihydrochloride and [DTrp⁸]- γ -MSH

To screen the effects of compounds visually, the treatments were done on co-culture of A375 melanoma and HaCaT keratinocytes. Here the effect of treatments can be detected on keratinocytes as well (Curry et al., 2001).

Figure 3.57 and Figure 3.58 were obtained from the treated co-culture plates over 24, 48, and 72 hours. The co-culture plates were imaged with DMEM inside the wells. Therefore, the effect of treatments was observed during 72 hours.

According to the images, the effect of encapsulated BMS-470539-dihydrochloride and [DTrp⁸]- γ -MSH on melanoma cells can be distinguished.

A375 cells are rapidly proliferating cells under normal culture conditions. In Figure 3.57 and Figure 3.58 both encapsulated BMS-470539-dihydrochloride and [DTrp⁸]- γ -MSH have inhibited A375 proliferation while HaCaT cells are proliferating. The A375 cells are labelled green (CMFDA) and HaCaT cells are labelled red (CMTPX).

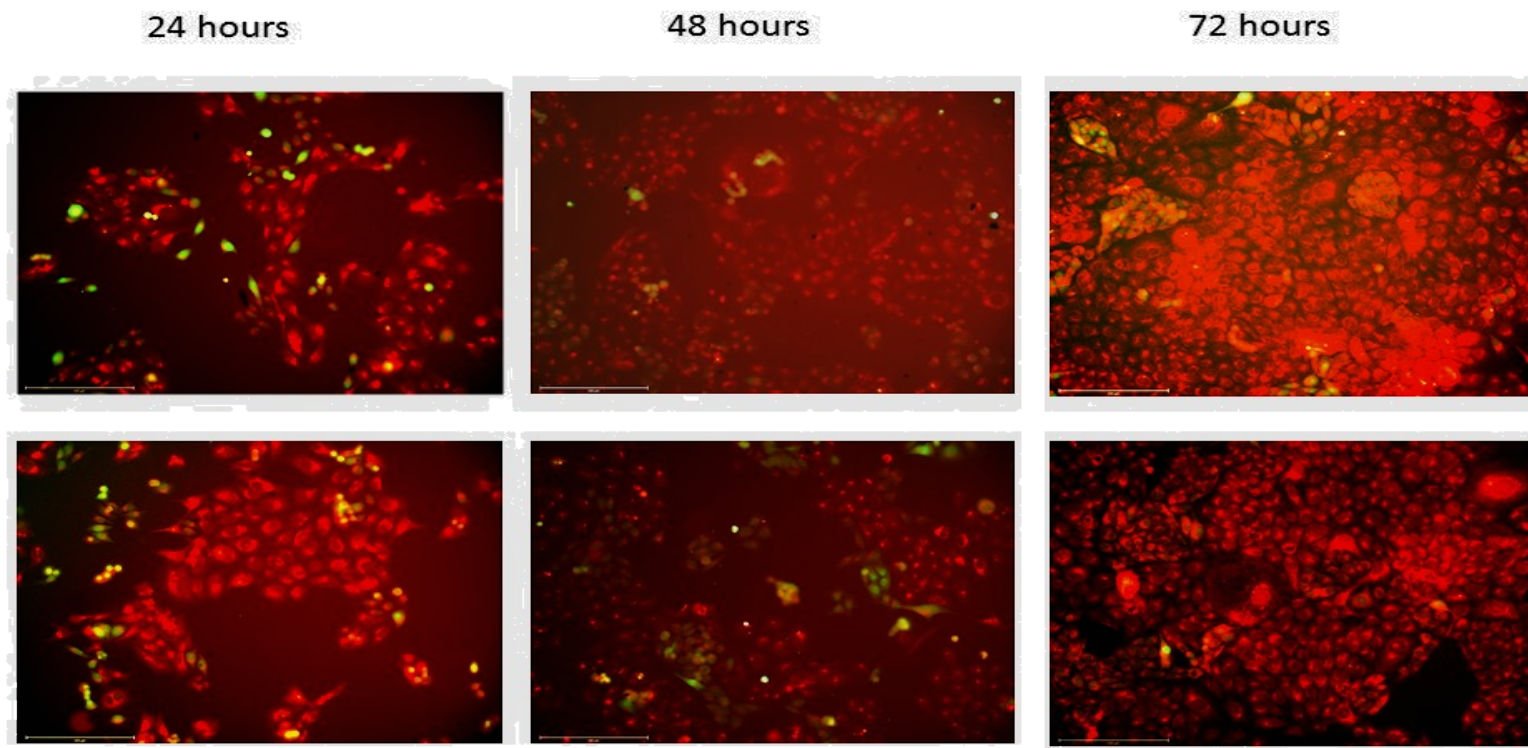


Figure 3.57 Fluorescent imaging of HaCaT and A375 co-cultures treated with encapsulated and naïve BMS-470539-dihydrochloride

The images are a single demonstration of three independent experiments. The cells labelled with CMFDA green (A375) and CMTPX red (HaCaT), incubated after treatments and imaged on 24th, 48th, and 72nd hours of incubation time. All images belong to a single multi-wall plate containing cells and treatments and contain DMEM. The cells were treated with 10µg/ml encapsulated and naïve BMS-470539-dihydrochloride, over 72 hours (scale bar 200µm).

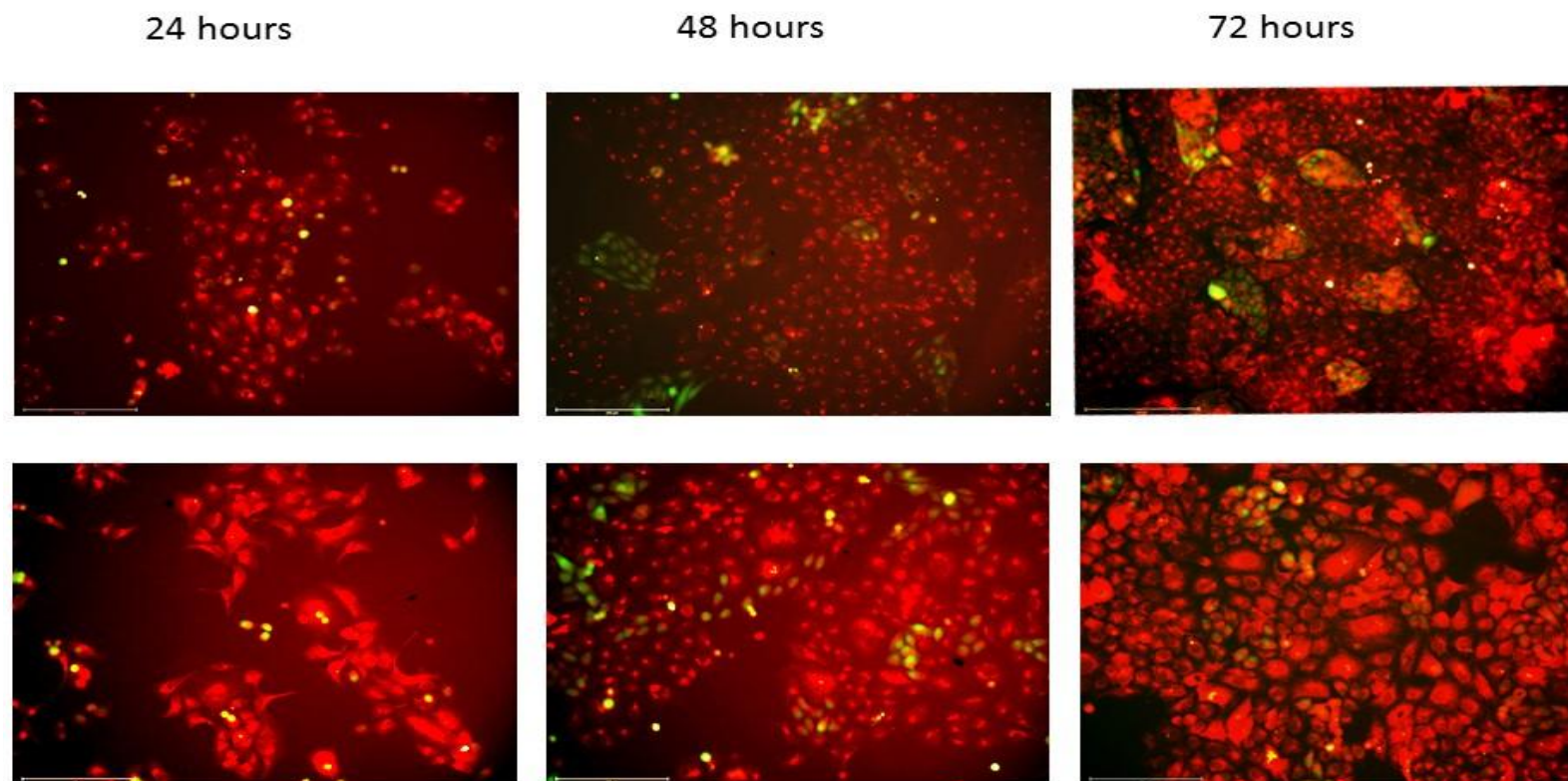


Figure 3.58 Fluorescent imaging of HaCaT and A375 co-cultures treated with encapsulated and naïve [DTrp⁸]-γ-MSH

The images are a single demonstration of three independent experiments. The cells labelled with CMFDA green (A375) and CMTPIX red (HaCaT), incubated after treatments and imaged on 24th, 48th, and 72nd hours of incubation time. All images belong to a single multi-wall plate containing cells and treatments and contain DMEM. The cells were treated with 10μg/ml encapsulated and naïve [DTrp⁸]-γ-MSH , over 72 hours (scale bar 200μm).

T

4 Discussion

4.1 Introduction

The development of chemo-resistance in response to cytotoxic drugs in the course of melanoma treatment was a major obstacle toward efficient therapy (Naves et al., 2017a). So far, researchers have vastly investigated approaches to defeat melanoma drug resistance, however, few have address flux-dependent melanoma chemo-resistance (Robey et al., 2018). This thesis aimed to design a drug delivery to alleviate melanoma by decreasing its resistance towards cytotoxic drugs. This was done by encapsulating the drug in a polymeric nano-emulsion providing a controlled release thereby controlled drug efflux. The nano-emulsion was also designed to facilitate the treatment procedure by using topical delivery administration for early-stage melanoma. The first part of this thesis was concerned with the development of a novel nano-emulsion delivery system to address melanoma and the associated chemo-resistant (Khalid and El-Sawy, 2017).

Efficient targeted therapy and controlled delivery of therapeutics have been successfully applied to provide enhanced apoptosis induction to A375 primary melanoma cells. Subsequently, controlled delivery of therapeutics via nano-emulsion was investigated as an efficient melanoma targeted therapy approach. As a consequence, the viability of A375 decreased by 15% while treated with doxorubicin and dacarbazine-loaded nano-emulsions, compared to untreated A375. Furthermore, the drug-carrying nano-emulsion was able to induce apoptosis to A375 cells by 80% after 72 hours.

In the second part of the study, as a novel approach, BMS470539 and [DTrp⁸]- γ -MSH were delivered to A375 cells using the nano-emulsion. The compounds were used to target the

regulation of iNOS and COX-2 in A375 cells. iNOS and COX-2 are two important markers for melanoma progression (Hao et al., 2018) hence this feature was investigated as potential progress for melanoma treatment. The anti-inflammatory compound loaded nano-emulsions decrease melanoma viability by 10% and 12% compared to non-encapsulated compounds. This was done in consequence of decreased iNOS and COX-2 expressions to 0% after 72 hours of treatment with encapsulated anti-inflammatory compounds.

4.2 Nano-emulsion optimisation

4.2.1 *In vitro* release test

In general, specific drug delivery systems are used as tools to retain the drug in the body or affected area (Sagbas and Sahiner, 2018). However, in cancer drug delivery, there are other aspects to be considered. For example, the patient's lifetime, the tumour should be able to be eliminated at the earliest in the host body (Koushik et al., 2016). In the meantime, the drug release should not be too fast to prevent chemo-resistance (Cavaco et al., 2017). Hence as a primary step drug release pattern has been optimised based on the “cancer drug delivery” criteria (Iturrioz-Rodríguez et al., 2019, Sun et al., 2020).

Nano-emulsions developed from each of the polymers (chitosan, pullulan, and alginate) successfully slowed down the drug release over the 21 days, however, they did not provide a steady release. Not all the samples presented a steady and controlled release profile to fulfill the criteria of this research. Minute details and fluctuations in the cumulative release trends of all nano-emulsions affect the final result (Senapati et al., 2018a). Alginate nano-emulsions

presented a lower initial burst compared to pullulan and chitosan, Yet, chitosan and pullulan nano-emulsions presented more fluctuations in the release profiles. However, pullulan and chitosan are reported to provide controlled release after further modifications (Soni et al., 2018, Shah et al., 2020, Mahdavinia et al., 2017).

The release pattern measurements were done over 21 days (section 3.1.2.1). Hence, major fluctuations detected after 72 hours were deemed to be due to the instability of coumarin-6 (Gupta et al., 2019). On the other hand, doxorubicin was separately encapsulated in the same nano-emulsions and the release profiles were screened. As was expected, more steady cumulative release patterns were detected assuming that blended nano-emulsions improved the bioavailability of doxorubicin (Khdaier et al., 2016). This was due to the more stable nature of doxorubicin compared to coumarin-6 (Bastiat et al., 2013, Li et al., 2019a). Hence coumarin-6 is a good option to track nano-particles but for short-term release or uptake (Chittasupho et al., 2009). It is recommended for the release test to be conducted using other chemotherapy drugs such as dacarbazine.

Not all the results obtained from the primary naïve polymeric nano-emulsions release show a steady and long-term controlled release profile. Hence, the best preparations from each group were chosen and blended to see the effect on the release profile (section 3.1.2.2). Obtained release profiles from blended nano-emulsions were greatly improved.

The hypothesis of chemo-resistance prevention requires avoiding a sudden burst of the drug and keeping the release pattern steady whiles increasing with time. For blended nano-emulsions, each release profile showed a different pattern, however, all increased during 21 days. Increased polymer amount had a positive effect, improving the steadiness of the drug

release profile. This may have happened through improved entrapment of the drug (Mohammed et al., 2017). It was noticeable that blended nano-emulsions presented a more controlled release. Hence, the chitosan-alginate-pullulan polymer blending seems to be successful.

There were fluctuations for both doxorubicin and coumarin-6 release profiles; albeit less for doxorubicin. This can be the indication of the unstable nature of coumarin-6 for long-term release experiments. The overall pattern of each individual nano-emulsion is dependent on several factors, such as polymer mass ratio, water solubility, and surface charge (Rizvi and Saleh, 2018). In the case of chitosan and alginate nano-emulsions, however, the hypothesis did not match with the obtained results. This means, albeit increased mass ratio of the polymer, the initial burst of the drug was still high and fluctuations were occurring during the release. Although alginate is soluble in neutral water, its initial burst is lowest. On the other hand, chitosan, soluble in acidic environments, has a higher initial burst compared to alginate.

The optimal nano-emulsion was chosen as pullulan-chitosan (1:2). According to the release pattern recorded for the optimal blended nano-emulsion, the release pattern was improved compared to previous investigations on chitosan-only nano-particles (Baghbani et al., 2017, Tai et al., 2020). Furthermore, this research contains the novel approach for using pullulan among the main components of a nano-emulsion for drug delivery. Utilisation of pullulan alone and as a blend led to a drug release up to 21 days. Previous investigations on drug release from pullulan provided a drug release for less than 72 hours (Xu et al., 2020, Yuan et al., 2019).

4.2.2 Cell viability test

MTT test was used as a primary test to screen the viability of the treated cells based on mitochondrial activity (A375 and HaCaT) (Rai et al., 2018b, Soe et al., 2019). HaCaT cells were used as a marker of non-cancerous control cells to monitor the possible toxicity of nano-emulsions as a topical delivery system.

Initially, a viability test was conducted on the cells treated with non-loaded blended nano-emulsions. Three concentrations of the nano-emulsions were used as treatments. As the result of increasing concentration, the overall viability of A375 treated with the non-loaded nano-emulsions was detected as a minimum of 25% and a maximum of 107%. Consequently, with the increased concentration of nano-emulsion, the cell viability decreased compared to control. On the other hand, the same treatments were conducted on HaCaT cells. Interestingly, a few of the nano-emulsion samples decreased the viability of HaCaT cells drastically against expectations (Sahu et al., 2019b). The rationale for effective delivery to A375 is to avoid harming the surrounding non-cancerous cells (Liu et al., 2018). Hence in the optimisation process, the high viability of HaCaT is important. Decreased viability of cells treated with nano-emulsions containing chitosan can be an indication of its cytotoxicity against cancer cell lines, according to previous investigations (Abedian et al., 2019, Gibot et al., 2015). Pullulan also has been extensively investigated for its increased uptake in cancer cells such as A375 cells (Nešić et al., 2020), and its anti-proliferative activity (Manitchotpisit et al., 2014, Bischoff et al., 2015). Hence, this can be a reason for the decrease of viability in the cells treated with pullulan-based nano-emulsions, compared to viable control untreated cells.

The action of nano-emulsion toward A375 cells is crucial. To this end in another experiment, the viability of A375 cells treated with both naïve and doxorubicin-loaded nano-emulsions was compared to non-loaded doxorubicin.

The cell viability was retained in the A375 cells treated with non-encapsulated doxorubicin. This indication may have two reasons behind it. The first, is that the drug is unable to decrease A375 cell viability despite its toxic nature. Secondly, the cells developed resistance to the drug. Out of the two, the latter is more probable, since the intrinsic resistance of melanoma cells to doxorubicin were previously stated and investigated (Oláh et al., 2018, Elliott and Al-Hajj, 2009). However, encapsulated doxorubicin drastically decreases the A375 cell viability compared to untreated A375. This can be an indication of the effective delivery of doxorubicin without the development of resistance in the cells. Hence the combination of doxorubicin and polymeric shell confirms the hypothesis of the drug being protected from degradation or being lysed. More importantly, the delivery of encapsulated doxorubicin with controlled efflux prevented the melanoma cells to develop resistance to the drug. This can be a confirmation of flux-dependent resistance development in melanoma (Kalal et al., 2017).

4.2.3 Cellular uptake and intracellular drug release studies

To address the cellular uptake of the nano-emulsions, confocal microscopy was conducted (Cutrona and Simpson, 2019). The experiment was done over 72 hours to screen the uptake of the nano-emulsions and consequent intracellular drug release by quantifying the fluorescent intensity of doxorubicin and coumarin-6 during the 72 hours. Using coumarin-6 as a fluorescent model was a primary experiment to make the drug delivery system traceable. It has been also

widely used as a drug model in delivery systems because of its good stability (Rivolta et al., 2011, Chirio et al., 2014). This experiment can also be further investigated using alternative fluorescent trackers to compare its effect on release and traceability (Yuan and Liu, 2017), and Coumarin-6 can be further investigated as a non-toxic drug model for *in vivo* animal models.

According to the quantified fluorescent intensity an increasing pattern was detected for most of the samples. Among drug-loaded nano-emulsions, a few samples performed a controlled release over 72 hours. Increased fluorescent intensity is an indication of intracellular drug release in the cytosol. However, in some samples, the release pattern showed a sudden increase or decrease. Several reasons can cause a sudden decrease or increase in fluorescent intensity (Pretor et al., 2015). Instability of dye and sudden degradation of nano-emulsion are among the causes leading to fluorescent fluctuations.

The confocal images were obtained for both doxorubicin and coumarin-6 loaded nano-emulsions. The treatments were applied to both cell lines (A375 and HaCaT). Among all, it was detected that nano-emulsions consisting of chitosan or pullulan had increased uptake in melanoma cells. This showed the increased affinity of these two polymers to bind to the A375 cells. This is consistent with the previous investigations of increased polysaccharide-based particle uptake in cancer cells (Salatin and Yari Khosroushahi, 2017). The nano-emulsions had successful uptake by cells and the encapsulated molecules were able to escape endosomes in the cell cytosol during 72 hours. As the nano-emulsions are made of polysaccharides without any surface modification, they have provides successful uptake as successfully as modified or non-polymeric nano-delivery systems (Capanema et al., 2019, Joseph et al., 2015).

4.2.4 Cellular apoptosis induction ability of the nano-emulsions

Initial optimisations based on release were performed to investigate the best delivery efflux from nano-emulsions. Melanoma cells are prone to develop flux-dependant drug-resistance and escape the apoptosis cycle, hence monitoring the effect of nano-emulsions on apoptosis induction is important. After the treatments over 4, 24, 48, and 72hours apoptosis induction ability of doxorubicin-loaded nano-emulsions were investigated. Even though the nano-emulsions presented successful uptake, their ultimate impact was investigated through DNA fragmentation ELISA.

Melanoma cells were treated with doxorubicin-loaded blended nano-emulsions. As indicated in Figure 3.24, all the doxorubicin-loaded blended non-emulsions were able to successfully induce apoptosis to melanoma cells over the time course of 72 hours. However, among them, pullulan-chitosan nano-emulsion (pullulan-chitosan 1:2) performed more prompt and had an increasing apoptosis induction pattern during the time. At the beginning of four hours, the apoptosis induction to melanoma cells was about 55% and increased to about 90% after 72 hours. The pullulan-chitosan nano-emulsion showed better performance since it was able to induce apoptosis fast enough. Its apoptosis induction pattern was consistent with its release profile. This is an indication of improved delivery of the drug which was carried by the nano-emulsion (pullulan-chitosan), without developing resistance. Sample nine consisted of chitosan and pullulan. Chitosan and pullulan are both polysaccharides that have been used in cancer drug delivery systems in earlier investigations (Scomparin et al., 2011). Chitosan intrinsically is an anti-cancer antioxidant (Gibot et al., 2015), which has a potency to adhere to skin cells

(Popat et al., 2014, Adhikari and Yadav, 2018) and can act as an anti-proliferative agent for cancer cells. Pullulan, as well, is a non-toxic and non-immunogenic polysaccharide, it can increase cellular uptake (Huang et al., 2018, Tao et al., 2016). Pullulan (Tao et al., 2018) and chitosan (Garg et al., 2019) were separately investigated in several cancer drug delivery systems as anti-proliferative polymers. However, the capability of the developed pullulan-chitosan nano-emulsion to induce apoptosis on other melanoma cell lines and various cancer cells can be further investigated.

In another aspect, nano-size nano-emulsion has provided a better uptake in A375 cells via the EPR effect due to the intrinsic characteristics of involved polymers. To summarise, the effect of pullulan-chitosan nano-emulsion was convincingly effective in inducing apoptosis to melanoma cells after 72 hours and consequent decrease of drug resistance.

In this research, ELISA was used as an anti-body-based experiment to detect the early apoptosis state of A375 cells. However, a more detailed study of A375 cell death mode, further investigations can be carried out by Annexin-V flow cytometry and tunnel assays.

4.2.5 Nano-emulsion characterisation

So far the experiments were conducted to come up with an optimised nano-emulsion. Before the surface modifications, the optimised nano-emulsion was characterised. The size range of nano-emulsion particles is an important factor defining their fate in cancer cells (Hui et al., 2019). Also, depending on the route of administration, the particle size and particle concentrations can be different (Rizvi and Saleh, 2018).

One of the disadvantages of nano-emulsions is their instability (Kale and Deore, 2017). Nano-particles having a zeta potential between -10 and +10 mV are considered neutral (Clogston and Patri, 2011). Interestingly in the results obtained and according to zeta potential (Table 3.1), the optimised nano-emulsion performs a neutral behaviour, due to the zeta potential of +5.

According to previous investigations, similar nano-emulsions of chitosan are measured with high positive zeta potential (Baghbani et al., 2017, Li et al., 2016), on the other hand, pullulan nano-emulsions have low negative zeta potential (Costa et al., 2019, Niu et al., 2020). This accounts for the neutral zeta potential of nano-emulsion consisting of chitosan and pullulan blend. Furthermore, scanning electron microscopy revealed the relative morphology of the nano-emulsion particles.

The encapsulation efficiency of the nano-emulsion was also investigated. This is an important factor for nano-emulsions to be effective in the delivery. Both dacarbazine and doxorubicin were encapsulated in the nano-emulsion successfully. The encapsulation efficiency of both drugs (doxorubicin and dacarbazine) was about 85%, which was lower compared to nano-emulsions consisting of only one polymer type (Abhinav et al., 2016). However, the encapsulation efficiency of the nano-emulsion is suitable for the aim of controlled delivery.

4.3 Modification of optimised chitosan-pullulan nano-emulsion

According to the results obtained, the developed nano-emulsion successfully provided controlled release and increased uptake via passive targeting by the EPR effect. However, the uptake test was done for both melanoma and keratinocyte cells, and uptake of the particles was detected in both cell lines. Hence, the motive for further modifications was to provide active targeting towards melanoma.

4.3.1 Folate-modification of nano-emulsion

Surface modification of the nano-emulsion was performed using folate (folic acid) (Dhas et al., 2015) to target folate receptors on A375 cells. Folate receptors are overexpressed in cancer cells and they exist excessively on their surfaces. According to the previous investigations and literature review, the A375 cell line was used as a folate receptor-negative (Ladino et al., 1997). Although, in comparison to non-cancerous cells, it has increased the expression of folate receptors (Ogboodu et al., 2015). On the same note, folate binding protein (FBP) ELISA was performed as a confirmation of folate receptor expression on the A375 cells (Chen et al., 2016). Zeta potential and size distribution were also done for the folic acid surface coated nano-emulsion Table 3.1. According to the results, a slight increase in particle size was observed. This could be due to surface coating, although the size difference is not considered high. However, according to zeta potential, the particles demonstrate neutral behaviour. Other than folate modification, the nano-emulsion can be further investigated to be modified using various

cancer-targeting receptors (Daniels et al., 2012). RGD peptide can be used as an alternative modification for the nano-emulsion to target A375 cells (Gajbhiye et al., 2019).

Modification of nano-emulsion using alternative receptors on A375 may increase or decrease the uptake of nano-emulsion particles depending on the concentration of receptors expressed in A375. Subsequently, by alterations in particle uptake, cellular viability may be affected.

4.3.2 Viability of melanoma and keratinocyte cells treated with surface modified optimized nano-emulsion

It is expected that after modification, the toxicity of nano-emulsions would be more on melanoma cells. Hence the MTT assay was performed to compare the viability of cells treated with drug-loaded nano-emulsion before and after modification.

The viabilities of both HaCaT and A375 cells treated with drug-loaded nano-emulsion and surface coated drug-loaded nano-emulsion, doxorubicin, and dacarbazine, was investigated (Jangdey et al., 2019). According to the MTT test, surface coated nano-emulsion significantly decreased the viability of melanoma cells while keratinocyte cells remained viable.

The results indicated an important point. The viability of melanoma treated by doxorubicin and dacarbazine was 93 and 53% respectively (Piotrowska et al., 2019, Andreucci et al., 2019). This may be due to emerging potential resistance in melanoma cells (Piotrowska et al., 2019, Movafegh et al., 2018). On the other hand, folate-functionalised nano-emulsion seems to have a protective effect on the non-cancerous control cell line (HaCaT). Figure 3.29 is an indication of an increased affinity of surface-modified nano-emulsion towards melanoma cells. The

mechanism of their uptake was predicted to be via folate receptors which are confirmed in the toxicity tests.

The findings of this experiment indicate a promising approach towards melanoma treatment. So, the encapsulated drugs in folate-modified nano-emulsion had more tendency to have uptake in melanoma cells and affect their viability without triggering cells to develop resistance. The decrease of A375 cell viability happens while the HaCaT cells remain viable (107 and 97% for folate-modified doxorubicin and dacarbazine loaded nano-emulsion treatments respectively). The outcome of this experiment can also be further investigated by Annexin-V flowcytometry assay to screen the state of the cells in the same treatments.

4.3.3 Fluorescent microscopy of melanoma and keratinocyte cells in co-culture

To visually monitor the melanoma and keratinocyte cells, each cell line was labelled with a different fluorescent marker. The A375 cells were labelled with CMFDA and the HaCaT cells with CMTPIX. DAPI stain was also utilized for the nucleus imaging. The images were captured both from melanoma and keratinocyte in mono-cultures and once more in the co-culture of both cell lines. Both mono-culture and co-culture were conducted to monitor the effect of nano-emulsion as a topical delivery system, on A375 and HaCaT as a monolayer model. In single-cell treatments, the images were captured from CMFDA labelled A375 cells and CMTPIX labelled HaCaT cells.

In the images obtained from fluorescent microscopy, the difference between the cells treated with folate-modified nano-emulsion, non-modified nano-emulsion, and blank drugs can be

detected according to the shape of the cells (apoptotic or healthy cell). Keratinocytes treated with surface-modified nano-emulsions, on the other hand, continue to proliferate, while many of the melanoma cells treated with folate-modified nano-emulsions show impeded growth and apoptosis.

The co-culture of the cells provided a more realistic model compared to a mono-culture (Chung et al., 2018), and it is feasible and quick compared to the preparation of a 3D culture. This method can be used as an alternative for mono-culture to study the effect of treatments on two or more cell lines. However, there are limitations to monolayer co-culture such as different doubling times of the cells. Furthermore, the co-culture of two adherent cell lines can be challenging if the time required for their detachment is similar (Gabbott et al., 2018).

For advanced investigations, a 3D co-culture model can provide a better resemblance to the actual tumour (Majety et al., 2015). Hence, the 3D tumour model helps to have a better understanding of the tumour microenvironment and paracrine signalling in two cell lines (Kapalczyńska et al., 2018) before translation of the drug delivery system to the clinical stage. The obtained images from the co-culture can give us a better understanding of the treatment's effect on the cells. However, the experiment was done for 72 hours containing DMEM in the wells, which had slightly affected the background noise of the images (Ettinger and Wittmann, 2014). According to the images obtained from co-culture, the A375 cells treated with the folate-modified nano-emulsion seem to have faded fluorescent intensity and scattered nucleolus as signs of early apoptosis compared to healthy HaCaT cells.

4.3.4 Polymerase chain reaction

PCR gel electrophoresis experiment was conducted to investigate the apoptosis-associated gene expressions in treated A375 and HaCaT cell lines (He et al., 2018, Del Puerto et al., 2010). In this regard, the regulation of five genes was investigated including reference gene and caspase-3, caspase-9, pre-apoptotic Bax, and anti-apoptotic Bcl2 genes (Lo et al., 2010). In this experiment, cDNA has been used instead of genomic DNA (Litwack, 2018) since the aim is to monitor the gene expression, upregulation, or downregulation of certain pro-apoptotic and anti-apoptotic genes rather than detection. Accordingly, cDNA was used to provide a more accurate analysis.

According to Figure 3.41 and Figure 3.42, in the A375 cells treated with doxorubicin and dacarbazine decreased expression of the pro-apoptotic gene (Bax) was detected. Bax and Bcl2 genes are known as an important apoptosis-related gene and has been investigated as a marker of resistance in the literature (Kale et al., 2018, Wang et al., 2017). This can be an indication of resistance towards both naïve drugs.

Upregulation of caspase-9 and Bax was detected in A375 cells treated with folate-modified nano-emulsion compared to non-modified drug-loaded nano-emulsion and naïve drug treatments. On the other hand, HaCaT had lower Bcl2 expressed rather than Bax.

An increase of the pro-apoptosis genes in A375 cells treated with folate-modified drug-loaded nano-emulsion was detected. Although the detection of this result indicates the increase in initial apoptosis markers, however, more investigations on the apoptosis of A375 can be done by quantitative-PCR (Jafarizad et al., 2018, Sarigöl-Kiliç and Ündeğer-Bucurgat, 2018) and

Annexin-V flow cytometry (Kotawong et al., 2018). A few researchers also investigated expression of caspase-3, caspase-9, Bax, and Bcl2 by western blot (Wang et al., 2019a, Shang et al., 2019) .

4.4 Investigation of cell viability and iNOS and COX-2 downregulation after treating with encapsulated anti- inflammatory compounds

In the second part of the thesis, melanocortin peptides were used to control melanoma progression. Melanocortin compounds are anti-inflammatory agents that have been used for both chronic and acute inflammation therapies (Tsatmali et al., 2002, Wang et al., 2019b). Cancer cells, most particularly melanoma cells, overexpress melanocortin receptors (Zhou et al., 2020). So far melanocortin peptides were used to target receptors on cancer cells as a targeted delivery tool (Li et al., 2019, Zhou et al., 2020, Dissanayake et al., 2017).

However, in current research using a novel approach, anti-inflammatory melanocortin compounds were used as potential tools to inhibit melanoma progression. Hence, this was done utilizing folate-modified pullulan-chitosan nano-emulsion developed and optimised according to section 2.2.5 and instead of the drugs, anti-inflammatory compounds were encapsulated in the optimal pullulan-chitosan nano-emulsion.

4.4.1 iNOS and COX-2 expression

iNOS and COX-2 protein upregulations have been investigated and reported as precursors for melanoma progression and metastasis (Johansson et al., 2009, Paulino et al., 2016). Hence, the effect of melanocortin compounds on iNOS and COX-2 expressions was investigated for the first time as a novel approach by BMS-470539-dihydrochloride and [DTrp⁸]- γ -MSH loaded optimal nano-emulsion to ascertain whether they were effective in modulating these inflammatory pathways.

The treatments were evaluated over 72 hours and their effect on cell viability and protein expression was confirmed by MTT and Western blot assays, subsequently imaged by fluorescent microscopy.

Evaluation of the cell viability via MTT assay has demonstrated that the melanoma cells treated with the melanocortin compound (BMS-470539-dihydrochloride and [DTrp⁸]- γ -MSH) loaded nano-emulsions caused a decrease to 12 and 9% respectively in A375 cell viability after 72 hours (Can et al., 2020). According to the investigations, COX-2 has been expressed in most of the malignant melanoma primary tumours and was confirmed in five malignant melanoma cell lines including MeWo, SK-Mel-13, SK-Mel-28, IGR 37, and A375 (Goulet et al., 2003, Denkert et al., 2001a). This leads to the progression of the melanoma cells. On the other hand, according to the studies conducted on benign nevi, no expression of COX-2 was detected (Denkert et al., 2001b, Lee et al., 2020). Inhibition of CXCL10 expression by iNOS also affects melanoma tumorigenesis and progression (Tanese et al., 2012). Therefore, iNOS is an important marker to target melanoma treatment (Tanese et al., 2012, Grimm et al., 2008).

Interestingly, the Western blot test showed a 100% knockdown of iNOS and COX-2 expression in A375 cells after 72 hours of encapsulated BMS470539-dihydrochloride and [DTrp⁸]- γ -MSH treatment and is a novel finding for these compounds on this cell line. According to the western blots, no band was detected for iNOS and COX-2 expressions in the cells treated with encapsulated compounds after 72 hours. Accordingly, the associated α -tubulin band was faint but detectable, this is most likely due to low levels of A375 cells left after treatment as can be seen from the data generated in the cell viability experiments (Figure 3.50 and 3.51), compared to untreated A375 cells. Whilst this data provides evidence of proof of concept it would be interesting to see if increasing the cell density would enable a higher number of cells for extraction to demonstrate this more clearly.

This is a promising point in melanoma treatment and prognosis. While the compounds used in this study decreased melanoma viability, according to the previous investigations they increase the viability of cells such as chondrocytes (Can et al., 2020). This happens following TNF- α stimulation, whereby the loss of chondrocytes within the cartilage leads to the development of osteoarthritis (Can et al., 2020). This indicates the potential of the current treatment procedure for targeted delivery applications.

There are certain problems with the delivery of small molecules and peptides. Most peptides have a very limited half-life starting from a few minutes to a few hours, thence they lack stability (Wei et al., 2016). Moreover, they are prone to oxidation and hydrolysis (Fosgerau and Hoffmann, 2015) which decreases their ability to function (Lau and Dunn, 2018). The administration route for them is usually the in-situ or subcutaneous injection. However, the delivery efficacy may not be always high (Pai et al., 2017).

In this study, the MC₁ agonist BMS470539-dihydrochloride and MC₃ agonist, [DTrp⁸]- γ -MSH (Tao et al., 2006) were encapsulated in the pullulan-chitosan optimised nano-emulsion, to ensure that the compounds would be protected against early degradation and therefore reach the target more efficiently (Bentz et al., 2017).

Although the approach is promising, there are certain challenges to address in further investigations. These include the sterilisation of the nano-emulsion after encapsulation of the compounds. In this study, short periods of UV light exposure were used to sterilise the nano-emulsion compound. The obtained results can be further confirmed by q-PCR or Annexin-V assays to detect the state of the cells (apoptotic/ necrotic).

4.4.2 Toxicity induced by encapsulated compounds on A375 cells

Measurement of the effect on cell viability induced by the naïve and encapsulated compounds on melanoma was used to ascertain their effects on the mitochondrial activity and subsequent viability of the melanoma (A375) cells. The viability of the melanoma cells treated with encapsulated BMS-470539-dihydrochloride and [DTrp⁸]- γ -MSH for 72 hours, caused a significant decrease in cell viability compared to naïve compounds. Which is consistent with the bands on the 72hour western blot.

As iNOS and COX-2 are known to have a substantial effect on melanoma progression and invasion (Kim et al., 2016), they also have an impact on melanoma viability (Herraiz et al.). In this study, the ultimate impact of the encapsulated compounds on iNOS and COX-2 expression was 100% downregulation after 72 hours. Encapsulation enhanced the compound's abilities to

downregulate the expression of both iNOS and COX-2 and decrease the A375 cell viability after 72 hours. However, the effect of the compounds on HaCaT cells is yet to be investigated.

4.4.3 Fluorescent microscopy of melanoma-keratinocyte co-culture treated with encapsulated compounds

The effect of encapsulated peptides on melanoma cells was investigated using Western blot and MTT. In further investigations, encapsulated BMS-470539-dihydrochloride, [DTrp⁸]- γ -MSH, and naïve BMS-470539-dihydrochloride, [DTrp⁸]- γ -MSH treatments were applied to the co-culture of pre-labelled A375 and HaCaT cells to visually screen their effectivity (Chung et al., 2018). Accordingly, the images were obtained, and the melanoma (green labelled) growth was monitored. Under normal conditions (without treatment) A375 cells proliferate rapidly and it was expected to grow within 72 hours. However, decreased numbers of A375 cells in the well (Figure 3.57 and 3.58) were detected while treated with encapsulated compounds. On the contrary, HaCaT cells (red labelled) continue to proliferate over the 72hours. This study suggests that BMS-470539-dihydrochloride and [DTrp⁸]- γ -MSH in both naïve and encapsulated form, do not affect effects on HaCaT cells. The results obtained from the microscopy also validated the Western blot and MTT results.

5 Conclusion

The aim of this thesis was achieved through two main phases. Firstly, development and optimisation of an appropriate drug-delivery platform for melanoma; secondly, investigation of inflammation control as a tool to control melanoma progression.

From the findings of the first part of the experimental work, polysaccharide-based nano-emulsions presented the promising potential for melanoma drug delivery. Alginate, chitosan, and pullulan each tested for their features in drug release. However, the blended alginate-pullulan, pullulan-chitosan, and chitosan-alginate demonstrated improved release profiles. The optimisation procedure of the blended nano-emulsions led to the optimal nano-emulsion “pullulan-chitosan”. The synthesized and folate-modified pullulan-chitosan nano-emulsion was found to have enhanced uptake in A375 cells. Furthermore, doxorubicin/dacarbazine loaded nano-emulsion substantially decreased the melanoma viability. In the meantime, the control cell line (HaCaT) was minimally affected by the drug-loaded folate-modified nano-emulsion. Hence the first part of the investigation showed that the drug-loaded pullulan-chitosan nano-emulsion can be used as melanoma targeted treatment.

The second part of the investigations pointed out that the nano-emulsion has the potential to be used as a highly efficient multi-propose delivery platform. Upregulation of the inflammation markers is reported to affect melanoma progression. Hence the delivery of anti-inflammatory compounds using the developed nano-emulsion was investigated. This novel approach led to a significant downregulation of the inflammation markers in A375 cells. This was due to the

efficient delivery of the anti-inflammatory compounds using the pullulan-chitosan nano-emulsion.

In conclusion, the developed formulation can be considered as an important tool toward the elimination of melanoma drug resistance. Moreover, the delivery of anti-inflammatory compounds using nano-emulsions was found to have a great impact in controlling melanoma progression.

6 Future work

In the results of the experimental part of this thesis, a novel folate modified pullulan-chitosan nano-emulsion was developed. This delivery platform had two unique features. First, targeted uptake in melanoma cells, and an ability to provide intracellular controlled release. Second, the potential to be used as a delivery platform for small molecules/compounds. This novel approach was used to deliver α -MSH-peptides into skin melanoma cells to downregulate iNOS and COX-2 and then using the same system, doxorubicin/dacarbazine was delivered into the A375 cells to induce apoptosis.

Although the obtained results depicted success in reducing A375 viability and inducing apoptosis, other features need to be investigated further. In this project, nano-emulsions were applied to mono-layer cell cultures on two cell lines. To get closer to a real-life system, the formulation can be tested in a 3D tumour model and a flow system. Furthermore, as the route of the delivery was aimed to be topical, the detailed study on nano-emulsion particle permeation through skin layers is crucial. This can be done via using a skin model or *ex vivo* flow tumour models. In such a system, the effects of the drug-loaded nano-emulsions on the tumour microenvironment, and the resulting interstitial fluid pressure on the uptake of the immobilised drugs can be investigated.

Investigation of the hepatotoxicity or any accumulations in distant organs can also be conducted before the translation of the nano-emulsion to clinical trial. Further research can be carried out to study the immunogenicity of the drug-loaded nano-emulsion.

As chemotherapy drugs have severe side effects, the developed nano-emulsion can be a tool to decrease the damages caused to healthy tissues during the course of treatment. The nano-emulsion can also be investigated as a tool to study the severe side effect of other cytotoxic drugs along with doxorubicin and dacarbazine.

Furthermore, effect of nano-emulsion can be investigated on the range of skin cancer cell lines such as SK-MEL-28, MeWo, and B16 F1. Ability of skin cancer to metastasis can also be investigated as the further effects of the optimal nano-emulsion.

Moreover, to use the nano-emulsion as a topical delivery formulation, the size of nano-emulsion particles can be further reduced to a range of 50-75 nm. Therefore, there will be a potential for the drug-loaded nano-emulsion particles to penetrate the skin.

Furthermore, the combined therapy of α -MSH-peptides-doxorubicin-dacarbazine loaded nano-emulsion can be investigated in melanoma treatments. The downregulation of inflammation modulators can significantly affect the progression of melanoma. Hence a combined therapy of anti-inflammatory compounds and chemotherapeutics can be a potential therapy for melanoma. Also, additional anti-inflammatory compounds such as NSAIDs (diclofenac) or COX-2 inhibitors (celecoxib) can be encapsulated in the nano-emulsion for investigation of cancer treatment or the prevention/treatment of severe inflammatory diseases.

7 Appendix

Appendix A. Evaluation of doxorubicin quantity

To evaluate encapsulation efficiency for doxorubicin-loaded nano-emulsion, HPLC was performed. The calibration curve was plotted based on various doxorubicin concentrations. Doxorubicin peak was detected at 2 minutes.

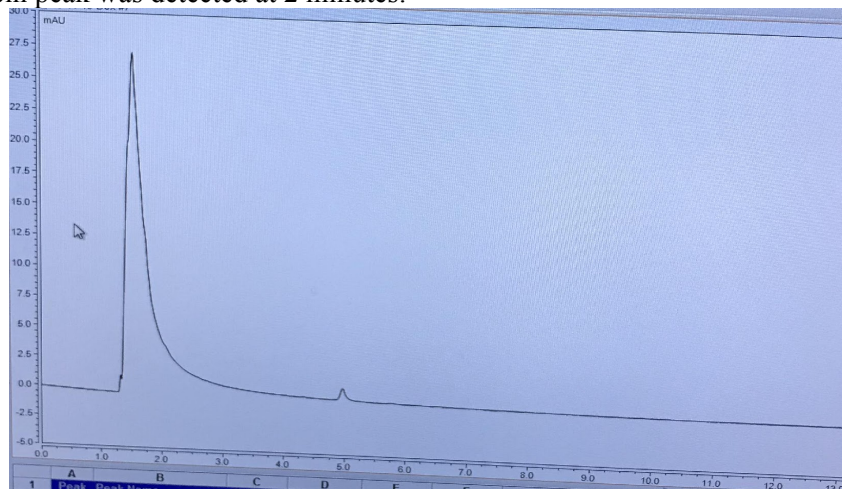


Figure 7.1 HPLC peak detected at 2 minutes for doxorubicin

UHPLC (Ultimate 3000 Thermo-scientific) was performed using a C18 column (4.6 mm x 100 mm, 2.7 μ m, Thermo-Scientific 071973). UV detection for doxorubicin was done at 233 nm. The mobile phase contained water and acetonitrile (25:75 v/v, adjusted to pH 3.0 using 85% w/v phosphoric acid) using the flow-rate of 1.0 ml per minute.

Appendix B. SEM imaging.

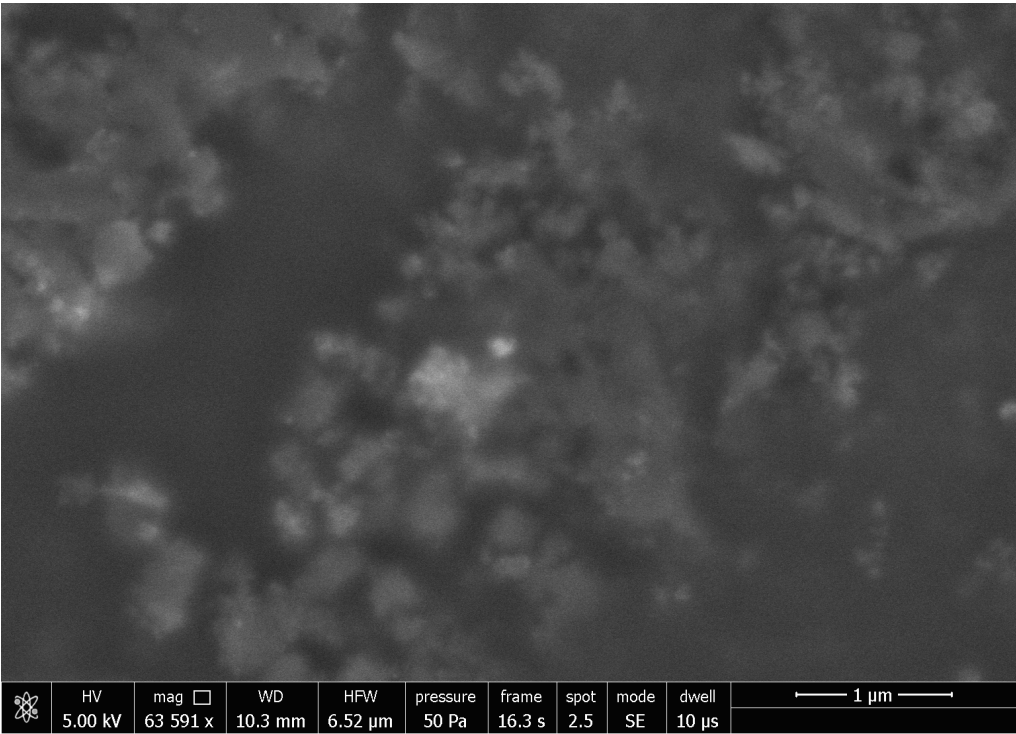
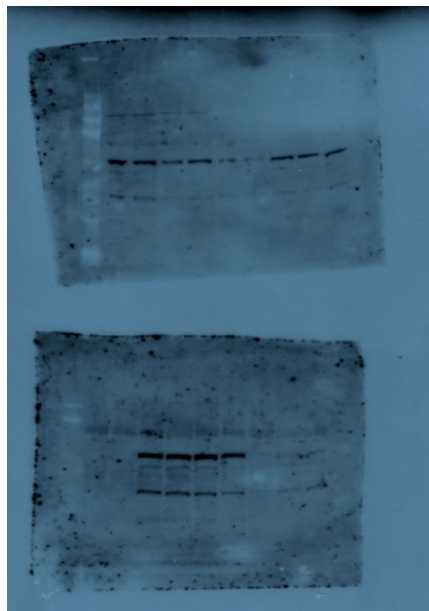


Figure 7.2 SEM image of the optimal pullulan-chitosan nano-emulsion

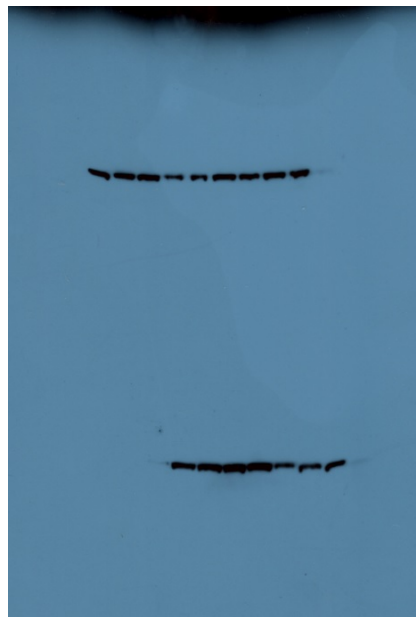
Scanning electron microscopy (SEM) was performed using FEI Quanta FEGSEM operating at 5.00 kV, 63k magnification, 50 pa pressure, dwelling 10 μseconds.

Appendix C. Western blots

A



B



C

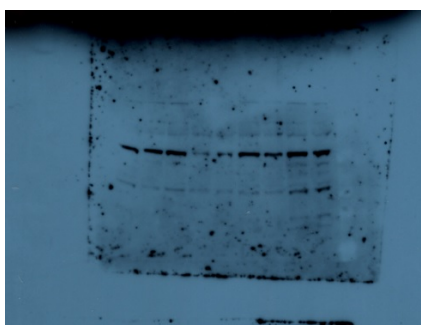


Figure 7.3 iNOS and COX-2 expression analysis by Western blot

This image is a single demonstration of three independent western blots (for each time point) conducted to analyse iNOS and COX-2 expressions in treated A375 cells. The experiment was conducted after 24, 48, and 72 of incubation with treatments. The results are normalised to α -tubulin. Blots demonstrated in the figure are the full demonstrations of figure 3.53. Figure 7.3A is indicating the α -tubulin bands and Figure 7.3 B and C are indicating the band obtained from the treatments.

REFERENCES

- ABDULKHALEQ, L. A., ASSI, M. A., ABDULLAH, R., ZAMRI-SAAD, M., TAUFIQ-YAP, Y. H. & HEZMEE, M. N. M. 2018. The crucial roles of inflammatory mediators in inflammation: A review. *Veterinary world*, 11, 627-635.
- ABEDINI, F., EBRAHIMI, M., ROOZBEHANI, A. H., DOMB, A. J. & HOSSEINKHANI, H. 2018. Overview on natural hydrophilic polysaccharide polymers in drug delivery. *Polymers for Advanced Technologies*, 29, 2564-2573.
- ABHINAV, M., NEHA, J., ANNE, G. & BHARTI, V. 2016. Role of novel drug delivery systems in bioavailability enhancement: at a glance. *International Journal of Drug Delivery Technology*, 6, 7-26.
- ABUDUKELIMU, A., BARBERIS, M., REDEGELD, F. A., SAHIN, N. & WESTERHOFF, H. V. 2018. Predictable irreversible switching between acute and chronic inflammation. *Frontiers in immunology*, 9, 1596.
- ADHIKARI, H. S. & YADAV, P. N. 2018. Anticancer activity of chitosan, chitosan derivatives, and their mechanism of action. *International Journal of Biomaterials*, 2018.
- AGLIANO, A., CALVO, A. & BOX, C. 2017. The challenge of targeting cancer stem cells to halt metastasis. *Seminars in Cancer Biology*, 44, 25-42.
- AHMED, S., ZHOU, Z., ZHOU, J. & CHEN, S.-Q. 2016. Pharmacogenomics of Drug Metabolizing Enzymes and Transporters: Relevance to Precision Medicine. *Genomics, proteomics & bioinformatics*, 14, 298-313.
- AHMED, T. A. & ALJAEID, B. M. 2016. Preparation, characterization, and potential application of chitosan, chitosan derivatives, and chitosan metal nanoparticles in pharmaceutical drug delivery. *Drug design, development and therapy*, 10, 483.
- ALFAROUC, K. O., STOCK, C.-M., TAYLOR, S., WALSH, M., MUDDATHIR, A. K., VERDUZCO, D., BASHIR, A. H. H., MOHAMMED, O. Y., ELHASSAN, G. O., HARGUINDEY, S., RESHKIN, S. J., IBRAHIM, M. E. & RAUCH, C. 2015. Resistance to cancer chemotherapy: failure in drug response from ADME to P-gp. *Cancer cell international*, 15, 71-71.
- ALFURHOOD, J. 2016. Poly (N-(2-Hydroxypropyl) Methacrylamide) Nanomaterials For Nanomedicine and Controlled Delivery.
- ALI, A. & AHMED, S. 2018. A review on chitosan and its nanocomposites in drug delivery. *International journal of biological macromolecules*, 109, 273-286.
- ALIBERT, C., GOUD, B. & MANNEVILLE, J. B. 2017. Are cancer cells really softer than normal cells? *Biology of the Cell*, 109, 167-189.
- ALLEN, T. M. & CULLIS, P. R. 2013. Liposomal drug delivery systems: from concept to clinical applications. *Advanced drug delivery reviews*, 65, 36-48.
- ALMEIDA, P. V., SHAHBAZI, M.-A., CORREIA, A., MÄKILÄ, E., KEMELL, M., SALONEN, J., HIRVONEN, J. & SANTOS, H. A. 2017. A multifunctional nanocomplex for enhanced cell uptake, endosomal escape and improved cancer therapeutic effect. *Nanomedicine*.

- AMJAD, M. T. & KASI, A. 2020. Cancer Chemotherapy. *StatPearls*. Treasure Island (FL): StatPearls Publishing
- Copyright © 2020, StatPearls Publishing LLC.
- ANDREUCCI, E., RUZZOLINI, J., PEPPICELLI, S., BIANCHINI, F., LAURENZANA, A., CARTA, F., SUPURAN, C. T. & CALORINI, L. 2019. The carbonic anhydrase IX inhibitor SLC-0111 sensitises cancer cells to conventional chemotherapy. *Journal of enzyme inhibition and medicinal chemistry*, 34, 117-123.
- ARNOLD, M., HOLTERHUES, C., HOLLESTEIN, L. M., COEBERGH, J. W. W., NIJSTEN, T., PUKKALA, E., HOLLECZEK, B., TRYGGVADOTTIR, L., COMBER, H. & BENTO, M. J. 2014. Trends in incidence and predictions of cutaneous melanoma across Europe up to 2015. *Journal of the European Academy of Dermatology and Venereology*, 28, 1170-1178.
- ARRUEBO, M., VILABOA, N., SÁEZ-GUTIERREZ, B., LAMBEA, J., TRES, A., VALLADARES, M. & GONZÁLEZ-FERNÁNDEZ, A. 2011. Assessment of the evolution of cancer treatment therapies. *Cancers*, 3, 3279-3330.
- BABIĆ, M. M., BOŽIĆ, B. Đ., BOŽIĆ, B. Đ., FILIPOVIĆ, J. M., UŠĆUMLIĆ, G. S. & TOMIĆ, S. L. 2016. Evaluation of novel antiproliferative controlled drug delivery system based on poly (2-hydroxypropyl acrylate/itaconic acid) hydrogels and nickel complex with Oxaprozin. *Materials Letters*, 163, 214-217.
- BÁCSKAY, I., NEMES, D., FENYVESI, F., VÁRADI, J., VASVÁRI, G., FEHÉR, P., VECSENYÉS, M. & UJHELYI, Z. 2018. *Role of cytotoxicity experiments in pharmaceutical development*, InTech: London, UK.
- BADAWI, A. A., EL-LAITHY, H. M., EL QIDRA, R. K. & EL MOFTY, H. 2008. Chitosan based nanocarriers for indomethacin ocular delivery. *Archives of pharmacal research*, 31, 1040.
- BADEA, I. 2017a. New strategies in melanoma therapy: can nanoparticles overcome chemoresistance? *Nanomedicine*, 12, 1623-1626.
- BADEA, I. 2017b. New strategies in melanoma therapy: can nanoparticles overcome chemoresistance? : Future Medicine.
- BAGDE, A., MONDAL, A. & SINGH, M. 2018. Drug delivery strategies for chemoprevention of UVB-induced skin cancer: A review. *Photodermatology, photoimmunology & photomedicine*, 34, 60-68.
- BAGHBANI, F., CHEGENI, M., MOZTARZADEH, F., HADIAN-GHAZVINI, S. & RAZ, M. 2017. Novel ultrasound-responsive chitosan/perfluorohexane nanodroplets for image-guided smart delivery of an anticancer agent: Curcumin. *Materials Science and Engineering: C*, 74, 186-193.
- BAGHERI, S., YASEMI, M., SAFAIE-QAMSARI, E., RASHIDIANI, J., ABKAR, M., HASSANI, M., MIRHOSSEINI, S. A. & KOOSHKI, H. 2018. Using gold nanoparticles in diagnosis and treatment of melanoma cancer. *Artificial Cells, Nanomedicine, and Biotechnology*, 46, 462-471.

- BAHRAMI, K. & ARABI, M. S. 2016. Copper immobilized ferromagnetic nanoparticle triazine dendrimer (FMNP@ TD-Cu (ii))-catalyzed regioselective synthesis of 1, 4-disubstituted 1, 2, 3-triazoles. *New Journal of Chemistry*, 40, 3447-3455.
- BAINS, S. N. & FONACIER, L. 2019. Irritant contact dermatitis. *Clinical reviews in allergy & immunology*, 56, 99-109.
- BANO, I., ARSHAD, M., YASIN, T., GHOURI, M. A. & YOUNUS, M. 2017. Chitosan: A potential biopolymer for wound management. *International journal of biological macromolecules*, 102, 380-383.
- BASTIAT, G., PRITZ, C. O., ROIDER, C., FOUCHET, F., LIGNIÈRES, E., JESACHER, A., GLUECKERT, R., RITSCH-MARTE, M., SCHROTT-FISCHER, A., SAULNIER, P. & BENOIT, J.-P. 2013. A new tool to ensure the fluorescent dye labeling stability of nanocarriers: A real challenge for fluorescence imaging. *Journal of Controlled Release*, 170, 334-342.
- BAUMAN, C. A., EMARY, P., DAMEN, T. & DIXON, H. 2018. Melanoma in situ: a case report from the patient's perspective. *The Journal of the Canadian Chiropractic Association*, 62, 56-61.
- BAUMANN, J. B., BAGUTTI, C., SIEGRIST, W., CHRISTEN, E., ZUMSTEG, U. & EBERLE, A. N. 1997. MSH receptors and the response of human A375 melanoma cells to interleukin-1 beta. *Journal of receptor and signal transduction research*, 17, 199-210.
- BAYAT MOKHTARI, R., HOMAYOUNI, T. S., BALUCH, N., MORGATSKAYA, E., KUMAR, S., DAS, B. & YEGER, H. 2017. Combination therapy in combating cancer. *Oncotarget*, 8, 38022-38043.
- BELLAMY, C. O., JENKINS, S. J., MCSORLEY, H. J., DORWARD, D. A. & KENDALL, T. J. 2020. 4 Inflammation and immunology. *Muir's Textbook of Pathology*.
- BELTER, B., HAASE-KOHN, C. & PIETZSCH, J. 2017. Biomarkers in malignant melanoma: recent trends and critical perspective. *Exon Publications*, 39-56.
- BENTZ, J., HILL, B. & ILLUM, L. 2017. Method for delivering alpha-melanocyte stimulating hormone mimetibody composition comprising propylene glycol for intranasal administration to the central nervous system. Google Patents.
- BERTRAM, J. S. 2000. The molecular biology of cancer. *Mol Aspects Med*, 21, 167-223.
- BERTRAND, N., WU, J., XU, X., KAMALY, N. & FAROKHZAD, O. C. 2014. Cancer nanotechnology: The impact of passive and active targeting in the era of modern cancer biology. *Advanced Drug Delivery Reviews*, 66, 2-25.
- BHUNCHU, S. & ROJSITTHISAK, P. 2014. Biopolymeric alginate-chitosan nanoparticles as drug delivery carriers for cancer therapy. *Die Pharmazie-An International Journal of Pharmaceutical Sciences*, 69, 563-570.
- BIABANIKHANKAHDANI, R., ALITHEEN, N. B. M., HO, K. L. & TAN, W. S. 2016. pH-responsive virus-like nanoparticles with enhanced tumour-targeting ligands for cancer drug delivery. *Scientific reports*, 6, 37891.
- BILLERO, V. L., JACOBSEN, A. A., MITEVA, M. I., WULKAN, A. J., MARASCA, C. & ROMANELLI, P. 2017. Nodular cutaneous amyloidoma of the extremity secondary to chronic

- granulomatous inflammation in setting of sarcoidosis. *Journal of cutaneous pathology*, 44, 801-804.
- BISWAS, S. & TORCHILIN, V. P. 2014. Nanopreparations for organelle-specific delivery in cancer. *Advanced drug delivery reviews*, 66, 26-41.
- BITTKAU, K. S., DÖRSCHMANN, P., BLÜMEL, M., TASDEMIR, D., ROIDER, J., KLETTNER, A. & ALBAN, S. 2019. Comparison of the Effects of Fucoidans on the Cell Viability of Tumor and Non-Tumor Cell Lines. *Marine drugs*, 17, 441.
- BLANCO, E., SHEN, H. & FERRARI, M. 2015. Principles of nanoparticle design for overcoming biological barriers to drug delivery. *Nature biotechnology*, 33, 941-951.
- BONIFACIO, B. V., DA SILVA, P. B., DOS SANTOS RAMOS, M. A., NEGRI, K. M. S., BAUAB, T. M. & CHORILLI, M. 2014. Nanotechnology-based drug delivery systems and herbal medicines: a review. *International journal of nanomedicine*, 9, 1.
- BORRELLI, A., TORNESELLO, A. L., TORNESELLO, M. L. & BUONAGURO, F. M. 2018. Cell Penetrating Peptides as Molecular Carriers for Anti-Cancer Agents. *Molecules (Basel, Switzerland)*, 23, 295.
- BOU-DARGHAM, M. J., KHAMIS, Z. I., COGNETTA, A. B. & SANG, Q. X. A. 2017. The Role of Interleukin-1 in Inflammatory and Malignant Human Skin Diseases and the Rationale for Targeting Interleukin-1 Alpha. *Medicinal research reviews*, 37, 180-216.
- BRAGTA, P., SIDHU, R. K., JYOTI, K., BALDI, A., JAIN, U. K., CHANDRA, R. & MADAN, J. 2018. Intratumoral administration of carboplatin bearing poly (ϵ -caprolactone) nanoparticles amalgamated with in situ gel tendered augmented drug delivery, cytotoxicity, and apoptosis in melanoma tumor. *Colloids and Surfaces B: Biointerfaces*, 166, 339-348.
- BRAY, F., FERLAY, J., SOERJOMATARAM, I., SIEGEL, R. L., TORRE, L. A. & JEMAL, A. 2018. Global cancer statistics 2018: GLOBOCAN estimates of incidence and mortality worldwide for 36 cancers in 185 countries. *CA: A Cancer Journal for Clinicians*, 68, 394-424.
- BROSSART, P., KEILHOLZ, U., WILLHAUCK, M., SCHEIBENBOGEN, C., MÖHLER, T. & HUNSTEIN, W. 1993. Hematogenous spread of malignant melanoma cells in different stages of disease. *Journal of investigative dermatology*, 101, 887-889.
- BULMAN, A., NEAGU, M. & CONSTANTIN, C. 2013. Immunomics in Skin Cancer - Improvement in Diagnosis, Prognosis and Therapy Monitoring. *Current proteomics*, 10, 202-217.
- BURAPAPADH, K., TAKEUCHI, H. & SRIAMORNSAK, P. 2012. Novel pectin-based nanoparticles prepared from nanoemulsion templates for improving in vitro dissolution and in vivo absorption of poorly water-soluble drug. *European Journal of Pharmaceutics and Biopharmaceutics*, 82, 250-261.
- CAIRNS, J. A. 2007. The coxibs and traditional nonsteroidal anti-inflammatory drugs: a current perspective on cardiovascular risks. *The Canadian journal of cardiology*, 23, 125-131.
- CAMARGO, L. E. A. D., BRUSTOLIN LUDWIG, D., TOMINAGA, T. T., CARLETTO, B., FAVERO, G. M., MAINARDES, R. M. & KHALIL, N. M. 2018. Bovine serum albumin nanoparticles

- improve the antitumour activity of curcumin in a murine melanoma model. *Journal of Microencapsulation*, 35, 467-474.
- CAMPBELL, K. J. & TAIT, S. W. G. 2018. Targeting BCL-2 regulated apoptosis in cancer. *Open biology*, 8, 180002.
- CAN, V. C., LOCKE, I. C., KANEVA, M. K., KERRIGAN, M. J. P., MERLINO, F., DE PASCALE, C., GRIECO, P. & GETTING, S. J. 2020. Novel anti-inflammatory and chondroprotective effects of the human melanocortin MC1 receptor agonist BMS-470539 dihydrochloride and human melanocortin MC3 receptor agonist PG-990 on lipopolysaccharide activated chondrocytes. *European Journal of Pharmacology*, 872, 172971.
- CARREAU, N. A. & PAVLICK, A. C. 2018. Nivolumab and ipilimumab: immunotherapy for treatment of malignant melanoma. *Future Oncology*, 15, 349-358.
- CAVACO, M. C., PEREIRA, C., KREUTZER, B., GOUVEIA, L. F., SILVA-LIMA, B., BRITO, A. M. & VIDEIRA, M. 2017. Evading P-glycoprotein mediated-efflux chemoresistance using Solid Lipid Nanoparticles. *European Journal of Pharmaceutics and Biopharmaceutics*, 110, 76-84.
- CHAN, M. S., LIU, L. S., LEUNG, H. M. & LO, P. K. 2017. Cancer-Cell-Specific Mitochondria-Targeted Drug Delivery by Dual-Ligand-Functionalized Nanodiamonds Circumvent Drug Resistance. *ACS Applied Materials & Interfaces*, 9, 11780-11789.
- CHANG, S.-C. & YANG, W.-C. V. 2016. Hyperglycemia, tumorigenesis, and chronic inflammation. *Critical reviews in oncology/hematology*, 108, 146-153.
- CHARI, R. V. 2008. Targeted cancer therapy: conferring specificity to cytotoxic drugs. *Acc Chem Res*, 41, 98-107.
- CHATTERJEE, N. & BIVONA, T. G. 2019. Polytherapy and Targeted Cancer Drug Resistance. *Trends in Cancer*, 5, 170-182.
- CHELLAPPAN, D. K., YEE, N. J., KAUR AMBAR JEET SINGH, B. J., PANNEERSELVAM, J., MADHESWARAN, T., CHELLIAN, J., SATIJA, S., MEHTA, M., GULATI, M. & GUPTA, G. 2019. Formulation and characterization of glibenclamide and quercetin-loaded chitosan nanogels targeting skin permeation. *Therapeutic delivery*, 10, 281-293.
- CHEN, L., DENG, H., CUI, H., FANG, J., ZUO, Z., DENG, J., LI, Y., WANG, X. & ZHAO, L. 2017. Inflammatory responses and inflammation-associated diseases in organs. *Oncotarget*, 9, 7204-7218.
- CHEN, X. Y., CHEN, Y., QU, C. J., PAN, Z. H., QIN, Y., ZHANG, X., LIU, W. J., LI, D. F. & ZHENG, Q. 2019. Vitamin C induces human melanoma A375 cell apoptosis via Bax-and Bcl-2-mediated mitochondrial pathways. *Oncology letters*, 18, 3880-3886.
- CHEN, Z., ZHANG, T., WU, B. & ZHANG, X. 2016. Insights into the therapeutic potential of hypoxia-inducible factor-1 α small interfering RNA in malignant melanoma delivered via folate-decorated cationic liposomes. *International journal of nanomedicine*, 11, 991.

- CHENG, N., JESCHKE, M. G., SHEIKHOESLAM, M., DATU, A. K., OH, H. H. & AMINI-NIK, S. 2019a. Promotion of dermal regeneration using pullulan/gelatin porous skin substitute. *Journal of tissue engineering and regenerative medicine*, 13, 1965-1977.
- CHENG, Y., HE, C., WANG, M., MA, X., MO, F., YANG, S., HAN, J. & WEI, X. 2019b. Targeting epigenetic regulators for cancer therapy: mechanisms and advances in clinical trials. *Signal Transduction and Targeted Therapy*, 4, 62.
- CHITTASUPHO, C., XIE, S.-X., BAOUM, A., YAKOVLEVA, T., SIAHAAN, T. J. & BERKLAND, C. J. 2009. ICAM-1 targeting of doxorubicin-loaded PLGA nanoparticles to lung epithelial cells. *European journal of pharmaceutical sciences*, 37, 141-150.
- CHO, K., WANG, X. U., NIE, S. & SHIN, D. M. 2008. Therapeutic nanoparticles for drug delivery in cancer. *Clinical cancer research*, 14, 1310-1316.
- CHOI, Y. H. & YU, A.-M. 2014. ABC transporters in multidrug resistance and pharmacokinetics, and strategies for drug development. *Current pharmaceutical design*, 20, 793-807.
- CHUNG, H., JUNG, H., JHO, E.-H., MULTHAUP, H. A. B., COUCHMAN, J. R. & OH, E.-S. 2018. Keratinocytes negatively regulate the N-cadherin levels of melanoma cells via contact-mediated calcium regulation. *Biochemical and Biophysical Research Communications*, 503, 615-620.
- CHUNG, Y.-C., SU, Y.-P., CHEN, C.-C., JIA, G., WANG, H.-L., WU, J. C. G. & LIN, J.-G. 2004. Relationship between antibacterial activity of chitosan and surface characteristics of cell wall. *Acta pharmacologica sinica*, 25, 932-936.
- CLOGSTON, J. D. & PATRI, A. K. 2011. Zeta Potential Measurement. In: MCNEIL, S. E. (ed.) *Characterization of Nanoparticles Intended for Drug Delivery*. Totowa, NJ: Humana Press.
- COCHRAN, M. C., EISENBREY, J., OUMA, R. O., SOULEN, M. & WHEATLEY, M. A. 2011. Doxorubicin and paclitaxel loaded microbubbles for ultrasound triggered drug delivery. *International journal of pharmaceutics*, 414, 161-170.
- COLCLOUGH, J. British society of Dermatological Surgeons.
- COLONE, M., CALCABRINI, A., TOCCACIELI, L., BOZZUTO, G., STRINGARO, A., GENTILE, M., CIANFRIGLIA, M., CIERVO, A., CARAGLIA, M. & BUDILLON, A. 2008. The multidrug transporter P-glycoprotein: a mediator of melanoma invasion? *Journal of Investigative Dermatology*, 128, 957-971.
- CONSTANTINIDES, P. P., CHAUBAL, M. V. & SHORR, R. 2008. Advances in lipid nanodispersions for parenteral drug delivery and targeting. *Advanced drug delivery reviews*, 60, 757-767.
- CORAS, R., NARASIMHAN, R., KAVANAUGH, A., SORIA, L. M., QUEHENBERGER, O., GUMA, M. & MARTÍNEZ-MORILLO, M. 2019. THU0044 PRO-AND ANTI-INFLAMMATORY MEDIATORS OF SYSTEMIC INFLAMMATION AND ARTHRITIS IN THE ELDERLY. BMJ Publishing Group Ltd.

- COSTA, A. M., BUENO, K. T. L., ROSA, A. P. C. D. & COSTA, J. A. V. 2019. The antioxidant activity of nanoemulsions based on lipids and peptides from *Spirulina* sp. LEB18. *LWT*, 99, 173-178.
- COSTANTINI, P., JACOTOT, E., DECAUDIN, D. & KROEMER, G. 2000. Mitochondrion as a novel target of anticancer chemotherapy. *Journal of the National Cancer Institute*, 92, 1042-1053.
- COSTIN, G.-E., TRIF, M., NICHITA, N., DWEK, R. A. & PETRESCU, S. M. 2002. pH-sensitive liposomes are efficient carriers for endoplasmic reticulum-targeted drugs in mouse melanoma cells. *Biochemical and biophysical research communications*, 293, 918-923.
- COUSSENS, L. M. & WERB, Z. 2002. Inflammation and cancer. *Nature*, 420, 860-867.
- COUTO, G. K., SEGATTO, N. V., OLIVEIRA, T. L., SEIXAS, F. K., SCHACHTSCHNEIDER, K. M. & COLLARES, T. 2019. The Melding of Drug Screening Platforms for Melanoma. *Frontiers in Oncology*, 9.
- COVIELLO, T., MATRICARDI, P., MARIANECCI, C. & ALHAIQUE, F. 2007. Polysaccharide hydrogels for modified release formulations. *Journal of controlled release*, 119, 5-24.
- COYLE, K. M., BOUDREAU, J. E. & MARCATO, P. 2017. Genetic Mutations and Epigenetic Modifications: Driving Cancer and Informing Precision Medicine. *BioMed Research International*, 2017, 9620870.
- CROCE, L., COPERCHINI, F., MAGRI, F., CHIOVATO, L. & ROTONDI, M. 2019. The multifaceted anti-cancer effects of BRAF-inhibitors. *Oncotarget*, 10, 6623-6640.
- CRUSZ, S. M. & BALKWILL, F. R. 2015. Inflammation and cancer: advances and new agents. *Nature Reviews Clinical Oncology*, 12, 584.
- CURRY, J. L., PINTO, W., NICKOLOFF, B. J. & SLOMINSKI, A. T. 2001. Human keratinocytes express functional α -MSH (MC1-R) receptors. *In vitro Cellular & Developmental Biology-Animal*, 37, 234-236.
- CUTRONA, M. B. & SIMPSON, J. C. 2019. A High-Throughput Automated Confocal Microscopy Platform for Quantitative Phenotyping of Nanoparticle Uptake and Transport in Spheroids. *Small*, 15, 1902033.
- D'SOUZA, G. G. M., WAGLE, M. A., SAXENA, V. & SHAH, A. 2011. Approaches for targeting mitochondria in cancer therapy. *Biochimica et Biophysica Acta (BBA) - Bioenergetics*, 1807, 689-696.
- DA SILVA, C. G., PETERS, G. J., OSSENDORP, F. & CRUZ, L. J. 2017. The potential of multi-compound nanoparticles to bypass drug resistance in cancer. *Cancer chemotherapy and pharmacology*, 80, 881-894.
- DADWAL, A., BALDI, A. & KUMAR NARANG, R. 2018. Nanoparticles as carriers for drug delivery in cancer. *Artificial Cells, Nanomedicine, and Biotechnology*, 46, 295-305.
- DAMSKY, W. E., ROSENBAUM, L. E. & BOSENBERG, M. 2010. Decoding melanoma metastasis. *Cancers*, 3, 126-163.

- DATE, A. A., DESAI, N., DIXIT, R. & NAGARSENKER, M. 2010. Self-nanoemulsifying drug delivery systems: formulation insights, applications and advances. *Nanomedicine*, 5, 1595-1616.
- DE SOUZA, R., ZAHEDI, P., ALLEN, C. J. & PIQUETTE-MILLER, M. 2010. Polymeric drug delivery systems for localized cancer chemotherapy. *Drug delivery*, 17, 365-375.
- DEBELE, T. A., MEKURIA, S. L. & TSAI, H.-C. 2016. Polysaccharide based nanogels in the drug delivery system: Application as the carrier of pharmaceutical agents. *Materials Science and Engineering: C*, 68, 964-981.
- DEINLEIN, T., RICHTIG, G., SCHWAB, C., SCARFI, F., ARZBERGER, E., WOLF, I., HOFMANN-WELLENHOF, R. & ZALAUDEK, I. 2016. The use of dermatoscopy in diagnosis and therapy of nonmelanocytic skin cancer. *JDDG: Journal der Deutschen Dermatologischen Gesellschaft*, 14, 144-151.
- DENKERT, C., KÖBEL, M., BERGER, S., SIEGERT, A., LECLERE, A., TREFZER, U. & HAUPTMANN, S. 2001a. Expression of cyclooxygenase 2 in human malignant melanoma. *Cancer research*, 61, 303-308.
- DENKERT, C., KÖBEL, M., BERGER, S., SIEGERT, A., LECLERE, A., TREFZER, U. & HAUPTMANN, S. 2001b. Expression of Cyclooxygenase 2 in Human Malignant Melanoma. *Cancer Research*, 61, 303.
- DEVARAJAN, P. V., DANDEKAR, P. & D'SOUZA, A. A. 2019. *Targeted Intracellular Drug Delivery by Receptor Mediated Endocytosis*, Springer.
- DEVITA, V. T. & CHU, E. 2008. A history of cancer chemotherapy. *Cancer research*, 68, 8643-8653.
- DEWANE, M. E., KELSEY, A., OLIVIERO, M., RABINOVITZ, H. & GRANT-KELS, J. M. 2019. Melanoma on chronically sun-damaged skin: Lentigo maligna and desmoplastic melanoma. *Journal of the American Academy of Dermatology*, 81, 823-833.
- DHARMALINGAM, S. R., RAMAMURTHY, S., CHIDAMBARAM, K. & NADARAJU, S. 2014. A simple HPLC bioanalytical method for the determination of doxorubicin hydrochloride in rat plasma: application to pharmacokinetic studies. *Tropical journal of pharmaceutical research*, 13, 409-415.
- DHAS, N. L., IGE, P. P. & KUDARHA, R. R. 2015. Design, optimization and in-vitro study of folic acid conjugated-chitosan functionalized PLGA nanoparticle for delivery of bicalutamide in prostate cancer. *Powder Technology*, 283, 234-245.
- DHEER, D., ARORA, D., JAGLAN, S., RAWAL, R. K. & SHANKAR, R. 2017. Polysaccharides based nanomaterials for targeted anti-cancer drug delivery. *Journal of Drug Targeting*, 25, 1-16.
- DIANZANI, C., ZARA, G. P., MAINA, G., PETTAZZONI, P., PIZZIMENTI, S., ROSSI, F., GIGLIOTTI, C. L., CIAMPORCERO, E. S., DAGA, M. & BARRERA, G. 2014. Drug delivery nanoparticles in skin cancers. *BioMed research international*, 2014, 895986-895986.
- DICKENS, E. & AHMED, S. 2018. Principles of cancer treatment by chemotherapy. *Surgery (Oxford)*, 36, 134-138.

- DIEKJÜRGEN, D. & GRAINGER, D. W. 2017. Polysaccharide matrices used in 3D in vitro cell culture systems. *Biomaterials*, 141, 96-115.
- DIELSCHNEIDER, R. F., HENSON, E. S. & GIBSON, S. B. 2017. Lysosomes as oxidative targets for cancer therapy. *Oxidative medicine and cellular longevity*, 2017.
- DIEPGEN, T. L. & MAHLER, V. 2002. The epidemiology of skin cancer. *British Journal of Dermatology*, 146, 1-6.
- DISSANAYAKE, S., DENNY, W. A., GAMAGE, S. & SAROJINI, V. 2017. Recent developments in anticancer drug delivery using cell penetrating and tumor targeting peptides. *Journal of Controlled Release*, 250, 62-76.
- DODDAPANENI, B. S., KYRYACHENKO, S., CHAGANI, S. E., ALANY, R. G., RAO, D. A., INDRA, A. K. & ALANI, A. W. G. 2015. A three-drug nanoscale drug delivery system designed for preferential lymphatic uptake for the treatment of metastatic melanoma. *Journal of Controlled Release*, 220, 503-514.
- DOMINGUES, B., LOPES, J. M., SOARES, P. & PÓPULO, H. 2018. Melanoma treatment in review. *ImmunoTargets and therapy*, 7, 35.
- DONG, K., WANG, Z., ZHANG, Y., REN, J. & QU, X. 2018. Metal–organic framework-based nanoplatfrom for intracellular environment-responsive endo/lysosomal escape and enhanced cancer therapy. *ACS applied materials & interfaces*, 10, 31998-32005.
- DORRANI, M., GARBUZENKO, O. B., MINKO, T. & MICHNIAK-KOHN, B. 2016. Development of edge-activated liposomes for siRNA delivery to human basal epidermis for melanoma therapy. *Journal of Controlled Release*, 228, 150-158.
- DRAKE, C. G., LIPSON, E. J. & BRAHMER, J. R. 2014. Breathing new life into immunotherapy: review of melanoma, lung and kidney cancer. *Nature reviews Clinical oncology*, 11, 24.
- DUAN, X., LIAO, Y., LIU, T., YANG, H., LIU, Y., CHEN, Y., ULLAH, R. & WU, T. 2020. Zinc oxide nanoparticles synthesized from *Cardiospermum halicacabum* and its anticancer activity in human melanoma cells (A375) through the modulation of apoptosis pathway. *Journal of Photochemistry and Photobiology B: Biology*, 202, 111718.
- DUESBERG, P. & MCCORMACK, A. 2013. Immortality of cancers: a consequence of inherent karyotypic variations and selections for autonomy. *Cell cycle (Georgetown, Tex.)*, 12, 783-802.
- ELDER, D. E. 2016. Melanoma progression. *Pathology*, 48, 147-154.
- ELLIOTT, A. M. & AL-HAJJ, M. A. 2009. ABCB8 mediates doxorubicin resistance in melanoma cells by protecting the mitochondrial genome. *Molecular Cancer Research*, 7, 79-87.
- ELMORE, S. 2007. Apoptosis: a review of programmed cell death. *Toxicologic pathology*, 35, 495-516.
- ERKURT, M. A., AYDOGDU, I., KUKU, I., KAYA, E. & BASARAN, Y. 2009. Nodular melanoma presenting with rapid progression and widespread metastases: a case report. *Journal of medical case reports*, 3, 50-50.

- ESTEVA, A., KUPREL, B., NOVOA, R. A., KO, J., SWETTER, S. M., BLAU, H. M. & THRUN, S. 2017. Dermatologist-level classification of skin cancer with deep neural networks. *Nature*, 542, 115.
- ETTINGER, A. & WITTMANN, T. 2014. Fluorescence live cell imaging. *Methods in cell biology*, 123, 77-94.
- FALZONE, L., SALOMONE, S. & LIBRA, M. 2018a. Evolution of Cancer Pharmacological Treatments at the Turn of the Third Millennium. *Frontiers in pharmacology*, 9, 1300-1300.
- FALZONE, L., SALOMONE, S. & LIBRA, M. 2018b. Evolution of Cancer Pharmacological Treatments at the Turn of the Third Millennium. *Frontiers in Pharmacology*, 9, 1300.
- FELDMAN, M. E. & SHOKAT, K. M. 2010. New inhibitors of the PI3K-Akt-mTOR pathway: insights into mTOR signaling from a new generation of Tor Kinase Domain Inhibitors (TORKinibs). *Curr Top Microbiol Immunol*, 347, 241-62.
- FERLAY, J., COLOMBET, M., SOERJOMATARAM, I., MATHERS, C., PARKIN, D., PIÑEROS, M., ZNAOR, A. & BRAY, F. 2019. Estimating the global cancer incidence and mortality in 2018: GLOBOCAN sources and methods. *International journal of cancer*, 144, 1941-1953.
- FERRARA, N., HILLAN, K. J. & NOVOTNY, W. 2005. Bevacizumab (Avastin), a humanized anti-VEGF monoclonal antibody for cancer therapy. *Biochem Biophys Res Commun*, 333, 328-35.
- FERRAZ, L. S., WATASHI, C. M., COLTURATO-KIDO, C., PELEGRINO, M. T., PAREDES-GAMERO, E. J., WELLER, R. B., SEABRA, A. B. & RODRIGUES, T. 2018. Antitumor Potential of S-Nitrosothiol-Containing Polymeric Nanoparticles against Melanoma. *Molecular Pharmaceutics*, 15, 1160-1168.
- FERRUCCI, L. & FABBRI, E. 2018. Inflammageing: chronic inflammation in ageing, cardiovascular disease, and frailty. *Nature Reviews Cardiology*, 15, 505-522.
- FIORENTZIS, M., KALIRAI, H., KATOPODIS, P., SEITZ, B., VIESTENZ, A. & COUPLAND, S. E. 2018. Electrochemotherapy with bleomycin and cisplatin enhances cytotoxicity in primary and metastatic uveal melanoma cell lines in vitro. *Neoplasma*, 65, 210-215.
- FOFARIA, N. M., QHATTAL, H. S. S., LIU, X. & SRIVASTAVA, S. K. 2016a. Nanoemulsion formulations for anti-cancer agent piplartine—Characterization, toxicological, pharmacokinetics and efficacy studies. *International Journal of Pharmaceutics*, 498, 12-22.
- FOFARIA, N. M., QHATTAL, H. S. S., LIU, X. & SRIVASTAVA, S. K. 2016b. Nanoemulsion formulations for anti-cancer agent piplartine—Characterization, toxicological, pharmacokinetics and efficacy studies. *International journal of pharmaceutics*, 498, 12-22.
- FORMAN, S. B., FERRINGER, T. C., PECKHAM, S. J., DALTON, S. R., SASAKI, G. T., LIBOW, L. F. & ELSTON, D. M. 2008. Is superficial spreading melanoma still the most common form of malignant melanoma? *J Am Acad Dermatol*, 58, 1013-20.

- FORNAGUERA, C., DOLS-PEREZ, A., CALDERO, G., GARCIA-CELMA, M., CAMARASA, J. & SOLANS, C. 2015. PLGA nanoparticles prepared by nano-emulsion templating using low-energy methods as efficient nanocarriers for drug delivery across the blood–brain barrier. *Journal of Controlled Release*, 211, 134-143.
- FOSGERAU, K. & HOFFMANN, T. 2015. Peptide therapeutics: current status and future directions. *Drug discovery today*, 20, 122-128.
- FRANZE, S. 2015. THE PERMEATION OF BIOMACROMOLECULES THROUGH HUMAN SKIN: AN INSIGHT INTO THE FAMILY OF GLYCOSAMINOGLYCANS.
- FROMHERZ, P. & RUPPEL, D. 1985. Lipid vesicle formation: the transition from open disks to closed shells. *FEBS letters*, 179, 155-159.
- FU, H., SHI, K., HU, G., YANG, Y., KUANG, Q., LU, L., ZHANG, L., CHEN, W., DONG, M., CHEN, Y. & HE, Q. 2015. Tumor-Targeted Paclitaxel Delivery and Enhanced Penetration Using TAT-Decorated Liposomes Comprising Redox-Responsive Poly(Ethylene Glycol). *Journal of Pharmaceutical Sciences*, 104, 1160-1173.
- FULFORD, M. R. & STANKIEWICZ, N. R. 2020. The Immune System. *Infection Control in Primary Dental Care*. Springer.
- GANDHI, J., KHERA, L., GAUR, N., PAUL, C. & KAUL, R. 2017. Role of Modulator of Inflammation Cyclooxygenase-2 in Gammaherpesvirus Mediated Tumorigenesis. *Frontiers in microbiology*, 8, 538-538.
- GANESHKUMAR, M., PONRASU, T., RAJA, M. D., SUBAMEKALA, M. K. & SUGUNA, L. 2014. Green synthesis of pullulan stabilized gold nanoparticles for cancer targeted drug delivery. *Spectrochimica Acta Part A: Molecular and Biomolecular Spectroscopy*, 130, 64-71.
- GARBE, C. & LEITER, U. 2009. Melanoma epidemiology and trends. *Clinics in dermatology*, 27, 3-9.
- GARBE, C., PERIS, K., HAUSCHILD, A., SAIAG, P., MIDDLETON, M., SPATZ, A., GROB, J.-J., MALVEHY, J., NEWTON-BISHOP, J. & STRATIGOS, A. 2010. Diagnosis and treatment of melanoma: European consensus-based interdisciplinary guideline. *European journal of cancer*, 46, 270-283.
- GARG, U., CHAUHAN, S., NAGAICH, U. & JAIN, N. 2019. Current Advances in Chitosan Nanoparticles Based Drug Delivery and Targeting. *Advanced pharmaceutical bulletin*, 9, 195-204.
- GEORGE, V. C., KUMAR, D. R. N., SURESH, P. K., KUMAR, S. & KUMAR, R. A. 2013. Comparative studies to evaluate relative in vitro potency of luteolin in inducing cell cycle arrest and apoptosis in HaCaT and A375 cells. *Asian Pacific Journal of Cancer Prevention*, 14, 631-637.
- GEORGE, V. C. & RUPASINGHE, H. 2017. Apple flavonoids suppress carcinogen-induced DNA damage in normal human bronchial epithelial cells. *Oxidative medicine and cellular longevity*, 2017.

- GERBER, D. E. 2008. Targeted therapies: a new generation of cancer treatments. *American family physician*, 77.
- GETTING, S. J., KANEVA, M., BHADRESA, Y., RENSCHAW, D., LEONI, G., PATEL, H. B., KERRIGAN, M. J. P. & LOCKE, I. C. 2009. Melanocortin peptide therapy for the treatment of arthritic pathologies. *The Scientific World Journal*, 9, 1394-1414.
- GETTING, S. J., LAM, C. W., CHEN, A. S., GRIECO, P. & PERRETTI, M. 2006. Melanocortin 3 receptors control crystal-induced inflammation. *The FASEB Journal*, 20, 2234-2241.
- GETTING, S. J., RIFFO-VASQUEZ, Y., PITCHFORD, S., KANEVA, M., GRIECO, P., PAGE, C. P., PERRETTI, M. & SPINA, D. 2008. A role for MC3R in modulating lung inflammation. *Pulmonary pharmacology & therapeutics*, 21, 866-873.
- GHAZ-JAHANIAN, M. A., ABBASPOUR-AGHDAM, F., ANARJAN, N., BERENJIAN, A. & JAFARIZADEH-MALMIRI, H. 2015. Application of chitosan-based nanocarriers in tumor-targeted drug delivery. *Molecular biotechnology*, 57, 201-218.
- GIBBS, P. A. & SEVIOUR, R. J. 2017. Pullulan. *Polysaccharides in medicinal applications*. Routledge.
- GIBOT, L., CHABAUD, S., BOUHOUT, S., BOLDUC, S., AUGER, F. A. & MOULIN, V. J. 2015. Anticancer properties of chitosan on human melanoma are cell line dependent. *International journal of biological macromolecules*, 72, 370-379.
- GILANI, S. J., JAHANGIR, M. A., RIZWANULLAH, M., TALEUZZAMAN, M., SHAHAB, M. S., SHAKEEL, K., AQIL, M. & IMAM, S. S. 2018. Nano-based therapy for treatment of skin cancer. *Recent patents on anti-infective drug discovery*, 13, 151-163.
- GOLIAS, C. H., TSOUTSI, E., MATZIRIDIS, A., MAKRIDIS, P., BATISTATOU, A. & CHARALABOPOULOS, K. 2007. Leukocyte and endothelial cell adhesion molecules in inflammation focusing on inflammatory heart disease. *In Vivo*, 21, 757-769.
- GONZAGA, E. R. 2009. Role of UV light in photodamage, skin aging, and skin cancer. *American journal of clinical dermatology*, 10, 19-24.
- GOULET, A.-C., EINSPHAR, J. G., ALBERTS, D. S., BEAS, A., BURK, C., BHATTACHARYYA, A. K., BANGERT, J., HARMON, J. M., FUJIWARA, H. & KOKI, A. 2003. Analysis of cyclooxygenase 2 (COX-2) expression during malignant melanoma progression. *Cancer biology & therapy*, 2, 713-718.
- GRETEN, F. R. & GRIVENNIKOV, S. I. 2019. Inflammation and cancer: triggers, mechanisms, and consequences. *Immunity*, 51, 27-41.
- GRILLO, R., DIAS, F. V., QUEROBINO, S. M., ALBERTO-SILVA, C., FRACETO, L. F., DE PAULA, E. & DE ARAUJO, D. R. 2019. Influence of hybrid polymeric nanoparticle/thermosensitive hydrogels systems on formulation tracking and in vitro artificial membrane permeation: A promising system for skin drug-delivery. *Colloids and Surfaces B: Biointerfaces*, 174, 56-62.
- GRIMM, E. A., ELLERHORST, J., TANG, C.-H. & EKMEKCIOGLU, S. 2008. Constitutive intracellular production of iNOS and NO in human melanoma: possible role in regulation of growth and resistance to apoptosis. *Nitric oxide : biology and chemistry*, 19, 133-137.

- GROSSMAN, D. & ALTIERI, D. C. 2001. Drug resistance in melanoma: mechanisms, apoptosis, and new potential therapeutic targets. *Cancer and Metastasis Reviews*, 20, 3-11.
- GUIMARÃES, C. A. & LINDEN, R. 2004. Programmed cell deaths. *European journal of biochemistry*, 271, 1638-1650.
- GUO, R. & SHI, X. 2012. Dendrimers in cancer therapeutics and diagnosis. *Current drug metabolism*, 13, 1097-1109.
- GUPTA, R. K., LIPMAN, M., JACKSON, C., SITCH, A., SOUTHERN, J., DROBNIEWSKI, F., DEEKS, J. J., TSOU, C.-Y., GRIFFITHS, C. & DAVIDSON, J. 2019. Quantitative Interferon Gamma Release Assay and Tuberculin Skin Test Results to Predict Incident Tuberculosis: A Prospective Cohort Study. *American Journal of Respiratory and Critical Care Medicine*.
- HAN, S., TOKER, A., LIU, Z. Q. & OHASHI, P. S. 2019. Turning the Tide Against Regulatory T Cells. *Frontiers in oncology*, 9, 279-279.
- HAO, J., XU, H., LUO, M., YU, W., CHEN, M., LIAO, Y., ZHANG, C., ZHAO, X., JIANG, W. & HOU, S. 2018. The Tumor-Promoting Role of TRIP4 in Melanoma Progression and its Involvement in Response to BRAF-Targeted Therapy. *Journal of Investigative Dermatology*, 138, 159-170.
- HE, W., GUO, X., XIAO, L. & FENG, M. 2009. Study on the mechanisms of chitosan and its derivatives used as transdermal penetration enhancers. *International journal of pharmaceutics*, 382, 234-243.
- HELFAND, M., MAHON, S. M., EDEN, K. B., FRAME, P. S. & ORLEANS, C. T. 2001. Screening for skin cancer. *American Journal of Preventive Medicine*, 20, 47-58.
- HELMBACH, H., ROSSMANN, E., KERN, M. A. & SCHADENDORF, D. 2001. Drug-resistance in human melanoma. *International Journal of Cancer*, 93, 617-622.
- HERRAIZ, C., JIMÉNEZ-CERVANTES, C., SÁNCHEZ-LAORDEN, B. & GARCÍA-BORRÓN, J. C. Functional interplay between secreted ligands and receptors in melanoma. 2018. Elsevier, 73-84.
- HIENTZ, K., MOHR, A., BHAKTA-GUHA, D. & EFFERTH, T. 2017. The role of p53 in cancer drug resistance and targeted chemotherapy. *Oncotarget*, 8, 8921-8946.
- HOANG, B., ERNSTING, M. J., ROY, A., MURAKAMI, M., UNDZYS, E. & LI, S.-D. 2015. Docetaxel-carboxymethylcellulose nanoparticles target cells via a SPARC and albumin dependent mechanism. *Biomaterials*, 59, 66-76.
- HODONICZKY, J., SIMS, C. G., BEST, W. M., BENTEL, J. M. & WILCE, J. A. 2008. The intracellular and nuclear-targeted delivery of an antiandrogen drug by carrier peptides. *Peptide Science*, 90, 595-603.
- HOLLOWAY, P. M., DURRENBERGER, P. F., TRUTSCHL, M., CVEK, U., COOPER, D., ORR, A. W., PERRETTI, M., GETTING, S. J. & GAVINS, F. N. E. 2015. Both MC1 and MC3 Receptors Provide Protection From Cerebral Ischemia-Reperfusion-Induced Neutrophil Recruitment. *Arteriosclerosis, thrombosis, and vascular biology*, 35, 1936-1944.
- HOSSEINI, F., HOSSEINI, F., JAFARI, S. M. & TAHERI, A. 2018. Bentonite nanoclay-based drug-delivery systems for treating melanoma. *Clay Minerals*, 53, 53-63.

- HOUSMAN, G., BYLER, S., HEERBOTH, S., LAPINSKA, K., LONGACRE, M., SNYDER, N. & SARKAR, S. 2014. Drug resistance in cancer: an overview. *Cancers*, 6, 1769-1792.
- HUA, C., BOUSSEMART, L., MATEUS, C., ROUTIER, E., BOUTROS, C., CAZENAVE, H., VIOLLET, R., THOMAS, M., ROY, S. & BENANNOUNE, N. 2016. Association of vitiligo with tumor response in patients with metastatic melanoma treated with pembrolizumab. *JAMA dermatology*, 152, 45-51.
- HUA, S. 2014. Comparison of in vitro dialysis release methods of loperamide-encapsulated liposomal gel for topical drug delivery. *International journal of nanomedicine*, 9, 735.
- HUANG, C.-Y., JU, D.-T., CHANG, C.-F., MURALIDHAR REDDY, P. & VELMURUGAN, B. K. 2017. A review on the effects of current chemotherapy drugs and natural agents in treating non-small cell lung cancer. *BioMedicine*, 7, 23-23.
- HUANG, L., CHAURASIYA, B., WU, D., WANG, H., DU, Y., TU, J., WEBSTER, T. J. & SUN, C. 2018. Versatile redox-sensitive pullulan nanoparticles for enhanced liver targeting and efficient cancer therapy. *Nanomedicine: Nanotechnology, Biology and Medicine*, 14, 1005-1017.
- HUGHES, J. 2018. HBOT: An Essential Component for the Regenerative Treatment of Pain from Sports Injuries, Chronic Inflammation and Infection.
- HUI, Y., YI, X., HOU, F., WIBOWO, D., ZHANG, F., ZHAO, D., GAO, H. & ZHAO, C.-X. 2019. Role of nanoparticle mechanical properties in cancer drug delivery. *ACS nano*, 13, 7410-7424.
- HUNTER, P. 2012. The inflammation theory of disease. The growing realization that chronic inflammation is crucial in many diseases opens new avenues for treatment. *EMBO reports*, 13, 968-970.
- IOANNIDES, T. 2017. Method and composition for treating cancer or skin lesion using a vaccine. Google Patents.
- IWAMOTO, T. 2013. Clinical application of drug delivery systems in cancer chemotherapy: review of the efficacy and side effects of approved drugs. *Biol Pharm Bull*, 36, 715-8.
- JABLONSKI, R. P., KIM, S.-J., CHERESH, P., WILLIAMS, D. B., MORALES-NEBRED, L., CHENG, Y., YELDANDI, A., BHORADE, S., PARDO, A., SELMAN, M., RIDGE, K., GIUS, D., SCOTT BUDINGER, G. R. & KAMP, D. W. 2017. SIRT3 deficiency promotes lung fibrosis by augmenting alveolar epithelial cell mitochondrial DNA damage and apoptosis. *The FASEB Journal*, 31, 2520-2532.
- JACQUELOT, N., ROBERTI, M. P., ENOT, D. P., RUSAKIEWICZ, S., TERNÈS, N., JEGOU, S., WOODS, D. M., SODRÉ, A. L., HANSEN, M. & MEIROW, Y. 2017. Predictors of responses to immune checkpoint blockade in advanced melanoma. *Nature communications*, 8, 592.
- JAIN, R. K. 1994. Barriers to drug delivery in solid tumors. *Scientific American*, 271, 58-65.
- JAISWAL, M., DUDHE, R. & SHARMA, P. K. 2015. Nanoemulsion: an advanced mode of drug delivery system. *3 Biotech*, 5, 123-127.
- JAN, R. & CHAUDHRY, G.-E. S. 2019. Understanding Apoptosis and Apoptotic Pathways Targeted Cancer Therapeutics. *Advanced pharmaceutical bulletin*, 9, 205-218.

- JANAKIRAM, N. B. & RAO, C. V. 2012. Chemoprevention of Colon Cancer by iNOS-Selective Inhibitors. *Forum on immunopathological diseases and therapeutics*, 3, 155-167.
- JANGDEY, M. S., KAUR, C. D. & SARAF, S. 2019. Efficacy of Concanavalin-A conjugated nanotransfersomal gel of apigenin for enhanced targeted delivery of UV induced skin malignant melanoma. *Artificial cells, nanomedicine, and biotechnology*, 47, 904-916.
- JAWORSKA, M., SAKURAI, K., GAUDON, P. & GUIBAL, E. 2003. Influence of chitosan characteristics on polymer properties. I: Crystallographic properties. *Polymer International*, 52, 198-205.
- JEFFE, D. B., PÉREZ, M., COLE, E. F., LIU, Y. & SCHOOTMAN, M. 2016. The Effects of Surgery Type and Chemotherapy on Early-Stage Breast Cancer Patients' Quality of Life Over 2-Year Follow-up. *Annals of surgical oncology*, 23, 735-743.
- JIANG, T., WANG, T., LI, T., MA, Y., SHEN, S., HE, B. & MO, R. 2018. Enhanced Transdermal Drug Delivery by Transfersome-Embedded Oligopeptide Hydrogel for Topical Chemotherapy of Melanoma. *ACS Nano*, 12, 9693-9701.
- JIANG, T., ZHOU, C. & REN, S. 2016. Role of IL-2 in cancer immunotherapy. *Oncoimmunology*, 5, e1163462-e1163462.
- JO, Y., CHOI, N., KIM, K., KOO, H.-J., CHOI, J. & KIM, H. N. 2018. Chemoresistance of Cancer Cells: Requirements of Tumor Microenvironment-mimicking In vitro Models in Anti-Cancer Drug Development. *Theranostics*, 8, 5259-5275.
- JOHANSSON, C. C., EGYHÁZI, S., MASUCCI, G., HARLIN, H., MOUGIAKAKOS, D., POSCHKE, I., NILSSON, B., GARBERG, L., TUOMINEN, R. & LINDEN, D. 2009. Prognostic significance of tumor iNOS and COX-2 in stage III malignant cutaneous melanoma. *Cancer immunology, immunotherapy*, 58, 1085-1094.
- JOO, W. D., VISINTIN, I. & MOR, G. 2013. Targeted cancer therapy--are the days of systemic chemotherapy numbered? *Maturitas*, 76, 308-314.
- KALAL, B. S., UPADHYA, D. & PAI, V. R. 2017. Chemotherapy resistance mechanisms in advanced skin cancer. *Oncology reviews*, 11.
- KALE, S. N. & DEORE, S. L. 2017. Emulsion micro emulsion and nano emulsion: a review. *Systematic Reviews in Pharmacy*, 8, 39.
- KALMOUNI, M., AL-HOSANI, S. & MAGZOUN, M. 2019. Cancer targeting peptides. *Cellular and Molecular Life Sciences*, 76, 2171-2183.
- KANEVA, M. K., KERRIGAN, M. J. P., GRIECO, P., CURLEY, G. P., LOCKE, I. C. & GETTING, S. J. 2012. Chondroprotective and anti-inflammatory role of melanocortin peptides in TNF- α activated human C-20/A4 chondrocytes. *British journal of pharmacology*, 167, 67-79.
- KAPALCZYŃSKA, M., KOLENDA, T., PRZYBYŁA, W., ZAJĄCZKOWSKA, M., TERESIAK, A., FILAS, V., IBBS, M., BLIŹNIAK, R., ŁUCZEWSKI, Ł. & LAMPERSKA, K. 2018. 2D and 3D cell cultures—a comparison of different types of cancer cell cultures. *Archives of medical science: AMS*, 14, 910.

- KAREWICZ, A., BIELSKA, D., LOBODA, A., GZYL-MALCHER, B., BEDNAR, J., JOZKOWICZ, A., DULAK, J. & NOWAKOWSKA, M. 2013. Curcumin-containing liposomes stabilized by thin layers of chitosan derivatives. *Colloids and Surfaces B: Biointerfaces*, 109, 307-316.
- KARIMI, M., SOLATI, N., GHASEMI, A., ESTIAR, M. A., HASHEMKHANI, M., KIANI, P., MOHAMED, E., SAEIDI, A., TAHERI, M. & AVCI, P. 2015. Carbon nanotubes part II: a remarkable carrier for drug and gene delivery. *Expert opinion on drug delivery*, 12, 1089-1105.
- KAWANISHI, S., OHNISHI, S., MA, N., HIRAKU, Y. & MURATA, M. 2017. Crosstalk between DNA damage and inflammation in the multiple steps of carcinogenesis. *International journal of molecular sciences*, 18, 1808.
- KESIK-BRODACKA, M. 2018. Progress in biopharmaceutical development. *Biotechnology and applied biochemistry*, 65, 306-322.
- KHALID, M. & EL-SAWY, H. S. 2017. Polymeric nanoparticles: Promising platform for drug delivery. *International journal of pharmaceutics*, 528, 675-691.
- KHANDAVILLI, S. & PANCHAGNULA, R. 2007. Nanoemulsions as versatile formulations for paclitaxel delivery: peroral and dermal delivery studies in rats. *Journal of Investigative Dermatology*, 127, 154-162.
- KHANDELIA, R., BHANDARI, S., PAN, U. N., GHOSH, S. S. & CHATTOPADHYAY, A. 2015. Gold nanocluster embedded albumin nanoparticles for two-photon imaging of cancer cells accompanying drug delivery. *Small*, 11, 4075-4081.
- KHAWAR, I. A., KIM, J. H. & KUH, H.-J. 2015. Improving drug delivery to solid tumors: priming the tumor microenvironment. *Journal of Controlled Release*, 201, 78-89.
- KHDAIR, A., HAMAD, I., ALKHATIB, H., BUSTANJI, Y., MOHAMMAD, M., TAYEM, R. & AIEDEH, K. 2016. Modified-chitosan nanoparticles: Novel drug delivery systems improve oral bioavailability of doxorubicin. *European Journal of Pharmaceutical Sciences*, 93, 38-44.
- KIM, J. B. Three-dimensional tissue culture models in cancer biology. 2005. Elsevier, 365-377.
- KIM, S.-H., HASHIMOTO, Y., CHO, S.-N., ROSZIK, J., MILTON, D. R., DAL, F., KIM, S. F., MENTER, D. G., YANG, P., EKMEKCIOGLU, S. & GRIMM, E. A. 2016. Microsomal PGE2 synthase-1 regulates melanoma cell survival and associates with melanoma disease progression. *Pigment cell & melanoma research*, 29, 297-308.
- KOHARA, Y. 2001. cDNA. In: BRENNER, S. & MILLER, J. H. (eds.) *Encyclopedia of Genetics*. New York: Academic Press.
- KORNILUK, A., KOPER, O., KEMONA, H. & DYMICKA-PIEKARSKA, V. 2017. From inflammation to cancer. *Irish Journal of Medical Science (1971-)*, 186, 57-62.
- KOSKI, C. & BOSE, S. 2019. Effects of amylose content on the mechanical properties of starch-hydroxyapatite 3D printed bone scaffolds. *Additive Manufacturing*, 30, 100817.
- KOUSHIK, O., RAO, Y., KUMAR, P. & KARTHIKEYAN, R. 2016. Nano drug delivery systems to overcome cancer drug resistance—a review. *J Nanomed Nanotechnol*, 7, 2.
- KOZOVSKA, Z., GABRISOVA, V. & KUCEROVA, L. 2016. Malignant melanoma: diagnosis, treatment and cancer stem cells. *Neoplasma*, 63, 510-517.

- KUFLIK, E. G. & GAGE, A. A. 1990. Cryosurgical Treatment for Skin Cancer, eds. *Kuflik, EG and Gage, AA, "History."* (Igaku-Shoin, New York), 1-13.
- KUMAR, A., AHMAD, A., VYAWAHARE, A. & KHAN, R. 2020. Membrane Trafficking and Subcellular Drug Targeting Pathways. *Frontiers in pharmacology*, 11, 629-629.
- KUMARI, A., YADAV, S. K. & YADAV, S. C. 2010. Biodegradable polymeric nanoparticles based drug delivery systems. *Colloids and surfaces B: biointerfaces*, 75, 1-18.
- LABALA, S. 2016. Layer-by-Layer Assembled Nanoparticles for Drug Delivery Through Skin.
- LADINO, C. A., CHARI, R. V., BOURRET, L. A., KEDERSHA, N. L. & GOLDMACHER, V. S. 1997. Folate-maytansinoids: Target-selective drugs of low molecular weight. *International journal of cancer*, 73, 859-864.
- LAI, Y.-L., CHENG, P.-Y., YANG, C.-C. & YEN, S.-K. 2018. Electrolytic deposition of hydroxyapatite/calcium phosphate-heparin/gelatin-heparin tri-layer composites on NiTi alloy to enhance drug loading and prolong releasing for biomedical applications. *Thin Solid Films*, 649, 192-201.
- LANDSKRON, G., DE LA FUENTE, M., THUWAJIT, P., THUWAJIT, C. & HERMOSO, M. A. 2014. Chronic inflammation and cytokines in the tumor microenvironment. *Journal of immunology research*, 2014.
- LASSALLE, V. & FERREIRA, M. L. 2007. PLA nano-and microparticles for drug delivery: an overview of the methods of preparation. *Macromolecular bioscience*, 7, 767-783.
- LAU, J. L. & DUNN, M. K. 2018. Therapeutic peptides: Historical perspectives, current development trends, and future directions. *Bioorganic & medicinal chemistry*, 26, 2700-2707.
- LEE, E.-H., LIM, S.-J. & LEE, M.-K. 2019. Chitosan-coated liposomes to stabilize and enhance transdermal delivery of indocyanine green for photodynamic therapy of melanoma. *Carbohydrate Polymers*, 224, 115143.
- LEE, S.-Y., CHO, S.-S., LI, Y., BAE, C.-S., PARK, K. M. & PARK, D.-H. 2020. Anti-inflammatory Effect of Curcuma longa and Allium hookeri Co-treatment via NF- κ B and COX-2 Pathways. *Scientific Reports*, 10, 1-11.
- LEE, S. Y., JU, M. K., JEON, H. M., JEONG, E. K., LEE, Y. J., KIM, C. H., PARK, H. G., HAN, S. I. & KANG, H. S. 2018. Regulation of Tumor Progression by Programmed Necrosis. *Oxidative Medicine and Cellular Longevity*, 2018, 3537471.
- LEHMANN, B. 1997. HaCaT cell line as a model system for vitamin D3 metabolism in human skin. *J Invest Dermatol*, 108, 78-82.
- LESLIE, E. M., DEELEY, R. G. & COLE, S. P. 2005. Multidrug resistance proteins: role of P-glycoprotein, MRP1, MRP2, and BCRP (ABCG2) in tissue defense. *Toxicol Appl Pharmacol*, 204, 216-37.
- LI, D., FENG, X., CHEN, L., DING, J. & CHEN, X. 2018a. One-Step Synthesis of Targeted Acid-Labile Polysaccharide Prodrug for Efficiently Intracellular Drug Delivery. *ACS Biomaterials Science & Engineering*, 4, 539-546.

- LI, H., JIN, H., WAN, W., WU, C. & WEI, L. 2018b. Cancer nanomedicine: mechanisms, obstacles and strategies. *Nanomedicine*, 13, 1639-1656.
- LI, H. S. 2018. The Effects of Cell Morphology on Nanoparticle Uptake and Uptake at the Leading Edge in MC3T3 Cells.
- LI, J., HWANG, I.-C., CHEN, X. & PARK, H. J. 2016. Effects of chitosan coating on curcumin loaded nano-emulsion: Study on stability and in vitro digestibility. *Food Hydrocolloids*, 60, 138-147.
- LI, J., WANG, Y., LIANG, R., AN, X., WANG, K., SHEN, G., TU, Y., ZHU, J. & TAO, J. 2015. Recent advances in targeted nanoparticles drug delivery to melanoma. *Nanomedicine: Nanotechnology, Biology and Medicine*, 11, 769-794.
- LI, J. & YUAN, J. 2008. Caspases in apoptosis and beyond. *Oncogene*, 27, 6194-6206.
- LI, K., ZHAN, W., CHEN, Y., JHA, R. K. & CHEN, X. 2019a. Docetaxel and Doxorubicin Codelivery by Nanocarriers for Synergistic Treatment of Prostate Cancer. *Frontiers in Pharmacology*, 10.
- LI, X. & HEYER, W.-D. 2008. Homologous recombination in DNA repair and DNA damage tolerance. *Cell research*, 18, 99-113.
- LI, X., QI, J., XIE, Y., ZHANG, X., HU, S., XU, Y., LU, Y. & WU, W. 2013. Nanoemulsions coated with alginate/chitosan as oral insulin delivery systems: preparation, characterization, and hypoglycemic effect in rats. *International journal of nanomedicine*, 8, 23.
- LI, Y., ZHANG, T., LIU, Q. & HE, J. 2019b. PEG-Derivatized Dual-Functional Nanomicelles for Improved Cancer Therapy. *Frontiers in pharmacology*, 10, 808-808.
- LIANG, X.-J., CHEN, C., ZHAO, Y. & WANG, P. C. 2010. Circumventing tumor resistance to chemotherapy by nanotechnology. *Methods in molecular biology (Clifton, N.J.)*, 596, 467-488.
- LIANG, Y., ZHAO, X., MA, P. X., GUO, B., DU, Y. & HAN, X. 2019. pH-responsive injectable hydrogels with mucosal adhesiveness based on chitosan-grafted-dihydrocaffeic acid and oxidized pullulan for localized drug delivery. *Journal of Colloid and Interface Science*, 536, 224-234.
- LIAO, B., YING, H., YU, C., FAN, Z., ZHANG, W., SHI, J., YING, H., RAVICHANDRAN, N., XU, Y., YIN, J., JIANG, Y. & DU, Q. 2016. (-)-Epigallocatechin gallate (EGCG)-nanoethosomes as a transdermal delivery system for docetaxel to treat implanted human melanoma cell tumors in mice. *International Journal of Pharmaceutics*, 512, 22-31.
- LIN, W.-C., YEH, I., NIYAMA, E., HUANG, W.-R., EBARA, M. & WU, C.-S. 2018. Electrospun poly (ϵ -caprolactone) nanofibrous mesh for imiquimod delivery in melanoma therapy. *Polymers*, 10, 231.
- LISAK, R. P. & BENJAMINS, J. A. 2017. Melanocortins, Melanocortin Receptors and Multiple Sclerosis. *Brain sciences*, 7, 104.
- LITWACK, G. 2018. Chapter 10 - Nucleic Acids and Molecular Genetics. In: LITWACK, G. (ed.) *Human Biochemistry*. Boston: Academic Press.

- LIU, F., FENG, L., ZHANG, L., ZHANG, X. & ZHANG, N. 2013. Synthesis, characterization and antitumor evaluation of CMCS–DTX conjugates as novel delivery platform for docetaxel. *International Journal of Pharmaceutics*, 451, 41-49.
- LIU, J., QI, C., TAO, K., ZHANG, J., ZHANG, J., XU, L., JIANG, X., ZHANG, Y., HUANG, L., LI, Q., XIE, H., GAO, J., SHUAI, X., WANG, G., WANG, Z. & WANG, L. 2016. Sericin/Dextran Injectable Hydrogel as an Optically Trackable Drug Delivery System for Malignant Melanoma Treatment. *ACS Applied Materials & Interfaces*, 8, 6411-6422.
- LIU, Q., CHAN, S. T. F. & MAHENDRAN, R. 2003. Nitric oxide induces cyclooxygenase expression and inhibits cell growth in colon cancer cell lines. *Carcinogenesis*, 24, 637-642.
- LIU, Q., DAS, M., LIU, Y. & HUANG, L. 2018. Targeted drug delivery to melanoma. *Advanced drug delivery reviews*, 127, 208-221.
- LIU, Y. & SHEIKH, M. S. 2014. Melanoma: Molecular Pathogenesis and Therapeutic Management. *Molecular and cellular pharmacology*, 6, 228-228.
- LIU, Z., JIAO, Y., WANG, Y., ZHOU, C. & ZHANG, Z. 2008. Polysaccharides-based nanoparticles as drug delivery systems. *Advanced drug delivery reviews*, 60, 1650-1662.
- LO, C., LAI, T.-Y., YANG, J.-H., YANG, J.-S., MA, Y.-S., WENG, S.-W., CHEN, Y.-Y., LIN, J.-G. & CHUNG, J.-G. 2010. Gallic acid induces apoptosis in A375. S2 human melanoma cells through caspase-dependent and-independent pathways. *International journal of oncology*, 37, 377-385.
- LOCH-NECKEL, G., SANTOS-BUBNIAK, L., MAZZARINO, L., JACQUES, A. V., MOCCELIN, B., SANTOS-SILVA, M. C. & LEMOS-SENNA, E. 2015. Orally Administered Chitosan-Coated Polycaprolactone Nanoparticles Containing Curcumin Attenuate Metastatic Melanoma in the Lungs. *Journal of Pharmaceutical Sciences*, 104, 3524-3534.
- LONGLEY, D. B. & JOHNSTON, P. G. 2005. Molecular mechanisms of drug resistance. *J Pathol*, 205, 275-92.
- LÓPEZ-GARCÍA, J., LEHOCKÝ, M., HUMPOLÍČEK, P. & SÁHA, P. 2014. HaCaT Keratinocytes Response on Antimicrobial Atelocollagen Substrates: Extent of Cytotoxicity, Cell Viability and Proliferation. *Journal of functional biomaterials*, 5, 43-57.
- LOVE, R. R., LEVENTHAL, H., EASTERLING, D. V. & NERENZ, D. R. 1989. Side effects and emotional distress during cancer chemotherapy. *Cancer*, 63, 604-612.
- LU, Y., CHAN, Y.-T., TAN, H.-Y., LI, S., WANG, N. & FENG, Y. 2020. Epigenetic regulation in human cancer: the potential role of epi-drug in cancer therapy. *Molecular Cancer*, 19, 79.
- LUGOWSKA, I., KOSEŁA-PATERCZYK, H., KOZAK, K. & RUTKOWSKI, P. 2015. Trametinib: a MEK inhibitor for management of metastatic melanoma. *OncoTargets and therapy*, 8, 2251-2259.
- LV, S., TANG, Z., ZHANG, D., SONG, W., LI, M., LIN, J., LIU, H. & CHEN, X. 2014. Well-defined polymer-drug conjugate engineered with redox and pH-sensitive release mechanism for efficient delivery of paclitaxel. *Journal of Controlled Release*, 194, 220-227.

- MAASER, C., KANNENGIESSER, K. & KUCHARZIK, T. 2006. Role of the Melanocortin System in Inflammation. *Annals of the New York Academy of Sciences*, 1072, 123-134.
- MADDOX, W. 2017. Causal Inference to Ascertain Causes of Metastasis in Melanoma. *Discussions*, 13.
- MAEDA, H., BHARATE, G. Y. & DARUWALLA, J. 2009. Polymeric drugs for efficient tumor-targeted drug delivery based on EPR-effect. *European journal of pharmaceuticals and biopharmaceutics*, 71, 409-419.
- MAHDAVINIA, G. R., MOSALLANEZHAD, A., SOLEYMANI, M. & SABZI, M. 2017. Magnetic-and pH-responsive κ -carrageenan/chitosan complexes for controlled release of methotrexate anticancer drug. *International journal of biological macromolecules*, 97, 209-217.
- MAJETY, M., PRADEL, L. P., GIES, M. & RIES, C. H. 2015. Fibroblasts influence survival and therapeutic response in a 3D co-culture model. *PLoS ONE*, 10.
- MARTÍNEZ-JIMÉNEZ, F., OVERINGTON, J. P., AL-LAZIKANI, B. & MARTI-RENOM, M. A. 2017. Rationally designed drug blending as a mechanism to overcome drug resistance in cancer: An application in EGFR.
- MARU, G. B., GANDHI, K., RAMCHANDANI, A. & KUMAR, G. 2014. The role of inflammation in skin cancer. *Inflammation and Cancer*. Springer.
- MASOUMI, Z., VAN GENDEREN, J. L. & MESGARI, M. S. 2018. Modelling and predicting the spatial dispersion of skin cancer considering environmental and socio-economic factors using a digital earth approach. *International Journal of Digital Earth*, 1-22.
- MATSUI, H., SHIMOKAWA, O., KANEKO, T., NAGANO, Y., RAI, K. & HYODO, I. 2011. The pathophysiology of non-steroidal anti-inflammatory drug (NSAID)-induced mucosal injuries in stomach and small intestine. *Journal of clinical biochemistry and nutrition*, 48, 107-111.
- MATTHEWS, N. H., LI, W.-Q., QURESHI, A. A., WEINSTOCK, M. A. & CHO, E. 2017. Epidemiology of melanoma. *Cutaneous melanoma: etiology and therapy [Internet]*. Codon Publications.
- MAYA, S., SARMENTO, B., NAIR, A., REJINOLD, N. S., NAIR, S. V. & JAYAKUMAR, R. 2013. Smart stimuli sensitive nanogels in cancer drug delivery and imaging: a review. *Current pharmaceutical design*, 19, 7203-7218.
- MAYERS, K. 2018. What is the scale of the skin cancer problem in the UK? *Journal of Aesthetic Nursing*, 7, 230-230.
- MCCARTHY, E. F. 2006a. The toxins of William B. Coley and the treatment of bone and soft-tissue sarcomas. *The Iowa orthopaedic journal*, 26, 154-158.
- MCCARTHY, E. F. 2006b. The toxins of William B. Coley and the treatment of bone and soft-tissue sarcomas. *The Iowa orthopaedic journal*, 26, 154.
- MCKINNON, C. M. & MELLOR, H. 2017. The tumor suppressor RhoBTB1 controls Golgi integrity and breast cancer cell invasion through METTL7B. *BMC cancer*, 17, 145.

- MCLEAN, S. R., GANA-WEISZ, M., HARTZOULAKIS, B., FROW, R., WHELAN, J., SELWOOD, D. & BOSHOF, C. 2005. Imatinib binding and cKIT inhibition is abrogated by the cKIT kinase domain I missense mutation Val654Ala. *Mol Cancer Ther*, 4, 2008-15.
- MEDRANO, R. F. V., HUNGER, A., MENDONÇA, S. A., BARBUTO, J. A. M. & STRAUSS, B. E. 2017. Immunomodulatory and antitumor effects of type I interferons and their application in cancer therapy. *Oncotarget*, 8, 71249-71284.
- MIAO, T., WANG, J., ZENG, Y., LIU, G. & CHEN, X. 2018. Polysaccharide-Based Controlled Release Systems for Therapeutics Delivery and Tissue Engineering: From Bench to Bedside. *Advanced Science*, 5, 1700513.
- MICHAEL, H., DAY, C.-P., YANG, H., MICHALOWSKI, A., LEE, M. & MERLINO, G. 2017. Progression from melanocytic nevi to melanoma is associated with increased genomic mutations in a UV-induced mouse model of human melanoma. AACR.
- MILLER, A. B., HOOGSTRAAT, B., STAQUET, M. & WINKLER, A. 1981. Reporting results of cancer treatment. *cancer*, 47, 207-214.
- MITCHISON, T. J. 2012. The proliferation rate paradox in antimitotic chemotherapy. *Molecular biology of the cell*, 23, 1-6.
- MO, R. & GU, Z. 2016. Tumor microenvironment and intracellular signal-activated nanomaterials for anticancer drug delivery. *Materials Today*, 19, 274-283.
- MOHNEN, D. 2008. Pectin structure and biosynthesis. *Current opinion in plant biology*, 11, 266-277.
- MOSETHAL, A. 2018. Inflammation, immune response and healing. *Fundamentals of Children's Applied Pathophysiology: An Essential Guide for Nursing and Healthcare Students*.
- MOVAFEGH, B., JALAL, R., MOHAMMADI, Z. & ALDAGHI, S. A. 2018. Poly-L-arginine: enhancing cytotoxicity and cellular uptake of doxorubicin and necrotic cell death. *Anti-Cancer Agents in Medicinal Chemistry (Formerly Current Medicinal Chemistry-Anti-Cancer Agents)*, 18, 1448-1456.
- MÜLLER, R. H., RÜHL, D., RUNGE, S., SCHULZE-FORSTER, K. & MEHNERT, W. 1997. Cytotoxicity of solid lipid nanoparticles as a function of the lipid matrix and the surfactant. *Pharmaceutical research*, 14, 458-462.
- MUNDRA, V., LI, W. & MAHATO, R. I. 2015. Nanoparticle-mediated drug delivery for treating melanoma. *Nanomedicine (London, England)*, 10, 2613-2633.
- MURAKAMI, A. & OHGASHI, H. 2007. Targeting NOX, INOS and COX-2 in inflammatory cells: Chemoprevention using food phytochemicals. *International Journal of Cancer*, 121, 2357-2363.
- MURPHY, M. P. 1997. Selective targeting of bioactive compounds to mitochondria. *Trends in biotechnology*, 15, 326-330.
- NAGY, G., DÉNES, N., KIS, A., SZABÓ, J. P., BERÉNYI, E., GARAI, I., BAI, P., HAJDU, I., SZIKRA, D. & TRENCSENYI, G. 2017. Preclinical evaluation of melanocortin-1 receptor (MC1-R)

- specific ⁶⁸Ga- and ⁴⁴Sc-labeled DOTA-NAPamide in melanoma imaging. *European Journal of Pharmaceutical Sciences*, 106, 336-344.
- NAIDOO, C., KRUGER, C. A. & ABRAHAMSE, H. 2018. Photodynamic therapy for metastatic melanoma treatment: A review. *Technology in cancer research & treatment*, 17, 1533033818791795.
- NAKAZAWA, H., CHANG, K., SHINOZAKI, S., YASUKAWA, T., ISHIMARU, K., YASUHARA, S., YU, Y.-M., MARTYN, J. A. J., TOMPKINS, R. G., SHIMOKADO, K. & KANEKI, M. 2017. iNOS as a Driver of Inflammation and Apoptosis in Mouse Skeletal Muscle after Burn Injury: Possible Involvement of Sirt1 S-Nitrosylation-Mediated Acetylation of p65 NF- κ B and p53. *PLoS one*, 12, e0170391-e0170391.
- NALLANTHIGHAL, S., HEISERMAN, J. P. & CHEON, D.-J. 2019. The Role of the Extracellular Matrix in Cancer Stemness. *Frontiers in Cell and Developmental Biology*, 7.
- NAVES, L. B. & ALMEIDA, L. 2015. Wound Healing Dressing and Some Composites Such as Zeolite, TiO₂, Chitosan and PLGA: A Review. *World Academy of Science, Engineering and Technology, International Journal of Medical, Health, Biomedical, Bioengineering and Pharmaceutical Engineering*, 9, 242-246.
- NAVES, L. B., ALMEIDA, L. & RAMAKRISHNA, S. 2017a. Understanding the microenvironment of melanoma cells for the development of target drug delivery systems. *ONCOLOGY*.
- NAVES, L. B., DHAND, C., VENUGOPAL, J. R., RAJAMANI, L., RAMAKRISHNA, S. & ALMEIDA, L. 2017b. Nanotechnology for the treatment of melanoma skin cancer. *Progress in biomaterials*, 6, 13-26.
- NAVYA, P. N., KAPHLE, A., SRINIVAS, S. P., BHARGAVA, S. K., ROTELLO, V. M. & DAIMA, H. K. 2019. Current trends and challenges in cancer management and therapy using designer nanomaterials. *Nano Convergence*, 6, 23.
- NEAGU, M., CONSTANTIN, C., CARUNTU, C., DUMITRU, C., SURCEL, M. & ZURAC, S. 2019. Inflammation: A key process in skin tumorigenesis. *Oncology letters*, 17, 4068-4084.
- NGUYEN, K. T. 2011. Targeted nanoparticles for cancer therapy: promises and challenge.
- NIGAM, S. & BAHADUR, D. 2018. Doxorubicin-loaded dendritic-Fe₃O₄ supramolecular nanoparticles for magnetic drug targeting and tumor regression in spheroid murine melanoma model. *Nanomedicine: Nanotechnology, Biology and Medicine*, 14, 759-768.
- NITISS, J. L. 2009. Targeting DNA topoisomerase II in cancer chemotherapy. *Nature reviews. Cancer*, 9, 338-350.
- NIU, B., SHAO, P. & SUN, P. 2020. Ultrasound-assisted emulsion electrosprayed particles for the stabilization of β -carotene and its nutritional supplement potential. *Food Hydrocolloids*, 102, 105634.
- NIU, Z., CONEJOS-SANCHEZ, I., GRIFFIN, B. T., O'DRISCOLL, C. M. & ALONSO, M. J. 2016. Lipid-based nanocarriers for oral peptide delivery. *Advanced drug delivery reviews*, 106, 337-354.

- NURGALI, K., JAGOE, R. T. & ABALO, R. 2018. Editorial: Adverse Effects of Cancer Chemotherapy: Anything New to Improve Tolerance and Reduce Sequelae? *Frontiers in pharmacology*, 9, 245-245.
- O'SULLIVAN, D. E., BRENNER, D. R., DEMERS, P. A., VILLENEUVE, P. J., FRIEDENREICH, C. M. & KING, W. D. 2019. Indoor tanning and skin cancer in Canada: A meta-analysis and attributable burden estimation. *Cancer Epidemiology*, 59, 1-7.
- OGAWARA, K.-I., ABE, S., UN, K., YOSHIZAWA, Y., KIMURA, T. & HIGAKI, K. 2014. Determinants for in vivo antitumor effect of angiogenesis inhibitor SU5416 formulated in PEGylated emulsion. *Journal of pharmaceutical sciences*, 103, 2464-2469.
- OGBODU, R. O., NDHUNDHUMA, I., KARSTEN, A. & NYOKONG, T. 2015. Photodynamic therapy effect of zinc monoamino phthalocyanine–folic acid conjugate adsorbed on single walled carbon nanotubes on melanoma cells. *Spectrochimica Acta Part A: Molecular and Biomolecular Spectroscopy*, 137, 1120-1125.
- OKADA, F. 2014. Inflammation-related carcinogenesis: current findings in epidemiological trends, causes and mechanisms. *Yonago acta medica*, 57, 65-72.
- OKE, J. L., O'SULLIVAN, J. W., PERERA, R. & NICHOLSON, B. D. 2018. The mapping of cancer incidence and mortality trends in the UK from 1980-2013 reveals a potential for overdiagnosis. *Scientific reports*, 8, 14663-14663.
- OLÁH, G., DOBOS, N., VÁMOSI, G., SZABÓ, Z., SIPOS, É., FODOR, K., HARDA, K., SCHALLY, A. V. & HALMOS, G. 2018. Experimental therapy of doxorubicin resistant human uveal melanoma with targeted cytotoxic luteinizing hormone-releasing hormone analog (AN-152). *European Journal of Pharmaceutical Sciences*, 123, 371-376.
- PAHWA, R. & JIALAL, I. 2018. Chronic inflammation. *StatPearls [Internet]*. StatPearls Publishing.
- PAI, V. V., BHANDARI, P. & SHUKLA, P. 2017. Topical peptides as cosmeceuticals. *Indian Journal of Dermatology, Venereology, and Leprology*, 83, 9.
- PAL, D. & SAHA, S. 2019. Chondroitin: a natural biomarker with immense biomedical applications. *RSC advances*, 9, 28061-28077.
- PAN, L., HE, Q., LIU, J., CHEN, Y., MA, M., ZHANG, L. & SHI, J. 2012. Nuclear-Targeted Drug Delivery of TAT Peptide-Conjugated Monodisperse Mesoporous Silica Nanoparticles. *Journal of the American Chemical Society*, 134, 5722-5725.
- PAN, Z., QU, C., CHEN, Y., CHEN, X., LIU, X., HAO, W., XU, W., YE, L., LU, P. & LI, D. 2019. Bufotalin induces cell cycle arrest and cell apoptosis in human malignant melanoma A375 cells. *Oncology reports*, 41, 2409-2417.
- PANG, L., PEI, Y., UZUNALLI, G., HYUN, H., LYLE, L. T. & YEO, Y. 2019. Surface modification of polymeric nanoparticles with M2pep peptide for drug delivery to tumor-associated macrophages. *Pharmaceutical research*, 36, 65.
- PARK, J., JEONG, D., JANG, B. & OH, E.-S. 2019. The melanocortin-1 receptor reversely regulates the melanin synthesis and migration of melanoma cells via dimerization-

- induced conformational changes. *Biochemical and Biophysical Research Communications*, 518, 739-745.
- PARVEEN, S., MISRA, R. & SAHOO, S. K. 2012. Nanoparticles: a boon to drug delivery, therapeutics, diagnostics and imaging. *Nanomedicine: Nanotechnology, Biology and Medicine*, 8, 147-166.
- PASQUAL-MELO, G., GANDHIRAJAN, R. K., STOFFELS, I. & BEKESCHUS, S. 2018. Targeting malignant melanoma with physical plasmas. *Clinical Plasma Medicine*, 10, 1-8.
- PATEL, H. B., LEONI, G., MELENDEZ, T. M., SAMPAIO, A. L. F. & PERRETTI, M. 2010. Melanocortin control of cell trafficking in vascular inflammation. *Melanocortins: Multiple Actions and Therapeutic Potential*. Springer.
- PATEL, P., HANINI, A., SHAH, A., PATEL, D., PATEL, S., BHATT, P. & PATHAK, Y. V. 2019. Surface Modification of Nanoparticles for Targeted Drug Delivery. In: PATHAK, Y. V. (ed.) *Surface Modification of Nanoparticles for Targeted Drug Delivery*. Cham: Springer International Publishing.
- PATEL, R. B., PATEL, M. R., THAKORE, S. D. & PATEL, B. G. 2017. Nanoemulsion as a valuable nanostructure platform for pharmaceutical drug delivery. *Nano-and Microscale Drug Delivery Systems*. Elsevier.
- PATHAK, K., PATTNAIK, S. & SWAIN, K. 2018. Chapter 13 - Application of Nanoemulsions in Drug Delivery. In: JAFARI, S. M. & MCCLEMENTS, D. J. (eds.) *Nanoemulsions*. Academic Press.
- PATRA, J. K., DAS, G., FRACETO, L. F., CAMPOS, E. V. R., RODRIGUEZ-TORRES, M. D. P., ACOSTA-TORRES, L. S., DIAZ-TORRES, L. A., GRILLO, R., SWAMY, M. K., SHARMA, S., HABTEMARIAM, S. & SHIN, H.-S. 2018. Nano based drug delivery systems: recent developments and future prospects. *Journal of nanobiotechnology*, 16, 71-71.
- PAULINO, N., PAULINO, A. S., DINIZ, S. N., DE MENDONÇA, S., GONÇALVES, I. D., FLORES, F. F., SANTOS, R. P., RODRIGUES, C., PARDI, P. C. & SUAREZ, J. A. Q. 2016. Evaluation of the anti-inflammatory action of curcumin analog (DM1): Effect on iNOS and COX-2 gene expression and autophagy pathways. *Bioorganic & medicinal chemistry*, 24, 1927-1935.
- PEARCE, A., HAAS, M., VINEY, R., PEARSON, S.-A., HAYWOOD, P., BROWN, C. & WARD, R. 2017. Incidence and severity of self-reported chemotherapy side effects in routine care: A prospective cohort study. *Plos one*, 12, e0184360.
- PEARSON, S., VITUCCI, D., KHINE, Y. Y., DAG, A., LU, H., SAVE, M., BILLON, L. & STENZEL, M. H. 2015. Light-responsive azobenzene-based glycopolymer micelles for targeted drug delivery to melanoma cells. *European Polymer Journal*, 69, 616-627.
- PEGORARO, C., CECCHIN, D., GRACIA, L. S., WARREN, N., MADSEN, J., ARMES, S. P., LEWIS, A., MACNEIL, S. & BATTAGLIA, G. 2013. Enhanced drug delivery to melanoma cells using PMPC-PDPA polymersomes. *Cancer Letters*, 334, 328-337.
- PEI, D. & BUYANOVA, M. 2019. Overcoming Endosomal Entrapment in Drug Delivery. *Bioconjugate chemistry*, 30, 273-283.

- PENSON, R. T., OLIVA, E., SKATES, S. J., GLYPTIS, T., FULLER, A. F., JR., GOODMAN, A. & SEIDEN, M. V. 2004. Expression of multidrug resistance-1 protein inversely correlates with paclitaxel response and survival in ovarian cancer patients: a study in serial samples. *Gynecologic Oncology*, 93, 98-106.
- PIAO, S. & AMARAVADI, R. K. 2016. Targeting the lysosome in cancer. *Annals of the New York Academy of Sciences*, 1371, 45-54.
- PIOTROWSKA, A., WIERZBICKA, J., RYBARCZYK, A., TUCKEY, R. C., SLOMINSKI, A. T. & ŻMIJEWSKI, M. A. 2019. Vitamin D and its low calcemic analogs modulate the anticancer properties of cisplatin and dacarbazine in the human melanoma A375 cell line. *International journal of oncology*, 54, 1481-1495.
- PISTONE, S., GOYCOOLEA, F. M., YOUNG, A., SMISTAD, G. & HIORTH, M. 2017. Formulation of polysaccharide-based nanoparticles for local administration into the oral cavity. *European Journal of Pharmaceutical Sciences*, 96, 381-389.
- POPAT, A., KARMAKAR, S., JAMBHRUNKAR, S., XU, C. & YU, C. 2014. Curcumin-cyclodextrin encapsulated chitosan nanoconjugates with enhanced solubility and cell cytotoxicity. *Colloids and Surfaces B: Biointerfaces*, 117, 520-527.
- POSOTTO, B., DREUSSI, E., DE SANTA, J., TOFFOLI, G., ABRAMI, M., MUSIANI, F., GRASSI, M., FARRA, R., TONON, F., GRASSI, G. & DAPAS, B. 2015. Polysaccharides for the Delivery of Antitumor Drugs. *Materials*, 8, 2569-2615.
- PRASAD, R. & KATYAR, S. K. 2017. Crosstalk among UV-induced inflammatory mediators, DNA damage and epigenetic regulators facilitates suppression of the immune system. *Photochemistry and photobiology*, 93, 930-936.
- PRASETYANTI, P. R. & MEDEMA, J. P. 2017. Intra-tumor heterogeneity from a cancer stem cell perspective. *Molecular cancer*, 16, 41-41.
- PRETOR, S., BARTELS, J., LORENZ, T., DAHL, K., FINKE, J. H., PETERAT, G., KRULL, R., AL-HALHOULI, A. T., DIETZEL, A., BÜTTGENBACH, S., BEHREND, S., REICHL, S. & MÜLLER-GOYMANN, C. C. 2015. Cellular Uptake of Coumarin-6 under Microfluidic Conditions into HCE-T Cells from Nanoscale Formulations. *Molecular Pharmaceutics*, 12, 34-45.
- PRICE, P. & SIKORA, K. 2020. *Treatment of cancer*, CRC Press.
- PROCKOP, D. J. 2016. Inflammation, fibrosis, and modulation of the process by mesenchymal stem/stromal cells. *Matrix Biology*, 51, 7-13.
- PUCCI, B., KASTEN, M. & GIORDANO, A. 2000. Cell cycle and apoptosis. *Neoplasia (New York, N.Y.)*, 2, 291-299.
- PUCCI, C., MARTINELLI, C. & CIOFANI, G. 2019. Innovative approaches for cancer treatment: current perspectives and new challenges. *Ecancermedicalscience*, 13.
- PUND, S., PAWAR, S., GANGURDE, S. & DIVATE, D. 2015. Transcutaneous delivery of leflunomide nanoemulgel: Mechanistic investigation into physicochemical characteristics, in vitro anti-psoriatic and anti-melanoma activity. *International Journal of Pharmaceutics*, 487, 148-156.
- QIAN, B.-Z. Inflammation fires up cancer metastasis. 2017. Elsevier, 170-176.

- QIU, C., TARRANT, M. K., CHOI, S. H., SATHYAMURTHY, A., BOSE, R., BANJADE, S., PAL, A., BORNMANN, W. G., LEMMON, M. A. & COLE, P. A. 2008. Mechanism of activation and inhibition of the HER4/ErbB4 kinase. *Structure*, 16, 460-467.
- QUEEN, L. 2017. Skin Cancer: Causes, Prevention, and Treatment.
- QUIST, S. R., WISWEDEL, I., QUIST, J. & GOLLNICK, H. P. 2016. Kinetic profile of inflammation markers in human skin in vivo following exposure to ultraviolet B indicates synchronic release of cytokines and prostanoids. *Acta dermato-venereologica*, 96, 911-917.
- RAI, V. K., MISHRA, N., YADAV, K. S. & YADAV, N. P. 2018a. Nanoemulsion as pharmaceutical carrier for dermal and transdermal drug delivery: Formulation development, stability issues, basic considerations and applications. *Journal of controlled release*, 270, 203-225.
- RAI, Y., PATHAK, R., KUMARI, N., SAH, D. K., PANDEY, S., KALRA, N., SONI, R., DWARAKANATH, B. S. & BHATT, A. N. 2018b. Mitochondrial biogenesis and metabolic hyperactivation limits the application of MTT assay in the estimation of radiation induced growth inhibition. *Scientific Reports*, 8, 1531.
- RAJPUT, S. & WILBER, A. 2010. Roles of inflammation in cancer initiation, progression, and metastasis. *Front Biosci (Schol Ed)*, 2, 176-183.
- RANGWALA, S. & TSAI, K. Y. 2011. Roles of the immune system in skin cancer. *The British journal of dermatology*, 165, 953-965.
- RAPOPORT, N. 2007. Physical stimuli-responsive polymeric micelles for anti-cancer drug delivery. *Progress in Polymer Science*, 32, 962-990.
- RASS, K. & REICHRATH, J. 2008. UV damage and DNA repair in malignant melanoma and nonmelanoma skin cancer. *Sunlight, Vitamin D and Skin Cancer*. Springer.
- RAWLA, P., SUNKARA, T. & GADUPUTI, V. 2019. Epidemiology of Pancreatic Cancer: Global Trends, Etiology and Risk Factors. *World journal of oncology*, 10, 10-27.
- RIZVI, S. A. A. & SALEH, A. M. 2018. Applications of nanoparticle systems in drug delivery technology. *Saudi pharmaceutical journal : SPJ : the official publication of the Saudi Pharmaceutical Society*, 26, 64-70.
- ROBEY, R. W., PLUCHINO, K. M., HALL, M. D., FOJO, A. T., BATES, S. E. & GOTTESMAN, M. M. 2018. Revisiting the role of efflux pumps in multidrug-resistant cancer. *Nature reviews. Cancer*, 18, 452.
- ROIDER, E. M. & FISHER, D. E. 2016. Red hair, light skin, and UV-independent risk for melanoma development in humans. *JAMA dermatology*, 152, 751-753.
- RUBIN, A. I., CHEN, E. H. & RATNER, D. 2005. Basal-cell carcinoma. *New England Journal of Medicine*, 353, 2262-2269.
- RUDDON, R. W. 2007. *Cancer biology*, Oxford University Press.
- RUTTALA, H. B., RAMASAMY, T., GUPTA, B., CHOI, H.-G., YONG, C. S. & KIM, J. O. 2017. Multiple polysaccharide–drug complex-loaded liposomes: A unique strategy in drug loading and cancer targeting. *Carbohydrate Polymers*, 173, 57-66.

- RYOO, H. D. & BERGMANN, A. 2012. The role of apoptosis-induced proliferation for regeneration and cancer. *Cold Spring Harbor perspectives in biology*, 4, a008797-a008797.
- SABITHA, M., SANOJ REJINOLD, N., NAIR, A., LAKSHMANAN, V.-K., NAIR, S. V. & JAYAKUMAR, R. 2013. Development and evaluation of 5-fluorouracil loaded chitin nanogels for treatment of skin cancer. *Carbohydrate Polymers*, 91, 48-57.
- SAGBAS, S. & SAHINER, N. 2018. Modifiable natural gum based microgel capsules as sustainable drug delivery systems. *Carbohydrate polymers*, 200, 128-136.
- SAHU, P., KASHAW, S. K., SAU, S., KUSHWAH, V., JAIN, S., AGRAWAL, R. K. & IYER, A. K. 2019a. pH Responsive 5-Fluorouracil Loaded Biocompatible Nanogels For Topical Chemotherapy of Aggressive Melanoma. *Colloids and Surfaces B: Biointerfaces*, 174, 232-245.
- SAHU, P., KASHAW, S. K., SAU, S., KUSHWAH, V., JAIN, S., AGRAWAL, R. K. & IYER, A. K. 2019b. pH triggered and charge attracted nanogel for simultaneous evaluation of penetration and toxicity against skin cancer: In-vitro and ex-vivo study. *International Journal of Biological Macromolecules*, 128, 740-751.
- SAKHRANI, N. M. & PADH, H. 2013. Organelle targeting: third level of drug targeting. *Drug design, development and therapy*, 7, 585-599.
- SALATIN, S. & YARI KHOSROUSHAHI, A. 2017. Overviews on the cellular uptake mechanism of polysaccharide colloidal nanoparticles. *Journal of cellular and molecular medicine*, 21, 1668-1686.
- SALGAME, P., VARADHACHARY, A. S., PRIMIANO, L. L., FINCKE, J. E., MULLER, S. & MONESTIER, M. 1997. An ELISA for detection of apoptosis. *Nucleic acids research*, 25, 680-681.
- SARKER, D. K. 2005. Engineering of nanoemulsions for drug delivery. *Current Drug Delivery*, 2, 297-310.
- SAWYERS, C. 2004. Targeted cancer therapy. *Nature*, 432, 294.
- SCHADENDORF, D., VAN AKKOOI, A. C. J., BERKING, C., GRIEWANK, K. G., GUTZMER, R., HAUSCHILD, A., STANG, A., ROESCH, A. & UGUREL, S. 2018. Melanoma. *The Lancet*, 392, 971-984.
- SCHIRRMACHER, V. 2019. From chemotherapy to biological therapy: A review of novel concepts to reduce the side effects of systemic cancer treatment (Review). *International journal of oncology*, 54, 407-419.
- SCOMPARIN, A., SALMASO, S., BERSANI, S., SATCHI-FAINARO, R. & CALICETI, P. 2011. Novel folated and non-folated pullulan bioconjugates for anticancer drug delivery. *European Journal of Pharmaceutical Sciences*, 42, 547-558.
- SENAPATI, S., MAHANTA, A. K., KUMAR, S. & MAITI, P. 2018a. Controlled drug delivery vehicles for cancer treatment and their performance. *Signal transduction and targeted therapy*, 3, 7-7.

- SENAPATI, S., MAHANTA, A. K., KUMAR, S. & MAITI, P. 2018b. Controlled drug delivery vehicles for cancer treatment and their performance. *Signal Transduction and Targeted Therapy*, 3, 7.
- SERHAN, C. N., WARD, P. A. & GILROY, D. W. 2010. *Fundamentals of inflammation*, Cambridge University Press.
- SEVERINO, P., DA SILVA, C. F., ANDRADE, L. N., DE LIMA OLIVEIRA, D., CAMPOS, J. & SOUTO, E. B. 2019. Alginate nanoparticles for drug delivery and targeting. *Current pharmaceutical design*, 25, 1312-1334.
- SEVERINO, P., FANGUEIRO, J. F., FERREIRA, S. V., BASSO, R., CHAUD, M. V., SANTANA, M. H. A., ROSMANINHO, A. & SOUTO, E. B. 2013. Nanoemulsions and nanoparticles for non-melanoma skin cancer: effects of lipid materials. *Clinical and Translational Oncology*, 15, 417-424.
- SGANTZOS, M., TSOUCALAS, G., LAIOS, K. & ANDROUTSOS, G. 2014. The physician who first applied radiotherapy, Victor Despeignes, on 1896. *Hellenic journal of nuclear medicine*, 17, 45-46.
- SHAH, A., ASHAMES, A. A., BUABEID, M. A. & MURTAZA, G. 2020. Synthesis, in vitro characterization and antibacterial efficacy of moxifloxacin-loaded chitosan-pullulan-silver-nanocomposite films. *Journal of Drug Delivery Science and Technology*, 55, 101366.
- SHAH, G. D., SOCCI, N. D., GOLD, J. S., WOLCHOK, J. D., CARVAJAL, R. D., PANAGEAS, K. S., VIALE, A., BRADY, M. S., COIT, D. G. & CHAPMAN, P. B. 2010a. Phase II trial of neoadjuvant temozolomide in resectable melanoma patients. *Annals of Oncology*, 21, 1718-1722.
- SHAH, S., PAL, A., GUDE, R. & DEVI, S. 2010b. Synthesis and characterization of thermo-responsive copolymeric nanoparticles of poly (methyl methacrylate-co-N-vinylcaprolactam). *European Polymer Journal*, 46, 958-967.
- SHAH, S., RASKIN, L., COHAN, D., HAMID, O. & FREEMAN, M. L. 2019. Treatment patterns of melanoma by BRAF mutation status in the USA from 2011 to 2017: a retrospective cohort study. *Melanoma management*, 6, MMT31-MMT31.
- SHARMA, A., BOISE, L. H. & SHANMUGAM, M. 2019. Cancer Metabolism and the Evasion of Apoptotic Cell Death. *Cancers*, 11, 1144.
- SHARMA, A., GARG, T., AMAN, A., PANCHAL, K., SHARMA, R., KUMAR, S. & MARKANDEYWAR, T. 2016. Nanogel—an advanced drug delivery tool: Current and future. *Artificial cells, nanomedicine, and biotechnology*, 44, 165-177.
- SHENG, Y., HU, J., SHI, J. & LEE, L. J. 2019. Stimuli-responsive Carriers for Controlled Intracellular Drug Release. *Curr Med Chem*, 26, 2377-2388.
- SHI, G.-N., ZHANG, C.-N., XU, R., NIU, J.-F., SONG, H.-J., ZHANG, X.-Y., WANG, W.-W., WANG, Y.-M., LI, C., WEI, X.-Q. & KONG, D.-L. 2017. Enhanced antitumor immunity by targeting dendritic cells with tumor cell lysate-loaded chitosan nanoparticles vaccine. *Biomaterials*, 113, 191-202.

- SHIFFMAN, M. L. 2001. Pegylated interferons: what role will they play in the treatment of chronic hepatitis C? *Curr Gastroenterol Rep*, 3, 30-7.
- SHINGEL, K. I. 2004. Current knowledge on biosynthesis, biological activity, and chemical modification of the exopolysaccharide, pullulan. *Carbohydrate Research*, 339, 447-460.
- SHUCK, S. C., SHORT, E. A. & TURCHI, J. J. 2008. Eukaryotic nucleotide excision repair: from understanding mechanisms to influencing biology. *Cell Research*, 18, 64-72.
- SI, L., YAN, X., HAO, W., MA, X., REN, H., REN, B., LI, D., DONG, Z. & ZHENG, Q. 2018. Licochalcone D induces apoptosis and inhibits migration and invasion in human melanoma A375 cells. *Oncology reports*, 39, 2160-2170.
- SIDDIQUI, I. A., BHARALI, D. J., NIHAL, M., ADHAMI, V. M., KHAN, N., CHAMCHEU, J. C., KHAN, M. I., SHABANA, S., MOUSA, S. A. & MUKHTAR, H. 2014. Excellent anti-proliferative and pro-apoptotic effects of (-)-epigallocatechin-3-gallate encapsulated in chitosan nanoparticles on human melanoma cell growth both in vitro and in vivo. *Nanomedicine: Nanotechnology, Biology and Medicine*, 10, 1619-1626.
- SIEGEL, R. L., MILLER, K. D. & JEMAL, A. 2019. Cancer statistics, 2019. *CA: A Cancer Journal for Clinicians*, 69, 7-34.
- SIEGEL, R. L., MILLER, K. D. & JEMAL, A. 2020. Cancer statistics, 2020. *CA: A Cancer Journal for Clinicians*, 70, 7-30.
- SILVERMAN, M. K., KOPF, A. W., GLADSTEIN, A. H., BART, R. S., GRIN, C. M. & LEVENSTEIN, M. J. 1992. Recurrence rates of treated basal cell carcinomas: part 4: X-ray therapy. *The Journal of dermatologic surgery and oncology*, 18, 549-554.
- SINGH, G., BHATTI, R., MANNAN, R., SINGH, D., KESAVAN, A. & SINGH, P. 2019. Osthole ameliorates neurogenic and inflammatory hyperalgesia by modulation of iNOS, COX-2, and inflammatory cytokines in mice. *Inflammopharmacology*, 27, 949-960.
- SINGH, S. K., SINGH, S., LILLARD JR, J. W. & SINGH, R. 2017. Drug delivery approaches for breast cancer. *International journal of nanomedicine*, 12, 6205.
- SMITH, J. & PURR, E. 2019. Preparation of PLGA Nanoparticles Encapsulated with Fluorescent Probe Coumarin-6. *bioRxiv*, 614875.
- SNAPE, JR. & COLLINS, S. M. 2020. *The Effects of Immune Cells and Inflammation On Smooth Muscle and Enteric Nerves*, CRC Press.
- SOE, Z. C., KWON, J. B., THAPA, R. K., OU, W., NGUYEN, H. T., GAUTAM, M., OH, K. T., CHOI, H.-G., KU, S. K., YONG, C. S. & KIM, J. O. 2019. Transferrin-Conjugated Polymeric Nanoparticle for Receptor-Mediated Delivery of Doxorubicin in Doxorubicin-Resistant Breast Cancer Cells. *Pharmaceutics*, 11, 63.
- SOMASUNDARAM, R., HERLYN, M. & WAGNER, S. N. 2016. The role of tumor microenvironment in melanoma therapy resistance. *Melanoma management*, 3, 23-32.

- SONG, H., SU, C., CUI, W., ZHU, B., LIU, L., CHEN, Z. & ZHAO, L. 2013. Folic acid-chitosan conjugated nanoparticles for improving tumor-targeted drug delivery. *BioMed research international*, 2013, 723158-723158.
- SONG, W., TANG, Z., ZHANG, D., ZHANG, Y., YU, H., LI, M., LV, S., SUN, H., DENG, M. & CHEN, X. 2014. Anti-tumor efficacy of c (RGDfK)-decorated polypeptide-based micelles co-loaded with docetaxel and cisplatin. *Biomaterials*, 35, 3005-3014.
- SONI, S. R., BHUNIA, B. K., KUMARI, N., DAN, S., MUKHERJEE, S., MANDAL, B. B. & GHOSH, A. 2018. Therapeutically Effective Controlled Release Formulation of Pirfenidone from Nontoxic Biocompatible Carboxymethyl Pullulan-Poly (vinyl alcohol) Interpenetrating Polymer Networks. *ACS omega*, 3, 11993-12009.
- SOUTO, E. B., ZIELINSKA, A., SOUTO, S. B., DURAZZO, A., LUCARINI, M., SANTINI, A., SILVA, A. M., ATANASOV, A. G., MARQUES, C., ANDRADE, L. N. & SEVERINO, P. 2020. (+)-Limonene 1,2-Epoxy-Loaded SLNs: Evaluation of Drug Release, Antioxidant Activity, and Cytotoxicity in an HaCaT Cell Line. *International Journal of Molecular Sciences*, 21, 1449.
- SPRING, L. M., WANDER, S. A., ZANGARDI, M. & BARDIA, A. 2019. CDK 4/6 Inhibitors in Breast Cancer: Current Controversies and Future Directions. *Current oncology reports*, 21, 25-25.
- SUDHAKAR, A. 2009. History of cancer, ancient and modern treatment methods. *Journal of cancer science & therapy*, 1, 1.
- SUGUMAR, S., MUKHERJEE, A. & CHANDRASEKARAN, N. 2015. Eucalyptus oil nanoemulsion-impregnated chitosan film: antibacterial effects against a clinical pathogen, *Staphylococcus aureus*, in vitro. *International journal of nanomedicine*, 10 Suppl 1, 67-75.
- SUI, X., LEI, L., CHEN, L., XIE, T. & LI, X. 2017. Inflammatory microenvironment in the initiation and progression of bladder cancer. *Oncotarget*, 8, 93279.
- SUN, Y., DU, L., LIU, Y., LI, X., LI, M., JIN, Y. & QIAN, X. 2014. Transdermal delivery of the in situ hydrogels of curcumin and its inclusion complexes of hydroxypropyl- β -cyclodextrin for melanoma treatment. *International Journal of Pharmaceutics*, 469, 31-39.
- SUTRADHAR, K. B. & AMIN, M. L. 2014. Nanotechnology in Cancer Drug Delivery and Selective Targeting. *ISRN Nanotechnology*, 2014, 939378.
- SUTTON, D., NASONGKLA, N., BLANCO, E. & GAO, J. 2007. Functionalized micellar systems for cancer targeted drug delivery. *Pharmaceutical research*, 24, 1029-1046.
- TAFRESHI, N. K., TICHACEK, C. J., PANDYA, D. N., DOLIGALSKI, M. L., BUDZEVICH, M. M., KIL, H., BHATT, N. B., KOCK, N. D., MESSINA, J. L. & RUIZ, E. E. 2019. Melanocortin 1 Receptor-Targeted α -Particle Therapy for Metastatic Uveal Melanoma. *Journal of Nuclear Medicine*, 60, 1124-1133.
- TANESE, K., GRIMM, E. A. & EKMEKCIOGLU, S. 2012. The role of melanoma tumor-derived nitric oxide in the tumor inflammatory microenvironment: its impact on the

- chemokine expression profile, including suppression of CXCL10. *International journal of cancer*, 131, 891-901.
- TANG, L. & WANG, K. 2016. Chronic Inflammation in Skin Malignancies. *Journal of molecular signaling*, 11, 2-2.
- TAO, J., TU, Y. T., LI, J. W., FENG, A. P., HUANG, C. Z., WU, Y. & SHEN, G. X. 2006. Endogenous production of nitric oxide contributes to proliferation effect of vascular endothelial growth factor-induced malignant melanoma cell. *Clinical and Experimental Dermatology: Experimental Dermatology*, 31, 94-99.
- TAO, X., XIE, Y., ZHANG, Q., QIU, X., YUAN, L., WEN, Y., LI, M., YANG, X., TAO, T. & XIE, M. 2016. Cholesterol-modified amino-pullulan nanoparticles as a drug carrier: comparative study of cholesterol-modified carboxyethyl pullulan and pullulan nanoparticles. *Nanomaterials*, 6, 165.
- TARRAGÓ-TRANI, M. T. & STORRIE, B. 2007. Alternate routes for drug delivery to the cell interior: Pathways to the Golgi apparatus and endoplasmic reticulum. *Advanced Drug Delivery Reviews*, 59, 782-797.
- TAVEIRA, S. F., NOMIZO, A. & LOPEZ, R. F. V. 2009. Effect of the iontophoresis of a chitosan gel on doxorubicin skin penetration and cytotoxicity. *Journal of Controlled Release*, 134, 35-40.
- TEYMOURI, M., BADIEE, A., GOLMOHAMMADZADEH, S., SADRI, K., AKHTARI, J., MELLAT, M., NIKPOOR, A. R. & JAAFARI, M. R. 2016. Tat peptide and hexadecylphosphocholine introduction into pegylated liposomal doxorubicin: An in vitro and in vivo study on drug cellular delivery, release, biodistribution and antitumor activity. *International journal of pharmaceutics*, 511, 236-244.
- THAM, H. P., XU, K., LIM, W. Q., CHEN, H., ZHENG, M., THNG, T. G. S., VENKATRAMAN, S. S., XU, C. & ZHAO, Y. 2018. Microneedle-Assisted Topical Delivery of Photodynamically Active Mesoporous Formulation for Combination Therapy of Deep-Seated Melanoma. *ACS Nano*, 12, 11936-11948.
- THARKAR, P., VARANASI, R., WONG, W. S. F., JIN, C. T. & CHRZANOWSKI, W. 2019. Nano-Enhanced Drug Delivery and Therapeutic Ultrasound for Cancer Treatment and Beyond. *Frontiers in bioengineering and biotechnology*, 7, 324-324.
- THOMAS, S. N., VOKALI, E., LUND, A. W., HUBBELL, J. A. & SWARTZ, M. A. 2014. Targeting the tumor-draining lymph node with adjuvanted nanoparticles reshapes the anti-tumor immune response. *Biomaterials*, 35, 814-824.
- TIETZE, R., ZALOGA, J., UNTERWEGER, H., LYER, S., FRIEDRICH, R. P., JANKO, C., PÖTTLER, M., DÜRR, S. & ALEXIOU, C. 2015. Magnetic nanoparticle-based drug delivery for cancer therapy. *Biochemical and biophysical research communications*, 468, 463-470.
- TOKUDA, E. Y., LEIGHT, J. L. & ANSETH, K. S. 2014. Modulation of matrix elasticity with PEG hydrogels to study melanoma drug responsiveness. *Biomaterials*, 35, 4310-4318.
- TOMALIA, D. A., REYNA, L. A. & SVENSON, S. 2007. Dendrimers as multi-purpose nanodevices for oncology drug delivery and diagnostic imaging. Portland Press Limited.

- TRAN, M. A., WATTS, R. J. & ROBERTSON, G. P. 2009. Use of liposomes as drug delivery vehicles for treatment of melanoma. *Pigment Cell & Melanoma Research*, 22, 388-399.
- TRÉDAN, O., GALMARINI, C. M., PATEL, K. & TANNOCK, I. F. 2007. Drug resistance and the solid tumor microenvironment. *Journal of the National Cancer Institute*, 99, 1441-1454.
- TSATMALI, M., ANCANS, J. & THODY, A. J. 2002. Melanocyte Function and Its Control by Melanocortin Peptides. *Journal of Histochemistry & Cytochemistry*, 50, 125-133.
- TUPAL, A., SABZICHI, M., RAMEZANI, F., KOUHSOLTANI, M. & HAMISHEHKAR, H. 2016. Dermal delivery of doxorubicin-loaded solid lipid nanoparticles for the treatment of skin cancer. *Journal of microencapsulation*, 33, 372-380.
- VÁCHA, R., MARTINEZ-VERACOECHEA, F. J. & FRENKEL, D. 2011. Receptor-mediated endocytosis of nanoparticles of various shapes. *Nano letters*, 11, 5391-5395.
- VAIDYA, F. U., SUFIYAN CHHIPA, A., MISHRA, V., GUPTA, V. K., RAWAT, S. G., KUMAR, A. & PATHAK, C. 2020. Molecular and cellular paradigms of multidrug resistance in cancer. *Cancer Reports*, n/a, e1291.
- VAN ZEIJL, M. C. T., VAN DEN EERTWEGH, A. J., HAANEN, J. B. & WOUTERS, M. 2017. (Neo) adjuvant systemic therapy for melanoma. *European Journal of Surgical Oncology (EJSO)*, 43, 534-543.
- VAN ZIJL, F., KRUPITZA, G. & MIKULITS, W. 2011. Initial steps of metastasis: cell invasion and endothelial transmigration. *Mutation research*, 728, 23-34.
- VASIR, J. K. & LABHASETWAR, V. 2005. Targeted drug delivery in cancer therapy. *Technology in cancer research & treatment*, 4, 363-374.
- VECCHIONE, R., QUAGLIARIELLO, V., GIUSTETTO, P., CALABRIA, D., SATHYA, A., MAROTTA, R., PROFETA, M., NITTI, S., SILVESTRI, N. & PELLEGRINO, T. 2017. Oil/water nano-emulsion loaded with cobalt ferrite oxide nanocubes for photo-acoustic and magnetic resonance dual imaging in cancer: in vitro and preclinical studies. *Nanomedicine: Nanotechnology, Biology and Medicine*, 13, 275-286.
- VELHO, T. R. 2012. Metastatic melanoma - a review of current and future drugs. *Drugs in context*, 2012, 212242-212242.
- VIGER, M. L., GROSSMAN, M., FOMINA, N. & ALMUTAIRI, A. 2013. Low power upconverted near-ir light for efficient polymeric nanoparticle degradation and cargo release. *Advanced Materials*, 25, 3733-3738.
- VIJAYARAGHAVALU, S. & LABHASETWAR, V. 2013. Efficacy of decitabine-loaded nanogels in overcoming cancer drug resistance is mediated via sustained DNA methyltransferase 1 (DNMT1) depletion. *Cancer Letters*, 331, 122-129.
- VOICULESCU, V.-M., CARUNTU, C., SOLOMON, I., LUPU, M., ILIE, M. A., BODA, D., CONSTANTIN, C. & NEAGU, M. 2018. Squamous cell carcinoma: Biomarkers and potential therapeutic targets. *Human Skin Cancers-Pathways, Mechanisms, Targets and Treatments. IntechOpen*, 135-159.

- VORA, L. K., COURTENAY, A. J., TEKKO, I. A., LARRAÑETA, E. & DONNELLY, R. F. 2020. Pullulan-based dissolving microneedle arrays for enhanced transdermal delivery of small and large biomolecules. *International Journal of Biological Macromolecules*, 146, 290-298.
- WADAJKAR, A. S., BHAVSAR, Z., KO, C.-Y., KOPPOLU, B., CUI, W., TANG, L. & NGUYEN, K. T. 2012. Multifunctional particles for melanoma-targeted drug delivery. *Acta biomaterialia*, 8, 2996-3004.
- WAKABAYASHI, R., SAKURAGI, M., KOZAKA, S., TAHARA, Y., KAMIYA, N. & GOTO, M. 2018. Solid-in-Oil Peptide Nanocarriers for Transcutaneous Cancer Vaccine Delivery against Melanoma. *Molecular Pharmaceutics*, 15, 955-961.
- WALKER, C., MOJARES, E. & DEL RÍO HERNÁNDEZ, A. 2018. Role of Extracellular Matrix in Development and Cancer Progression. *International journal of molecular sciences*, 19, 3028.
- WAN, T., STYLIOS, G. K., GIANNOUDI, M. & GIANNOUDIS, P. V. 2015. Investigating a new drug delivery nano composite membrane system based on PVA/PCL and PVA/HA(PEG) for the controlled release of biopharmaceuticals for bone infections. *Injury*, 46, S39-S43.
- WANG, L., ZHANG, H., QIN, A., JIN, Q., TANG, B. Z. & JI, J. 2016. Theranostic hyaluronic acid prodrug micelles with aggregation-induced emission characteristics for targeted drug delivery. *Science China Chemistry*, 59, 1609-1615.
- WANG, M., ZHAO, J., ZHANG, L., WEI, F., LIAN, Y., WU, Y., GONG, Z., ZHANG, S., ZHOU, J. & CAO, K. 2017a. Role of tumor microenvironment in tumorigenesis. *Journal of Cancer*, 8, 761.
- WANG, Q.-M., GAO, Z., LIU, S., FAN, B., KANG, L., HUANG, W. & JIN, M. 2014. Hybrid polymeric micelles based on bioactive polypeptides as pH-responsive delivery systems against melanoma. *Biomaterials*, 35, 7008-7021.
- WANG, R.-F. 2017. A special issue on cancer immunotherapy. *Cell research*, 27, 1-2.
- WANG, W., GUO, D.-Y., LIN, Y.-J. & TAO, Y.-X. 2019a. Melanocortin Regulation of Inflammation. *Frontiers in endocrinology*, 10, 683-683.
- WANG, W., LIU, X., XIE, Y., ZHANG, H. A., YU, W., XIONG, Y., XIE, W. & MA, X. 2006. Microencapsulation using natural polysaccharides for drug delivery and cell implantation. *Journal of Materials Chemistry*, 16, 3252-3267.
- WANG, X.-Y., ZUO, D., SARKAR, D. & FISHER, P. B. 2011. Blockade of cytotoxic T-lymphocyte antigen-4 as a new therapeutic approach for advanced melanoma. *Expert opinion on pharmacotherapy*, 12, 2695-2706.
- WANG, X., ZHANG, H. & CHEN, X. 2019b. Drug resistance and combating drug resistance in cancer. *Cancer Drug Resistance*, 2, 141-160.
- WANG, Y., ZHANG, Z., XU, S., WANG, F., SHEN, Y., HUANG, S. & GUO, S. 2017b. pH, redox and photothermal tri-responsive DNA/polyethylenimine conjugated gold nanorods as nanocarriers for specific intracellular co-release of doxorubicin and chemosensitizer pyronaridine to combat multidrug resistant cancer. *Nanomedicine: Nanotechnology, Biology and Medicine*, 13, 1785-1795.

- WEBER, D., WHEAT, J. M. & CURRIE, G. M. 2010. Inflammation and cancer: tumor initiation, progression and metastasis, and Chinese botanical medicines. *Journal of Chinese Integrative Medicine*, 8, 1006-1013.
- WEI, P., YANG, Y., LIU, Z., HUANG, J., GONG, Y. & SUN, H. 2016. Oral Bifidobacterium longum expressing alpha-melanocyte-stimulating hormone to fight experimental colitis. *Drug Delivery*, 23, 2058-2064.
- WEI, X., LIAO, J., DAVOUDI, Z., ZHENG, H., CHEN, J., LI, D., XIONG, X., YIN, Y., YU, X. & XIONG, J. 2018. Folate receptor-targeted and gsh-responsive carboxymethyl chitosan nanoparticles containing covalently entrapped 6-mercaptopurine for enhanced intracellular drug delivery in leukemia. *Marine drugs*, 16, 439.
- WEINBERG, R. A. 2013. *The Biology of Cancer: Second International Student Edition*, WW Norton & Company.
- WEISSLEDER, R., KELIHER, E. J. & NAHRENDORF, M. 2018. Dextran nanoparticles for macrophage specific imaging and therapy. Google Patents.
- WEYERS, W. 2018. Screening for malignant melanoma-a critical assessment in historical perspective. *Dermatology practical & conceptual*, 8, 89-103.
- WINDER, M. & VIRÓS, A. 2017. Mechanisms of drug resistance in melanoma. *Mechanisms of Drug Resistance in Cancer Therapy*. Springer.
- WIRADHARMA, N., ZHANG, Y., VENKATARAMAN, S., HEDRICK, J. L. & YANG, Y. Y. 2009. Self-assembled polymer nanostructures for delivery of anticancer therapeutics. *Nano Today*, 4, 302-317.
- WOLINSKY, J. B. & GRINSTAFF, M. W. 2008. Therapeutic and diagnostic applications of dendrimers for cancer treatment. *Advanced drug delivery reviews*, 60, 1037-1055.
- WONG, R. S. Y. 2011. Apoptosis in cancer: from pathogenesis to treatment. *Journal of experimental & clinical cancer research : CR*, 30, 87-87.
- WONGKANYA, R., CHUYSINUAN, P., PENGSAK, C., TECHASAKUL, S., LIRDPRAPAMONGKOL, K., SVASTI, J. & NOOEAI, P. 2017. Electrospinning of alginate/soy protein isolated nanofibers and their release characteristics for biomedical applications. *Journal of Science: Advanced Materials and Devices*, 2, 309-316.
- WOODS, D. & TURCHI, J. J. 2013. Chemotherapy induced DNA damage response: convergence of drugs and pathways. *Cancer biology & therapy*, 14, 379-389.
- WU, C. F., WANG, H. M., HUANG, W. K. & CHANG, J. W. 2015. Efficacy and safety of bio-chemotherapy with dacarbazine plus interleukin-2 in patients with unresectable malignant melanoma. *Asia Pac J Clin Oncol*, 11, 314-8.
- WU, Q., YANG, Z., NIE, Y., SHI, Y. & FAN, D. 2014. Multi-drug resistance in cancer chemotherapeutics: mechanisms and lab approaches. *Cancer letters*, 347, 159-166.
- WU, W., SHEN, J., GAI, Z., HONG, K., BANERJEE, P. & ZHOU, S. 2011. Multi-functional core-shell hybrid nanogels for pH-dependent magnetic manipulation, fluorescent pH-sensing, and drug delivery. *Biomaterials*, 32, 9876-9887.

- XIA, J., DU, Y., HUANG, L., CHAURASIYA, B., TU, J., WEBSTER, T. J. & SUN, C. 2018. Redox-responsive micelles from disulfide bond-bridged hyaluronic acid-tocopherol succinate for the treatment of melanoma. *Nanomedicine: Nanotechnology, Biology and Medicine*, 14, 713-723.
- XIAO, D., BARRY, S., KMETZ, D., EGGER, M., PAN, J., RAI, S. N., QU, J., MCMASTERS, K. M. & HAO, H. 2016. Melanoma cell-derived exosomes promote epithelial-mesenchymal transition in primary melanocytes through paracrine/autocrine signaling in the tumor microenvironment. *Cancer letters*, 376, 318-327.
- XIE, Z., SU, Y., KIM, G. B., SELVI, E., MA, C., ARAGON-SANABRIA, V., HSIEH, J.-T., DONG, C. & YANG, J. 2017. Immune Cell-Mediated Biodegradable Theranostic Nanoparticles for Melanoma Targeting and Drug Delivery. *Small*, 13, 1603121.
- XU, P., VAN KIRK, E. A., ZHAN, Y., MURDOCH, W. J., RADOSZ, M. & SHEN, Y. 2007. Targeted Charge-Reversal Nanoparticles for Nuclear Drug Delivery. *Angewandte Chemie International Edition*, 46, 4999-5002.
- XU, X., ZHENG, L., YUAN, Q., ZHEN, G., CRANE, J. L., ZHOU, X. & CAO, X. 2018. Transforming growth factor- β in stem cells and tissue homeostasis. *Bone research*, 6, 1-31.
- XUE, X. & LIANG, X.-J. 2012. Overcoming drug efflux-based multidrug resistance in cancer with nanotechnology. *Chinese journal of cancer*, 31, 100-109.
- YANG, L. 2010. TGF β and cancer metastasis: an inflammation link. *Cancer and Metastasis Reviews*, 29, 263-271.
- YANG, S. & GAO, H. 2017. Nanoparticles for modulating tumor microenvironment to improve drug delivery and tumor therapy. *Pharmacological research*, 126, 97-108.
- YASUHARA, N., TAKEDA, E., INOUE, H., KOTERA, I. & YONEDA, Y. 2004. Importin alpha/beta-mediated nuclear protein import is regulated in a cell cycle-dependent manner. *Exp Cell Res*, 297, 285-93.
- YOKOYAMA, M. 2011. Clinical Applications of Polymeric Micelle Carrier Systems in Chemotherapy and Image Diagnosis of Solid Tumors. *Journal of Experimental & Clinical Medicine*, 3, 151-158.
- YONCHEVA, K., MERINO, M., SHENOL, A., DASKALOV, N. T., PETKOV, P. S., VAYSSILOV, G. N. & GARRIDO, M. J. 2019. Optimization and in-vitro/in-vivo evaluation of doxorubicin-loaded chitosan-alginate nanoparticles using a melanoma mouse model. *International journal of pharmaceutics*, 556, 1-8.
- YU, W., JIANG, G., ZHANG, Y., LIU, D., XU, B. & ZHOU, J. 2017. Polymer microneedles fabricated from alginate and hyaluronate for transdermal delivery of insulin. *Materials Science and Engineering: C*, 80, 187-196.
- YUAN, Y., CAI, T., XIA, X., ZHANG, R., CHIBA, P. & CAI, Y. 2016. Nanoparticle delivery of anticancer drugs overcomes multidrug resistance in breast cancer. *Drug Delivery*, 23, 3350-3357.

- ZAID, A., GÉRARDIN, P., TAYLOR, A., MOSTAFAVI, H., MALVY, D. & MAHALINGAM, S. 2018. Chikungunya arthritis: implications of acute and chronic inflammation mechanisms on disease management. *Arthritis & Rheumatology*, 70, 484-495.
- ZARGHI, A. & ARFAEI, S. 2011. Selective COX-2 Inhibitors: A Review of Their Structure-Activity Relationships. *Iranian journal of pharmaceutical research : IJPR*, 10, 655-683.
- ZETOUNE, F. S., SERHAN, C. N. & WARD, P. A. 2014. Inflammatory Disorders☆. *Reference Module in Biomedical Sciences*. Elsevier.
- ZHANG, C., LIN, K.-S. & BÉNARD, F. 2017. Molecular imaging and radionuclide therapy of melanoma targeting the melanocortin 1 receptor. *Molecular imaging*, 16, 1536012117737919.
- ZHANG, C., ZHANG, J., QIN, Y., SONG, H., HUANG, P., WANG, W., WANG, C., LI, C., WANG, Y. & KONG, D. 2018a. Co-delivery of doxorubicin and pheophorbide A by pluronic F127 micelles for chemo-photodynamic combination therapy of melanoma. *Journal of Materials Chemistry B*, 6, 3305-3314.
- ZHANG, Y., ZHAN, X., XIONG, J., PENG, S., HUANG, W., JOSHI, R., CAI, Y., LIU, Y., LI, R. & YUAN, K. 2018b. Temperature-dependent cell death patterns induced by functionalized gold nanoparticle photothermal therapy in melanoma cells. *Scientific reports*, 8, 8720.
- ZHOU, Y. 2019. Development of Selective Peptide Ligands Targeting Melanocortin Receptors for Melanoma Prevention and Therapy.
- ZHU, L.-F., ZHENG, Y., FAN, J., YAO, Y., AHMAD, Z. & CHANG, M.-W. 2019. A novel core-shell nanofiber drug delivery system intended for the synergistic treatment of melanoma. *European Journal of Pharmaceutical Sciences*, 137, 105002.
- ZOUANI, O. F., LEI, Y. & DURRIEU, M. C. 2013. Pericytes, Stem-Cell-Like Cells, but not Mesenchymal Stem Cells are Recruited to Support Microvascular Tube Stabilization. *Small*, 9, 3070-3075.
- ABEDIAN, Z., MOGHADAMNIA, A. A., ZABIHI, E., POURBAGHER, R., GHASEMI, M., NOURI, H. R., TASHAKORIAN, H. & JENABIAN, N. 2019. Anticancer properties of chitosan against osteosarcoma, breast cancer and cervical cancer cell lines. *Caspian journal of internal medicine*, 10, 439-446.
- AGARWAL, S. & KRISHNAMURTHY, K. 2019. Histology, skin.
- BAGHBANI, F., CHEGENI, M., MOZTARZADEH, F., HADIAN-GHAZVINI, S. & RAZ, M. 2017. Novel ultrasound-responsive chitosan/perfluorohexane nanodroplets for image-guided smart delivery of an anticancer agent: Curcumin. *Materials Science and Engineering: C*, 74, 186-193.
- BARONI, A., BUOMMINO, E., DE GREGORIO, V., RUOCCO, E., RUOCCO, V. & WOLF, R. 2012. Structure and function of the epidermis related to barrier properties. *Clinics in Dermatology*, 30, 257-262.

- BARUA, S. & MITRAGOTRI, S. 2014. Challenges associated with Penetration of Nanoparticles across Cell and Tissue Barriers: A Review of Current Status and Future Prospects. *Nano today*, 9, 223-243.
- BISCHOFF, K. M., LEATHERS, T. D., PRICE, N. P. J. & MANITCHOTPISIT, P. 2015. Liamocin oil from *Aureobasidium pullulans* has antibacterial activity with specificity for species of *Streptococcus*. *The Journal of Antibiotics*, 68, 642-645.
- BLANK, C. U., ROZEMAN, E. A., FANCHI, L. F., SIKORSKA, K., VAN DE WIEL, B., KVISTBORG, P., KRIJGSMAN, O., VAN DEN BRABER, M., PHILIPS, D. & BROEKS, A. 2018. Neoadjuvant versus adjuvant ipilimumab plus nivolumab in macroscopic stage III melanoma. *Nature medicine*, 24, 1655-1661.
- BRENNER, M. & HEARING, V. J. 2008. The protective role of melanin against UV damage in human skin. *Photochemistry and photobiology*, 84, 539-549.
- CAO, Z., LI, D., WANG, J., XIONG, M. & YANG, X. 2019. Direct Nucleus-Targeted Drug Delivery Using Cascade pH/Photo Dual-Sensitive Polymeric Nanocarrier for Cancer Therapy. *Small*, 15, 1902022.
- CAPANEMA, N. S. V., CARVALHO, I. C., MANSUR, A. A. P., CARVALHO, S. M., LAGE, A. P. & MANSUR, H. S. 2019. Hybrid Hydrogel Composed of Carboxymethylcellulose–Silver Nanoparticles–Doxorubicin for Anticancer and Antibacterial Therapies against Melanoma Skin Cancer Cells. *ACS Applied Nano Materials*, 2, 7393-7408.
- CARROLL, R. G. 2007. 2 - The Integument. In: CARROLL, R. G. (ed.) *Elsevier's Integrated Physiology*. Philadelphia: Mosby.
- CHEN, Q., KANG, J. & FU, C. 2018. The independence of and associations among apoptosis, autophagy, and necrosis. *Signal Transduction and Targeted Therapy*, 3, 18.
- CHEUNG, A., BAX, H. J., JOSEPHS, D. H., ILIEVA, K. M., PELLIZZARI, G., OPZOOMER, J., BLOOMFIELD, J., FITTALL, M., GRIGORIADIS, A., FIGINI, M., CANEVARI, S., SPICER, J. F., TUTT, A. N. & KARAGIANNIS, S. N. 2016. Targeting folate receptor alpha for cancer treatment. *Oncotarget*, 7, 52553-52574.
- CHIRIO, D., GALLARATE, M., PEIRA, E., BATTAGLIA, L., MUNTONI, E., RIGANTI, C., BIASIBETTI, E., CAPUCCHIO, M. T., VALAZZA, A., PANCANI, P., LANOTTE, M., ANNOVAZZI, L., CALDERA, V., MELLAI, M., FILICE, G., CORONA, S. & SCHIFFER, D. 2014. Positive-charged solid lipid nanoparticles as paclitaxel drug delivery system in glioblastoma treatment. *European Journal of Pharmaceutics and Biopharmaceutics*, 88, 746-758.
- CICHOREK, M., WACHULSKA, M., STASIEWICZ, A. & TYMIŃSKA, A. 2013. Skin melanocytes: biology and development. *Postępy dermatologii i alergologii*, 30, 30-41.
- DANIELS, T. R., BERNABEU, E., RODRÍGUEZ, J. A., PATEL, S., KOZMAN, M., CHIAPPETTA, D. A., HOLLER, E., LJUBIMOVA, J. Y., HELGUERA, G. & PENICHET, M. L. 2012. The transferrin receptor and the targeted delivery of therapeutic agents against cancer. *Biochimica et Biophysica Acta (BBA)-General Subjects*, 1820, 291-317.

- DANIELS, T. R., DELGADO, T., HELGUERA, G. & PENICHET, M. L. 2006. The transferrin receptor part II: targeted delivery of therapeutic agents into cancer cells. *Clin Immunol*, 121, 159-76.
- DEL PUERTO, H., MARTINS, A., MORO, L., MILSTED, A., ALVES, F., BRAZ, G. & VASCONCELOS, A. 2010. Caspase-3/-8/-9, Bax and Bcl-2 expression in the cerebellum, lymph nodes and leukocytes of dogs naturally infected with canine distemper virus. *Genetics and Molecular Research*, 9, 151-161.
- DISSANAYAKE, S., DENNY, W. A., GAMAGE, S. & SAROJINI, V. 2017. Recent developments in anticancer drug delivery using cell penetrating and tumor targeting peptides. *Journal of Controlled Release*, 250, 62-76.
- EFTEKHARI, A., AHMADIAN, E., SALATIN, S., SHARIFI, S., DIZAJ, S. M., KHALILOV, R. & HASANZADEH, M. 2019. Current analytical approaches in diagnosis of melanoma. *TrAC Trends in Analytical Chemistry*, 116, 122-135.
- ERDEI, E. & TORRES, S. M. 2010. A new understanding in the epidemiology of melanoma. *Expert review of anticancer therapy*, 10, 1811-1823.
- ERDMANN, S., SEIDEL, D., JAHNKE, H.-G., EICHLER, M., SIMON, J.-C. & ROBITZKI, A. A. 2019. Induced cross-resistance of BRAF V600E melanoma cells to standard chemotherapeutic dacarbazine after chronic PLX4032 treatment. *Scientific reports*, 9, 1-11.
- FERNALD, K. & KUROKAWA, M. 2013. Evading apoptosis in cancer. *Trends in cell biology*, 23, 620-633.
- GAJBHIYE, K., GAJBHIYE, V., SIDDIQUI, I. A. & GAJBHIYE, J. 2019. cRGD functionalised nanocarriers for targeted delivery of bioactives. *Journal of drug targeting*, 27, 111-124.
- GARG, U., CHAUHAN, S., NAGAICH, U. & JAIN, N. 2019. Current Advances in Chitosan Nanoparticles Based Drug Delivery and Targeting. *Advanced pharmaceutical bulletin*, 9, 195-204.
- GIACONE, D. V., DARTORA, V. F., DE MATOS, J. K., PASSOS, J. S., MIRANDA, D. A., DE OLIVEIRA, E. A., SILVEIRA, E. R., COSTA-LOTUFO, L. V., MARIA-ENGLER, S. S. & LOPES, L. B. 2020. Effect of nanoemulsion modification with chitosan and sodium alginate on the topical delivery and efficacy of the cytotoxic agent piplartine in 2D and 3D skin cancer models. *International Journal of Biological Macromolecules*, 165, 1055-1065.
- GIBOT, L., CHABAUD, S., BOUHOUT, S., BOLDUC, S., AUGER, F. A. & MOULIN, V. J. 2015. Anticancer properties of chitosan on human melanoma are cell line dependent. *International Journal of Biological Macromolecules*, 72, 370-379.
- GIRDHAR, V., PATIL, S., BANERJEE, S. & SINGHVI, G. 2018. Nanocarriers for drug delivery: mini review. *Current Nanomedicine (Formerly: Recent Patents on Nanomedicine)*, 8, 88-99.
- HAFEEZ, A. & KAZMI, I. 2017. Dacarbazine nanoparticle topical delivery system for the treatment of melanoma. *Scientific Reports*, 7, 16517.
- HARRISON, S. C. & BERGFELD, W. F. 2009. Ultraviolet light and skin cancer in athletes. *Sports health*, 1, 335-340.

- HASSANZADEH, P., ATYABI, F. & DINARVAND, R. 2019. The significance of artificial intelligence in drug delivery system design. *Advanced Drug Delivery Reviews*, 151-152, 169-190.
- HE, X., SUN, J. & HUANG, X. 2018. Expression of caspase-3, Bax and Bcl-2 in hippocampus of rats with diabetes and subarachnoid hemorrhage. *Experimental and therapeutic medicine*, 15, 873-877.
- ITURRIOZ-RODRÍGUEZ, N., CORREA-DUARTE, M. A. & FANARRAGA, M. L. 2019. Controlled drug delivery systems for cancer based on mesoporous silica nanoparticles. *International journal of nanomedicine*, 14, 3389-3401.
- JAFARIZAD, A., JAYMAND, M., TAGHIZADEHGHAEHJOUGI, A., MOHAMMADI-NASR, S. & JABBARI, A. M. The magnetic graphene-based nanocomposite: an efficient anticancer delivery system. AIP Conference Proceedings, 2018. AIP Publishing LLC, 020039.
- JOSEPH, M. M., ARAVIND, S., GEORGE, S. K., PILLAI, K. R., MINI, S. & SREELEKHA, T. 2015. Anticancer activity of galactoxyloglucan polysaccharide-conjugated doxorubicin nanoparticles: Mechanistic insights and interactome analysis. *European Journal of Pharmaceutics and Biopharmaceutics*, 93, 183-195.
- KALE, J., KUTUK, O., BRITO, G. C., ANDREWS, T. S., LEBER, B., LETAI, A. & ANDREWS, D. W. 2018. Phosphorylation switches Bax from promoting to inhibiting apoptosis thereby increasing drug resistance. *EMBO reports*, 19, e45235.
- KAPLAN, A. B. U., CETIN, M., ORGUL, D., TAGHIZADEHGHAEHJOUGH, A., HACİMUFTUOĞLU, A. & HEKİMOĞLU, S. 2019. Formulation and in vitro evaluation of topical nanoemulsion and nanoemulsion-based gels containing daidzein. *Journal of Drug Delivery Science and Technology*, 52, 189-203.
- KHALID, M. & EL-SAWY, H. S. 2017. Polymeric nanoparticles: Promising platform for drug delivery. *International journal of pharmaceutics*, 528, 675-691.
- KOSTER, B. D., VAN DEN HOUT, M. F., SLUIJTER, B. J., MOLENKAMP, B. G., VUYLSTEKE, R. J., BAARS, A., VAN LEEUWEN, P. A., SCHEPER, R. J., VAN DEN TOL, M. P. & VAN DEN EERTWEGH, A. J. 2017. Local adjuvant treatment with low-dose CpG-B offers durable protection against disease recurrence in clinical stage I–II melanoma: data from two randomized phase II trials. *Clinical Cancer Research*, 23, 5679-5686.
- KOTAWONG, K., CHAIJAROENKUL, W., MUHAMAD, P. & NA-BANGCHANG, K. 2018. Cytotoxic activities and effects of atractylodin and β -eudesmol on the cell cycle arrest and apoptosis on cholangiocarcinoma cell line. *Journal of pharmacological sciences*, 136, 51-56.
- LASON, E. 2020. Topical Administration of Terpenes Encapsulated in Nanostructured Lipid-Based Systems. *Molecules (Basel, Switzerland)*, 25, 5758.
- LEE, C. L. 1953. Structure and Development of Hypodermis in *Dacrydium taxoides* Leaves. *American Journal of Botany*, 40, 366-371.
- LI, M., LIU, D., LEE, D., KAPOOR, S., GIBSON-CORLEY, K. N., QUINN, T. P., SAGASTUME, E. A., MOTT, S. L., WALSH, S. A. & ACEVEDO, M. R. 2019. Enhancing the efficacy of melanocortin 1 receptor-targeted radiotherapy by

- pharmacologically upregulating the receptor in metastatic melanoma. *Molecular pharmaceutics*, 16, 3904-3915.
- LIN, Z. 2018. *Characterization and functional studies of electrospun/sprayed complexes loaded with phytochemicals*. Rutgers University-School of Graduate Studies.
- LIU, Q., DAS, M., LIU, Y. & HUANG, L. 2018. Targeted drug delivery to melanoma. *Advanced drug delivery reviews*, 127, 208-221.
- LOPES-RODRIGUES, V., DI LUCA, A., MLECZKO, J., MELEADY, P., HENRY, M., PESIC, M., CABRERA, D., VAN LIEMPD, S., LIMA, R. T., O'CONNOR, R., FALCON-PEREZ, J. M. & VASCONCELOS, M. H. 2017. Identification of the metabolic alterations associated with the multidrug resistant phenotype in cancer and their intercellular transfer mediated by extracellular vesicles. *Scientific reports*, 7, 44541-44541.
- MANITCHOTPISIT, P., WATANAPOKSIN, R., PRICE, N. P. J., BISCHOFF, K. M., TAYEH, M., TEERAWORAWIT, S., KRIWONG, S. & LEATHERS, T. D. 2014. Aureobasidium pullulans as a source of liamocins (heavy oils) with anticancer activity. *World Journal of Microbiology and Biotechnology*, 30, 2199-2204.
- MAZZONE, R., ZWERGEL, C., ARTICO, M., TAURONE, S., RALLI, M., GRECO, A. & MAI, A. 2019. The emerging role of epigenetics in human autoimmune disorders. *Clinical Epigenetics*, 11, 34.
- MCDONALD, T. O., SICCARDI, M., MOSS, D., LIPTROTT, N., GIARDIELLO, M., RANNARD, S. & OWEN, A. 2015. Chapter 2.2 - The Application of Nanotechnology to Drug Delivery in Medicine. In: DOLEZ, P. I. (ed.) *Nanoengineering*. Amsterdam: Elsevier.
- MISHRA, H., MISHRA, P. K., EKIELSKI, A., JAGGI, M., IQBAL, Z. & TALEGAONKAR, S. 2018. Melanoma treatment: from conventional to nanotechnology. *J Cancer Res Clin Oncol*, 144, 2283-2302.
- MOHAMMADPOUR, A., DERAKHSHAN, M., DARABI, H., HEDAYAT, P. & MOMENI, M. 2019. Melanoma: Where we are and where we go. *Journal of cellular physiology*, 234, 3307-3320.
- MOHAMMED, M. A., SYEDA, J. T. M., WASAN, K. M. & WASAN, E. K. 2017. An Overview of Chitosan Nanoparticles and Its Application in Non-Parenteral Drug Delivery. *Pharmaceutics*, 9, 53.
- MOSTAFA, W. Z. & HEGAZY, R. A. 2015. Vitamin D and the skin: Focus on a complex relationship: A review. *Journal of advanced research*, 6, 793-804.
- NAVES, L. B., DHAND, C., VENUGOPAL, J. R., RAJAMANI, L., RAMAKRISHNA, S. & ALMEIDA, L. 2017. Nanotechnology for the treatment of melanoma skin cancer. *Progress in biomaterials*, 6, 13-26.
- NEŠIĆ, M. D., DUČIĆ, T., LIANG, X., ALGARRA, M., MI, L., KORIĆANAC, L., ŽAKULA, J., KOP, T. J., BJELAKOVIĆ, M. S., MITROVIĆ, A., GOJGIĆ CVIJOVIĆ, G. D., STEPIĆ, M. & PETKOVIĆ, M. 2020. SR-FTIR spectro-microscopic interaction study of biochemical changes in HeLa cells induced by Levan-C60, Pullulan-C60, and their cholesterol-derivatives. *International Journal of Biological Macromolecules*, 165, 2541-2549.

- NIKOLAOU, M., PAVLOPOULOU, A., GEORGAKILAS, A. G. & KYRODIMOS, E. 2018. The challenge of drug resistance in cancer treatment: a current overview. *Clinical & Experimental Metastasis*, 35, 309-318.
- OGBODU, R. O., NDHUNDHUMA, I., KARSTEN, A. & NYOKONG, T. 2015. Photodynamic therapy effect of zinc monoamino phthalocyanine–folic acid conjugate adsorbed on single walled carbon nanotubes on melanoma cells. *Spectrochimica Acta Part A: Molecular and Biomolecular Spectroscopy*, 137, 1120-1125.
- PARKIN, A., MAN, J., TIMPSON, P. & PAJIC, M. 2019. Targeting the complexity of Src signalling in the tumour microenvironment of pancreatic cancer: from mechanism to therapy. *The FEBS journal*, 286, 3510-3539.
- PFANNENSTIEL, L. W., MCNEILLY, C., XIANG, C., KANG, K., DIAZ-MONTERO, C. M., YU, J. S. & GASTMAN, B. R. 2019. Combination PD-1 blockade and irradiation of brain metastasis induces an effective abscopal effect in melanoma. *Oncoimmunology*, 8, e1507669.
- RAI, V. K., MISHRA, N., YADAV, K. S. & YADAV, N. P. 2018a. Nanoemulsion as pharmaceutical carrier for dermal and transdermal drug delivery: Formulation development, stability issues, basic considerations and applications. *J Control Release*, 270, 203-225.
- RAI, Y., PATHAK, R., KUMARI, N., SAH, D. K., PANDEY, S., KALRA, N., SONI, R., DWARAKANATH, B. S. & BHATT, A. N. 2018b. Mitochondrial biogenesis and metabolic hyperactivation limits the application of MTT assay in the estimation of radiation induced growth inhibition. *Scientific Reports*, 8, 1531.
- RIA, R. & VACCA, A. 2020. Bone Marrow Stromal Cells-Induced Drug Resistance in Multiple Myeloma. *International journal of molecular sciences*, 21, 613.
- RIVOLTA, I., PANARITI, A., LETTIERO, B., SESANA, S., GASCO, P., GASCO, M. R., MASSERINI, M. & MISEROCCHI, G. 2011. Cellular uptake of coumarin-6 as a model drug loaded in solid lipid nanoparticles. *J Physiol Pharmacol*, 62, 45-53.
- ROBERTSON, F. M.-L. & FITZGERALD, L. 2017. Skin cancer in the youth population of the United Kingdom. *Journal of cancer policy*, 12, 67-71.
- ROMA-RODRIGUES, C., MENDES, R., BAPTISTA, P. V. & FERNANDES, A. R. 2019. Targeting Tumor Microenvironment for Cancer Therapy. *International journal of molecular sciences*, 20, 840.
- SÁNCHEZ-LÓPEZ, E., GUERRA, M., DIAS-FERREIRA, J., LOPEZ-MACHADO, A., ETTCHETO, M., CANO, A., ESPINA, M., CAMINS, A., GARCIA, M. L. & SOUTO, E. B. 2019. Current applications of nanoemulsions in cancer therapeutics. *Nanomaterials*, 9, 821.
- SARIGÖL-KILIÇ, Z. & ÜNDEĞER-BUCURGAT, Ü. 2018. The apoptotic and anti-apoptotic effects of pendimethalin and trifluralin on A549 cells in vitro. *Turkish Journal of Pharmaceutical Sciences*, 15, 364.
- SHAKEEL, F., SHAFIQ, S., HAQ, N., ALANAZI, F. K. & ALSARRA, I. A. 2012. Nanoemulsions as potential vehicles for transdermal and dermal delivery of hydrophobic compounds: an overview. *Expert Opin Drug Deliv*, 9, 953-74.

- SHANG, J., CHEN, W.-M., LIU, S., WANG, Z.-H., WEI, T.-N., CHEN, Z.-Z. & WU, W.-B. 2019. CircPAN3 contributes to drug resistance in acute myeloid leukemia through regulation of autophagy. *Leukemia research*, 85, 106198.
- SINGH, T., MURTHY, A. S. N., YANG, H.-J. & IM, J. 2018. Versatility of cell-penetrating peptides for intracellular delivery of siRNA. *Drug Delivery*, 25, 1996-2006.
- STYLIANOPOULOS, T., MUNN, L. L. & JAIN, R. K. 2018. Reengineering the Physical Microenvironment of Tumors to Improve Drug Delivery and Efficacy: From Mathematical Modeling to Bench to Bedside. *Trends in cancer*, 4, 292-319.
- SUN, Z., SONG, C., WANG, C., HU, Y. & WU, J. 2020. Hydrogel-Based Controlled Drug Delivery for Cancer Treatment: A Review. *Molecular Pharmaceutics*, 17, 373-391.
- TAGNE, J.-B., KAKUMANU, S. & NICOLOSI, R. J. 2008. Nanoemulsion Preparations of the Anticancer Drug Dacarbazine Significantly Increase Its Efficacy in a Xenograft Mouse Melanoma Model. *Molecular Pharmaceutics*, 5, 1055-1063.
- TAI, K., RAPPOLT, M., MAO, L., GAO, Y., LI, X. & YUAN, F. 2020. The stabilization and release performances of curcumin-loaded liposomes coated by high and low molecular weight chitosan. *Food Hydrocolloids*, 99, 105355.
- TAO, X., TAO, T., WEN, Y., YI, J., HE, L., HUANG, Z., NIE, Y., YAO, X., WANG, Y., HE, C. & YANG, X. 2018. Novel Delivery of Mitoxantrone with Hydrophobically Modified Pullulan Nanoparticles to Inhibit Bladder Cancer Cell and the Effect of Nano-drug Size on Inhibition Efficiency. *Nanoscale Research Letters*, 13, 345.
- TESTORI, A., RUTKOWSKI, P., MARSDEN, J., BASTHOLT, L., CHIARION-SILENI, V., HAUSCHILD, A. & EGGERMONT, A. 2009. Surgery and radiotherapy in the treatment of cutaneous melanoma. *Annals of Oncology*, 20, vi22-vi29.
- UGUREL, S., RÖHMEL, J., ASCIERTO, P. A., FLAHERTY, K. T., GROB, J. J., HAUSCHILD, A., LARKIN, J., LONG, G. V., LORIGAN, P. & MCARTHUR, G. A. 2017. Survival of patients with advanced metastatic melanoma: the impact of novel therapies—update 2017. *European Journal of Cancer*, 83, 247-257.
- WANG, K., DAI, J., LIU, T., WANG, Q. & PANG, Y. 2019a. LncRNA ZEB2-AS1 regulates the drug resistance of acute myeloid leukemia via the miR-142-3p/INPP4B axis. *RSC Advances*, 9, 39495-39504.
- WANG, W., GUO, D.-Y., LIN, Y.-J. & TAO, Y.-X. 2019b. Melanocortin Regulation of Inflammation. *Frontiers in endocrinology*, 10, 683-683.
- WANG, X., LIOW, S. S., WU, Q., LI, C., OWH, C., LI, Z., LOH, X. J. & WU, Y. L. 2017. Codelivery for Paclitaxel and Bcl-2 Conversion Gene by PHB-PDMAEMA Amphiphilic Cationic Copolymer for Effective Drug Resistant Cancer Therapy. *Macromolecular bioscience*, 17, 1700186.
- XIAO, J., EGGER, M. E., MCMASTERS, K. M. & HAO, H. 2018. Differential expression of ABCB5 in BRAF inhibitor-resistant melanoma cell lines. *BMC Cancer*, 18, 675.
- XIN, Y., YIN, M., ZHAO, L., MENG, F. & LUO, L. 2017. Recent progress on nanoparticle-based drug delivery systems for cancer therapy. *Cancer biology & medicine*, 14, 228-241.

- XU, T., MA, Y., HUANG, J., LAI, H., YUAN, D., TANG, X. & YANG, L. 2020. Self-organized thermo-responsive poly (lactic-co-glycolic acid)-graft-pullulan nanoparticles for synergistic thermo-chemotherapy of tumor. *Carbohydrate polymers*, 237, 116104.
- YANG, N. J. & HINNER, M. J. 2015. Getting across the cell membrane: an overview for small molecules, peptides, and proteins. *Methods in molecular biology (Clifton, N.J.)*, 1266, 29-53.
- YONCHEVA, K., MERINO, M., SHENOL, A., DASKALOV, N. T., PETKOV, P. S., VAYSSILOV, G. N. & GARRIDO, M. J. 2019. Optimization and in-vitro/in-vivo evaluation of doxorubicin-loaded chitosan-alginate nanoparticles using a melanoma mouse model. *International journal of pharmaceutics*, 556, 1-8.
- YU, B., TAI, H. C., XUE, W., LEE, L. J. & LEE, R. J. 2010. Receptor-targeted nanocarriers for therapeutic delivery to cancer. *Molecular membrane biology*, 27, 286-298.
- YUAN, L., GUO, B., ZHONG, W., NIE, Y., YAO, X., PENG, X., WANG, R., YU, H., YANG, S. & HE, C. 2019. Interaction of mitoxantrone-loaded cholesterol modified pullulan nanoparticles with human serum albumin and effect on drug release. *Journal of Nanomaterials*, 2019.
- YUAN, Y. & LIU, B. 2017. Visualization of drug delivery processes using AIEgens. *Chemical science*, 8, 2537-2546.
- ZAIDI, M. R., DAY, C.-P. & MERLINO, G. 2008. From UVs to Metastases: Modeling Melanoma Initiation and Progression in the Mouse. *Journal of Investigative Dermatology*, 128, 2381-2391.
- ZHOU, Y., MOWLAZADEH HAGHIGHI, S., LIU, Z., WANG, L., HRUBY, V. J. & CAI, M. 2020. Development of Ligand-Drug Conjugates Targeting Melanoma through the Overexpressed Melanocortin 1 Receptor. *ACS Pharmacology & Translational Science*, 3, 921-930.
- ZUNUNI VAHED, S., FATHI, N., SAMIEI, M., MALEKI DIZAJ, S. & SHARIFI, S. 2019. Targeted cancer drug delivery with aptamer-functionalized polymeric nanoparticles. *Journal of drug targeting*, 27, 292-299.